8-2016

Kinetics and Mechanisms of Amine Bis-phenolate Polymerization Catalysts Featuring Titanium, Zirconium, or Hafnium Centers

Paul Daniel Pletcher
Purdue University

Graduate School Form 30
(Updated 11/20/2014)

PURDUE UNIVERSITY
GRADUATE SCHOOL
Thesis/Dissertation Acceptance

This is to certify that the thesis/dissertation prepared

By Paul Daniel Pletcher

Entitled KINETICS AND MECHANISMS OF AMINE BIS-PHENOLATE POLYMERIZATION CATALYSTS FEATURING TITANIUM, ZIRCONIUM, OR HAFNIUM CENTERS

For the degree of Doctor of Philosophy

Is approved by the final examining committee:

Mahdi Abu-Omar

David R. McMillin

James Caruthers

W. Nicholas Delgass

To the best of my knowledge and as understood by the student in the Thesis/Dissertation Agreement, Publication Delay, and Certification/Disclaimer (Graduate School Form 32), this thesis/dissertation adheres to the provisions of Purdue University's "Policy on Integrity in Research" and the use of copyrighted material.

Mahdi Abu-Omar

Approved by Major Professor(s): _____

_____

Approved by: Timothy Zwier 05/26/2016

Head of the Department Graduate Program Date

KINETICS AND MECHANISMS OF AMINE BIS-PHENOLATE POLYMERIZATION CATALYSTS FEATURING TITANIUM, ZIRCONIUM, OR HAFNIUM CENTERS

A Dissertation

Submitted to the Faculty

of

Purdue University

by

Paul Daniel Pletcher

In Partial Fulfillment of the

Requirements for the Degree

of

Doctor of Philosophy

August 2016

Purdue University

West Lafayette, Indiana

This dissertation is dedicated to my family, friends, and mentors.

ACKNOWLEDGMENTS

I would like to first thank my advisor and research mentor, Professor Mahdi Abu-Omar, for his support, enthusiasm, guidance, and patience over my time at Purdue. I do not believe I would have had such a positive graduate experience without him as an advisor.

I would also like to express gratitude and thanks to past present collaborators: Dr. Erin Smith, Dr. David Steelman, Thilina N. Gunasekara, Andrew Preston. Dr. Grigori A. Medvedev, Dr. Silei Xiong, Dr. Jeffrey Switzer, and Jungsuk Kim.

In terms of my other mentors, I want to give my utmost thanks to Professors W. Nicholas Delgass, James M. Caruthers, and David McMillin. My future professional success will be in a large part due to the guidance and faith that they have given me in past.

Thanks must be given to my group members in the Chemistry Department for their help and support through this time together. Mike Mazzotta, I wish the best in the rest of his academic career and thank him for friendly discussions, science or otherwise. My other friends in the department, too numerous to name individually, I also give my undying gratitude and best wishes in their dreams, professionally and personally.

And last, I give thanks to the support from my family as it has grown and continues to grow. My fiancé, Chelsey, has been my rock and kept me grounded during my time here.

TABLE OF CONTENTS

Page

Page

Page

LIST OF TABLES

Table Page

LIST OF FIGURES

Figure Page

Figure Page

Figure Page

Figure Page

Figure Page

Figure Page

Figure Page

LIST OF SCHEMES

Scheme Page

Scheme Page

ABSTRACT

Pletcher, Paul Daniel, Ph.D., Purdue University, August 2016. Kinetics and Mechanisms of Amine Bis-phenolate Polymerization Catalysts Featuring Titanium, Zirconium, or Hafnium Centers. Major Professor: Mahdi Abu-Omar.

The story of Group IV metallocene polymerization catalysts has been a tremendous success in the ability to tune chemical reactivity through structural design. As new, nonmetallocene catalyst systems are being investigated, there has been a lack of quantitative relationships for predicting optimal catalyst design for both desired reactivity and polymeric properties. By utilizing a rational catalyst design strategy that focuses on obtaining a quantitative kinetic analysis of all relevant chemical steps from a family of related catalysts, we have attempted to correlate the fundamental reactivity within the olefin polymerization mechanism to distinctive chemical structures. Such studies have revealed both predictive, quantitative correlations and new, unexpected reactivity in a family of Group IV amine bis-phenolate catalysts.

CHAPTER 1. QUANTITATIVE KINETIC ANALYSIS OF SINGLE-SITE OLEFIN POLYMERIZATION CATALYSIS

1.1 Introduction

The ability to convert olefins and α-olefins into high molecular weight materials via insertion between metal and alkyl chain is one of the fundamental chemical reactions that has built the modern world, with projected estimates of nearly 170 billion kg of materials produced by 2018.[1] The discovery of heterogeneous Ziegler-Natta catalysts has eventually led to homogeneous catalysts capable of systematic design.[2-5] Further progress in terms of cocatalyst design from methylaluminoxane (MAO) to well-defined, molecular borate/aluminate/aminate catalysts have allowed for kinetic and chemical reactivity studies.[6] In fact, the field of organometallic, coordination-insertion polymerization has developed a mature understanding in terms of the different types of fundamental chemical reactions.[2-7] In contrast, development of quantitative structure-functional relationships has lagged. The hope and purpose behind this research has been to develop kinetic models in terms of Group IV olefin polymerization to discover chemical descriptors that can be used to develop the next generation of catalysts and polymeric materials.

Systematic development of qualitative relationships between structure and function with Group IV catalysts featuring metallocene ligands has suggested that rationale design of olefin polymerization species may be possible.[8-9] Through careful kinetic and computational analysis, a study by Abu-Omar and coworkers on the polymerization of 1-hexene through different Titanium cyclopentadienyl/aryloxide catalysts has shown a quantitative structure-function relationship between the ion pair separation energy of the cationic Ti center to the inner-sphere $MeB(C_6F_5)_3^-$ counter anion and the propagation rate constant.[9c] Despite this example of correlating catalyst chemical structure to reactive functionality, there is a lack of fundamental, quantitative studies connecting structure and function.

The development of group IV coordination catalysts and polymeric products has been accelerated through the development of high-throughput screening processes. Such design strategies have led to Dow's catalyst systems for block copolymer products[10] or the rapid development of phenoxy imine catalysts.[11] These studies often rely solely on catalytic activity on monomer (ethylene, α-olefins, or multiple monomers) consumption and analysis of the polymer produced. Reliance on these limited measurements fails to capture both the entire mechanism and the associated rate constants for each step. Without such information, developing quantitative chemical descriptors for rational catalyst design remains an elusive goal.

In the attempt to replicate the success of structure-activity relationships studies in heterogeneous systems, such as with CO oxidation[12] or water gas shift reaction,[13] an overall design strategy has been conceptualized, Figure 1.1. After synthesis of a catalyst family, an array of quantitative studies of the kinetics, structural, and polymer bulk properties will

be analyzed to understand the behavior of both the chemical reactivity of the catalyst as well as the corresponding polymer properties that arise from the corresponding rate constants. Through analysis of a family of catalysts, a forward model can be quantified to develop catalyst descriptors that can be used as an inverse search for new group IV compounds. Alternatively, an inverse model approach to the coordination polymerization design scheme exists: experiments with a known family of catalyst structures produces polymeric materials which can be used to describe properties such as molecular weight, tacticity, or other structural features that influence the polymer bulk properties. For the purpose of this thesis, the forward model approach will be utilized to study and determine catalyst descriptors for the purpose of designing new catalysts and polymeric materials. This requires and relies on the acquiring an overall mechanism with quantified kinetic rate constants for each elementary step.

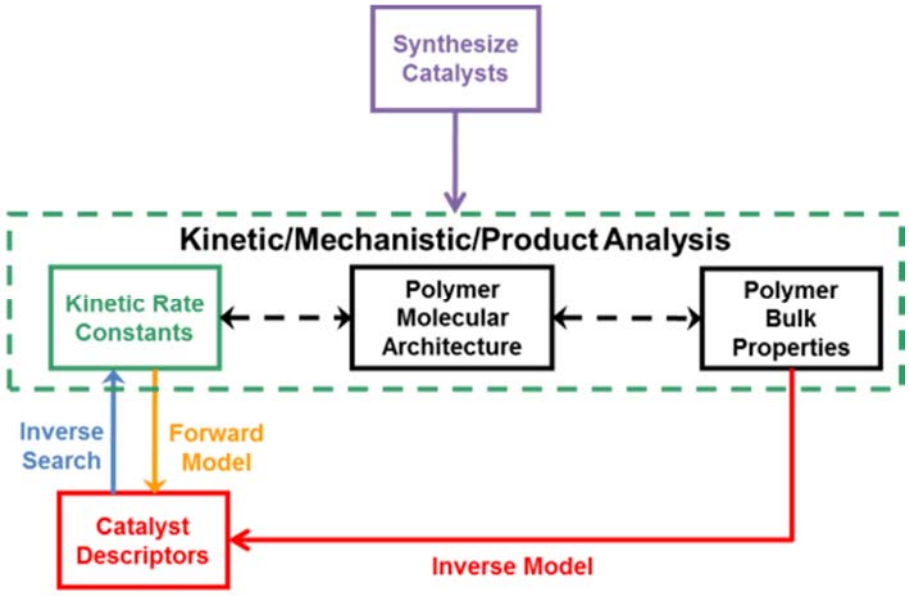

Figure 1.1 Idealized Group IV Coordination Polymerization Design Scheme

In many reports, rate constants for elementary steps in the catalyst cycle are determined over limited conditions and do not capture the entirety of the mechanism or assume total catalyst participation.[14-17] For example, a common method of determining catalytic activity is to run an experiment in a massive loading of monomer before quenching the reaction at a specified time and weighing the mass of polymeric material.[18] This experiment captures a single measurement point and assumes total catalyst participation, no catalyst deactivation, and a fast induction period. Such experiments only consider one elementary step of the mechanism instead of breaking down the results into the complete collection of different chemical reactions. In recent years, kinetic analysis including a comprehensive collection of a diverse set of multi-response data that comprises monomer consumption, production and quantification of vinyl end groups, and active site analysis has shown the potential to not only capture the entirety of the catalytic mechanism but also quantify the rate constants of all elementary steps.[15,18] This has been further improved through the inclusion of time-evolved molecular weight distributions of the polymeric material.[19] Through this level of analysis, reliable rate constants can be matched to catalyst molecular architecture to build a forward model for reliable descriptor determination.

Using the aforementioned analysis tools, it is possible to consider α-olefin insertion polymerization as a collection of six distinctive steps: (1) activation, (2) initiation, insertion of the first olefin molecule, (3) propagation, repeated insertions of successive monomers (in a 1,2-fashion), (4) 2,1 mis-insertion (and possible recovery by a 1,2-insertion), (5) chain transfer, and (6) reinitiation (Scheme 1.1).

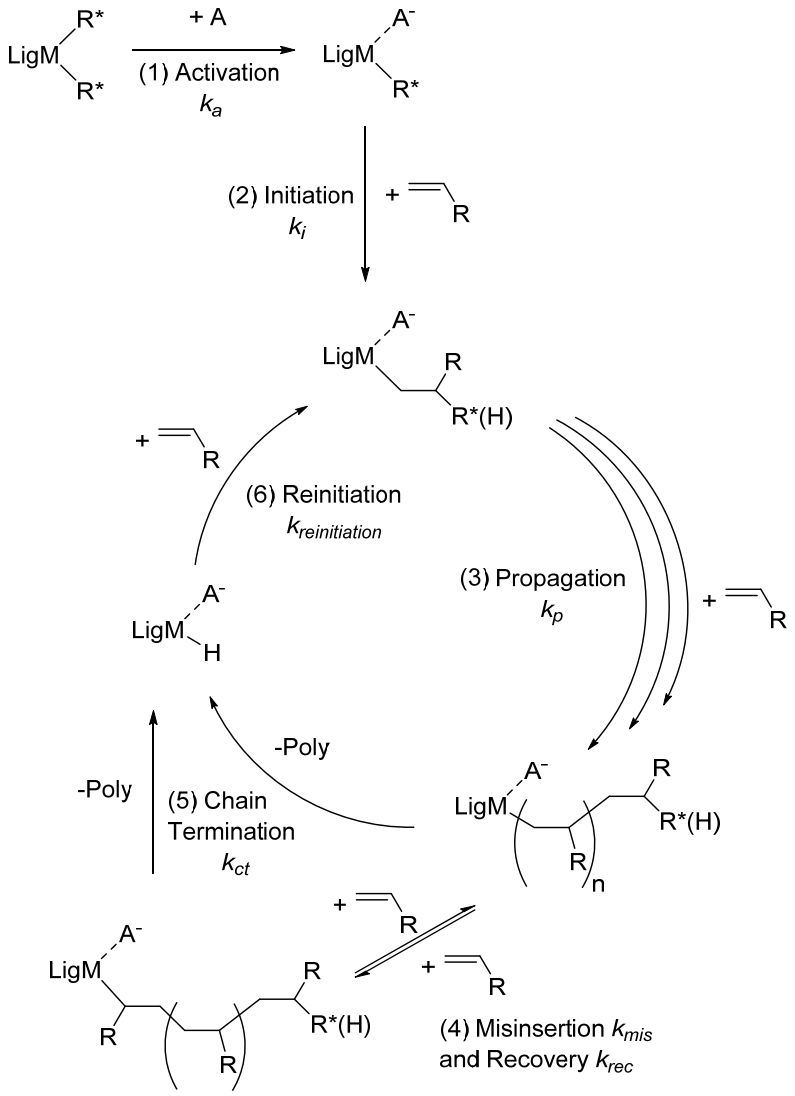

Scheme 1.1 Simple mechanism for α-olefin polymerization

The first step of catalysis is activation by abstraction of an alkyl group (-R*) from the precatalyst by a Lewis acid activator (co-catalyst), k_a. For most cases, the abstraction of the R* is caused directly by either protonation or direct α-carbon abstraction. In the specific case where R* = ^{i}Pr, a β-hydride is abstracted from one of the ^{i}Pr groups to form isobutene and an ion pair consisting of the activated metal center and activator, Scheme

1.2.[20] After the cation-anion pair is formed, initiation, with the rate constant denoted as k_i, occurs through the first olefin insertion.

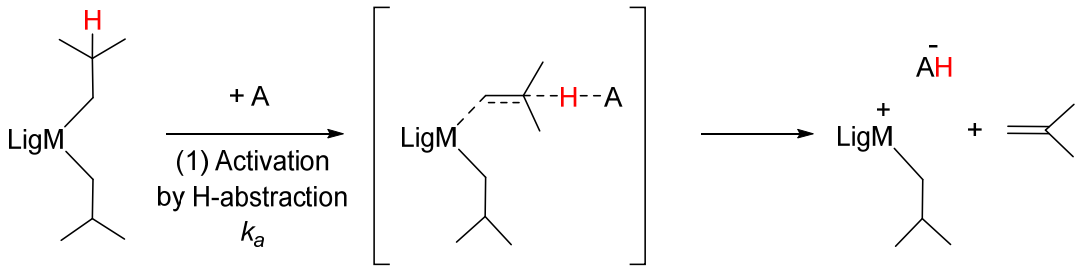

Scheme 1.2 Unique initiation and activation from ^{i}Pr starting groups on the precatalyst

Propagation, k_p, is the portion of the cycle where an olefin inserts into the metal-carbon bond, typically in a 1,2-fashion for α-olefins to grow the chain length. In the formation of long polymer chains, this phase dominates the catalysis. During this propagation period, a catalyst site can undergo a 2,1 mis-insertion of an α-olefin and may form a dormant site that removes the catalyst from the catalytic cycle, k_{mis}. This dormant species may return to an active site through a recovery, k_{rec}, 1,2-insertion of an α-olefin. Chain transfer typically occurs when the polymer chain undergoes an interaction with the metal center to separate the two, k_{ct}. This process has been known to be either monomer dependent or monomer independent, forming a metal-hydride. The subsequent insertion of an olefin into the metal-hydride is known as reinitiation, $k_{reinitiaion}$, and allows for more polymer chains to grow.

While previous works have expounded on the importance of obtaining a rich set of multi-response data to determine both the exact catalyst mechanism and the robust rate constants for the elementary steps involved,[14-19] this chapter and works contained within

will focus on the understanding factors that control the steps within the traditional coordination insertion catalytic mechanism as well as utilizing more exotic pathways for further catalytic control. Further developments of these pathways will be examined more closely in Chapters 3, 4, and 5.

1.2 Activation

The development and study of olefin coordination insertion polymerization has relied on forming a stable, zwitterionic complex. Originally, heterogeneous Ziegler-Natta catalysts of titanium chloride on magnesium chloride could be reacted with alkyl aluminums to form such species.[21] In homogeneous systems, the fortuitous discovery of methylaluminoxanes (MAO) would allow for methylation of halogenated Group IV catalysts before subsequent methyl abstraction to form an ion pair.[22] However, such systems require several hundredfold excess of MAO to catalyst to prepare the zwitterion.[23] Development and experimentation of well-defined, molecular Lewis acids has allowed for replacements to MAO (**1**) to a series of different borane (**2**), borate (**3**/**4**), aluminate (**5**), and other fluorinated species (**6**), Figure 1.2.[24]

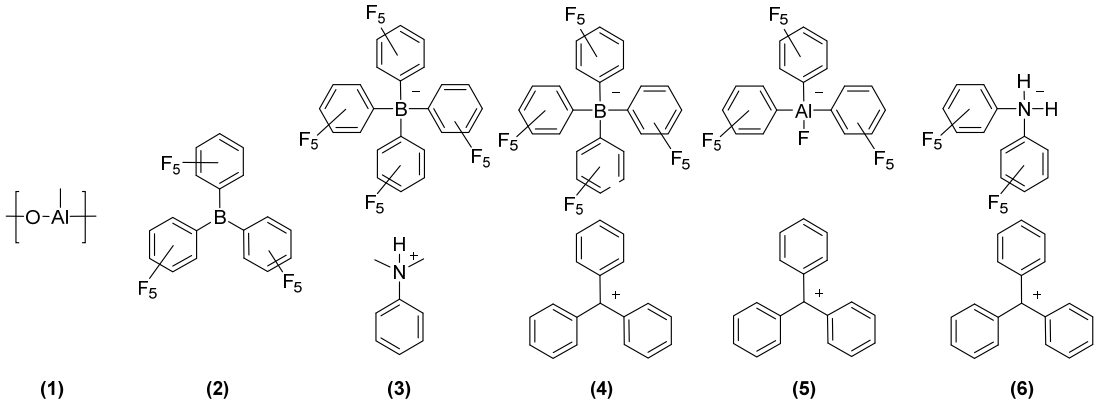

Figure 1.2 Different structures of common activators: (1) MAO (2) borane (3-4) borates (5) aluminate and (6) aminate activators

The reaction between the catalyst and molecular activators can produce a series of different zwitterionic pairs and potential side products based off of the catalyst/activator identities. The tris(pentafluoroaryl) borane (FAB) is a unique activator in that it can act as both an inner or outer sphere counter ion depending on the both the extracted alkyl group and the steric hindrance surrounding the metal active site,[24-25] while trityl salts form protonated triphenyl methane side products, and protonated-amine-type activators that cleave an alkyl group from the precatalyst using the proton and form an amine side product that is capable of coordinating to the metal center, scheme 1.3.[26] These interactions will have a further impact that will be discussed later in section 1.4 and chapter 5.

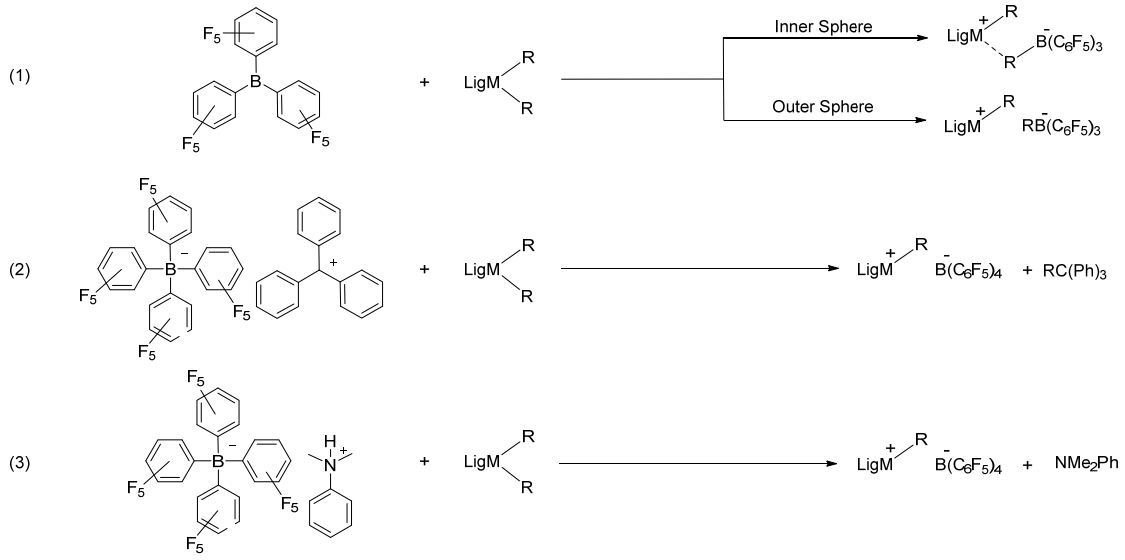

Scheme 1.3 Activation products between different molecular activators and catalysts

1.3 Initiation

The initiation of an olefin into the first metal-alkyl bond in typically a unique event whose elementary reaction is distinct from the normal propagation event. Typical alkyl initiating groups for this class of catalysts are methyl, isopropyl, and benzyl groups, the identity of which can have a pronounced effect on polymerization.[27] The rate of initiation directly affects the polydisperisive index (PDI) of the growing chains i.e. a slow initiation relative to propagation will cause a large distribution in the M_w while a fast initiation is necessary but not solely sufficient in producing a narrow polymer distribution.[28] The type of ion pair, inner- or outer-sphere, can also be a contributing factor in the ability in entering the catalytic cycle.[29] Reports with inner-sphere precatalysts with benzyl alkyl groups have been shown to have no activity to 1-hexene polymerization while in some cases have been shown to have some reactivity towards ethylene or acetylene insertion.[29-30]

1.4 Propagation and Misinsertion

The propagation step of the polymerization reaction, k_p, constitutes the bulk of the monomer consumption and one of the most important reactions within the cycle. While the exact active site structure to the insertion mechanism has not been experimentally proven, the Cossee mechanism has become the dominant model for coordination insertion polymerization.[31] Theoretical calculations have been used to predict the formation of an agostic α-hydrogen stabilizing the polymer-metal bond for outer-sphere zwitterions.[32] The subsequent coordination of an olefin to the metal center displaces either the agostic α-hydrogen or the coordinated inner-sphere anion, called the ion pair separation energy ΔE^{IPS}.[9c] The interaction of the olefin with the metal center weakens the double bond before breakage of the metal-polymer bond and subsequent insertion of the olefin into the polymer-metal bond. For many α-olefins, the insertion is predominately determined by sterics where a 1,2-insertion is the preferred mode of insertion.[33] In contrast, there have been reports of predominately 2,1-insertion preferred propagation in sterically bulky Ti phenoxy imine catalysts.[34] Further studies into olefin insertion with the copolymerization of ethylene with polar monomers have shown an electronic dependence into the insertion mode, where polar monomers with electronic donating groups discriminate a 1,2-insertion while electronic withdrawing groups will direct the olefin to a 2,1-insertion.[35]

The effect of sterics and electronics of the catalyst itself also plays a complex role on the propagation rate constant. The role of electronics on the insertion of ethylene into polyethylene chains is said to be stabilized by electronic donation while electronic withdrawing groups have also been shown to increase or decrease the propagation rate for α-olefins.[36] For sterics, increasing bulk can lower monomer insertion while decreasing

steric bulk can reduce the stability of the catalyst and drastically reduce the active species' lifetime.[37] Furthermore, sterics can also have further influences on other aspects of the catalytic mechanism.[38]

Another important influence on the propagation rate constant is the ion pair separation energy between the anionic activator and the cationic metal center.[24,25] The ΔE^{IPS} is the energy required to remove the coordinated ion from the cationic metal center, freeing an empty coordination site for next olefin to dock before insertion. The identity of the activated cocatalyst is of particular importance to the scale of this binding energy between the zwitterion pair.[39] Using activators such as the trityl tetrakis(pentafluoroaryl)borate or MAO, the ion pairing energy is typically weaker and allows for facile docking of olefins.[40] With FAB cocatalysts, the anion produced can have tremendous effect based on the initiating group. Benzyl initiating groups have been reported to make for a "sticky" ion pair that reduces overall catalytic activity.[24,25] When the initiating group is instead a methyl group, the ion pair becomes strong enough to become an inner sphere coordinated cocatalyst-catalyst.[24] DFT calculations in conjunction with kinetic experiments have shown that the ΔE^{IPS} can be the dominating influence on the propagation rate constant.[9c]

The enthalpy of 1-hexene polymerization, ΔE^{poly}, has been reported as -23 kJ/mole to -20 kJ/mole while the entropy of the system is always negative since the process takes a large number of monomer compounds and reduces the total number of chemical species to form the longer polymer chains.[41] The activation energy for the propagation step can be further reduced into a three, or potentially 2, step mechanism that contains a possible dissociation of the zwitterionic pair, an equilibrium docking of the polymerizing olefin,

and the subsequent insertion of the olefin into the metal-polymer chain, Scheme 1.4. In Scheme 1.4, it is possible that dissociation of the inner-sphere ion pair occurs in tandem through with the docking of the incoming monomer. The rate controlling step of these interactions should be identifiable through the reaction order of olefin in the monomer consumption kinetics. For many catalysts, the kinetic experiments show a first order monomer dependence and show an increase in the catalyst activity when run in a more polar solvent.[18] Both of these factors suggest that the ΔE^{IPS} is the key factor in controlling the propagation rate constant, similar to the studies with the Ti aryl phenoxide catalysts in polyhexene polymerization mentioned previously, as the insertion step should not show a first order dependence on monomer or solvent polarity.[9c]

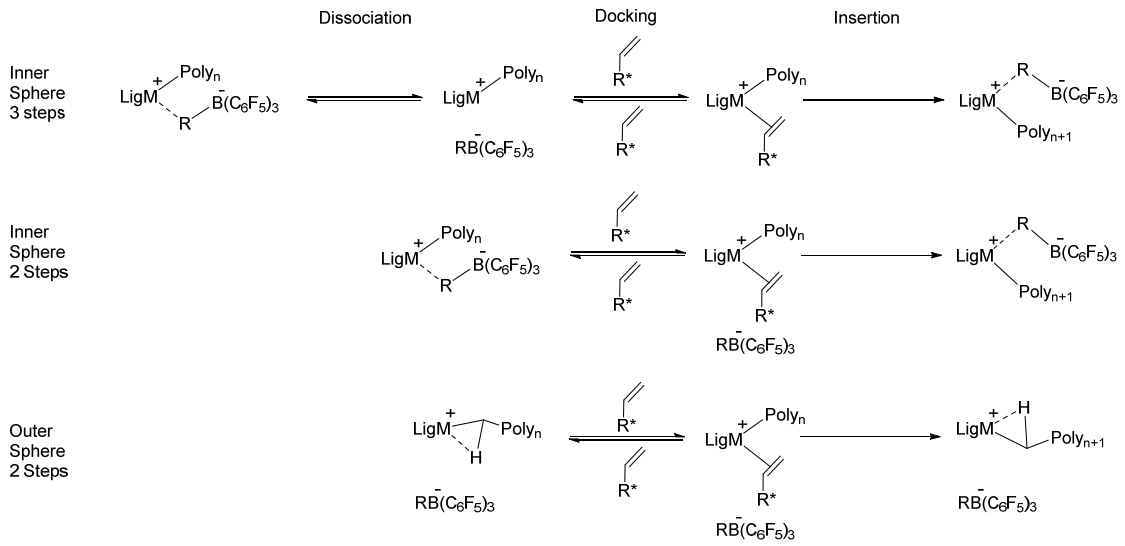

Scheme 1.4 Possible insertion mechanisms including dissociation, docking, and insertion

The insertion step is also an important step due to the stereoregularity of the polymeric chain for polymers containing α-olefins. The structure of the polymer chain can form either an isotactic form, a syndiotactic form, or a mixture of the two forms called atactic.[42] The two proposed mechanisms used to explain this phenomenon are either catalytic site or enantiomeric directing control over the tacticity of the polymer product.[42-43] Catalyst site control has been correlated strongly to the symmetry of the catalyst active site while enantiomeric site control has been linked closely to the temperature of the reaction, where the reaction pathway with the lowest activation energy produces a singly tactic product due to the interaction of the docking monomer to the tacticity of the last inserted monomer of the polymer chain.

While the insertion of an α-olefin occurs primarily through 1,2-insertion, it is possible for 2,1-insertion of an α-olefin to occur to act as a misinsertions, k_{mis}, shown in scheme 1.5.[44] This step within the mechanisms has a tremendous effect on the polymer molecular weight distribution, chain growth, and vinyl formation.[45] A 2,1-misinserted monomer can act as either a dormant site to the chain growth process, affecting polymer PDI by preventing activity at this particular catalyst site while other active sites continue to grow, or even cause immediate chain transfer, reducing the size of polymer chain lengths.[19a] The implications of the formation of these catalyst sites will be discussed in section 1.5 and section 1.6.

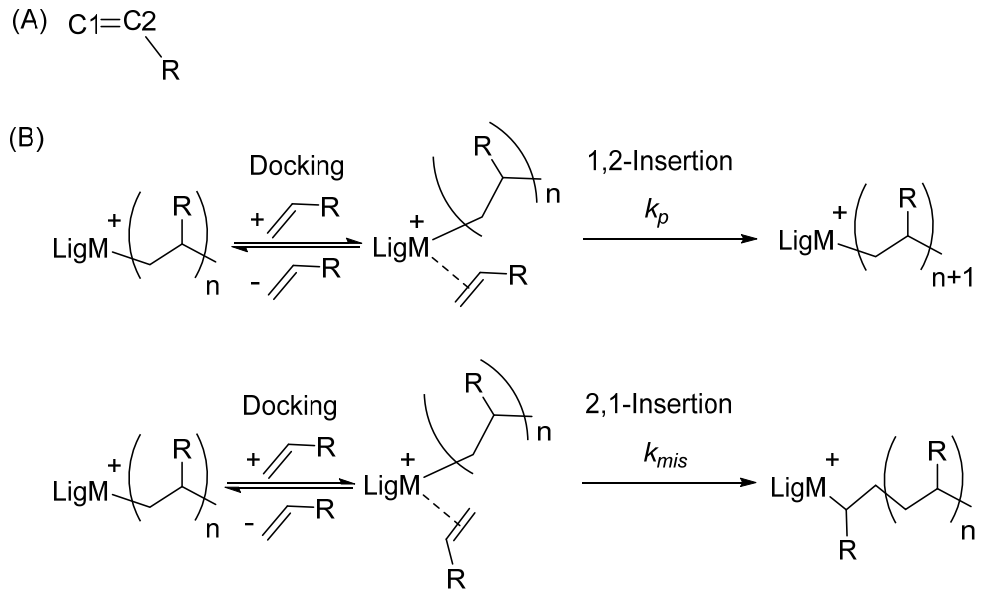

Scheme 1.5 (A) Numbering convention for insertion of α-olefins (B) mechanisms of k_p and k_{mis}

1.5 Recovery

A dormant site, formed via 2,1-insertion, can reenter the cycle through the recovery elementary step, k_{rec}. This particular elementary reaction rate has been particularly difficult to analyze since misinsertion occurs so infrequently, relative to 1,2-insertion, and has been a lack of experiments to discriminate this rate constant from the rest of the mechanism. Regardless, some reports have shown there is a particular metal based effect on the recovery rate constant.[46] In addition, this reaction rate constant, like all rate constants that are monomer dependent, can be effected by catalyst electronics.[47] Such a step in the overall mechanism is important when compared to the chain transfer elementary step, and is shown in Scheme 1.6. The formation of regioerrors appear when the recovery elementary step occurs more frequently than the chain termination of the last, misinserted monomer.

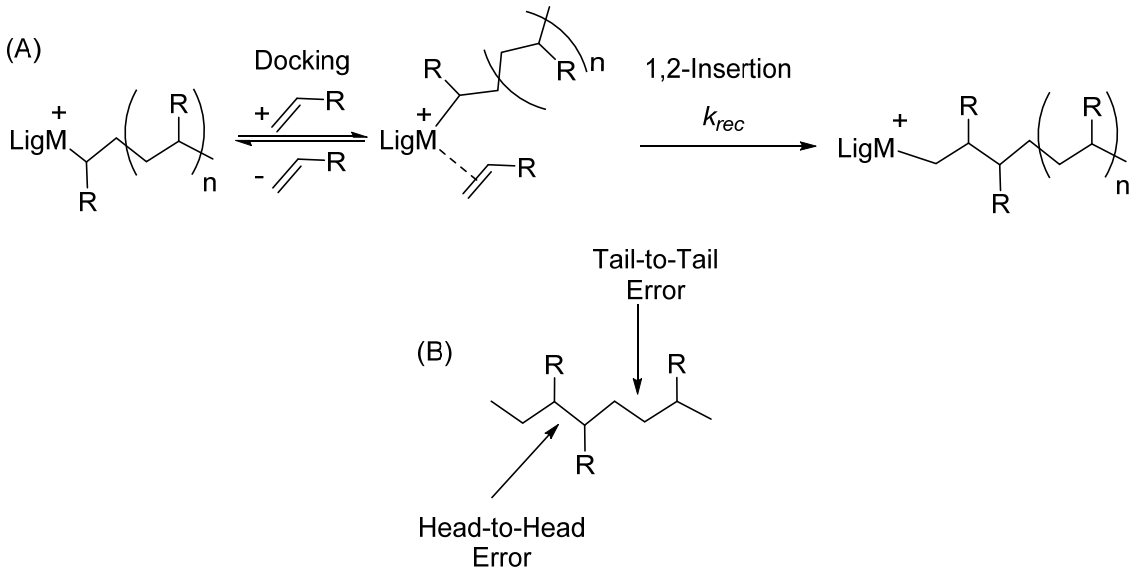

Scheme 1.6 (A) Reaction pathway producing a regioerror by recovery from a misinserted site and (B) types of errors in the polymer that form from a recovery step

1.6 Chain Transfer

One of the most fundamental changes in the kinetic mechanism is the elementary chain transfer reaction, k_{ct}. The magnitude of this rate constant has tremendous effects on both the length and PDI of the MWD.[48] Tuning this elementary reaction in conjunction with the propagation rate constant can shift the product distribution from an oligomer product to a polymer one.[49] Factors affecting this rate constant include catalyst sterics,[50] activator/cocatalysts,[51] and the presence of a chain transfer agent.[52] Moreover, this rate constant is unique in the fact that it can be monomer independent or monomer dependent depending on the monomer or catalyst structure, each mechanism shown in Scheme 1.7. Most important, the mechanism produces a metal-hydride after chain transfer. A metal-

hydride species can reenter the catalyst cycle via the reinitiation elementary step to continue to produce new polymer products.

In terms of catalyst sterics, it has been shown that the monomer dependence of polyolefin termination process is strongly tied to catalyst structure.[53] The relative openness of the active site affects both monomer independent and monomer dependent chain transfer.[54] Reduced steric bulk has been correlated to chain transfer to monomer, a process where a beta-hydride is transferred from the outgoing polymer to a docked monomer.[55] Furthermore, the sterics of these catalysts are shown to correlate to the amount of chain transferred product.[56] Such a chemical descriptor is important in design of future catalysts or polymer products.

The chain transfer rate constant has also been shown to be influenced by the identity of cocatalyst. Work by Marks and Bochmann have independently shown that the nature, inner- or outer-sphere, and the identity of the outer-sphere anion have a large effect on the type and amount of chain terminated products. Metallocenes using inner-sphere zwitterions using FAB over the Trityl salts showed higher amounts of vinylidene terminated chain ends while vinylene chain ends remained unaffected.[24]

The presence of chain transfer agent also has a tremendous effect on the MWD.[57] One such species is molecular hydrogen. The presence of molecular hydrogen causes coordination and sigma bond metastasis to form a protonated polymer chain and metal-hydride. Subsequently, metal alkyl species such as diethyl zinc or trimethyl aluminum can cause chain transfer from the active metal center to the zinc or aluminum center.[58] The diethyl zinc compound is also a known chain shuttling agent capable of moving the polymer chain from metal center to metal center while trimethyl aluminum can act either

as a chain shuttling agent or as a chain termination agent where the polymer ends its growth on the organoaluminum complex.[59] The different chain transfer pathways are shown in Scheme 1.7.

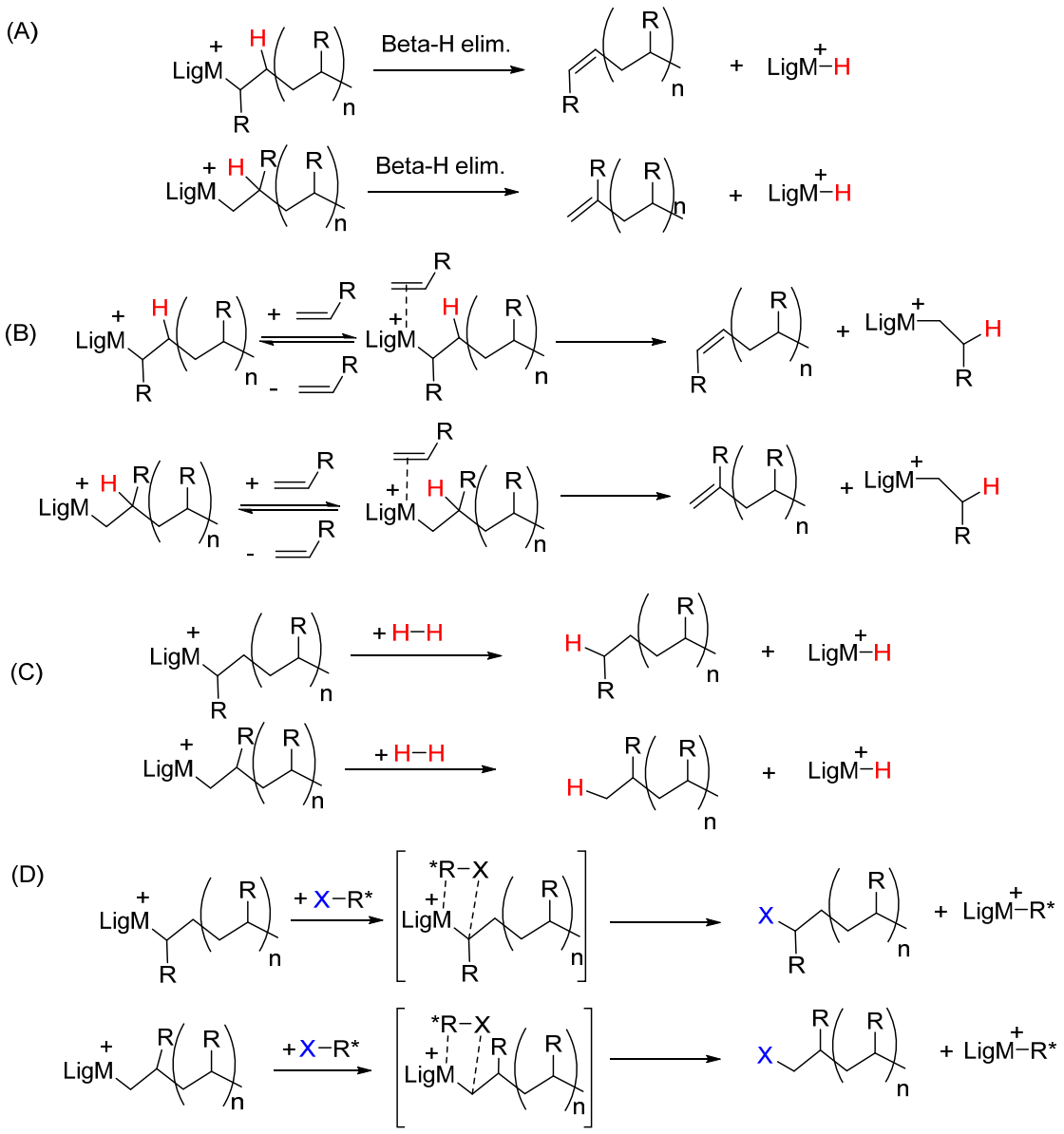

Scheme 1.7 (A) Chain transfer from β-hydride elimination, (B) chain transfer to monomer, (C) chain transfer by the chain termination agent hydrogen, and (D) chain transfer via transmetallation to a metal-alkyl group X-R*

Another important influence on the chain transfer rate constants is the reaction temperature for the monomer independent process.[60] The thermodynamics of the chain transfer reaction are described as an endothermic process that breaks a weaker metal-carbon bond for a stronger metal-hydride. This feature of the chain transfer elementary step has a tremendous effect on the MWD of the polymer product. As such, reports in the literature on the molecular weight (M_w) and PDI of the produced polymer can be tuned to produce ultralong M_w polymers with PDIs closer to unity by dropping the reaction temperature.[61]

While the prevailing wisdom is that each catalyst will exhibit either monomer dependent or monomer independent chain transfer, it may be possible that a catalyst exhibits both pathways but with one pathway more dominate at a certain reaction temperature. A combination of mechanisms would be difficult to measure and would require experiments at many different reaction conditions to determine the monomer order for this elementary reaction.

1.7 Reinitiation

The metal-hydride complex produced during the monomer independent chain termination pathway can complete the mechanistic cycle through insertion of olefin into the metal hydride. Thorough studies on the olefin insertion process into metal-hydride have shown both a range of different activity and possible products.[62] In the presence of olefins, the magnitude of this rate constant also influences both the consumption of monomer and the MWD of the polymeric products. It has been reported that slow reinitiation, $k_{reintitiation}$,

of monomer results in a metal-hydride at acts as a dormant site in the polymerization cycle.[19b] Other reports have shown that the insertion of olefin into metal hydrides is one of the fastest rate constants within the cycle, being faster or on par with k_p.[19a,c-f]

1.8 Vinyl Isomerization or Chain Walking

The activation, insertion, and transformation of vinylidene substituted polymeric hydrocarbons has been reported in high temperature copolymerization of ethylene with 1-hexene.[63] These mechanisms have been further explored by the Bercaw lab with the use of a 5 coordinate Zr carbene oligomerization catalyst for the reaction to 1-hexene as well as other Zr and Ti oligomerization catalysts.[30,54] The formation of these products through the insertion of a vinylidene chain end into a metal-hydride before subsequent β-hydride, Scheme 1.8, transfers produces an incredibly stable trisubstituted olefinic product. Further reactivity of one such species or the polymerization of vinylidene terminated species has not been found in the literature.

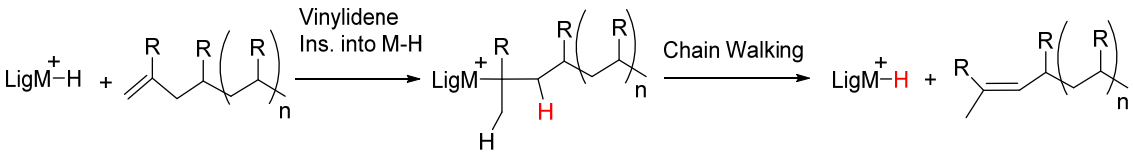

Scheme 1.8 Chain walking mechanism of M-H with vinylidene terminated polymers

1.9 Lewis Base Coordination and Influence on Polymerization

The development of molecular cocatalysts featuring Lewis bases such as N,N-dimethyl anilinium tetrakis(pentafluoroaryl) borate has raised the question of the interaction of the N,N dimethyl aniline or even other Lewis base with the activated metal center in a batch scale reaction.[26] Reports by Schrock where different Lewis bases were added to batch polymerization reactions showed no effect or even reaction inhibition.[64] Incredibly, there have been recent reports of Lewis acids modifying the reactivity of the metal center into producing unique products based on the identity of the Lewis bases.[30] The coordination of the base to the metal center seems to be an irreversible binding for some systems that can reduce the chain transfer rate constant by increasing steric congestion around the metal center and increase the relative activity of the olefin polymerization by increasing the regioselectivity of the olefin insertion to reduce the number of dormant secondary sites. This reactivity has yet to be replicated in the literature reports for other systems.

1.10 Degenerative Chain Transfer

One of the interesting and unexpected interactions with the electropositive group IV organometallic complexes that comprise this field of catalysis is the ability to form alkyl or halogenated bridged species to relieve the strain of electron deficiency.[70] Using molecular cocatalysts in a substiochiometric amount, it has been noted repeatedly that the an unactivated precatalyst species can displace the anion and form an unstable bridged metal dimer that can break apart to have the different catalyst sites active for polymerization at separate times, Scheme 1.9. This feature has a remarkable impact on the

catalyst cycle through subsequent discrimination of the catalyst species towards primary insertion,[19d] as well as producing polymers with blocks of alternating isotatic chains in reports from the Sita laboratory.[71] Copolymerization studies from the Marks lab with different degenerative Zr and Ti catalysts showed equivalent or greater activity when compared to catalysts with 1:1 ratios of catalyst:activator.[72] Additional reports from the Abu-Omar lab show that the degenerative alkyl group includes benzyl initiating groups and increases the initiation rate constant for 1-hexene polymerization.[19d] Unfortunately, there has been a lack of research on the effect of degenerative chain transfer on the bimetallic or oligomerization Group IV catalysts.

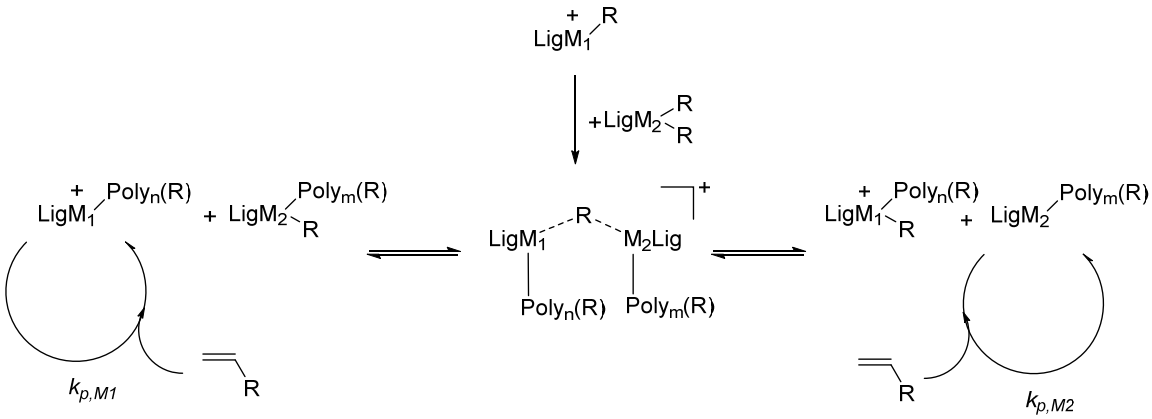

Scheme 1.9 Degenerative group transfer from a substiochiometric amount of activator

1.11 Modeling and New Understanding of α-Olefin Insertion Catalysts

In this thesis, kinetic analysis has been applied to a series of different Group IV amine bis-phenolate complexes, first reported by Kol and coworkers,[73] using boron-based, molecular activators. The work that follows can be separated into two distinctive areas.

Chapters 2, 3, and 4 look to model structure-activity relationships in α-olefin polymerization of catalyst families already reported in the literature while chapters 5 and looks into new reactivity of 5 coordinate Zr amine bis-phenolates, catalyst structures shown in Figure 1.3. Building off of the work previously published by previous members from this collaboration, Chapters 2, focuses on my contributions to the comparison of pendant and metal centers for select Zr/Hf catalysts. Chapter 3 covers comparisons with Ti metal centered polymerization catalysts and the effects of metal electronics and sterics to the effect of polymerization. In Chapter 4, a brief overview on the quantitative effects of temperature on the polymerization mechanism is explored.

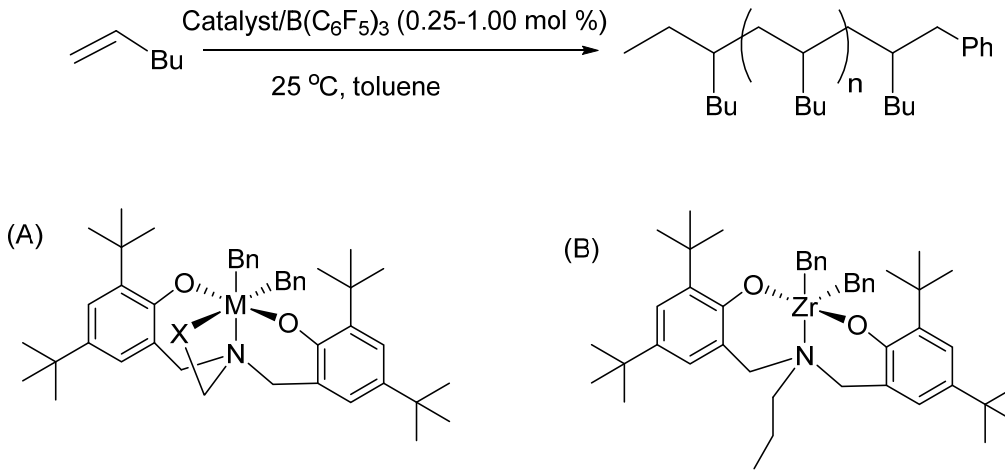

Figure 1.3 Catalyst systems studied in this work where (A) constitutes catalysts studied quantitatively for structure activity relationships while (B) represents a catalyst with featuring new reactivity.

In terms of structure-activity comparisons, there has been some important qualitative discoveries. Quantitative kinetic studies were undertaken with catalysts

containing a series of different metal centers and pendants to probe the effects of structure to catalytic activity.[19a,b] From these studies, it was shown that for the zirconium precatalyst containing a SMe pendant, there was a change in chain transfer mechanism for the unimolecular (β-H elimination) chain transfer in making vinylidene terminated polymer chains in comparison to THF, Py, and NMe_2 pendants. While the THF, Py, and NMe_2 pendant catalysts showed a direct correlation between the Zr-pendant bond distance in the precatalyst crystal structures and the $k_{vinylidene}$ rate constant, the Zr[SMe] catalyst showed the formation of vinylidene terminated polymers became dependent on the concentration of monomer if this bond distance grew too long. Furthermore, similar studies were repeated with Hf centered catalyst featuring Py and NMe_2 pendants. These catalysts showed an order of magnitude reduction of activity for reactions between monomer and catalyst (k_{ini}, k_p, k_{mis}, and k_{rec}) and a similar dependence in the monomer independent chain transfer reaction rate, $k_{vinylidene}$, and the Hf-pendant bond length.

From this basic entrance to the effect of ligand and metal center, a third study was conducted focusing on the synthesis and reactivity studies of Ti amine bis-phenolate catalysts.[46] Again a linear relationship was shown between the metal-pendant crystal structure bond length and the $k_{vinylidene}$ rate constant, showing the dependence of chain termination reactions on catalyst sterics. The metal center has a pronounced effect on the number of 2,1-insertions, where the trend follows Ti > Zr > Hf. This was followed by counting the number of regioerrors through the simple equation below, Equation 1.1, where a regioerror is considered a misinserted monomer within a polymer chain, not a vinylene chain terminated polymer or a dormant catalyst site from a 2,1-insertion as those errors are at the polymer end. Additionally, it was shown that the longest polymers should be

produced using with the metal center as Zr > Ti > Hf in comparison to the literature reported trend of Ti > Zr > Hf. This study has outlined the need for experiments requiring consistent reaction conditions from the same starting concentrations to allow for comparative studies between catalyst systems.

$$\#\ Regioerrors = \#\ Misinsertions - \#Vinyidene - \#\ Secondary\ Sites \qquad \text{Equation 1.1}$$

The next logical step after determining the mechanisms and related rate constants at 25 Celsius was to perform temperature dependent studies to calculate the thermodynamic quantities of Eyring enthalpy and entropy. Such a study focused on a series of different Zr based amine bis-phenolate catalysts containing the THF, NMe_2, and SMe pendants over a 40-degree range of temperatures. The calculations showed adequate fits for the rate constants k_p and k_{ct} while other constants could not be fit to a high degree of precision.

Recent reports with the effect of activators and Lewis base on the reactivity of 5 coordinate Zr polymerization catalysts have refocused our group's attention on a previously reported Zr amine bis-phenolate catalyst that exhibited rapid deactivation when paired with the FAB activator.[30] Reactions with the trityl tetrakis(pentafluoroaryl) borate and N,N dimethyle anilinium tetrakis(pentafluoroaryl) borate activators showed distinct reactivity with the trityl activator converting over 99% of the initial monomer into short, oligomer products. Further reactivity was studied using different monomers, different temperatures, substiochiometric amounts of trityl activator, and the addition of stiochiometric/substiochiometric Lewis base. These changes were able to shift the product

distribution towards shorter chains, in the case of higher temperatures and substiochiometric activator, or to form polymers, with the addition of Lewis base.

In previous work through our group we have shown the potential insight that can be obtained by obtaining rigorous kinetic data to distinguish and calculate quantitative rate constants for the fundamental rate constants within the polymerization mechanism. In this work, we hope to show a new method of rational catalyst development by understanding and predicting catalyst reactivity by the addition of structural characteristics. Beyond that, we also look to examine new, unexplained phenomena in coordination insertion polymerzation using state-of-the art kinetic analytical methods.

1.12 References

(1) Markets and Markets, Inc. Polyolefins Market By Types (Low, Linear & High Density Polyethylene, Polypropylene And Ethylene Vinyl Acetate), By Applications (Film & Sheet, Injection Molding, Fibers & Tapes, Blow Molding, Others) & Geography - Global Trends & Forecasts To 2018, www.marketsandmarkets.com

(2) (a) Chen, E. Y-X.; Marks, T. J. *Chem. Rev.* **2000**, *100*, 1391-1434. (b) Li, H.; Marks, T. J. *Proc. Natl. Sci. U.S.A.* **2006**, *103*, 15295-15302. (c) Delferro, M.; Marks, T. J. *Chem. Rev.* **2011**, *111*, 2450-2485.

(3) (a) Krauledat, H.; Brintzinger, H.H. *Angew. Chem., Int. Ed.* **1990**, *29*, 1412-1413. (b) Piers, W. E.; Bercaw, J. E. *J. Am. Chem. Soc.* **1990**, *112*, 9406-9707. (c) Coates, G. W.; Waymouth, R. M. *J. Am. Chem. Soc.* **1991**, *113*, 6270-6271. (d) Coates, G. W.; Waymouth, R. M. *Science* **1995**, *267*, 217-218.

(4) Manz, T.A.; Phomphrai, K.; Medvedev, G. A.; Krishnamurthy, B. B.; Sharma, S.; Haq, J.; Novstrup, K. A.; Thomson, K. T.; Delgass, W. N.; Caruthers, J. M.; Abu-Omar, M. M. *J. Am. Chem. Soc.* **2007**, *129*, 3776-3777.

(5) Britovsek, G. J. P.; Gibson, V. C.; Wass, D. F. *Angew. Chem., Int. Ed.* **1999**, *38*, 428-447.

(6) Bochman, M. *Organometallics* **2010**, *29*, 4711-4740.

(7) Huang, J.; Rempel, G. L. *Prog. Polym. Sci.*, **1995**, 20, 459-526.

(8) (a) Möhring, P. C.; Coville, N. J. *Coord. Chem. Rev.* **2006**, *250*, 18-35. (b) Möhring, P. C.; Coville, N. J. *J. Organometallic Chem.* **1994**, *479*, 1-29.

(9) (a) Liu, Z.; Somsook, E.; Landis, C. R. *J. Am. Chem. Soc.* **2001**, *123*, 2915-2916. (b) Liu, Z.; Somsook, E.; White, C. B.; Rosaaen, K. A.; Landis, C. R. *J. Am. Chem. Soc.* **2001**, *123*, 11193-11207. (c) Novstrup, K. A.; Travia, N. E.; Medvedev, G. A.; Stanciu, C; Switzer, J. M.; Thomson, K. T.; Delgass, W. N.; Abu-Omar, M. M.; Caruthers, J. M. *J. Am. Chem. Soc.* **2010**, *132*, 558-566.

(10) Arriola, D. J.; Carnahan, E. M.; Hustad, P. D.; Kuhlman, R. L.; Wenzel, T. T. *Science* **2006**, *312*, 714-719.

(11) Jones, D. J.; Gibson, V. C.; Green, S. M.; Maddox, P. J.; White, A. J. P.; Williams, D. J. *J. Am. Chem. Soc.* **2005**, *127* (31), 11037-11046.

(12) Falsig, H.; Hvolbaek, B.; Kristensen, I. S.; Jiang, T.; Bligaard, T.; Christensen, C. H.; Norskov, J. K. *Angew. Chem. Int. Ed.* **2008**, *47*, 4835-4839.

(13) Schumacher, N.; Boisen, A.; Dahl, S.; Gokhale, A. A.; Kandoi, S.; Grabow, L. C.; Dumesic, J. A.; Mavrikakis, M.; Chorkendorff, I. *Journal of Catalysis* **2005**, *229*, 265-275.

(14) Liu, Z.; Somsook, E.; White, C. B.; Rosaaen, K. A.; Landis, C. R. *Journal of the American Chemical Society* **2001**, *123*, 11193-11207.

(15) Liu, Z.; Somsook, E.; Landis, C. R. *Journal of the American Chemical Society* **2001**, *123*, 2915-2916.

(16) Moscato, B. M.; Zhu, B.; Landis, C. R. *Journal of the American Chemical Society* **2010**, *132*, 14352-14354.

(17) Moscato, B. M.; Zhu, B.; Landis, C. R. *Organometallics* **2012**, *31*, 2097-2107.

(18) Song, F.; Cannon, R. D.; Bochmann, M. *Journal of the American Chemical Society* **2003**, *125*, 7641-7653.

(19) (a) Switzer, J. M.; Travia, N. E.; Steelman, K. D.; Medvedev, G. A.; Thomson, K. T.; Delgass, W. N.; Abu-Omar, M. M.; Caruthers, J. M. *Macromolecules* **2012**, *45*, 4978-4988. (b) Steelman, D. K.; Xiong, S.; Pletcher, P. D.; Smith, E.; Switzer, J. M.; Medvedev, G. A.; Delgass, W. N.; Caruthers, J. M.; Abu-Omar M. M. *J. Am. Chem. Soc.* **2013**, *135*, 6280-6288. (c) Steelman, D. K.; Pletcher, P. D.; Switzer, J. M.; Xiong, S.; Medvedev, G. A.; Delgass, W. N.; Caruthers, J. M.; Abu-Omar M. M. *Organometallics* **2013**, *32*, 4862-4867. (d) Xiong, S.; Steelman, D. K.; Medvedev, G. A.; Delgass, W. N.; Abu-Omar M. M.; Caruthers, J. M. *ACS Catal.* **2014**, *4*, 1162-1170.

(20) (a) Mehrkhodavandi, P.; Bonitatebus, P. J.; Schrock, R. R. *J. Am. Chem. Soc.* **2000**, *122*, 7841-7842. (b) Mehrkhodavandi, P. and Schrock, R. R. *J. Am. Chem. Soc.* **2001**, *123*, 10746-10747. (c) Mehrkohavandi, P.; Pryor, L. L.; Schrock, R. R. *Organometallics*, **2003**, *22*, 4569-4583.

(21) (a) Natta, G. *J. Am. Chem. Soc*. **1955**, *77*, 1708. (b) Sinn, H.; Kaminsky, W. "Zieg1er—Natta Catalysis." *ADVANCES ORGANOMETALLIC CHEMISTRY*, Academic Press: San Diego, 1980; 18.

(22) Kaminsky, W. *Macromolecules*, **2012**, *45* (8), 3289-3297.

(23) Coevoet, D.; Cramail, H.; Deffieux, A. *Macromol. Chem. Phys.* **1996**, *197*, 855–867.

(24) (a) Delferro, M.; Marks, T. J. *Chem. Rev*. **2011**, *111*, 2450. (b) Wilson, P. A.; Hannant, M. H.; Wright, J. A.; Cannon, R. D.; Bochmann, M. *Macromol. Symp.* **2006**, *236*, 100-110. (c) Bochmann, M. *Organometallics*, **2010**, *29*, 4711-4740.

(25) (a) Ciancaleoni, G.; Fraldi, N.; Budzelaar, P. H. M.; Busico, V.; Macchioni, A. *Organometallics,* **2011**, *30* (11), 3096-3105. (b) Zuccaccia, C.; Macchioni, A.; Busico, V.; Cipullo, R.; Talarico, G.; Alfano, F.; Boone, H. W.; Frazier, K. A.; Hustad, P. D.; Stevens, J. C.; Vosejpka, P. C.; Abboud, K. A. *J. Am. Chem. Soc.* **2008**, *130*, 10354-10368.

(26) Dagorne, S.; Bellemin-Laponnaz, S.; Romain, C. *Organometallics*, **2013**, *32*, 2736.

(27) Denner, C. E.; Alt, H. G.; *J. App. Poly. Sci.* **2003**, *89*, 1336-1340.

(28) Quirk, R. P.; Lee, B. *Polymer International* **1992**, *27*, 359-367.

(29) Shafi, A.; Arnold, J. *Organometallics* **2003**, *22*, 567-575.

(30) Despagnet-Ayoub, E.; Takase, M. K.; Henling, L. M.; Labinger, J. A.; Bercaw, J. E. *Organometallics* **2015**, *34*, 4707-4716.

(31) Cossee; P. *Tetrahedron Letters* **1960**, *17*, 12-16.

(32) Nifant'ev, I. E.; Ustynyuk, L. Y.; Laikov, D. N. *Organometallics*, **2001**, *20*, 5375-5393.

(33) Odian, G. *Principles of Polymerization*. John Wiley & Sons, **2004**.

(34) Saito, J.; Suzuki, Y.; Makio, H.; Tanaka, H.; Onda, M.; Fujita, T. *Macromolecules* **2006**, *39* (12), 4023-4031.

(35) Nakamura, A.; Ito, S.; Nozaki, K. *Chem. Rev.* **2009**, *109*, 5215-5244.

(36) (a) Sernetz, F. G.; Mulhaupt, R.; Fokken, S.; Okuda, J. *Macromolecules* **1997**, *30*, 1562-1569. (b) Porri, L.; Ripa, A.; Colombo, P.; Miano, E.; Capelli, S.; Meille, S. V. *J. Organomet. Chem.* **1996**, *514*, 213-217.

(37) (a) Groysman, S.; Tshuva, E. Y.; Goldberg, I.; Kol, M.; Goldschmidt, Z.; Shuster, M. *Organometallics*, **2004**, *23*, 5291-5299. (b) Gendler, S.; Groysman, S.; Goldschmidt, Z.; Shuster, M.; Kol, M. *J. Poly. Sci: Part A: Poly Chem.* **2006**, *44*, 1136-1146.

(38) Miller, S. A.; Bercaw, J. E. *Organometallics* **2006**, *25*, 3576-3592.

(39) Song, F.; Cannon, R. D.; Bochmann, M. *Chem. Commun.* **2004**, 542-543.

(40) Reybuck, S. E.; Lincoln, A. L.; Ma, S.; Waymouth, R. M. *Macromolecules* **2005**, *38* (7), 2552-2558.

(41) Roberts, D. E. *J. Res. Nat. Bureau. Standards* **1950**, *44*, 221-232.

(42) Baugh, L. S.; Canich, J. A. M. *Stereoselective Polymerization with Single-Site Catalysts*; CRC Press: Boca Raton, 2008.

(43) Resconi, L.; Cavallo, L.; Fait, A.; Piemontesi, F. *Chem. Rev.* **2000**, *100* (4), 1253-1346.

(44) Busico, V.; Cipullo, R.; Corradini, P. *Die Makromolekulare Chemie, Rapid Communications* **1993**, *14*, 97-103.

(45) (a) Roll, W.; Britzinger, H-H.; Rieger, B.; Zolk, R. *Angew. Chem., Int. Ed.* **1990**, *29*, 279-280. (b) Chadwick, J. C.; van der Burgt, F. P. T.; Rastogi, S. *Macromolecules* **2004**, *37*, 9722-9727. (c) Klingelhofer, S.; Schellengerg, C.; Pommerehne, J.; Bassler, H.; Greiner, A.; Heitz, W. *Macro. Chem. Phys.* **1997**, *198*, 1511-1530.

(46) Pletcher, P. D**.**; Switzer, J. M.; Steelman, D. K.; Medvedev, G. A.; Delgass, W. N.; Caruthers, J. M.; Abu-Omar, M. M. "Quantitative Comparative Kinetics of 1-Hexene Polymerization across Group IV Bis-phenolate Catalysts" *ACS Catalysis*, Submitted.

(47) Steelman, D. K.; Xiong, S.; Medvedev, G. A.; Delgass, W. N.; Caruthers, J. M.; Abu-Omar M. M. *ACS Catal.* **2014**, *4*, 2186-2190.

(48) Kawai, T. *Colloid and Polymer Science* **1965**, *201*, 15-20.

(49) Mecking, S. *Angewandte Chemie International Edition* **2001**, *40*, 534-540.

(50) Mohring, P. C.; Coville, N. J. *Coordination Chem. Rev.* **2006**, *250*, 18-35.

(51) Chen, M.-C.; Roberts, J. A. S.; Marks, T. J. *J. Am. Chem. Soc*. **2004**, *126*, 4605−4625.

(52) Tsutui, T.; Kashiwa, N.; Mizuno, A. *Macrom. Rapid Comm.* **2003**, *11*, 565-570.

(53) Groysman, S.; Goldberg, I.; Kol, M.; Genizi, E.; Goldschmidt, Z. *Organometallics* **2003**, *22*, 3013−3015.

(54) Agapie, T.; Henling, L. M.; DiPasquale, A. G.; Rheingold, A. L.; Bercaw, J. E. *Organometallics* **2008**, *27*, 6245-6256.

(55) Margl, P.; Deng, L.; Ziegler, T. *J. Am. Chem. Soc.* **1999**, *121* (1), 154-162.

(56) Burger, B. J.; Thompson, M. E.; Cotter, W. D.; Bercaw, J. E. *J. Am. Chem. Soc.* **1990**, *112*, 1566-1577.

(57) Chu, K-J.; Soares, J. B. P.; Penlidis, A. *Macromol. Chem. Phys.* **2000**, *201*, 552-557.

(58) Valente, A.; Mortreaux, A.; Visseaux, M.; Zinck, P. *Chem. Rev.* **2013**, *113*, 3836-3857.

(59) Alfano, F.; Boone, H. W.; Busico, V.; Cipullo, R.; Stevens, J. *Macromolecules* **2007**, *40*, 7736-7738.

(60) (a) Thorshaug, K.; Stovneng, J. A.; Rytter, E.; Ystenes, M. *Macromolecules* **1998**, *31*, 7149. (b) Wester, T. S.; Johnsen, H.; Kittilsen, P.; Rytter, E. *Macromolecular Chemistry and Physics* **1998**, *199*, 1989.

(61) (a) Razavi, A.; Ferrara, J. *Journal of Organometallic Chemistry* **1992**, *435*, 299. (b) Rieger, B.; Jany, G.; Fawzi, R.; Steimann, M. *Organometallics* **1994**, *13*, 647. (c) Miyake, S.; Okumura, Y.; Inazawa, S. *Macromolecules* **1995**, *28*, 3074.

(62) Chirik, P. J.; Bercaw, J. E. *Organometallics* **2005**, *24* (22), 5407-5423.

(63) Grumel, V.; Brull, R.; Pasch, H.; Raubenheimer, H. G.; Sanderson, R.; Wahner, U. M. *Macromolecular Mat. Eng.* **2001**, *286*, 480-487.

(64) Goodman, J. T.; Schrock, R. R. *Organometallics* **2001**, *20*, 5201-5211.

(65) Delferro, M.; Marks, T. J. *Chem. Rev.* **2011**, *111* (3), 2450-2485.

(66) Radlauer, M. R.; Agapie, T. *Organometallics* **2014**, *33* (13), 3247-3250.

(67) Rodriguez, B. A.; Delferro, M. D.; Marks, T. J. *Organometallics*, **2008**, *27* (10), 2166-2168.

(68) Liu, S.; Motta, A.; Delferro, M.; Marks, T. J. *J. Am. Chem. Soc.* **2013**, *135* (24), 8830-8833.

(69) Radlauer, M. R.; Buckley, A. K.; Henling, L. M.; Agapie, T. *J. Am. Chem. Soc.* **2013**, *135* (10), 3784-3787.

(70) Zhang, Y.; Keaton, R. J.; Sita, L. R. *J. Am. Chem. Soc.* **2003**, *125* (30), 9062-9069.

(71) Zhang, Y.; Sita, L. R. *J. Am. Chem. Soc.* **2004**, *126* (25), 7776-7777.

(72) Chen, Y.-X.; Metz, M. V.; Li, L.; Stern, C. L.; Marks, T. J. *J. Am. Chem. Soc.* **1998**, *120*, 6287-6305.

(73) Tshuva, E. Y.; Goldberg, I.; Kol, M. *J. Am. Chem. Soc.* **2000**, *122* (43), 10706-10707.

CHAPTER 2. EFFECTS OF PENDANT LIGAND BINDING AFFINITY ON CHAIN TRANSFER FOR 1-HEXENE POLYMERIZATION CATALYZED BY SELECT SINGLE-SITE ZIRCONIUM AND HAFNIUM AMINE BIS-PHENOLATE COMPLEXES

2.1 Introduction

The production of polyolefins is a major chemical industry with the current capacity of ca. 110 billion kg per year.[1] While most of these polyolefins are made using heterogeneous Ziegler-Natta catalysts, a growing interest has focused on developing new homogeneous single-site catalysts due to the potential for controlling catalytic activity, and subsequently polymer properties.[2,3,4] In the past decades, an explosion of research into different homogeneous, Group IV catalyst designs have included metallocenes, constrained geometry, aryloxide, aminodate, Salan, and amine bis-phenolate ligand designs. [2-5]

Reproduced with permission from Steelman, D. K.; Xiong, S.; Pletcher, P. D.; Smith, E.; Switzer, J. M.; Medvedev, G. A.; Delgass, W. N.; Caruthers, J. M.; Abu-Omar, M. M. *Journal of the American Chemical Society* **2013**, *135*, 6280. DOI: 10.1021/ja401474v

Reproduced with permission from Steelman, D. K.; Pletcher, P. D.; Xiongs, S.; Switzer, J. M.; Medvedev, G. A.; Delgass, W. N.; Caruthers, J. M.; Abu-Omar, M. M. *Organometallics,* **2013**, *32*, 4862. DOI: 10.1021/om4006005

In developing these catalysts, intuitive understanding on the relationship between catalyst structure and polymer structure has been used successfully in designing new catalysts systems, such as Dow's catalysts for olefin block copolymer synthesis.[6] Unfortunately, directly comparing kinetic rate constants of families of catalytic systems to determine the controlling chemical descriptors has not been realized. Due to the difficulty in determining the fundamental rate constants for the relevant steps within the catalytic mechanism, this field has relied on the chemist's intuition to design the next generation of olefin polymerization catalysts. As an alternative to this intuition based method, we have instead focused on rational catalyst design methods based on correlating quantitative rate constants to catalyst structure.

In the heterogeneous fields of carbon monoxide oxidation[7] and water gas shift,[8] there has been a shift in research design to include computational and kinetic experiments into design of experiments called discovery informatics. By correlating experimental activity measurements to binding energies of the catalyst to different substrates for a series of different catalysts, predictive volcano plots have been constructed to show which catalyst system will show an eruption of activity and which systems will exhibit lower activity. In the polymerization field, there has been an encouraging report by Abu-Omar and coworkers on correlating the ion pair separation energy between the zwitterionic pair of Ti aryl phenoxides with $MeB(C_6F_5)_3$ of individual catalyst structures to the propagation rate constant. [9] We have used this framework and past successes in predicting both new catalysts and polymer structures by first obtaining quantitative kinetic rate constants in 1-hexene polymerization.

Focusing on a particular catalyst family, we have studied the 1-hexene polymerization reactivity of an amine bis-phenolate ligand system first reported by Kol and coworkers, shown in Figure 2.1. [10, 11] In particular, the catalyst structures **5a**, **2b**, and **3b** will be discussed here within the context that they were reported. The work presented was done in collaboration with Dr. Jeffrey Switzer of Purdue Chemical Engineering, where he provided the modeling of all experimental data. The experimental data collection and kinetic the modeling of the catalysts **2a**, **3a**, **4a**, and **1b** were completed by Dr. David K. Steelman and Dr. Silei Xiong, respectively. The experimental data collection and kinetic the modeling of the catalyst **1a** was completed by Dr. David K. Steelman and Dr. Jeffrey Switzer, respectively.

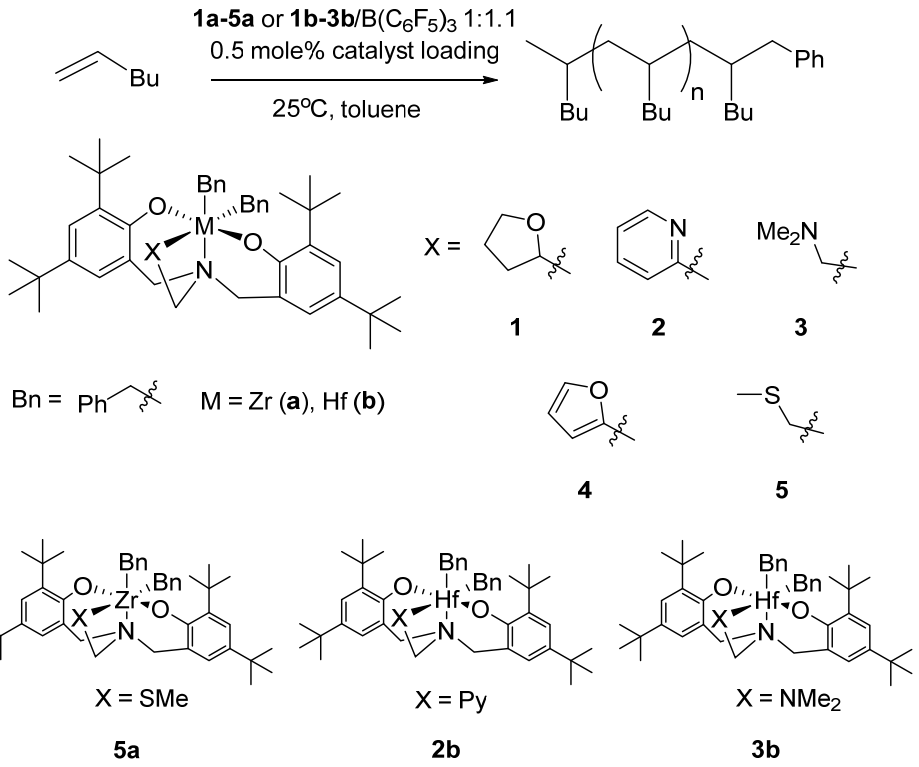

Figure 2.1 1-hexene polymerization catalyzed by zirconium and hafnium amine bis-phenolate-type catalysts when combined with the activator $B(C_6F_5)_3$. Catalysts **5a**, **2b**, and **3b** will be discussed in reference to the reactivity of the other catalysts

In the reported studies of zirconium and hafnium amine bis-phenolate catalysts, Kol reported that the metal (M), the pendant ligand (X), and the distance between M-X had implications on both reactivity and chain transfer. [10] Using this observation, we focused on quantifying both the rate constants within the polymerization mechanism for the purpose of finding chemical descriptors. We will show in following sections that a minimal set of rate constants can be used to completely describe the datasets of monomer consumption, vinyl formation, active site counting, and time-evolution of the molecular weight distribution.

Considering the influence of metal and X on overall catalytic mechanisms, the metal has a considerable effect on the reaction rate constants between catalyst and monomer. Zirconium catalysts with analogous pendants exhibited an increase in activity by roughly an order of magnitude when compared to their hafnium counterparts.[11] Focusing on changes to the ligand structures, the identity of the pendant has a considerable effect on both olefin insertion reactions and the vinylidene specific termination chain transfer reaction rate constants.

Of the catalysts studied for Group IV coordination insertion polymerization of olefins, zirconium compounds have been the most studied. However, there are often comparative studies between complexes containing identical ligands with zirconium and hafnium metal centers. These metals access the same electropositive 4+ oxidation state and are similar in size. In fact, many crystal structures of analogous Zr and Hf complexes are nearly identical.[12-14] However, the reactivity of these species towards olefin polymerization can be drastically different due to differences in the metal electronics. Zr compounds are typically reported with much larger activities compared to their Hf counterparts. [12-14] This

is typically rationalized as the difference between the enthalpies of the metal-carbon bond: Zr-C bonds are typically weaker than Hf-C bonds and may allow for more facile olefin insertion.[15] Furthermore, in metallocene catalyst systems, it is typically Hf catalysts that exhibit larger molecular weight, M_w, polymers when compared to those made from zirconium analogues.[12-15]

In the area of chain transfer, this process most commonly occurs through 4 distinctive mechanisms. These mechanisms include: (1) a monomer independent β-H elimination to form a vinylidene or vinylene terminated end; (2) a monomer dependent elimination reaction where the incoming monomer accepts a β-H from the metal-polymer chain and results in a vinylidene or vinylene terminated end; (3) cleavage of the M-Polymer bond through the use of a chain transfer agent, such as molecular hydrogen, or (4) chain transfer to activator, where the polymer chain transmetallates between the Group IV catalyst to an aluminum alkyl activator to form a non-growing polymer chain on the Al and a new smaller alkane attached catalyst center.

Looking through the chemical literature, the intuitive method of controlling chain transfer typically relies on steric bulk to reduce the chain transfer pathway for these types of catalysts.[16] Bercaw and co-workers observed that catalysts with an open metal center led to faster propagation but also increased β-H elimination. They speculated that an increased active site could more easily accommodate a docking monomer for insertion or β-H agostic bonding interactions necessary for β-H elimination.[17] These insights have led to modifications to late transition metal catalysts, based on Fe, Co, and Ni, with bulky

ligands systems to bias ethylene insertion towards polymer products over short chain oligomers.[18]

Detailed computational studies on ethylene polymerization using a variety of organometallic catalysts by Ziegler and coworkers have suggested that the activation energy for chain transfer is influenced by both the metal and the presence of steric bulk.[19] They concluded that β-H transfer to monomer is preferred versus β-H elimination, except with low concentrations of monomer or when the coordination of monomer to the catalyst center is severely hindered. These findings have been used by a range of laboratories to reduce chain transfer to produce high molecular weight polymers under a variety of conditions.[20-22]

The identity of the cocatalyst activator also has an impact on the effect of chain transfer. Systems such as $V(acac)_3$ or metallocenes can exhibit different pathways, β-H chain transfer pathway or chain transfer to activator, depending on the alkylaluminum activator present.[23,24] Using fluorinated aryl borane/borate/aluminum activators, Marks and coworkers have looked at the effect of catalyst-cocatalyst ion pair on chain transfer.[25] Their work, along with those of Bochmann and coworkers, found that the ion pair has a direct effect on both the preferred termination pathway and the magnitude of such a rate.[25,26]

In this study, we describe a detailed kinetic analysis for catalysts **5a**, **2b**, and **3b** in relation to other zirconium and hafnium catalysts. Contained in Table 2.1, the relevant rate constants of these systems, as well as similar catalysts, have been analyzed to observe the appearance of certain trends. Using a minimum number of necessary reaction steps to describe the entire data set for each catalytic system, rate constants were optimized such that the predictions of the polymer molecular weight distribution matched those observed

experimentally. These data sets include monomer consumption kinetics, molecular weight evolution of the growing polymer chains, active-site counts of deuterated polymer chain ends, and analysis of terminated vinyl groups. The chain transfer mechanisms and corresponding rate constants as the pendant ligand (X) changes will be discussed. A linear quantitative structure-activity relationship (QSAR) between the logarithm of the chain transfer rate constant and the M-X bond length will be shown and discussed.

2.2 Experimental Procedure

General Procedure: All manipulations were performed under a dry, inert atmosphere in a glove box or at a vacuum manifold using air sensitive techniques under N_2 or Ar atmosphere. Toluene and pentane were distilled over activated alumina and a copper catalyst using a solvent purification system (Anhydrous Technologies) and degassed through freeze-pump-thaw cycles. Both solvents were stored over activated molecular sieves. Tetrabenzylzirconium was purchased from STREM and used as received. The monomer 1-hexene was purchased from Aldrich and purified by distillation over a small amount of dimethyl bis(cyclopentadienyl)zirconium and stored over molecular sieves. Tris(pentafluorophenyl)boron was purchased from STREM and purified by sublimation. Diphenylmethane was purchased from Aldrich and stored over molecular sieves. CH_3OD was purchased from Cambridge Isotopes and used as received. D_8-toluene was used as received and stored over molecular sieves. ^1H and ^2H NMR experiments were performed on a Varian INOVA600 MHz or Bruker DRX500 MHz spectrometer.

The ligands and precatalysts (**5a. 2b, and 3b**) were prepared following modified literature procedures.[10,11]

Synthesis of 6,6'-(((2-(methylthio)ethyl)azanediyl)bis(methylene))bis(2,4-di-tert-butylphenol), ^{t}Bu-ON^{SMe}O ligand. The synthesis procedure is based on literature,[10,11] Scheme 2.1. In a typical synthesis, an 80 mL reaction vessel was charged with 2,4-di-tert-butylphenol (8.87 g, 42.6 mmol), 2-(methylthio)ethylamine (2.0 mL, 22 mmol) and 37% histological grade formaldehyde (8 mL, 71 mmol), and distilled water, and a stir bar while maintaining a maximum volume of 80 mL. The biphasic reaction mixture was placed in a CEM microwave reactor and allowed to warm to 100 ºC over 5 min while stirring. The reaction was allowed to stand at 100 ºC for 30 min, and then cooled to room temperature. The aqueous layer was removed, and cold, dry methanol was added to the organic phase. This mixture was shaken for 30 min, and the resulting solid isolated by vacuum filtration. The crude ligand product was purified by crystallization from ethanol (30% yield).

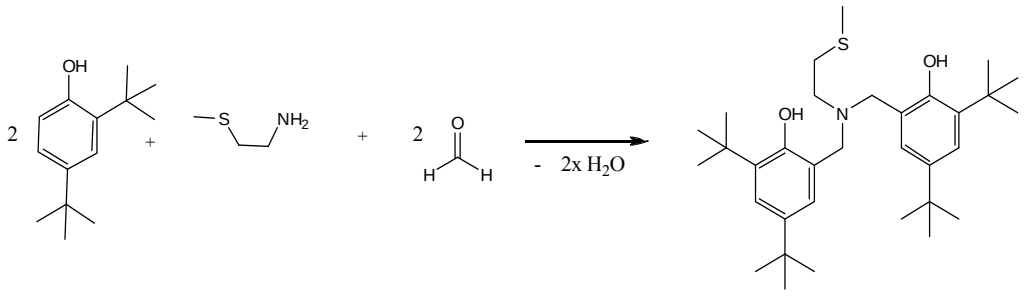

Scheme 2.1. Synthesis of the ^{t}Bu-ON^{SMe}O ligand

Synthesis of Zr[^{t}Bu-ON^{SMe}O]Bn$_2$. The synthesis procedure is based on literature,[10,11] Scheme 2.2. In a typical synthesis, a 100 mL flask was charged with tetrabenzylzirconium (1.17 g, 2.57 mmol), 20 mL toluene, and a stir bar and fitted with a rubber septum. A second 100 mL flask was charged with the ^{t}Bu-ON^{SMe}O ligand (1.43 g, 2.70 mmol) and 20 mL of toluene. The two flasks were placed under an inert atmosphere, and the ligand solution was added to the tetrabenzylzirconium solution via a cannula. The reaction was allowed to warm to 60 º C and stir for 2 hours resulting in a yellow solution. The solution was evaporated to dryness and washed with pentane. The resulting solid (84% yield) was recrystallized by vapor diffusion of pentane into a precatalyst/toluene solution to afford an analytically pure complex.

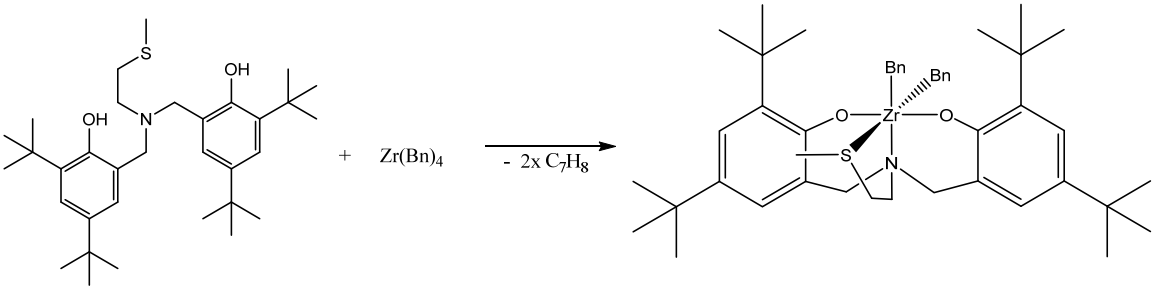

Scheme 2.2. Synthesis of the Zr[^{t}Bu-ON^{SMe}O]Bn$_2$ catalyst

NMR scale polymerization of 1-hexene with Zr[tBu-ON^{SMe}O]Bn$_2$ at 25 ºC. The procedure for NMR scale polymerization is based on literature.[27] For a typical polymerization, Zr[^{t}Bu-ON^{SMe}O]Bn$_2$ (6.0 mg, 0.0075 mmol) was dissolved in 0.5 mL toluene in a small vial and sealed with a screw-cap septum. The vial containing the

precatalyst solution was pierced with a 1 mL syringe. The vial and syringe were placed in an N_2 bag and allowed to equilibrate to 25 ºC. Tris(pentafluorophenyl)boron (3.8 mg, 0.0075 mmol), 1-hexene (0.124 grams, 1.47 mmol), and diphenylmethane (13.9 mg 0.082 mmol) were added to a 2 mL volumetric flask and diluted to the mark with d^8-toluene. This solution was placed in an NMR tube and sealed with a septum. The monomer/activator solution was placed in the spectrometer and allowed to equilibrate to 25 ºC using a VT controller. A measurement was taken to determine the initial concentration of monomer relative to the internal standard. The NMR tube was removed from the spectrometer, and the catalyst precursor solution was added to the activator/monomer solution by piercing the septum while the syringe remained in the N_2 bag. The reaction mixture was allowed to shaken for 30 seconds and injected back into the spectrometer. Measurements were taken at predetermined time intervals until the reaction reached completion. Each sample was prepared for GPC analysis by evaporation over mild heat before dissolution in hexanes and filtration through an alumina plug to remove the quenched catalyst. Evaporation of solvent yielded clear, colorless poly(1-hexene). The array of spectra was collected on an INOVA 600 MHz spectrometer and analyzed using MestReNova.

Batch polymerization of 1-hexene with Zr[^{t}Bu-ON^{SMe}O]Bn$_2$ at 25 ºC. The procedure for Manual Quench is based on literature.[27] For a typical polymerization, Zr[^{t}Bu-ON^{SMe}O]Bn$_2$ (0.024 g, 0.030 mmol) was dissolved in 3.0 mL toluene and placed in a small vial that was sealed with a screw-cap septum. The vial containing the precatalyst solution was pierced with a 3 mL syringe. The vial and syringe were placed in an N_2 bag and allowed to equilibrate to 25 ºC. Tris(pentafluorophenyl)boron (0.061 grams, 0.12 mmol), and 1-hexene (1.81 g, 21.4 mmol) were dissolved in 25 mL of toluene. A 1 mL aliquot of

this solution was removed for quantification of the initial monomer concentration through NMR analysis. A 7 mL aliquot of this solution was placed in a flask, and the flask was sealed with a septum and moved from an N_2 filled glovebox to a vacuum manifold and placed under argon. The monomer/activator solution was allowed to equilibrate to 25 ºC using a temperature-controlled silicone oil bath. The catalyst precursor solution was added to the activator/monomer solution by piercing the septum while the syringe remained in the N_2 bag. The resulting yellow solution was allowed to stir until a selected time point and quenched with 1 mL of d_4-methanol. A 1 mL aliquot from the quenched solutions was removed and a 0.5 mL solution of d-toluene spiked with diphenylmethane as an internal standard for quantification of 1-hexene consumption (via ^{1}H NMR on Varian Inova600). Each sample was prepared for GPC analysis by evaporation over mild heat before dissolution in hexanes and filtration through an alumina plug to remove the quenched catalyst. Evaporation of solvent yielded clear, colorless poly(1-hexene).

In the case of vinyl analysis, A 1 mL aliquot was worked up as described above. The resulting polymer was dissolved in $CDCl_3$, and diluted to the mark in a 2 mL volumetric flask. Diphenylmethane was used as an internal standard and the method of standard additions was used in quantification of the end groups by ^{1}H NMR. All end-group analysis measurements were taken on a Bruker DRX500 spectrometer at 25 ºC.

In the case of ^{2}H analysis, the remaining quenched reaction solution (8 mL) was worked up as described above. The resulting polymer was dissolved in CH_2Cl_2, and diluted to the mark in a 2 mL volumetric flask. d_6-benzene was used as an internal standard and the method of standard additions was used in quantification of active sites by ^{2}H NMR. All active site measurements were taken on a Bruker DRX500 spectrometer at 25 ºC.

Gel Permeation Chromatography (GPC) Analysis. The procedure used to analyze polymer samples using GPC methods was taken from Novstrup et al.,[9] and it is summarized below. Poly(1-hexene) samples were added to THF at room temperature and allowed to dissolve for 4 h. Solutions were then passed through a 0.2 μm filter to remove any particulate matter. The GPC analysis was performed on a Waters GPCV 2000 for system **1a** and **3a**, and on a Viscotek GPCmax VE 2001 for system **2a**, **4a**, and **5a**. On the Waters GPCV 2000, samples were injected through a 101.3 μL injection loop and passed through two Polymer Laboratories PLGel 5 μm Mixed-C columns in series in a 45 °C oven at a flow rate of 1.0 mL min-1. On Viscotek GPCmax VE 2001, samples were injected through a 200 μL injection loop and passed through three Viscotek T6000M 10 μm General Mixed Org columns in series in a 35 °C oven at a flow rate of 1.0 mL min^{-1}. The analysis made use of the differential RI detector and a capillary viscometer. Molecular weights were assigned by way of a universal calibration curve created with polystyrene standards ranging from 580 g mol-1 to 3,114,000 g mol-1. The calibration was verified through the analysis of a broad standard, SRM 706a, provided by the National Institute of Standards and Technology.

Synthesis of 6,6'-(((pyridin-2-ylmethyl)azanediyl)bis(methylene))bis(2,4-di-tert-butyl-phenol), ^{t}Bu-ON^{Py}O ligand. The synthesis procedure is based on literature,[10,11] Scheme 2.3. In a typical synthesis, an 80 mL reaction vessel was charged with 2,4-di-tert-butylphenol (24.7 g, 119 mmol), 2-picolylamine (7.0 mL, 68 mmol) and 37% histological grade formaldehyde (24.0 mL, 319 mmol), and distilled water, and a stir bar while maintaining a maximum volume of 80 mL. The biphasic reaction mixture was placed in a CEM microwave reactor and allowed to warm to 100 ºC over 5 min while stirring. The

reaction was allowed to stand at 100 ºC for 10 min, and then cooled to room temperature. The aqueous layer was removed, and cold, dry methanol was added to the organic phase. This mixture was shaken for 30 min, and the resulting solid isolated by vacuum filtration. The crude ligand product was purified by crystallization from ethanol (34% yield).

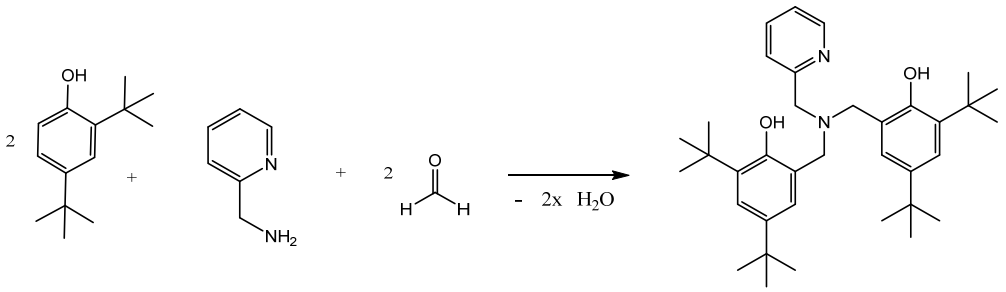

Scheme 2.3. Synthesis of the ^{t}Bu-ON^{Py}O ligand

Synthesis of Hf[tBu-ON^{Py}O]Bn$_2$. The synthesis procedure is based on the literature procedure of the zirconium analog[10,11], Scheme 2.4. In a typical synthesis, a 100 mL flask was charged with tetrabenzylhafnium (2.00 g, 3.68 mmol), 20 mL toluene, and a stir bar and fitted with a rubber septum. A second 100 mL flask was charged with the ^{t}Bu-ON^{Pyr}O ligand (2.11 g, 3.87 mmol) and 20 mL of toluene. The two flasks were placed under an inert atmosphere, and the ligand solution was added to the tetrabenzyhafnium solution via a cannula. The reaction was allowed to warm to 60 º C and stir for 2 hours resulting in a colorless solution. The solution was evaporated to dryness and washed with pentane. The resulting solid (62% yield) was recrystallized by vapor diffusion of pentane into a precatalyst/toluene solution to afford an analytically pure complex.

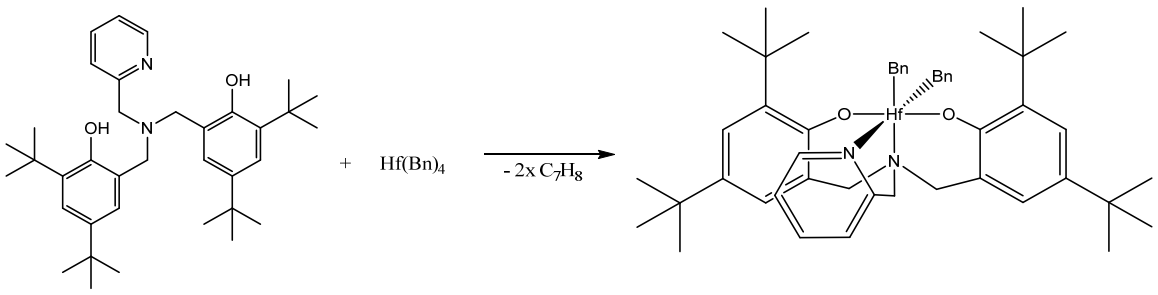

Scheme 2.4. Synthesis of the Hf[^{t}Bu-ON^{Py}O]Bn$_2$ catalyst

NMR scale polymerization of 1-hexene with Hf[tBu-ON^{Py}O]Bn$_2$ at 25 ºC. The procedure for NMR scale polymerization is based on literature.[27] For a typical polymerization, Hf[^{t}Bu-ON^{Py}O]Bn$_2$ (6.9 mg, 0.0075 mmol) was dissolved in 0.5 mL toluene in a small vial and sealed with a screw-cap septum. The vial containing the precatalyst solution was pierced with a 1 mL syringe. The vial and syringe were placed in an N_2 bag and allowed to equilibrate to 25 ºC. Tris(pentafluorophenyl)boron (4.2 mg, 0.0083 mmol), 1-hexene (0.126 grams, 1.50 mmol), and diphenylmethane (9.7 mg 0.058 mmol) were added to a 2 mL volumetric flask and diluted to the mark with d^8-toluene. This solution was placed in an NMR tube and sealed with a septum. The monomer/activator solution was placed in the spectrometer and allowed to equilibrate to 25 ºC using a VT controller. A measurement was taken to determine the initial concentration of monomer relative to the internal standard. The NMR tube was removed from the spectrometer, and the catalyst precursor solution was added to the activator/monomer solution by piercing the septum while the syringe remained in the N_2 bag. The reaction mixture was allowed to shaken for 30 seconds and injected back into the spectrometer. Measurements were taken at predetermined time intervals until the reaction reached completion. Each sample was

prepared for GPC analysis by evaporation over mild heat before dissolution in hexanes and filtration through an alumina plug to remove the quenched catalyst. Evaporation of solvent yielded clear, colorless poly(1-hexene). The array of spectra was collected on an INOVA 600 MHz spectrometer and analyzed using MestReNova.

Batch polymerization of 1-hexene with Hf[^{t}Bu-ON^{Py}O]Bn$_2$ at 25 ºC. The procedure for Manual Quench is based on literature.[27] For a typical polymerization, Hf[^{t}Bu-ON^{Py}O]Bn$_2$ (0.083g, 0.090 mmol) was dissolved in 6.0 mL toluene in a small vial that was sealed with a screw-cap septum. The vial containing the precatalyst solution was pierced with a 10 mL syringe. The vial and syringe were placed in an N_2 bag and allowed to equilibrate to 25 ºC. Tris(pentafluorophenyl)boron (0.053 grams, 0.103 mmol), and 1-hexene (1.60 g, 19.0 mmol) were added to a 25 mL flask and diluted to the mark with toluene. This solution was diluted to 26 mL with 1 mL of toluene, and 1mL of the resulting solution was removed for quantification of the initial monomer concentration through NMR analysis. The flask was sealed with a septum and moved from an N_2 filled glovebox to a vacuum manifold and placed under argon. The monomer/activator solution was allowed to equilibrate to 25 ºC using a temperature-controlled silicone oil bath. The catalyst precursor solution was added to the activator/monomer solution by piercing the septum while the syringe remained in the N_2 bag. The resulting yellow solution was allowed to stir while aliquots were removed at selected times and each was injected into a 10 mL volumetric flask containing 1 mL of deutero-methanol. A 1 mL aliquot from the quenched solutions was removed and a 0.5 mL solution of d-toluene spiked with diphenylmethane as an internal standard for quantification of 1-hexene consumption (via ^{1}H NMR on Varian Inova600). Each sample was prepared for GPC analysis by evaporation over mild heat

before dissolution in hexanes and filtration through an alumina plug to remove the quenched catalyst. Evaporation of solvent yielded clear, colorless poly(1-hexene).

In the case of vinyl analysis, A 1 mL aliquot was worked up as described above. The resulting polymer was dissolved in $CDCl_3$, and diluted to the mark in a 2 mL volumetric flask. Diphenylmethane was used as an internal standard and the method of standard additions was used in quantification of the end groups by ^1H NMR. All end-group analysis measurements were taken on a Bruker DRX500 spectrometer at 25 ºC.

In the case of ^2H analysis, the remaining quenched reaction solution (8 mL) was worked up as described above. The resulting polymer was dissolved in CH_2Cl_2, and diluted to the mark in a 2 mL volumetric flask. d_6-benzene was used as an internal standard and the method of standard additions was used in quantification of active sites by ^2H NMR. All active site measurements were taken on a Bruker DRX500 spectrometer at 25 ºC.

Synthesis of 6,6'-((dimethylamino)methylazanediyl)bis(methylene)bis(2,4-di-tert-butylphenol), ^{t}Bu-ON^{NMe2}O ligand. The ligand synthesis procedure is based on literature,[10,11] Scheme 2.5. In a typical synthesis, a 30 mL reaction vessel was charged with 2,4-di-tert-butylphenol (7.62 g, 36.0 mmol), N,N-dimethylethylenediamine (1.89 mL, 15 mmol) and 37% histological grade formaldehyde (3.00 mL, 36 mmol), 6.7 mL of distilled water. The biphasic reaction mixture was placed in a CEM microwave reactor and allowed to warm to 100 ºC over 10 min while being stirred. The reaction mixture was allowed to stand at 100 ºC for 10 min, and then cooled to room temperature. The aqueous layer was removed, and cold, dry methanol was added to the organic phase. This mixture was shaken for 30 min, and the resulting solid was isolated by vacuum filtration. The crude ligand product was purified by crystallization from ethanol (52% yield).

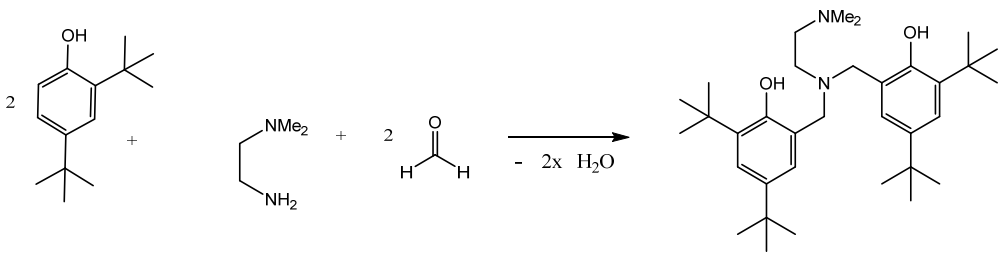

Scheme 2.5. Synthesis of the tBu-ON^{NMe2}O ligand

Synthesis of Hf(^{t}Bu-ON^{NMe2}O)Bn$_2$. The catalyst synthesis procedure is based on literature, Scheme 2.6.[10.11] In a typical synthesis, a 100 mL flask was charged with tetrabenzylhafnium (2.00 g, 3.68 mmol), 20 mL toluene, and a stir bar and fitted with a rubber septum. A second 100 mL flask was charged with the ^{t}Bu-ON^{NMe2}O ligand (2.03 g, 3.87mmol) and 20 mL of toluene. The two flasks were placed under an inert atmosphere, and the ligand solution was added to the tetrabenzylhafnium solution via a cannula. The reaction mixture was allowed to warm to 65 ºC and stir for 2 h, resulting in a bright yellow solution. The reaction mixture was then allowed to cool to yield small yellow crystals (2.3597 g). By ^{1}H NMR analysis the product appeared to be ca. 92% pure. Recrystallization by vapor diffusion of pentane into a toluene solution of Hf[^{t}Bu-ON^{NMe2}O]Bn$_2$ afforded an analytically pure complex (72% yield).

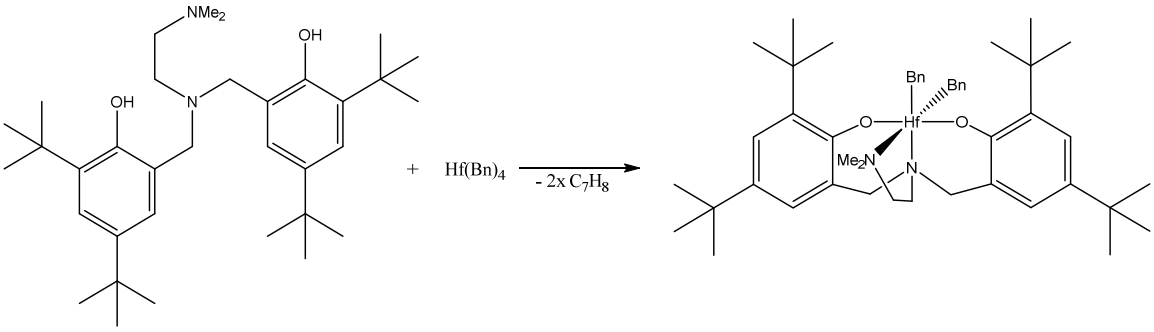

Scheme 2.6. Synthesis of the Hf[^{t}Bu-ON^{NMe2}O]Bn$_2$ catalyst

NMR scale polymerization of 1-hexene with Hf[^{t}Bu-ON^{NMe2}O]Bn$_2$ at 25 ºC. The procedure for NMR scale polymerization is based on literature.[27] For a typical polymerization, Hf[^{t}Bu-ON^{NMe2}O]Bn$_2$ (6.6 mg, 0.008 mmol) was dissolved in 0.5 mL toluene in a small vial and sealed with a screw-cap septum. The vial containing the precatalyst solution was pierced with a 1 mL syringe. The vial and syringe were placed in an N_2 bag and allowed to equilibrate to 25 ºC. Tris(pentafluorophenyl)boron (4.2 mg, 0.0083 mmol), 1-hexene (0.1262 grams, 1.5 mmol), and diphenylmethane (9.5 mg, 0.056 mmol) were added to a 2 mL volumetric flask and diluted to the mark with d^8-toluene. This solution was placed in an NMR tube and sealed with a septum. The monomer/activator solution was placed in the spectrometer and allowed to equilibrate to 25 ºC using a VT controller. A measurement was taken to determine the initial concentration of monomer relative to the internal standard. The NMR tube was removed from the spectrometer, and the catalyst precursor solution was added to the activator/monomer solution by piercing the septum while the syringe remained in the N_2 bag. The reaction mixture was allowed to shaken for 30 seconds and injected back into the spectrometer. Measurements were taken at predetermined time intervals until the reaction reached completion. Each sample was

prepared for GPC analysis by evaporation over mild heat before dissolution in hexanes and filtration through an alumina plug to remove the quenched catalyst. Evaporation of solvent yielded clear, colorless poly(1-hexene). The array of spectra was collected on an INOVA 600 MHz spectrometer and analyzed using MestReNova.

Batch polymerization of 1-hexene with Hf[^{t}Bu-ON^{NMe2}O]Bn$_2$ at 25 ºC. The procedure for manual quench is based on literature.[27] For a typical polymerization, Hf[^{t}Bu-ON^{NMe2}O]Bn$_2$ (0.0756 g, 0.09 mmol) was dissolved in 6 mL of toluene. This solution was placed in a small vial and sealed with a screw-cap septum. The vial containing the catalyst precursor solution was pierced with a 10 mL syringe. The vial and syringe were placed in an N_2 bag and allowed to equilibrate to 25 ºC. Tris(pentafluorophenyl)boron (0.0528 g, 0.103 mmol), and 1-hexene (1.80 g, 18.75 mmol) were added to a 25 mL volumetric flask and diluted to the mark with toluene. A 1 mL aliquot of this solution was removed for quantification of the initial monomer concentration through NMR analysis. 24 mL aliquot of this solution was placed in a 50 mL flask which was sealed with a septum and moved from an N_2 filled glovebox to a vacuum manifold and placed under argon. The monomer/activator solution was allowed to equilibrate to 25 ºC using a temperature-controlled silicone oil bath. The catalyst precursor solution was added to the activator/monomer solution by piercing the septum while the syringe remained in the N_2 bag. The resulting yellow solution was allowed to stir while aliquots were removed at selected times and each was injected into a 10 mL volumetric flask containing 1 mL of deutero-methanol. A 1 mL aliquot from the quenched solutions was removed and a 0.5 mL solution of d-toluene spiked with diphenylmethane as an internal standard for quantification of 1-hexene consumption (via ^{1}H NMR on Varian Inova600). Each

quenched sample was prepared for GPC analysis by evaporation over mild heat before dissolution in hexane and filtration through an alumina plug to remove the quenched catalyst. Evaporation of solvent yielded clear, colorless poly(1-hexene).

For vinyl/end group analysis, a 1 mL aliquot was worked up as described above. The resulting polymer was dissolved in $CDCl_3$, and diluted to the mark in a 2 mL volumetric flask. Diphenylmethane was used as an internal standard and the method of standard additions was used for quantification of the end groups by ^1H NMR. All end-group analysis measurements were taken on a Bruker DRX500 spectrometer at 25 ºC.

In the case of ^2H NMR analysis for the active-site count, the remaining quenched reaction solution (8 mL) was worked up as described above. The resulting polymer was dissolved in CH_2Cl_2, and diluted to the mark in a 2 mL volumetric flask. D_6-benzene was used as an internal standard, and the method of standard additions was employed in quantification of active sites by ^2H NMR. All active site measurements were taken on a Bruker DRX500 spectrometer at 25 ºC.

2.3 Results

Here we present a complete kinetic analysis for 1-hexene polymerization by catalysts **5a**, **2b**, and **3b**. In approaching each system, we followed our previously developed kinetic modeling method[28] based on the analysis of multi-response data that includes GPC traces where we did not make any a priori assumptions about the elementary reaction steps taking place. However, when this independent analysis was completed for each catalyst system, it emerged that all three systems described herein follow a similar kinetic mechanism including initiation, propagation via normal insertion, 2,1-misinsertion,

recovery from misinsertion, and two types of chain transfer resulting in the formation of vinylidene and vinylene species. The kinetic steps are illustrated in Scheme 2.7. The activation step is fast on the timescale of polymerization and as a result was not used in the kinetic modeling. Chain transfer resulting in vinylidene and vinylene terminated polymers follows either unimolecular (monomer independent) β-H elimination or bimolecular β-H transfer to monomer.

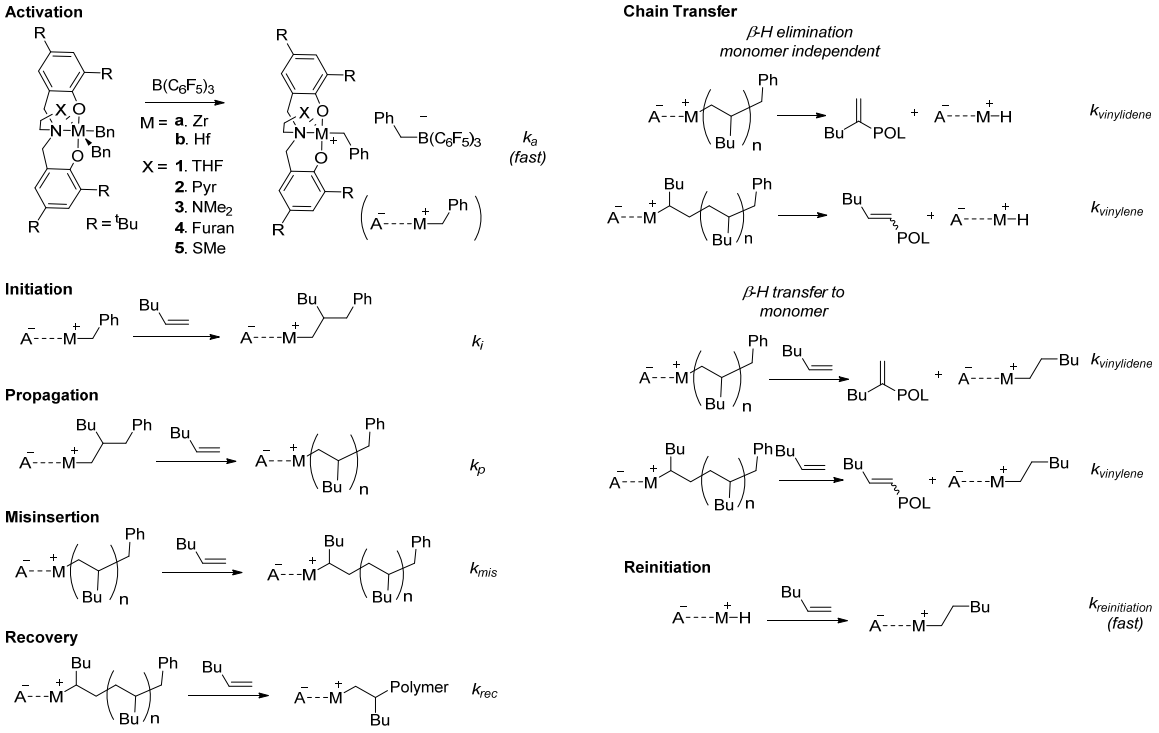

Scheme 2.7. The elementary kinetic steps used in fitting the data for catalysts **5a**, **2b**, and **3b**. The ordinary differential equations (ODEs) that describe the mass-action kinetics associated with this mechanism are provided in Section 2.2.

Examining the available data, the reasons for the mechanism (Scheme 2.7) are as follows:

I. Misinsertion (k_{mis}) and recovery (k_{rec}) are necessary because

1. We observe two types of chains attached to the active sites (primary and secondary) in active-site counting experiments with MeOD quenches (^{2}H NMR of isolated polymer gives δ 0.83 (DH_2C—Polymer) and 1.22 (DH(Bu)C—Polymer).
2. When analyzing the produced polymer, there are two types of vinyl end groups are observed: one with a terminal double bond at the end of the chain (vinylidene), and another with an internal double bond inside the chain (vinylene). We believe the latter arises from chain transfer of misinserted chains.
3. The secondary sites (Zr-CH(Bu)-Polymer) do not accumulate over time. We assume this is the case because they are able to recover via normal 1-hexene insertion.
4. Although there is an alternative explanation for points 1 through 3, namely, that there are two different sites growing separately, it is expected that such a mechanism would at least under some experimental conditions produce bimodal MWD. The fact that none of the systems exhibit a bimodal MWD and all yield narrow PDI values strongly suggest that these systems are single-site catalysts.

II. Chain transfer reactions are necessary because we observe polymer chains with vinyl end groups. It should be noted that there are two possible mechanisms through monomer dependent and monomer independent pathways. The monomer dependent pathway (β-H transfer to monomer) results in an active site with one repeat unit, while the monomer independent pathway (β-H elimination) results in the formation of a zirconium hydride.

There is an ongoing discussion whether the insertion of a monomer in the zirconium hydride i.e. re-initiation ($k_{reinitiation}$) is facile or hindered as compared to the normal initiation (k_i) for a given catalyst system. If the rate constant of re-initiation ($k_{reinitiation}$) of the zirconium hydride is slow, it effectively renders affected catalyst sites inactive, which in turn has an effect on the monomer consumption curve, active sites count, and the MWDs. As a result the value of the re-initiation rate constant ($k_{reinitiation}$) can be determined. On the other hand, when the rate constant of the re-initiation of zirconium hydride is fast, the data are usually not sensitive enough to determine its value precisely**,** similarly to how the data are not sensitive enough to determine the normal initiation rate when it is not significantly slower than the propagation rate. In practice we have set the re-initiation rate to be equal to the propagation rate in cases when the re-initiation rate is determined to be fast.

An important caveat is that the catalyst participation for each system may vary and not be 100%. The catalyst participation can be estimated from the active site counting experiments (quench with MeOD followed by ^{2}H NMR analysis of polymer chains). Also, for the systems where the chain transfer is low (catalysts **1a** and **5a**) the catalyst participation is readily estimated from the slope of M_w vs. conversion plot, which is linear in these cases. When applicable, these two methods give consistent results.

For each system we simultaneously fit the following: (1) monomer consumption, (2) MWD, (3) active site counts, and (4) end group counts. The data set usually includes several initial conditions of different $[C]_0$ (C = precatalyst/$B(C_6F_5)_3$) and $[M]_0$ (M = 1-hexene). For some conditions, multiple repeats were carried out, and the results were consistent when small variation in active-site catalyst participation was accounted for; however, only one repeat is shown in the figures below.

In determining error margins of the estimates for the six rate constants for each catalyst system (see Scheme 2.7), the following considerations apply: (1) the experimental data has an inherent error resulting from the measurement procedure. Specifically, the NMR spectrum is characterized by the uncertainty of roughly 5% for the peak integration; the GPC trace is characterized by the uncertainty of the weight average, M_w, of approximately 3%, where the uncertainty in the shape of the distribution is more difficult to ascertain (see discussion in reference 28). However, these estimates are based on the best experimental conditions, such sufficient concentration of the species of interest in the case of NMR, which holds for the monomer concentration. (2) In the case of the active sites and vinyl end group analyses, the concentrations are relatively low, causing the uncertainty to increase. Three separate measurements were performed for each sample, where the concentration varied slightly from measurement to measurement. The standard deviation calculated on the basis of these three measurements is compared to the inherent NMR integration error, and the larger error is chosen. (3) In the case of the GPC measurements, repeat runs result in minimal scatter such that the GPC curves appear overlapping. This, however, should not be taken as an actual estimate of the experimental error, since the error in the GPC measurements may be systematic rather than random due to various reasons described in the literature.[28] Instead, we assumed that the potential error in the GPC outputs caused by the uncertainty in the *dn/dc* values, inter-detector time, etc., amounts to at most a 10% up or down shift of each slice molecular weight and hence the shift of the entire MWD. (This actually translates in the -0.05/+0.04 shifts on log scale). For most of the studied systems, error from the GPC measurements were determined to

cause the largest uncertainty in the rate constants, and therefore this method was used to generate the uncertainty reported in this paper.

In the rest of this section we provide first the detailed analysis including fits to the data for each catalyst system, and then a summary of all the rate constants in Table 2.1

Zr-SMe catalyst 5a. The experimental data along with the kinetic modeling fits are presented in Figure 2.2.

The specific features of this system are:

(1) secondary Zr-polymer sites (Zr-CH(Bu)-Polymer) resulting from misinsertion dominate over primary active-sites (Zr-CH_2-Polymer). The model-based explanation is that the k_{mis}/k_p ratio is high while k_{rec}/k_p is low. These values for this catalyst are similar to those for catalyst **1a**, where secondary sites are roughly equal to primary sites.

(2) vinylene end groups, which are formed from chain transfer of secondary sites, are more abundant than vinylidene end groups. This is because of the higher concentration of secondary sites rather than a larger $k_{vinylene}$ rate constant.

(3) vinyl groups form via chain transfer to monomer, affording second-order rate constants. The data, however, is not definitive, and a first-order reaction (β-H elimination) cannot be definitively ruled out. In either case, the vinyl concentrations are relatively small, and the effect of the chain transfer rate constants on the responses other than the vinyl end group analysis data (e.g. the MWDs) is small.

(4) the total active site concentration (primary plus secondary) decreases over the course of the reaction. In addition, the monomer consumption slows late in the

reaction. These behaviors imply a first order (in catalyst) deactivation reaction. The deactivation rate constant is approximately half of the initiation rate constant, with the result that the total active site concentration remains low throughout the reaction.

(5) while 100% of the catalyst is available to initiate (in contrast to the other systems where only a fraction participates), no more than about one third (ca. 33%) of the zirconium active sites contain a growing polymer chain at any time

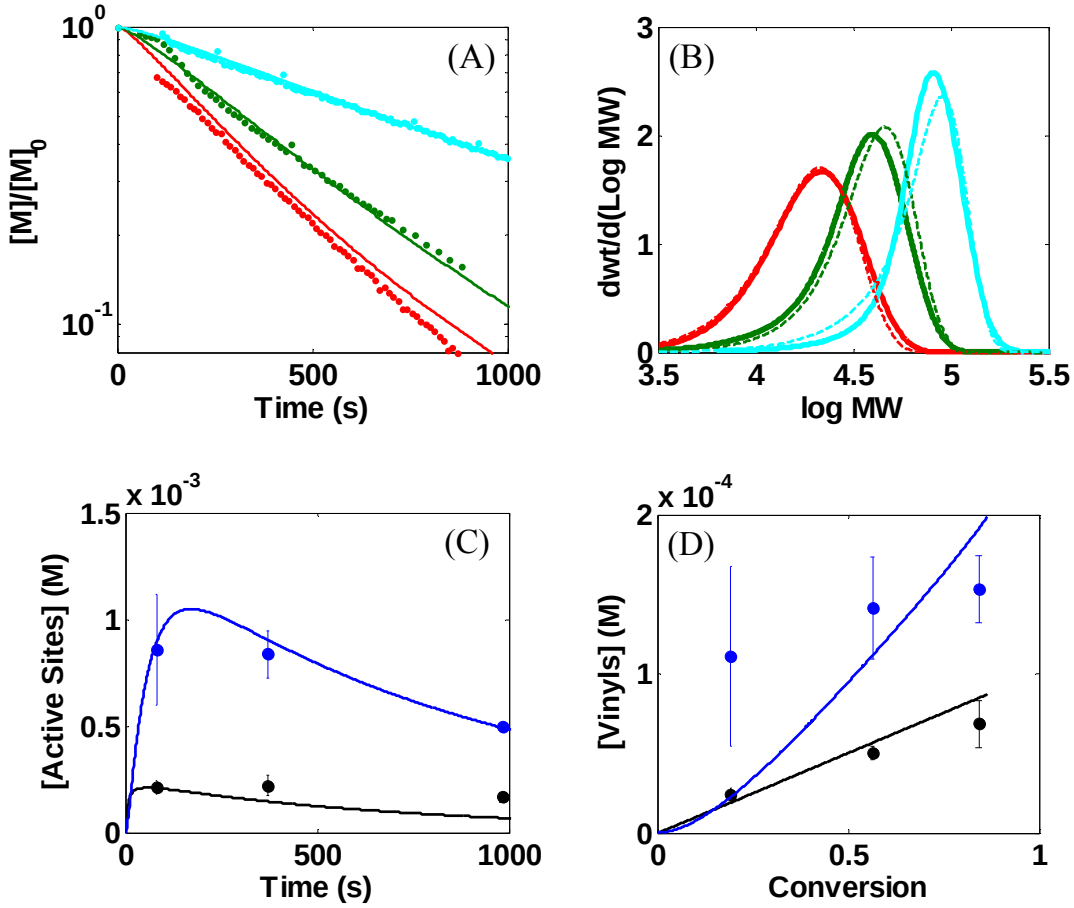

Figure 2.2. Multi-response data set with fits for Zr[^{t}Bu-ON^{SMe}O]Bn$_2$/B(C$_6$F$_5$)$_3$ catalyst 5. (A) Monomer consumption of selected NMR scale reactions having catalyst to monomer ratios of 1:100 (red, $[C]_0$ = 3.0 mM, $[M]_0$ = 0.30 M), 1:200 (green, $[C]_0$ = 3.0 mM, $[M]_0$ = 0.60 M), and 1:400 (cyan, $[C]_0$ = 1.5 mM, $[M]_0$ = 0.60 M). Symbols are data, solid lines are modeling fits. (B) MWDs of the polymer resulting from the reactions shown in (A). Solid curves are data, dashed curves are fits. (C) Active site counts of selected batch scale reaction with three quenches using MeOD at different reaction time. $[C]_0$ = 3.0 mM, $[M]_0$ = 0.60 M. Black symbols: primary active-site count; blue symbols: secondary active-site count. Solid curves are modeling fits. (D) Vinyls analyses of selected batch scale reaction with three quenches at different reaction time. $[C]_0$ = 3.0 mM, $[M]_0$ = 0.60 M. Black symbols: vinylidene count; blue symbols: vinylene count. Squares are vinyls counts taken after 12 h. Lines represent kinetic modeling fits.

Hf-Pyridine catalyst 2b. The experimental data along with the kinetic modeling fits are presented in Figure 2.3.

The specific features of this system are:

(1) Catalyst participation is nearly 100%;

(2) In case of the batch scale experiments, significant catalyst deactivation is observed as evidenced by bending of the monomer consumption curve in Figure 2.3C and the steep decline in primary active site counts over the course of the reaction in Figure 2.3E. In case of the NMR scale experiments, the deactivation either does not occur or is much less significant. For that reason, deactivation is not considered as part of the catalytic reactions;

(3) The amount of chain transfer is relatively high as evidenced by the significant vinylidene concentration in Figure 2.3F and the fact that MWD does not change much after 30% conversion of the monomer. The vinylidene formation is via a monomer independent reaction as evidenced by the upward curvature in the vinylidene concentration versus monomer conversion plot (Figure 2.3F);

(4) The vinylene end group concentration is much lower than that of vinylidene (Figure 2.3F), where the vinylene formation is via monomer dependent reaction as evidenced by the linear accumulation in Figure 2.3F.

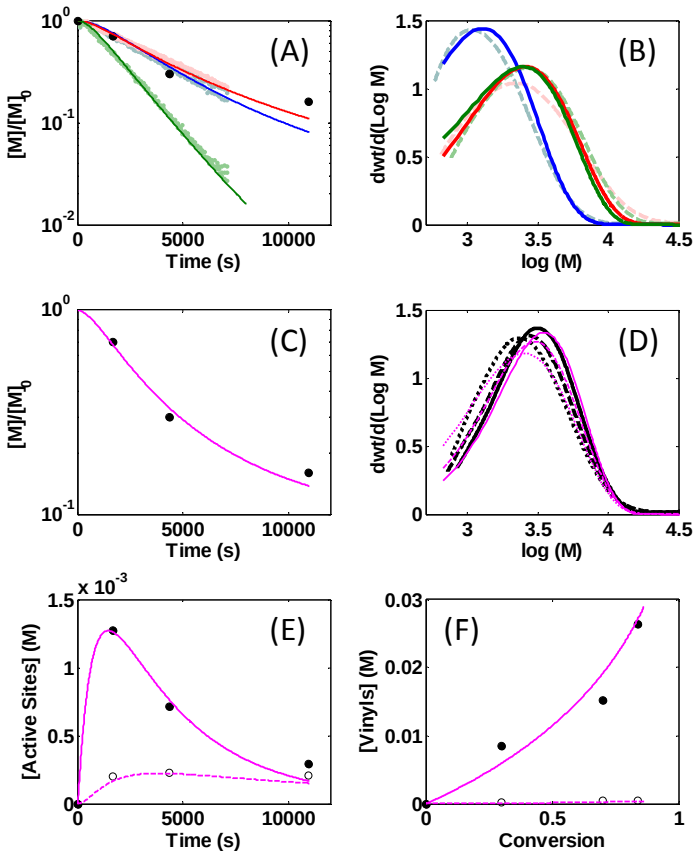

Figure 2.3. Multi-response data set with fits for catalyst **2b**. NMR-scale experiments: (A - B); (A) Monomer consumption. Data: symbols, fits: lines. (B) MWDs at the end. {Blue, Red, Green}: $[C]_0$ = {3.0, 3.0, 6.0} mM and $[M]_0$ = {0.30, 0.60, 0.60} M. Data: solid, fits: dashed. Batch scale experiments ($[C]_0$ = 3.0 mM, $[C]_0$ = 0.60 M): (C - F). (C) Monomer consumption. Data: symbols, fit: line. (D) MWDs at: — 1694 s, – – 4352 s, ⋯ 10963 s. Data: black, fits: magenta. (E) Active site counts. Primary - filled circles (data)/solid line (fit); secondary - open circles (data)/dashed line (fit). (F) End group analysis. Filled circles (data)/solid line (fit): vinylidene; open circles (data)/dashed line (fit): vinylene. In (A), black circles same as in (C) for comparison.

Hf-NMe$_2$ catalyst 3b. The experimental data along with the kinetic modeling fits are presented in the Supporting Information. The specific features of this system are:

(1) Catalyst participation is approximately 40%;

(2) There is a decline in active catalyst sites over the course of the reaction, although it is not as steep as in Systems **1b** and **2b**;

(3) No secondary catalyst sites were measured, although a small amount of vinylene end groups were detected. This peculiar behavior was also observed for the EBIZrMe$_2$/B(C$_6$F$_5$)$_3$ catalyst.[3] Vinylene is typically expected to form following chain transfer of secondary sites. It is likely in this system that secondary sites do form, but they rapidly undergo either chain transfer or monomer-dependent recovery. Since no secondary sites are observed even late in the reaction when monomer concentration is low, a fast monomer independent chain transfer event is more probable.

2.3.1 Detailed Kinetic Modeling

The modeling perspectives used in this communication (i) start with the simplest possible polymerization mechanism, (ii) determine if it fits the data, and (iii) if it does not fit the data within experimental error, postulate the next simplest mechanism. Using this procedure the simplest model consistent with the data is discovered.

2.3.1.1 Kinetic Modeling of Zr[^{t}Bu-ON^{SMe}O]Bn$_2$ Catalyst System (**5a**)

The results for system **5** were somewhat unique among the five systems studied as this was the only system where the data could be modeled with the assumption that 100% of the precatalyst is available for polymer growth. However, the data could also only be reconciled with the introduction of a first order deactivation pathway. To demonstrate this,

Figure 2.4 shows the best possible fit by optimization of representative vinyl and MWD data from batch scale experiments quenched at different reaction times. While rate constants can be selected to satisfy the monomer consumption data reasonably well, there is a tradeoff in fitting the vinyl and MWD data. The model with slow initiation and fast chain transfer fits the MWDs moderately well but fits the vinyls poorly (cyan curves in Figure 2.4), while the model with fast initiation and slow chain transfer does the opposite (red curves in Figure 2.4). Neither of these model types matches the active site behavior well at the end of the reaction. Introducing a deactivation pathway, which seems intuitively reasonable based on the shape of the monomer consumption and active site data, allows a good fit of all data simultaneously (i.e. green curves in Figure 2.4), where all of the catalysts is active.

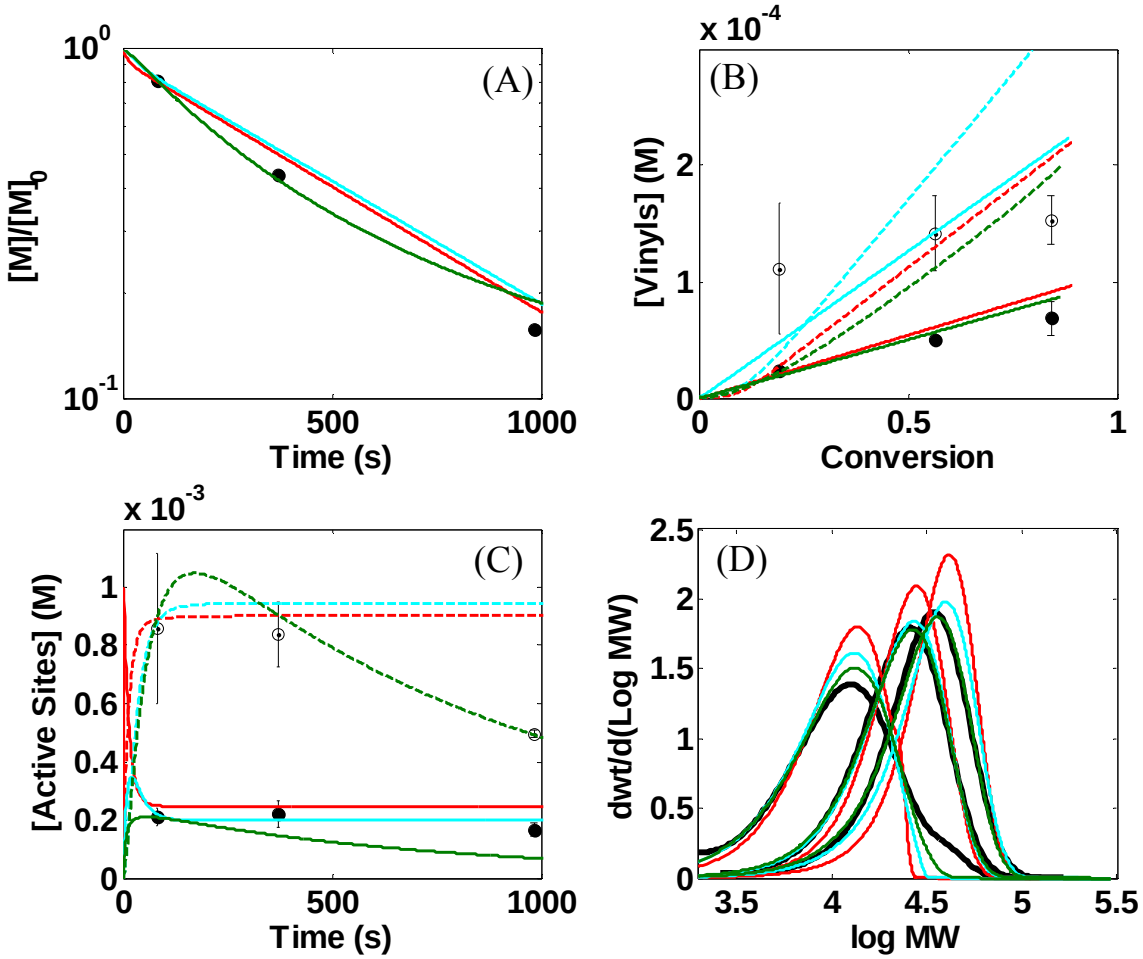

Figure 2.4. Experimental data for three selected batch scale reactions, quenched at different reaction times. $[C]_0$ = 3.0 mM, $[M]_0$ = 0.60 M. Black: data. Colored lines represent kinetic modeling fits. Red: $k_i = k_p$ = 6.5 M^{-1} s^{-1}, k_{mis} = 0.11 M^{-1} s^{-1}, k_{rec} = 0.029 M^{-1} s^{-1}, k_{dene} = 0.0012 M^{-1} s^{-1}, k_{ene} = 0.0008 M^{-1} s^{-1}, active site fraction = 0.38; Cyan: k_i = 0.080 M^{-1} s^{-1}, k_p = 7.9 M^{-1} s^{-1}, k_{mis} = 0.12 M^{-1} s^{-1}, k_{rec} = 0.024 M^{-1} s^{-1}, k_{dene} = 0.0035 M^{-1} s^{-1}, k_{ene} = 0.0012 M^{-1} s^{-1}, active site fraction = 0.38; Green: k_d = 0.0079 s^{-1}, all other rates are in Table 1. (A) Monomer consumption data. (B) Vinyl measurements. Filled symbols/solid lines: vinylidene count; open symbols/dashed lines: vinylene count. (C) Active site measurements. Filled symbols/solid lines: primary site count; open symbols/dashed lines: secondary site count. (D) MWD data at (from left to right) 81 s, 371 s, 983 s.

One concern with determining a model for this catalyst system is predicting the vinylidene data. In one experiment where vinylene concentrations were measured (Figure 2.4B), the vinylene concentration appears to be relatively high at the lowest monomer conversion, where there is minimal additional increase in vinylene concentration as the polymerization proceeds. This implies that vinylene formation slows down later into the reaction, and therefore likely depends on monomer concentration. When plotted as vinylene concentration vs. monomer conversion a straight line is expected (in the absence of events that alter catalyst concentration, which do occur in this system), whereas when chain transfer is monomer independent the line would curve upwards. The behavior seen in the data is most closely modeled by monomer dependent vinylene formation (Figure 2.5, green curve) rather than monomer independent vinylene formation (Figure 2.5, blue curve), although no rate constants could be found that were completely satisfactory at fitting the initial measurement. One possible issue is the uncertainty in the NMR measurement of vinyl concentration at such low values, which may cause errors even larger than displayed in the figure.

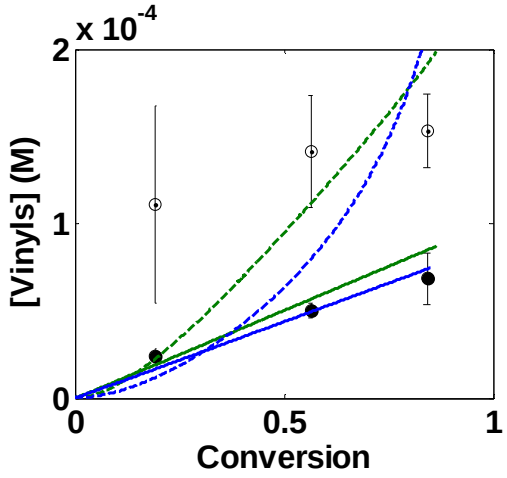

Figure 2.5. Vinyl concentration data for three selected batch scale reactions, quenched at different reaction times. $[C]_0$ = 3.0 mM, $[M]_0$ = 0.60 M. Black: data. Colored lines represent kinetic modeling fits.; Green: Monomer dependent vinylene formation: k_d = 0.0079 s^{-1}, all other rates are in Table 1; Blue: Monomer independent vinylene formation: k_i = 0.018 M^{-1} s^{-1}, k_p = 11.9 M^{-1} s^{-1}, k_{mis} = 0.20 M^{-1} s^{-1}, k_{rec} = 0.038 M^{-1} s^{-1}, k_{dene} = 0.0018 M^{-1} s^{-1}, k_{ene} = 0.00026 s^{-1}, k_d = 0.0081 s^{-1}, active site fraction = 1.0. Filled symbols/solid lines: vinylidene count; open symbols/dashed lines: vinylene count.

2.3.1.2 Kinetic Modeling of Hf[^{t}Bu-ON^{Py}O]Bn$_2$ Catalyst System (**2b**)

2.3.1.2.1 Mechanism I. Living Polymerization

Again, we start by using the living polymerization model. It is immediately apparent from the monomer consumption data (2.6A) that the logarithm of monomer consumption is not linear. It is therefore not surprising that this simplified model is inadequate to fit the data. The MWD fits are also poor (Figure 2.6B), predicting higher MW than expected MWDs.

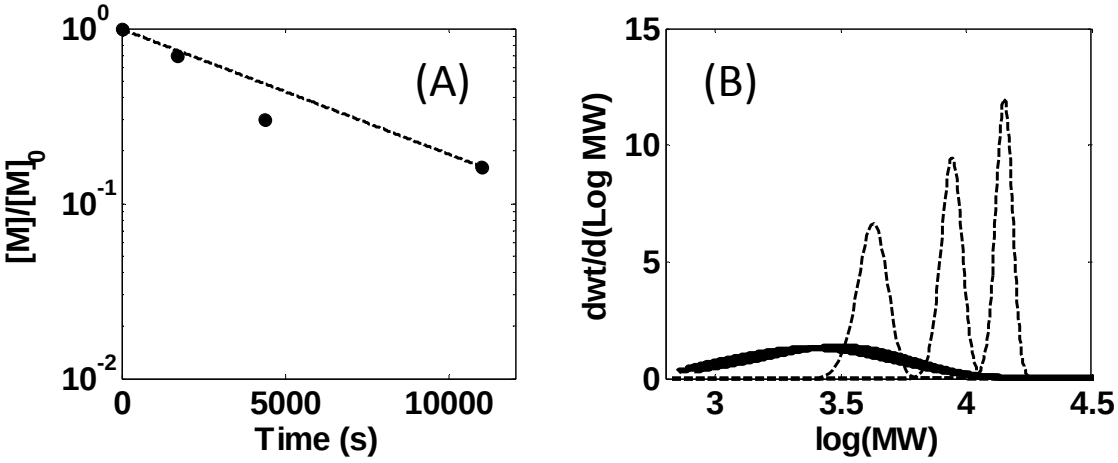

Figure 2.6. Modeling using Mechanism I; data (A) monomer consumption from three batch quenches at 1694, 4352, 10963 s (circles), (B) corresponding MWD of each quench (bold solid lines); fits (dashed lines); rate constants: $k_i = k_p = 0.55$ M^{-1} s^{-1}. $[C]_0 = 3.0$ mM, $[M]_0 = 0.60$ M.

2.3.1.2.2 Mechanism II. Vinylidene Formation Via Chain Transfer

Vinyl end groups were measured during polymerization of this system, indicating that chain transfer is likely present. Inclusion of a chain transfer pathway into the kinetic mechanism will also produce the smaller MW chains that we expect compared with Mechanism I, and it will also produce broader distributions. We start with only vinylidene formation because it is the dominant vinyl species. Vinylidene may form in a unimolecular reaction, i.e. β-H elimination (Mechanism II(i)), or it may form in a bimolecular reaction with monomer, i.e. β-H transfer (Mechanism II(ii)). The elimination reaction results in the formation of Hf-H species. For the current mechanism it is assumed that these species enchain monomer at a rate equal to the propagation rate. Results of the model fits are in Figure 2.7. One additional comment is that the active sites reported in Figure 2.7C only

represent long chain active sites, that is, chains longer than two repeat units. Smaller chains are lost in polymer workup, and so the active site prediction of the model corrects for this.

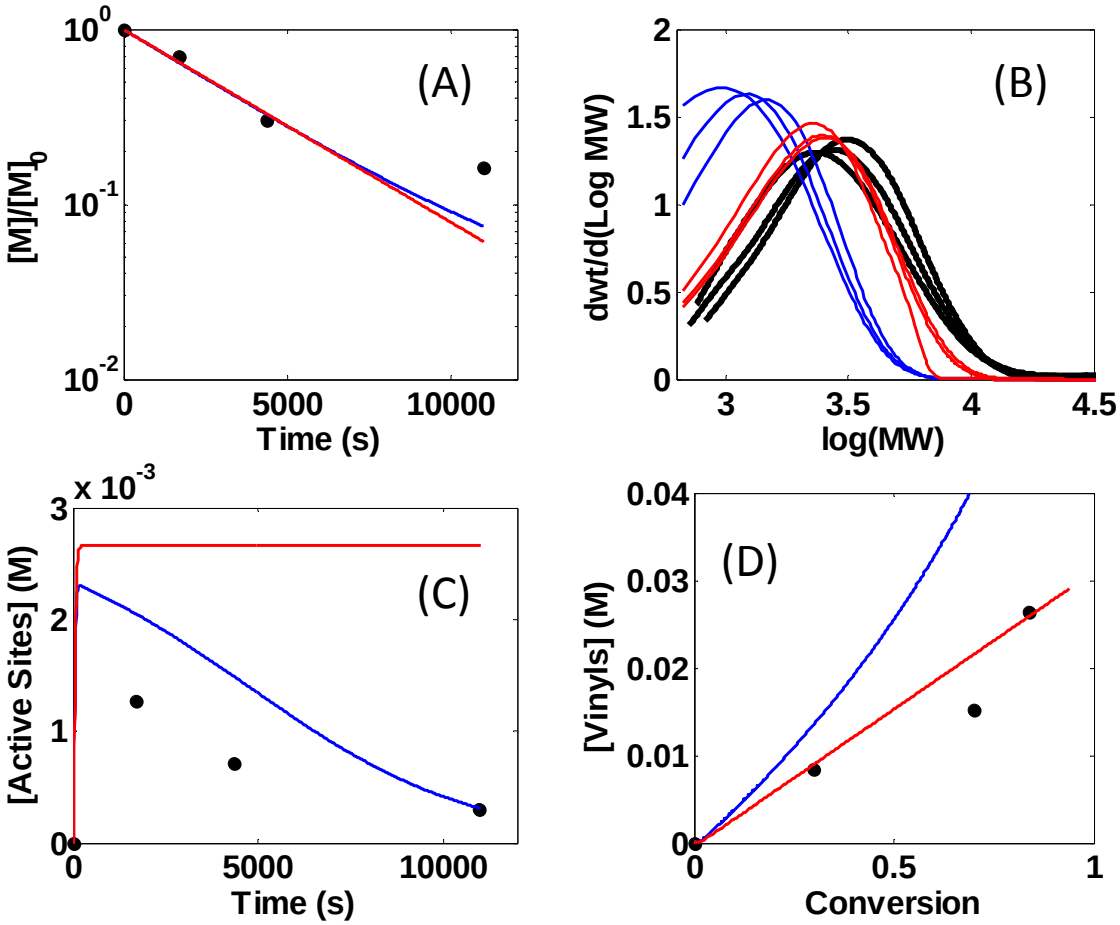

Figure 2.7. Modeling using Mechanism II; data (A) monomer consumption from three batch quenches at 1694, 4352, 10963 s (circles), (B) corresponding MWD of each quench (bold solid lines); fits (colored lines), (C) primary active site concentration; circles: data; solid lines: fit, (D) vinylidene concentration vs. monomer conversion; circles: data; lines: fit. $[C]_0$ = 3.0 mM, $[M]_0$ = 0.60 M. Blue: Mechanism II(i), rate constants: k_p = 0.087 M^{-1} s^{-1}, $k_{vinylidene}$ = 0.0046 s^{-1}. Red: Mechanism II(ii), rate constants: k_p = 0.08 M^{-1} s^{-1}, $k_{vinylidene}$ = 0.005 M^{-1} s^{-1}.

Both mechanisms shown in Figure 2.7 have advantages and disadvantages. The elimination mechanism (blue) captures the drop in active site concentration and the curvature of the vinyl concentration, but the transfer mechanism (red) has a better absolute fit to the distributions and vinyl data. In either case, additional refinement to the mechanism is necessary.

2.3.1.2.3 Mechanism III. Misinsertion with Slow Recovery and Monomer Independent Chain Transfer

Additional data was collected for this system that shows that secondary Hf-alkyls are present during polymerization. To account for such a species, a monomer misinsertion reaction has been added to the mechanism, along with a slow recovery rate, which allows for secondary site accumulation. (The absence of a recovery rate altogether would lead to an ever increasing concentration of secondary sites over the course of the reaction, which is not supported by the data.) These reaction steps, along with monomer independent chain transfer, were used to predict the data, and the result is in Figure 2.8. The fit does an excellent job at fitting all the data shown except for the secondary active sites. Also, this model does not have the capability to fit vinylene data (not shown in Figure 2.8). An alternate mechanism is therefore required.

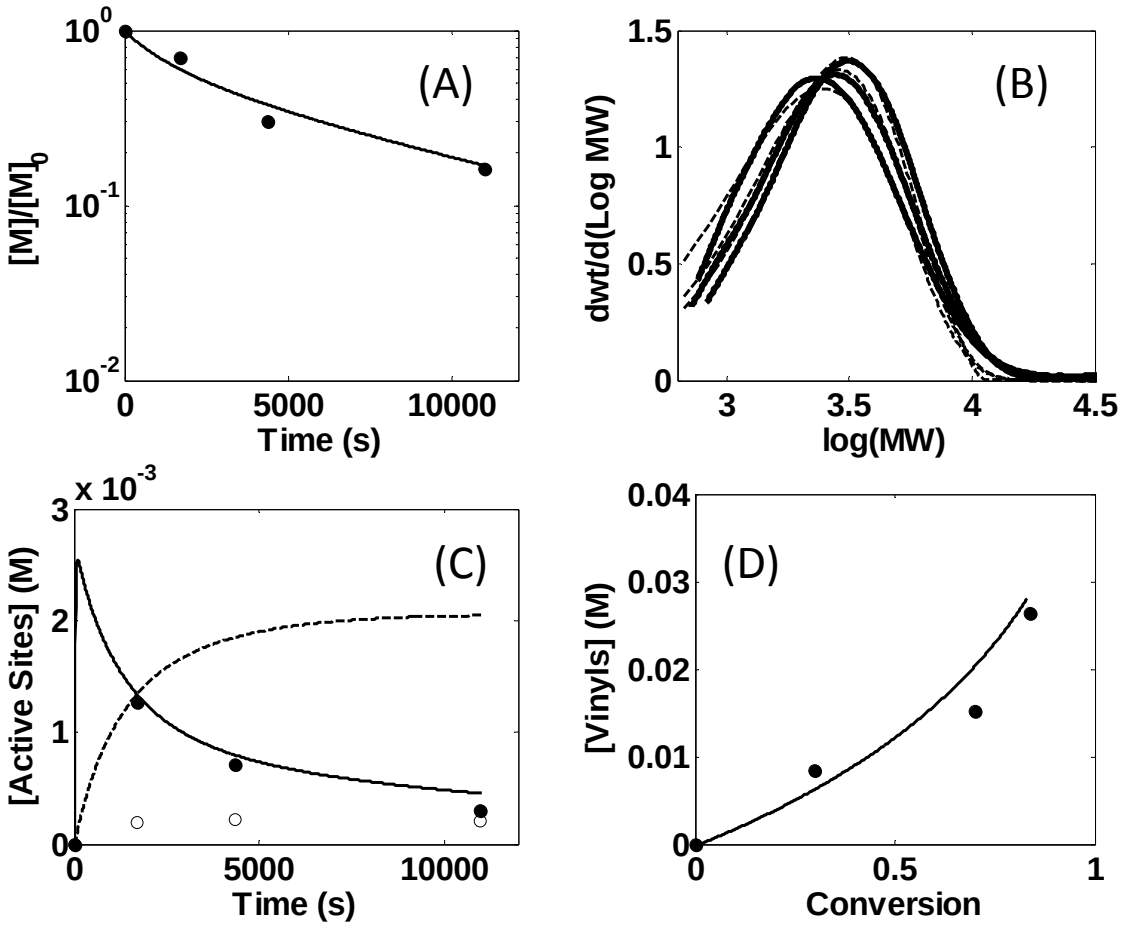

Figure 2.8. Modeling using Mechanism III; (A) monomer consumption from three batch quenches at 1694, 4352, 10963 s (circles), (B) corresponding MWD of each quench (bold solid lines) with different fits; fits (dashed lines), (C) active site concentrations; filled circles: primary sites, open circles: secondary sites; solid line: primary site fit; dashed line: secondary site fit, (D) vinylidene concentration vs. monomer conversion; circles: data; line: fit. Rate constants: $k_i = k_p = 0.14$ M^{-1} s^{-1}, $k_{vinylidene} = 0.0029$ s^{-1}, $k_{mis} = 0.00097$ M^{-1} s^{-1}, $k_{rec} = 0.00024$ M^{-1} s^{-1}. $[C]_0 = 3.0$ mM, $[M]_0 = 0.60$ M.

2.3.1.2.4 Mechanism IV. Slow Initiation and Chain Transfer

The overprediction of the active site concentrations and the underprediction of the MWD peaks in Mechanism II suggest that chain initiation may be slow relative to propagation. If this mechanism is amended by a slow initiation process (in the absence of

misinsertion) the resulting model prediction can be improved, as shown in Figure 2.9. As in Mechanism II, Mechanism IV(i) uses β-H elimination (monomer independent), while Mechanism IV(ii) uses β-H transfer.

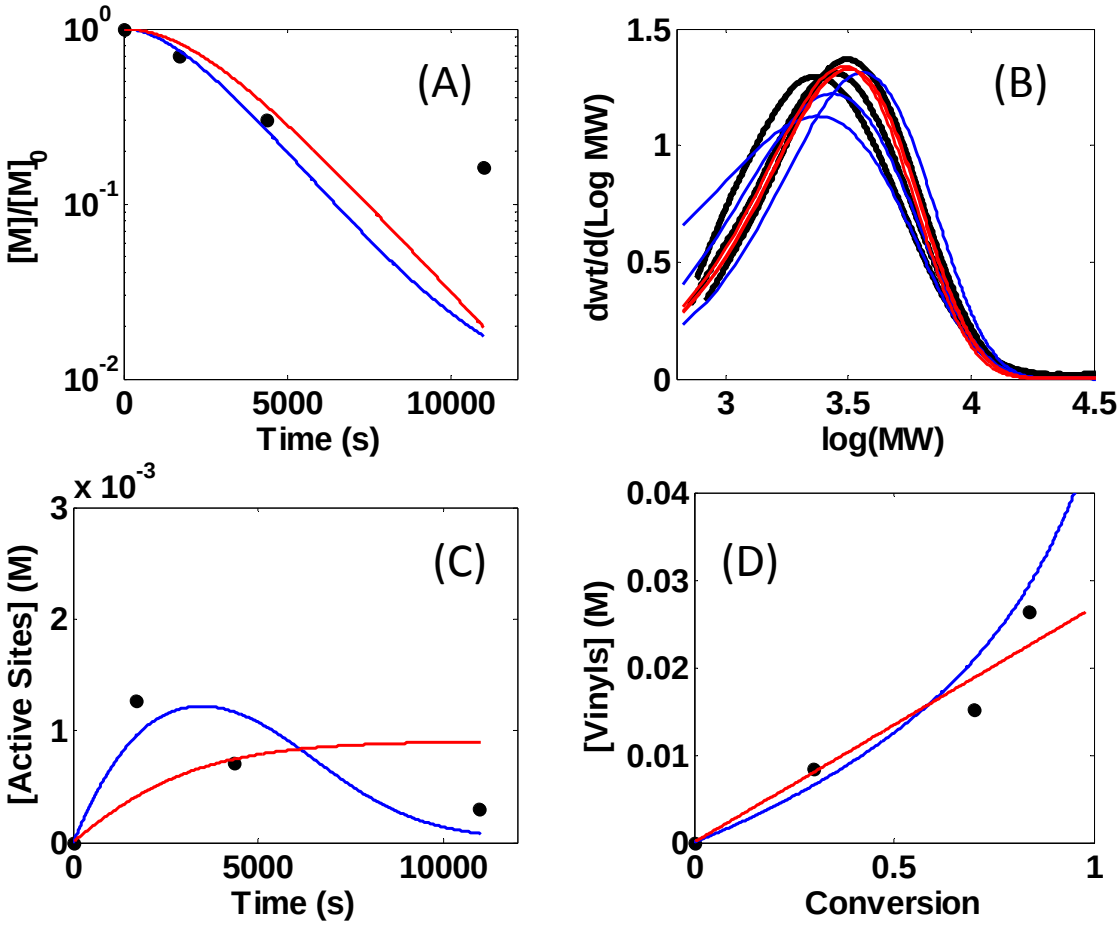

Figure 2.9. Modeling using Mechanism IV; data (A) monomer consumption from three batch quenches at 1694, 4352, 10963 s (circles), (B) corresponding MWD of each quench (bold solid lines); fits (colored lines), (C) primary active site concentration; circles: data; solid lines: fit, (D) vinylidene concentration vs. monomer conversion; circles: data; lines: fit. $[C]_0$ = 3.0 mM, $[M]_0$ = 0.60 M. Blue: Mechanism IV(i), rate constants: k_p = 0.27 M^{-1} s^{-1}, k_i = 0.00049 M^{-1} s^{-1}, $k_{vinylidene}$ = 0.0057 s^{-1}. Red: Mechanism IV(ii), rate constants: k_p = 0.44 M^{-1} s^{-1}, k_i = 0.00017 M^{-1} s^{-1}, $k_{vinylidene}$ = 0.023 M^{-1} s^{-1}.

Relative to Mechanism II, the elimination mechanism (blue) is much improved compared to the transfer mechanism (red). Nonetheless, there is still the need for a model that can predict secondary active sites, which have not yet been shown due to clarity.

2.3.1.2.5 Mechanism V. Slow Initiation, Chain Transfer, and Misinsertion with Slow Recovery

To account for all observed species, the additions to all previous mechanisms are here considered simultaneously. Monomer independent vinylidene formation is preferred to monomer dependent formation due to its ability to predict the curvature in the vinylidene data. In addition, chain transfer following misinsertion of monomer is added due to the vinylene groups that are observed. Vinylene may potentially form via monomer independent β-H elimination or monomer dependent β-H transfer to monomer. Both are presented in Figure 2.10, with blue representing elimination and red representing transfer. The vinylene fits in Figure 2.10D show that the monomer dependent transfer reaction is preferred due to its linear behavior, similar to the data. However, neither series of pathways is able to capture the late reaction monomer concentration behavior. Additional changes to the model are necessary.

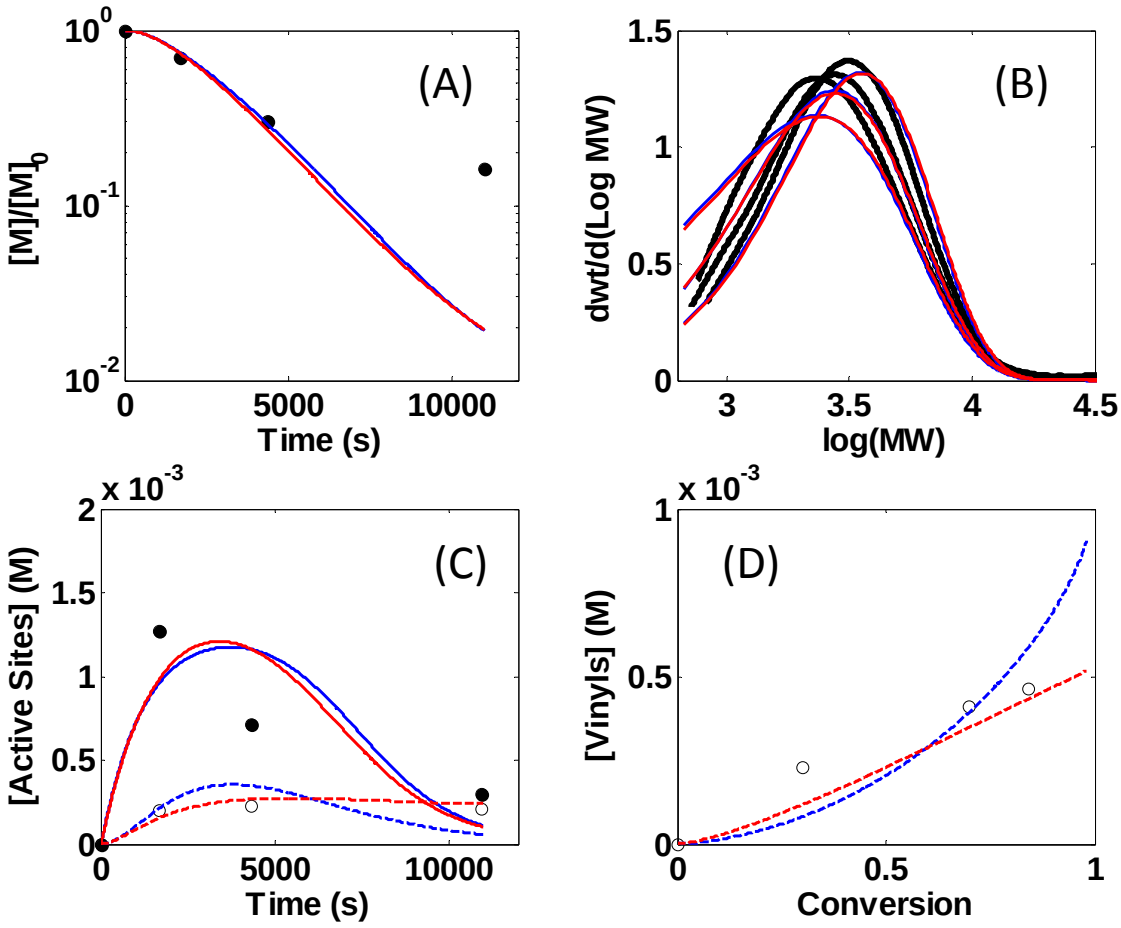

Figure 2.10. Modeling using Mechanism V; data (A) monomer consumption from three batch quenches at 1694, 4352, 10963 s (circles), (B) corresponding MWD of each quench (bold solid lines); fits (colored lines), (C) active site concentrations; filled circles: primary sites, open circles: secondary sites; solid line: primary site fit; dashed line: secondary site fit, (D) vinylene concentration vs. monomer conversion; open circles: data; dashed lines: fit. $[C]_0$ = 3.0 mM, $[M]_0$ = 0.60 M. Blue: Mechanism V(i), rate constants: k_p = 0.25 M^{-1} s^{-1}, k_i = 0.00064 M^{-1} s^{-1}, $k_{vinylidene}$ = 0.0052 s^{-1}, $k_{vinylene}$ = 0.0004 s^{-1}, k_{mis} = 0.0005 M^{-1} s^{-1}, k_{rec} = 0. Red: Mechanism V(ii), rate constants: k_p = 0.26 M^{-1} s^{-1}, k_i = 0.00062 M^{-1} s^{-1}, $k_{vinylidene}$ = 0.0053 s^{-1}, $k_{vinylene}$ = 0.0016 M^{-1} s^{-1}, k_{mis} = 0.00056 M^{-1} s^{-1}, k_{rec} = 0.00087 M^{-1} s^{-1}.

2.3.1.2.6 Mechanism VI. Slow Initiation, Chain Transfer, Misinsertion with Slow Recovery, and Deactivation

In order to account for the monomer consumption behavior, a deactivation reaction is assumed to occur. This reaction in first order in active catalyst concentration and does not involve monomer. This reaction may be due to air sensitivity of the catalyst or a poison introduced during the experiment. When this pathway is added to Mechanism V, the result is much improved. This model is reported in the main text, and the rate constants are reported in Table 2.1, along with the values: $k_{vinylene}$ = 0.00097 M^{-1} s^{-1} and $k_{deactivation}$ = 0.00020 s^{-1}. This model also provides a good fit of data collected in smaller NMR-scale experiments, which were performed at different initial concentrations (Figure 2.11).

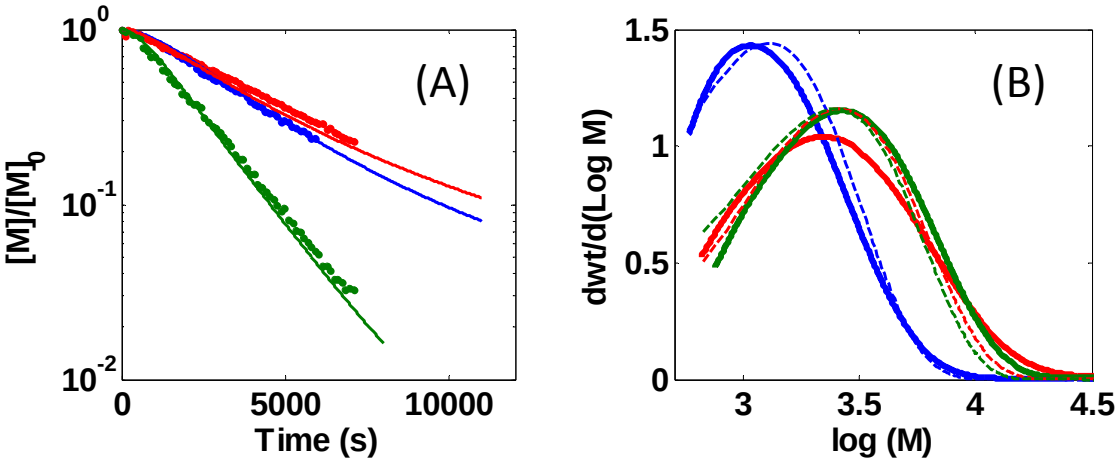

Figure 2.11. Modeling using Mechanism VI; data (A) monomer consumption from three NMR trials (circles), (B) corresponding endpoint MWD (bold solid lines); fits (dashed lines). Blue: $[C]_0$ = 3.0 mM, $[M]_0$ = 0.30 M, Red: $[C]_0$ = 3.0 mM, $[M]_0$ = 0.60 M, Green: $[C]_0$ = 6.0 mM, $[M]_0$ = 0.60 M. Rate constants: reported in Table 3.1.

2.3.1.3 Kinetic Modeling of Hf[^{t}Bu-ON^{NMe2}O]Bn$_2$ Catalyst System (**3b**)

2.3.1.3.1 Mechanism I. Living Polymerization

As before, we start by using the living polymerization model with the initiation rate constant equal to the propagation rate. The monomer consumption data (Figure 2.12A) is somewhat accurate, but the MWD fits are very poor (Figure 2.12B), predicting distributions that are much narrower than the data and have incorrect peak MWs.

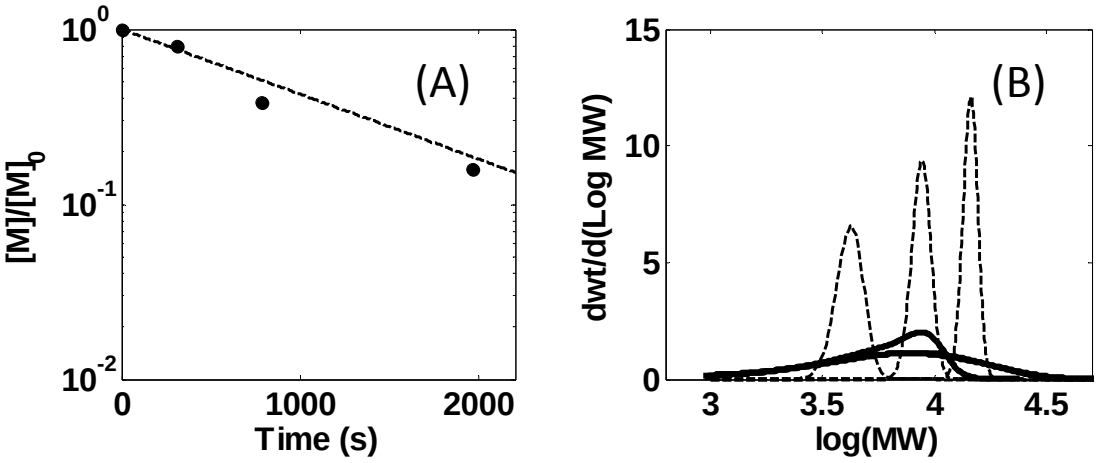

Figure 2.12. Modeling using Mechanism I; data (A) monomer consumption from three batch quenches at 310, 788, 1961 s (circles), (B) corresponding MWD of each quench (bold solid lines); fits (dashed lines); rate constants: $k_i = k_p = 0.30$ M^{-1} s^{-1}. $[C]_0 = 2.85$ mM, $[M]_0 = 0.60$ M.

2.3.1.3.2 Mechanism II. Vinylidene Formation Via Chain Transfer

To account for the broader distributions and vinyl species measured by experiment, chain transfer will also be included in the mechanism. Vinylidene groups may once again be formed through either a β-H elimination (monomer independent; Mechanism II(i)) pathway or a β-H transfer to monomer (mechanism II(ii)) pathway. Both are compared in

Figure 2.13. The elimination pathway (blue) seems to provide a better fit of the vinylidene data due to its ability to predict an upward curve at higher monomer conversion.

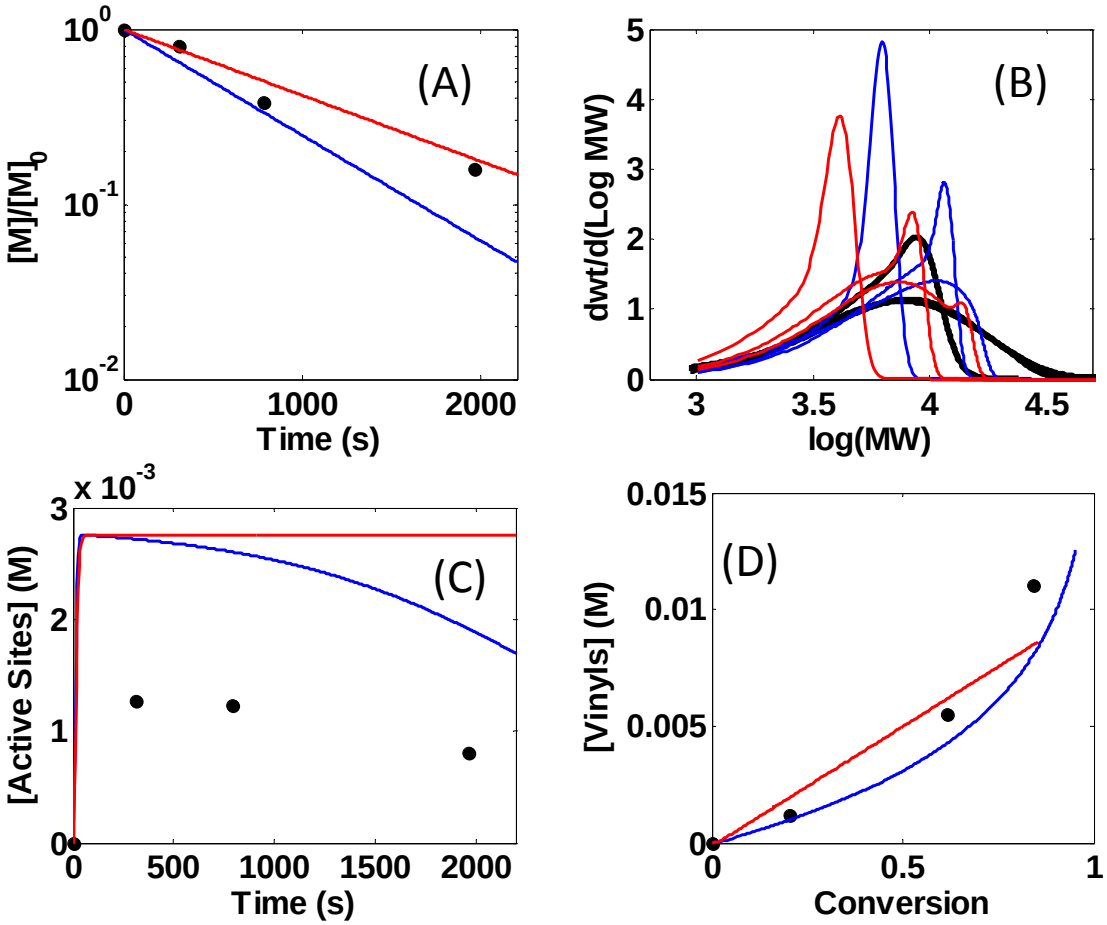

Figure 2.13. Modeling using Mechanism II; data (A) monomer consumption from three batch quenches at 310, 788, 1961 s (circles), (B) corresponding MWD of each quench (bold solid lines); fits (colored lines), (C) primary active site concentration; circles: data; solid lines: fit, (D) vinylidene concentration vs. monomer conversion; circles: data; lines: fit. $[C]_0$ = 2.85 mM, $[M]_0$ = 0.60 M. Blue: Mechanism II(i), rate constants: k_p = 0.49 M^{-1} s^{-1}, $k_{vinylidene}$ = 0.0023 s^{-1}. Red: Mechanism II(ii), rate constants: k_p = 0.30 M^{-1} s^{-1}, $k_{vinylidene}$ = 0.0054 M^{-1} s^{-1}.

2.3.1.3.3 Mechanism III. Slow Initiation and Chain Transfer

A slow initiation rate constant may be present in this system. Its effect can be seen in the initial points of the monomer consumption data. Furthermore, a slow initiation rate would push the early MWDs to higher molecular weights. When this model is fit to the data, an improved fit can indeed be seen (Figure 2.14). This mechanism is an improvement over Mechanism II, but it still lacks the ability to predict vinylene end groups (not shown in Figure 2.14), and it over predicts the concentration of active sites late in the reaction.

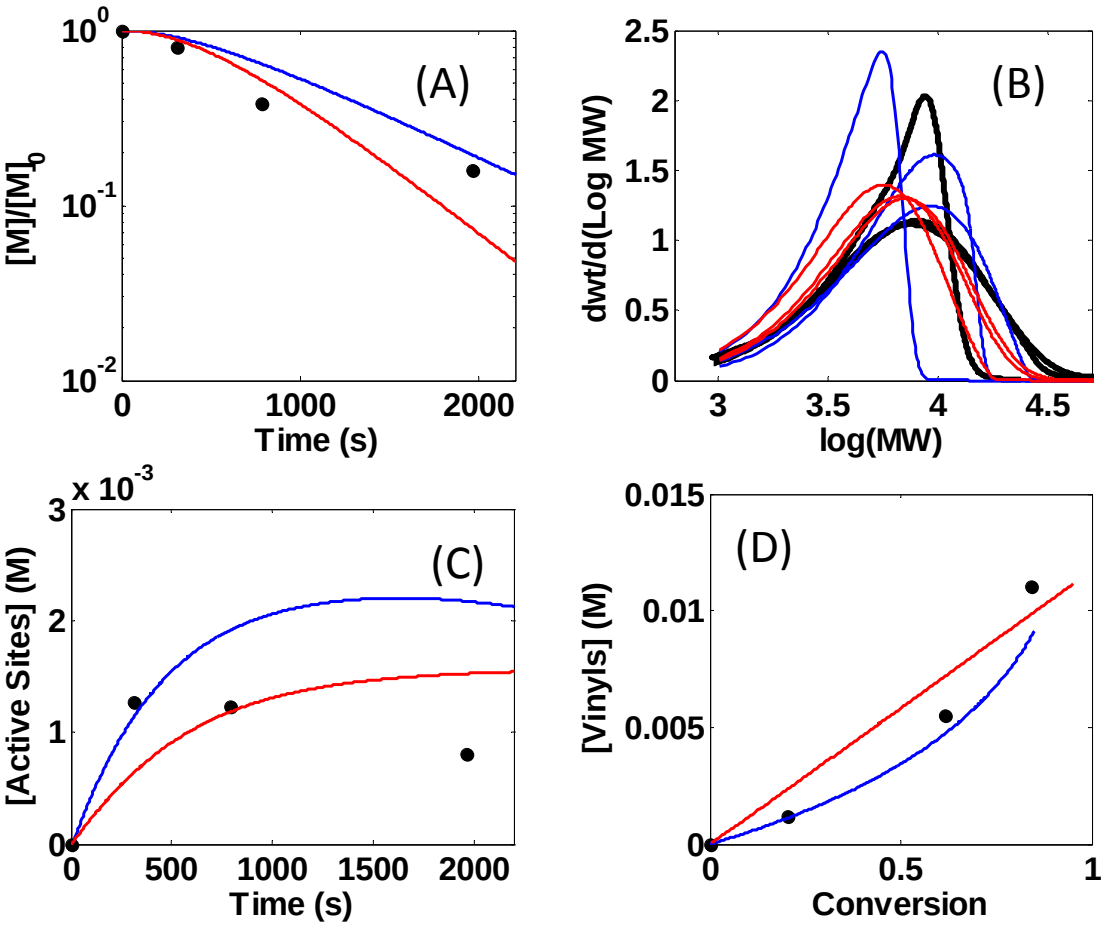

Figure 2.14. Modeling using Mechanism IV; data (A) monomer consumption from three batch quenches at 310, 788, 1961 s (circles), (B) corresponding MWD of each quench (bold solid lines); fits (colored lines), (C) primary active site concentration; circles: data; solid lines: fit, (D) vinylidene concentration vs. monomer conversion; circles: data; lines: fit. $[C]_0$ = 2.85 mM, $[M]_0$ = 0.60 M. Blue: Mechanism III(i), rate constants: k_p = 0.44 M^{-1} s^{-1}, k_i = 0.0030 M^{-1} s^{-1}, $k_{vinylidene}$ = 0.0023 s^{-1}. Red: Mechanism III(ii), rate constants: k_p = 1.1 M^{-1} s^{-1}, k_i = 0.0015 M^{-1} s^{-1}, $k_{vinylidene}$ = 0.023 M^{-1} s^{-1}.

2.3.1.3.4 Mechanism IV. Slow Initiation, Chain Transfer, and Incomplete Catalyst Participation

Mechanism III(i) is preferable to Mechanism III(ii) due to its ability to capture the curve in the vinylidene data (Figure 2.15D). However, this mechanism over predicts the

primary active site concentration (Figure 2.15C). In addition, the early time MWD has a higher MW than predicted. Both of these differences may be accounted for with the assumption that not all of the catalyst actively participates in the reaction. This new assumption is used to predict the data in Mechanism IV, along with a monomer-dependent reaction that will generate vinylene species. No secondary active sites were detected, so the model predicts that vinylene is formed from a reaction involving a primary active site and a monomer even though the true reaction may involve a two step process of monomer misinsertion followed by fast chain transfer. The result for this model is in Figure 2.16.

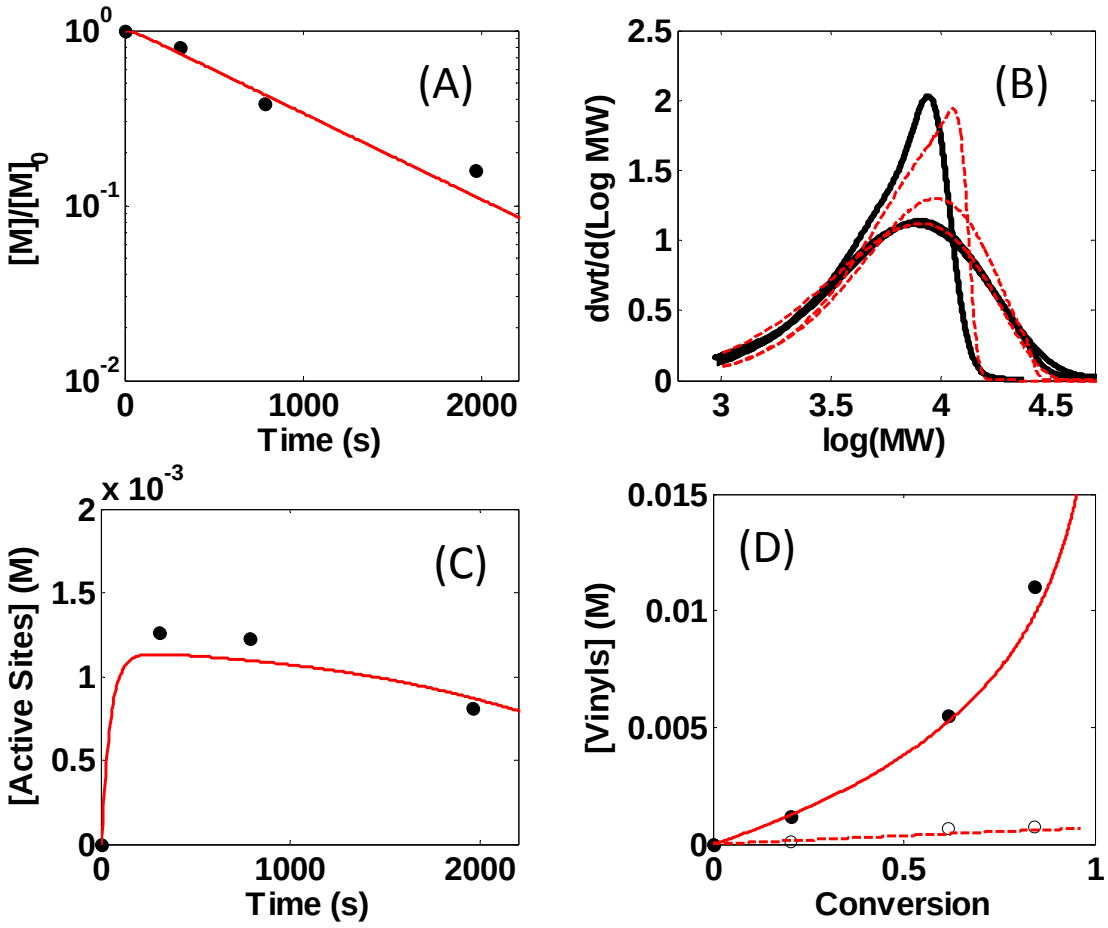

Figure 2.15. Modeling using Mechanism IV; data (A) monomer consumption from three batch quenches at 310, 788, 1961 s (circles), (B) corresponding MWD of each quench (bold solid lines); fits (red lines), (C) active site concentrations; circles: primary sites; solid line: fit, (D) vinyl concentration vs. monomer conversion; filled circles: vinylidene concentration, open circles: vinylene concentration, solid line: vinylidene fit, dashed line: vinylene fit. $[C]_0$ = 2.85 mM, $[M]_0$ = 0.60 M. Red: Mechanism IV, rate constants: k_p = 0.95 M^{-1} s^{-1}, k_i = 0.037 M^{-1} s^{-1}, $k_{vinylidene}$ = 0.0055 s^{-1}, k_{mis} = 0.0012 M^{-1} s^{-1} (forms vinylene), active catalyst = 42%. Rates also reported in main text.

Additional data was collected for this catalyst in NMR scale reactions with different initial catalyst and monomer concentrations. The fit using Mechanism IV and the rate constants in the main text (also in the Figure 2.15 caption) to these data are in Figure 2.16.

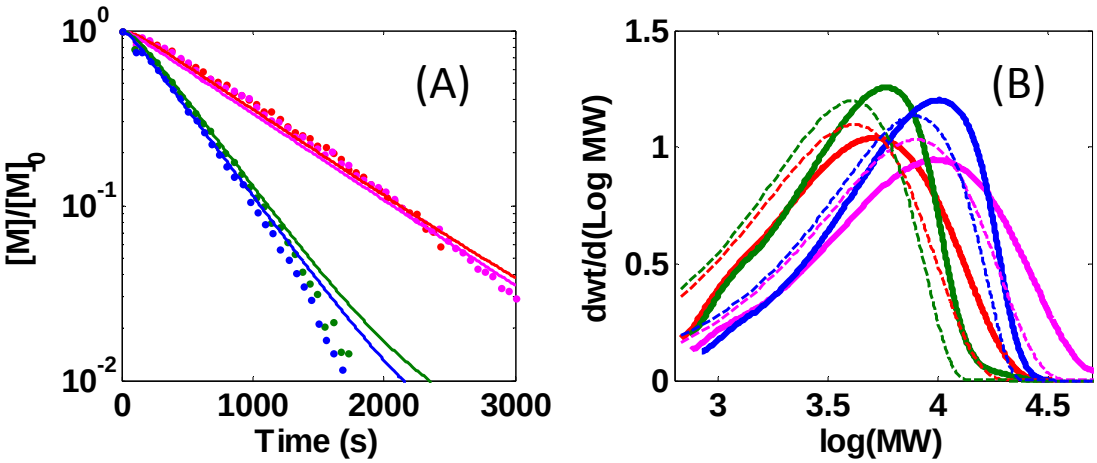

Figure 2.16. Modeling using Mechanism IV; data (A) monomer consumption from four NMR trials (circles), (B) corresponding endpoint MWD (bold solid lines); fits (dashed lines). Blue: $[C]_0$ = 6.0 mM, $[M]_0$ = 0.60 M, Green: $[C]_0$ = 6.0 mM, $[M]_0$ = 0.30 M, Magenta: $[C]_0$ = 3.0 mM, $[M]_0$ = 0.60 M. Red: $[C]_0$ = 3.0 mM, $[M]_0$ = 0.30 M. Rate constants: reported in Figure 3.20 caption.

2.4 Discussion

In this chapter, the complete set of kinetic rate constants for a zirconium amine bis-phenolate catalyst system and two hafnium amine bis-phenolate catalysts systems have been presented. By successfully fitting the diverse data sets using comprehensive kinetic modeling, the 1-hexene polymerization mechanisms for these catalysts (**5a**, **2b**, and **3b**) have been shown to consists of the following elementary reaction steps: initiation, normal propagation, misinsertion, recovery, and chain transfer, with these values shown in Table 2.1 along with other Zr and Hf catalysts**.**

Table 2.1. Rate constants for 1-hexene polymerization by M[tBu-ON^{X}O]Bn$_2$/B(C_6F_5)$_3$ catalysts **1a-5a** and **1b-3b**.[a]

M	Zr(a)					Hf(b)		
X	THF (1)	Py (2)	NMe_2 (3)	Furan (4)	SMe (5)[b]	THF (1)	Py (2)	NMe_2 (3)
M—X/ Å	2.37	2.51	2.59	2.69	2.89	2.33	2.47	2.56
k_i/ M^{-1} s^{-1}	0.08	0.017	0.16	0.0031	0.017	0.04	0.0017	0.04
k_p/ M^{-1} s^{-1}	8.0	1.35	11	3.52	12	0.53	0.20	0.95
k_{mis}/ M^{-1} s^{-1}	0.054	0.077	0.055	0.0064	0.20	0.0081	0.00028	0.0012[c]
k_{rec}/ M^{-1} s^{-1}	0.047	0.052	0.04	0[c]	0.036	0.06	0.0002	*N/A*
$k_{vinylidene}$ (10^{-3})/ s^{-1}	0.14	1.34	12.2	1.00	0	0.84	3.8	5.5
$k_{vinylene}$ (10^{-3})/ s^{-1}	0.051	0.44	8.72	0	0	0.27	0	[b]
$k_{vinylidene}$ (10^{-3})/ M^{-1} s^{-1}	0	0	0	12.1	2.2	0	0	0
$k_{vinylene}$ (10^{-3})/ M^{-1} s^{-1}	0	0	0	6.9	0.95	0	Fast	0

[a] In toluene at 25 °CSee Figure 2.1 for precatalyst structures and Scheme 2.1 for reactions steps. [b] The misinsertion reaction in the system **3b** mechanism is followed immediately by monomer independent β-H elimination to form vinylene.

As shown in in Table 2.1, the M-X bond distances were determined by single crystal X-ray crystallography and the catalyst structures were organized by increasing bond length for catalysts with the same metal center. Comparing this structural trend to the reaction rate constants, it is clear that the size of this M-X bond distances as well as the identity of the metal center has an effect on the chain transfer reaction pathway that produces vinylidene terminated polymers. Catalysts **1a-3a** and **1b-3b** exhibit increasing monomer independent vinylidene termination, $k_{vinylidene}$, with increasing M-X distance while catalysts **4a** and **5a** exhibited monomer dependent chain transfer. We believe that this specific chain transfer pathway is controlled by the catalyst sterics where the increased size in the active site correlates to increased chain transfer. In fact, a quantitative structure activity relationship, QSAR, can be calculated for **1a-3a** and **1b-3b** between the logarithm of the M-X bond distance and the $k_{vinylidene}$ rate constant, shown in Figure 2.17. Along this line of reasoning, there is a point where the decreased steric bulk opens up enough that the chain transfer path way changes from a monomer independent mechanism to a monomer dependent mechanism, such as in catalyst **5a**.

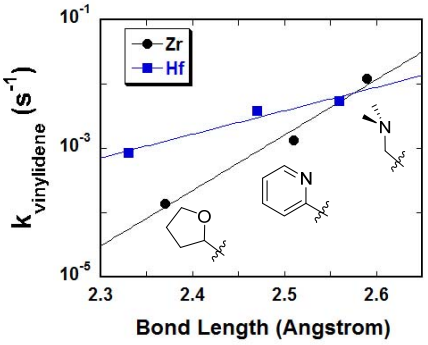

Figure 2.17 $k_{vinylidene}$ (s^{-1}) vs M-X distance for **1a-3a** and **1b-3b**

In terms of other reaction rate constants and mechanistic insight, the Hf catalysts **2b**, and **3b** exhibited decreasing k_{mis} while the Zr catalyst **5a** exhibited the largest k_{mis}. This suggests that the Hf catalysts seem to disfavors M-$C_{secondary}$ bond formation while the **5a** is more amendable to this type of insertion due to the different metal and sterically open active site. Furthermore, the Hf catalysts exhibit very fast chain transfer of the secondary carbon to form vinylene terminated groups when compared to their Zr analogues, along with a change in mechanism to a monomer dependent $k_{vinylene}$. These changes suggest that the identity of the metal center can play a dynamic role in terms of overall activity, 2,1-insertion, and the subsequent recovery or chain transfer of the misinserted sites.

2.5 Conclusion

Two relatable kinetic study of three catalytic systems based on Zr and Hf amine bis-phenolate complexes has been completed. Having determined the quantitative, elementary rate constants for initiation, propagation, misinsertions, recovery, and chain transfer, we have found a QSAR relating the distance between the metal-to-pendant crystal structure distance to the monomer-independent, vinylidene-forming chain transfer rate constant kvinylidene for Hf catalysts **2b** and **3b**. The zirconium catalyst **5a** did not follow such a correlation as we believe that the larger M-X distance causes a change in mechanism to become a monomer-dependent $k_{vinylidene}$ rate constant. Such insights are valuable in designing new catalysts and show the nuance required in determining mechanistic insight of catalyst structure.

2.6 References

(1) Chemical Market Associates, Inc. (CMAI), **2005** *World Polyolefins Analysis*, www.cmaiglobal.com.

(2) (a) Chen, E. Y-X.; Marks, T. J. *Chem. Rev.* **2000**, *100*, 1391-1434. (b) Li, H.; Marks, T. J. *Proc. Natl. Acad. Sci. USA* **2006**, *103*, 15295-15302.

(3) Manz, T. A.; Phomphrai, K.; Medvedev, G. A.; Krishnamurthy, B. B.; Sharma, S.; Haq, J.; Novstrup, K. A.; Thomson, K. T.; Delgass, W. N.; Caruthers, J. M.; Abu-Omar, M. M. *J. Am. Chem. Soc.* **2007**, *129*, 3776-3777.

(4) (a) Krauledat, H.; Brintzinger, H. H. *Angew. Chem. Int. Ed.* **1990**, *29*, 1412-1413. (b) Piers, W. E.; Bercaw, J. E. *J. Am. Chem. Soc.* **1990**, *112*, 9406-9707. (c) Coates, G. W.; Waymouth, R. M. *J. Am. Chem. Soc.* **1991**, *113*, 6270-6271.

(5) Britovsek, G. J. P.; Gibson, V. C.; Wass, D. F. *Angew. Chem. Int. Ed.* **1999**, *38*, 428-447.

(6) Arriola, D. J.; Carnahan, E. M.; Hustad, P. D.; Kuhlman, R. L.; Wenzel, T. T. *Science* **2006**, *312*, 714-719.

(7) Falsig, H.; Hvolbaek, B.; Kristensen, I. S.; Jiang, T.; Bligaard, T.; Christensen, C. H.; Norskov, J. K. *Angew. Chem. Int. Ed.* **2008**, *47*, 4835-4839.

(8) Schumacher, N.; Boisen, A.; Dahl, S.; Gokhale, A. A.; Kandoi, S.; Grabow, L. C.; Dumesic, J. A.; Mavrikakis, M.; Chorkendorff, I. *JCat* **2005**, *229*, 265-275.

(9) Novstrup, K. A.; Travia, N. E.; Medvedev, G. A.; Stanciu, C.; Switzer, J. M.; Thomson, K. T.; Delgass, W. N.; Abu-Omar, M. M.; Caruthers, J. M. *J. Am. Chem. Soc.* **2010**, *132*, 558-566.

(10) Tshuva, E.Y.; Goldberg, I.; Kol, M.; Goldschmidt, Z. *Organometallics*, **2001**, *20*, 3017-3028.

(11) Tshuva, E.Y.; Groysman, S.; Goldberg, I.; Kol, M.; Goldschmidt, Z. *Organometallics*, **2002**, *21*, 662-670.

(12) (a) Gauthier, W. J.; Corrigan, J. F.; Taylor, N. J.; Collins, S. *Macromolecules* **1995**, *28*, 3771−3778. (b) Razavi, A.; Ferrara, J. *J. Organomet. Chem*. **1992**, *435*, 299−310.

(13) Resconi, L.; Piemontesi, F.; Franciscono, G.; Abist, L.; Fioranit,T. *J. Am. Chem. Soc*. **1992**, *114*, 1025−1032.

(14) Abbas, R.; Ferrara, J. *J. Organomet. Chem*. **1992**, *435*, 299−310.

(15) Kissounko, D. A.; Zhang, Y.; Harney, M. B.; Sita, L. R. *Adv. Synth. Catal*. **2005**, *347*, 426−432.

(16) Mecking, S. *Angew. Chem. Int. Ed.* **2001**, *40*, 534-540, and references therein.

(17) Agapie, T.; Henling, L. M.; DiPasquale, A. G.; Rheingold, A. L.; Bercaw, J. E. *Organometallics*, **2008**, *27*, 6245-6256.

(18) Camacho, D. H.; Guan, Z. B. *Macromolecules* **2005**, *38*, 2544-2546.

(19) Margl, P.; Deng, L. Q.; Ziegler, T. *J. Am. Chem. Soc.* **1999**, *121*, 154-162.

(20) Busico, V.; Cipullo, R.; Friederichs, N.; Ronca, S.; Talarico, G.; Togrou, M.; Wang, B. *Macromolecules* **2004**, *37*, 8201-8203.

(21) Camacho, D. H.; Guan, Z. B. *Macromolecules* **2005**, *38*, 2544-2546.

(22) (a) Meinhard, D.; Wegner, M.; Kipiani, G.; Hearley, A.; Reuter, P.; Fischer, S.; Marti, O.; Rieger, B.*J. Am. Chem. Soc.,* **2007**, *129*, 9182-9191. (b) Anselment, T. M. J.; Wichmann, C.; Anderson, C. E.; Herdtweck, E.; Rieger, B. *Organometallics,* **2011**, *30*, 6602-6611.

(23) Doi, Y.; Ueki, S.; Keii, T. *Macromolecules* **1979**, *12*, 814-819.

(24) Naga, N.; Mizunuma, K. *Polymer* **1998**, *39*, 5059-5067.

(25) Chen, M-C.; Roberts, J. A. S.; Marks, T. J. *J. Am. Chem. Soc.* **2004**, *126*, 4605-4625.

(26) Wilson, P. A.; Hannant, M. H.; Wright, J. A.; Cannon, R. D.; Bochmann, M. *Macromol. Symp.* **2006**, *236*, 100-110.

(27) Liu, Z.; Somsook, E.; Landis, C. R. *J. Am. Chem. Soc.* **2001**, *123*, 2915−2916.

(28) Switzer, J. M.; Travia, N. E.; Steelman, D. K.; Medvedev, G. A.; Thomson, K. T.; Delgass, W. N.; Abu-Omar, M. M.; Caruthers, J. M. *Macromolecules*, **2012**, *45*, 4978-4988.

CHAPTER 3. QUANTITATIVE COMPARATIVE KINETICS OF 1-HEXENE POLYMERIZATION ACROSS GROUP IV BIS-PHENOLATE CATALYSTS

3.1 Introduction

Homogeneous olefin polymerization catalysts provide a well-defined, single-site structure that is attractive to study because a deeper understanding of structure–function relationships can be developed.[1-4] Such relationships are not only interesting academically but also industrially as polyolefin capacity is projected to grow to nearly 170 billion kg by 2018.[5] While much of the underlying organometallic reaction chemistry of olefin polymerization has been uncovered over the past decades,[6] quantitative kinetic data enabling direct comparison of the rate constants of elementary steps is lacking. Many of the structure–function relationships have been driven by qualitative comparisons based on activity measurements or turnover frequency (TOF).[7] Caution must be exercised in using TOFs, as they represent a combination of rate constants—i.e. multiple effects are embedded in one measurement—and are strongly dependent on the reaction initial conditions. A feature of catalytic olefin polymerization that makes it an excellent candidate for quantitative kinetic studies is the richness of data that can be obtained from time-dependent batch reactions. In recent years, it has been demonstrated how a data set including monomer consumption, active site counting, and vinyl end group analysis can robustly determine the catalytic mechanism and quantify rate constants.[8,9]

A primary example is the comparison of different group IV metal centers for organometallic olefin polymerization. Reports of group IV dichloride metallocenes utilizing methylaluminoxane (MAO) cocatalysts reveal that the ethylene polymerization activities are ordered by metal center: Zr > Ti > Hf.[10] These observations are rationalized via difference in metal–carbon bond enthalpies, i.e. breaking a strong Hf–carbon bond via monomer insertion results in a lower TOF while more labile Ti/Zr–carbon bonds allow for higher TOFs.[10g] This activity trend has also been reported in constrained geometry catalysts.[11] Additional work by Ihm and coworkers suggest that the difference in activity between the Ti and Zr catalysts could be attributed to deactivation of Ti active sites.[10h] Additionally, computational work by Ziegler and coworkers showed increases to the monomer insertion activation energy going down group IV (Ti < Zr < Hf).[12] They rationalized that while this trend did not match the experimental trends, side reactions reduced the number of Ti active sites, whereas their calculations reflected the reactivity of the metal center. Furthermore, experimental polyethylene activities by group IV bis(phenoxy-imine) catalysts exhibit a different trend (Zr > Hf > Ti), which could be the result of unstable Ti species.[12] These studies underscore the fact that the metal center is only one of many factors (e.g. active site concentration) that influence the activity measurement.[6,10,11]

The polymerization activity of linear α-olefins, e.g. 1-hexene, by group IV catalysts does not necessarily follow the metallocene polyethylene activity trends. Group IV [OSSO] bis(phenolato)/tris(pentafluoroaryl) borane ($B(C_6F_5)_3$) systems[6] yield 1-hexene activity trends of Ti > Zr > Hf,[13a] while group IV [ONNO] Salan/$B(C_6F_5)_3$ systems instead exhibit

1-hexene activity trends of Zr > Ti ~ Hf.[13b] These studies suggest that the monomer is another factor that influences the activity of group IV catalysts.

Within the activity measurement of α-olefins, the salient reaction is the propagation step, typically by 1,2-insertion. A 2,1-insertion is regarded as a misinsertion and directly affects polymer properties.[14] For some catalysts, a 2,1-insertion results in immediate chain termination. This produces a vinylene terminated polymer and reduces the overall molecular weight (M_w) and molecular number (M_n) of the polymer. For other systems, a 2,1-insertion produces an inactive catalyst, a dormant site that reduces the rate of polymerization.[14d] The dormant catalyst can chain terminate or recover to the active species via 1,2-insertion and the formally misinserted monomer then becomes a regioerror.[8,14b]

The type of α-olefin insertion affects the regioselectivity. For some metallocene catalysts, increased steric bulk suppresses 2,1-misinsertion.[14a,15] Alternatively, some nonmetallocene systems, with overly constrained sterics, have been reported to propagate normally a 2,1-insertion.[16] Marks and coworkers also reported that binuclear constrained geometry catalysts influenced the mechanism of ethylene–styrene copolymers by increasing 1,2-insertion for styrene.[17] Regioselectivity is also affected by monomer electronics.[18] Nozaki and coworkers, as well as others, noted that the regioselectivity of functionalized monomers shows a dependence on the electron donating (1,2-insertion favored) or electron withdrawing (2,1-insertion favored) substituents of the monomer in copolymerization with ethylene for palladium catalysts.[19]

Prior to this report, we are not aware of studies that use quantitative kinetic modeling tools to study the influence of the group IV metal center on misinsertions and regioerrors of 1-hexene.[20] However, there are some literature examples on the effect of

group IV metal center on regioselectivity and regioerrors. The Oliva group was able to affect the regioselectivity in styrene insertion for hydro-oligomerization; specifically, by changing the metal center from Zr to Hf while reacting p-methyl styrene instead of styrene, they increased selectivity for the 1,2-insertion product.[21] They reasoned that the change in regioselectivity was due to increased electron density at the incoming metal–carbon bond for Hf and p-methyl styrene, where the increased electron density favors 1,2-insertion over 2,1-insertion. Also, Busico et al. reported a ~4x drop in polypropylene regioerrors catalyzed by Hf Salans when compared to Zr Salan catalysts.[22]

Polymer chain length is an important feature in olefin polymerization. The average length of a polymer chain at the moment termination occurs is related to the ratio of the propagation rate to the chain transfer rate, which is typically inferred from the endpoint polymer M_n. Polyethylene polymerization studies of group IV metallocene catalysts reveal that the highest M_n polymers are produced by the metal center in the order of Ti > Hf > Zr.[10] These values are indicative of differences between metal–carbon to metal–hydride bond strengths among the group IV metal centers.[10g] Computational work by Ziegler et al. also supports the conclusion that changes in the metal–carbon and metal–hydride bond enthalpies are an important factor in the termination reaction.[23]

In this study, we describe detailed kinetics of the Ti catalysts **1a**–**3a**, Figure 3.1, and compare these rate constants to those for Zr (**1b**–**3b**) and Hf (**1c**–**3c**) catalysts, in Table 3.1.[9c,9d] The M–X bond length for these catalysts is ordered as M–THF < M–Pyridine < M–NMe_2. These catalysts were initially synthesized and studied by Kol and co-workers.[24–26] Using TOFs and M_n from the end of reaction, they determined a 1-hexene activity trend of Zr > Hf > Ti and polymer M_n trend of Ti > Zr > Hf; however, they did not determine

how the underlying fundamental rate constants change with the metal site. In this study, we will quantitatively show the difference in magnitude of elementary rate constants across the group IV catalysts. The effect of metal on 2,1-insertion and regioerrors is quantified. The polymer M_n, which is influenced by the ratio of the propagation rate to the termination rate, follows the trend of Zr > Ti > Hf, which is different compared to the relationship reported by Kol using the M_n reported from the end of reaction. Finally, we show a linear relationship between the logarithm of the rate constant of vinylidene formation and the precatalyst Ti–pendant bond length that is similar to the relationships observed previously with other group IV complexes.[9c]

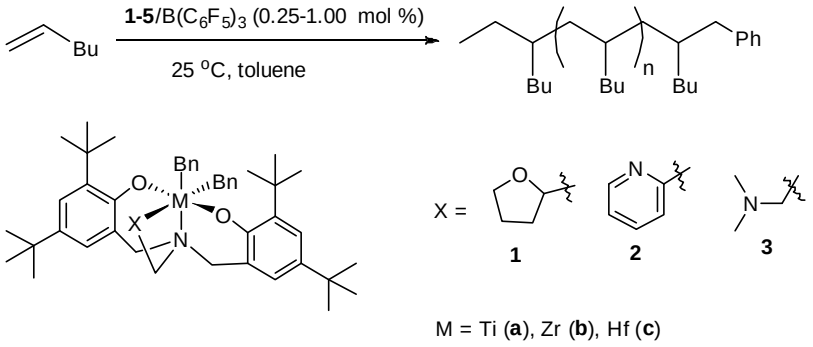

Figure 3.1. 1-hexene polymerization catalyzed by titanium/zirconium/hafnium salan-type catalysts **1a-3c** when combined with the activator $B(C_6F_5)_3$

3.2 Experimental Procedure

General Procedure: All manipulations were performed under dry inert atmosphere in a glove box or at a vacuum manifold using air sensitive techniques under N_2 or Ar atmosphere. Toluene and pentane were distilled over activated alumina and a copper catalyst using a solvent purification system (Anhydrous Technologies) and degassed

through freeze-pump-thaw cycles. Both solvents were stored over activated molecular sieves. Tetrabenzylzirconium was purchased from STREM and used as received. The monomer 1-hexene was purchased from Aldrich and purified by distillation over a small amount of dimethyl bis(cyclopentadienyl)zirconium and stored over molecular sieves. Tris(pentafluorophenyl)boron was purchased from STREM and purified by sublimation. Diphenylmethane was purchased from Aldrich and stored over molecular sieves. CH_3OD was purchased from Cambridge Isotopes and used as received. D_8-toluene was used as received and stored over molecular sieves. ^1H and ^2H NMR experiments were performed on a Varian INOVA600 MHz or Bruker DRX500 MHz spectrometer.

The ligands and precatalysts (**1a-3c**) were prepared following modified literature procedures.[24-26] We describe herein the details for the titanium based systems. The zirconium/hafnium analogs, previously described in Chapter 2, will not be shown here.

Synthesis of 6,6'-((((Tetrahydrofuran-2-yl)methyl)-azanediyl)bis(methylene))bis(2,4-di-tert-butylphenol), ^{t}Bu-ON^{THF}O ligand (1). In a typical synthesis,[24-26] Scheme 3.1, an 80 ml reaction vessel was charged with 2,4-di-tert-butylphenol (6.19g, 30.0 mmol), 2-(aminomethyl)tetrahydrofuran (1.55 mL, 15 mmol), and 37% histological grade formaldehyde (6.00 mL, 80 mmol), distilled water, and a stir bar while maintaining a maximum volume of 80 ml. The biphasic reaction mixture was placed in a CEM microwave reactor and allowed to warm to 100^{o}C over 5 min while stirring. The reaction was allowed to stand at 100^{o}C for 30 min and cold, dry methanol was added to the organic phase. This mixture was shaken for 30 min and the resulting solid was isolated by vacuum

filtration. The crude ligand product was purified by crystallization from ethanol (28% yield).

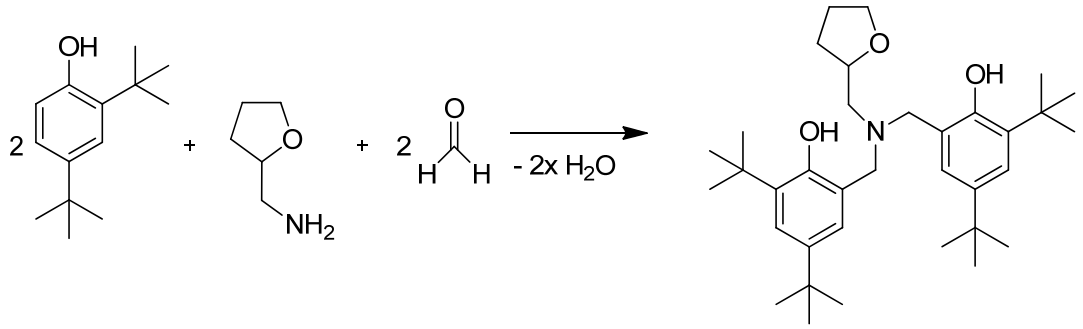

Scheme 3.1. Synthesis of the ^{t}Bu-ON^{THF}O ligand (**1**)

Synthesis of Ti[^{t}Bu-ON^{THF}O]Bn$_2$ (1a). In a typical synthesis,[24-26] Scheme 3.2, a 100 ml flask was charged with titanium(IV) tetrachloride (.361 g, 1.9 mmol), 20 ml toluene, and a stir bar before being fitted with a rubber septum. A second 100 ml flask was charged with **1** (1 g, 1.9 mmol) and 20 ml of toluene. A third 100 ml flask, 2 equivalents of benzylmagnesium chloride (3.8 ml, 3.8 mmol) and 20 ml of diethyl ether were charged. The three flasks were placed under an inert atmosphere, and the ligand solution from the second flask was slowly added to the tetrachlorotitanium solution in the first flask via cannula. The reaction stirred for 2 hours while nitrogen was bubbled through the solution. Afterwards, the solvent were evaporated off and 20 ml of diethyl ether were added. The contents of the third flask were then transferred via cannula dropwise into the first flask. After stirring for 2 hours, the solution was filtered and the resulting liquid was removed yielding a dark red product. Subsequent crystallization in pentane afforded analytically pure compound **1a** (>90% yield).

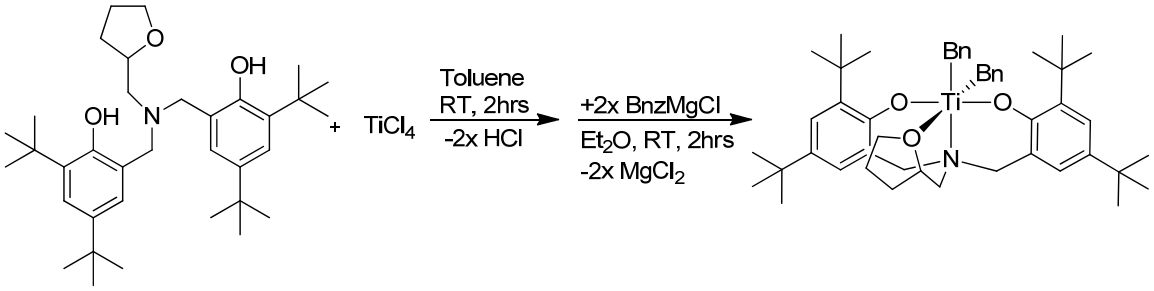

Scheme 3.2. Synthesis of the Ti[^{t}Bu-ON^{THF}O]Bn$_2$ catalyst

Synthesis of 6,6'-(((pyridin-2-ylmethyl)azanediyl)bis(methylene))bis(2,4-di-tert-butylphenol), ^{t}Bu-ON^{Py}O ligand (2). This synthesis procedure is based on previous literature,[24-26] Scheme 3.3. In a typical synthesis, an 80 mL reaction vessel was charged with 2,4-di-tert-butylphenol (24.7 g, 119 mmol), 2-picolylamine (7.0 mL, 68 mmol) and 37% histological grade formaldehyde (24.0 mL, 319 mmol), and distilled water, and a stir bar while maintaining a maximum volume of 80 mL. The biphasic reaction mixture was placed in a CEM microwave reactor and allowed to warm to 100ºC over 5 min while stirring. The reaction was allowed to stand at 100ºC for 10 min, and then cooled to room temperature. The aqueous layer was removed, and cold, dry methanol was added to the organic phase. This mixture was shaken for 30 min, and the resulting solid isolated by vacuum filtration. The crude ligand product was purified by crystallization from ethanol (34% yield).

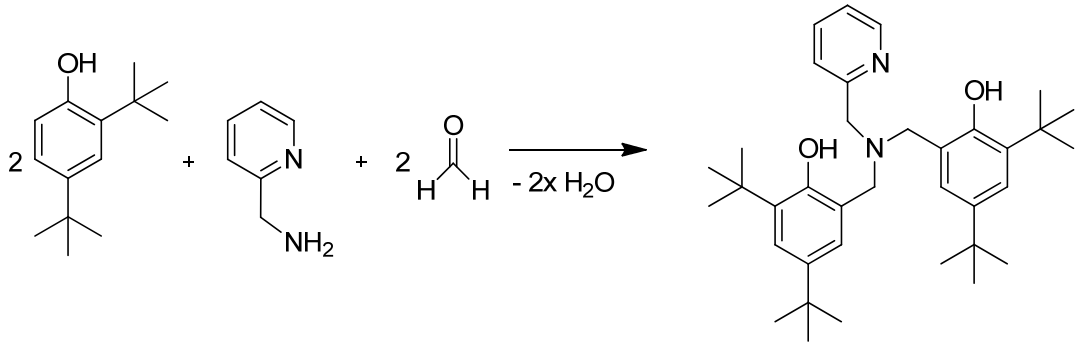

Scheme 3.3. Synthesis of the ^{t}Bu-ON^{Py}O ligand (**2**)

Synthesis of Ti[^{t}Bu-ON^{Py}O]Bn$_2$ (2a). In a typical synthesis,[24-26] Scheme 3.4, a 100 ml flask was charged with titanium(IV) tetrachloride (.35 g, 1.8 mmol), 20 ml toluene, and a stir bar before being fitted with a rubber septum. A second 100 ml flask was charged with **2** (1 g, 1.8 mmol) and 20 ml of toluene. A third 100 ml flask, 2 equivalents of benzylmagnesium chloride (3.8 ml, 3.8 mmol) and 20 ml of diethyl ether were charged. The three flasks were placed under an inert atmosphere, and the ligand solution from the second flask was slowly added to the tetrachlorotitanium solution in the first flask via cannula. The reaction stirred for 2 hours while nitrogen was bubbled through the solution. Afterwards, the solvent were evaporated off and 20 ml of diethyl ether were added. The contents of the third flask were then transferred via cannula dropwise into the first flask. After stirring for 2 hours, the solution was filtered and the resulting liquid was removed yielding a dark red product. Subsequent crystallization in pentane afforded analytically pure compound **2a** (>90% yield).

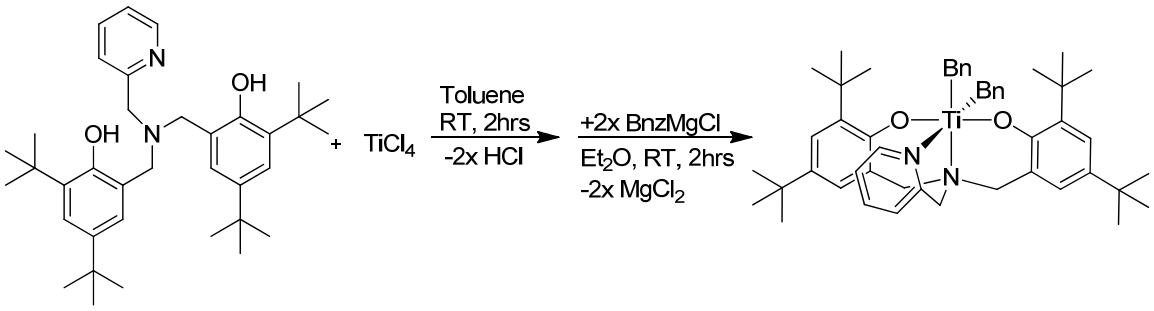

Scheme 3.4. Synthesis of the Ti[^{t}Bu-ON^{Py}O]Bn$_2$ catalyst

Synthesis of 6,6'-((dimethylamino)methylazanediyl)bis(methylene)bis(2,4-di-tert-butylphenol), ^{t}Bu-ON^{NMe2}O ligand. The ligand synthesis procedure is based on literature,[24-26] Scheme 3.5. In a typical synthesis, a 30 mL reaction vessel was charged with 2,4-di-tert-butylphenol (7.62 g, 36.0 mmol), N,N-dimethylethylenediamine (1.89 mL, 15 mmol) and 37% histological grade formaldehyde (3.00 mL, 36 mmol), 6.7 mL of distilled water. The biphasic reaction mixture was placed in a CEM microwave reactor and allowed to warm to 100^{o}C over 10 min while being stirred. The reaction mixture was allowed to stand at 100^{o}C for 10 min, and then cooled to room temperature. The aqueous layer was removed, and cold, dry methanol was added to the organic phase. This mixture was shaken for 30 min, and the resulting solid was isolated by vacuum filtration. The crude ligand product was purified by crystallization from ethanol (52% yield).

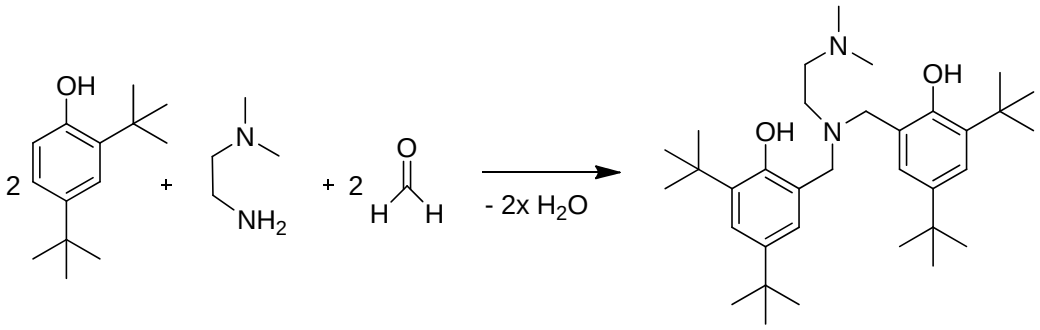

Scheme 3.5. Synthesis of the ^{t}Bu-ON^{NMe2}O ligand (**3**)

Synthesis of Ti[tBu-ON^{NMe2}O]Bn$_2$. In a typical synthesis,[24-26] Scheme 3.6, a 100 ml flask was charged with titanium(IV) tetrachloride (.361 g, 1.9 mmol), 20 ml toluene, and a stir bar before being fitted with a rubber septum. A second 100 ml flask was charged with 3 (1 g, 1.9 mmol) and 20 ml of toluene. A third 100 ml flask, 2 equivalents of benzylmagnesium chloride (3.8 ml, 3.8 mmol) and 20 ml of diethyl ether were charged. The three flasks were placed under an inert atmosphere, and the ligand solution from the second flask was slowly added to the tetrachlorotitanium solution in the first flask via cannula. The reaction stirred for 2 hours while nitrogen was bubbled through the solution. Afterwards, the solvent were evaporated off and 20 ml of diethyl ether were added. The contents of the third flask were then transferred via cannula dropwise into the first flask. After stirring for 2 hours, the solution was filtered and the resulting liquid was removed yielding a dark red product. Subsequent crystallization in pentane afforded analytically pure compound **3a** (>90% yield).

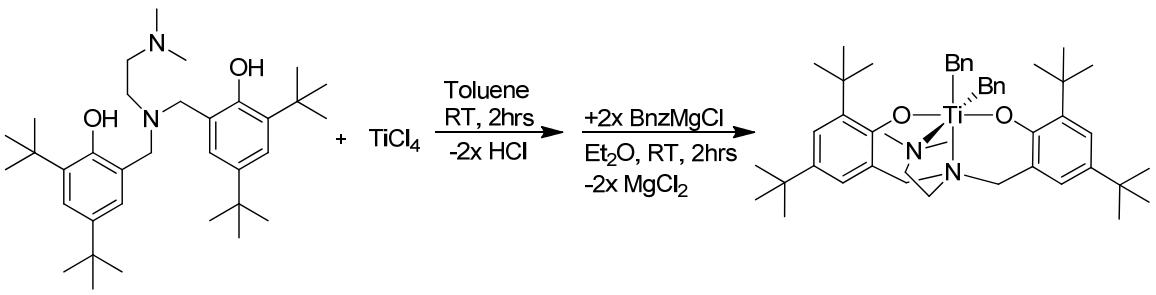

Scheme 3.6. Synthesis of the Ti[^{t}Bu-ON^{NMe2}O]Bn$_2$ catalyst

NMR Scale Polymerization of 1-Hexene Arrays. The procedure for NMR scale polymerization is based on literature.[9] As an example of a typical reaction, Ti[^{t}Bu-ON^{THF}O]Bn$_2$(**1a**) (16.9 mg, 0.0225 mmol) was dissolved in 1.5 mL of toluene and sealed in a vial with a screw-cap septum. This vial was pierced with a 1 mL syringe and placed in an N_2 bag and equilibrated to 25 °C. B(C_6F_5)$_3$ (63.4 mg, 0.124 mmol), 1-hexene (1.89 g, 22.5 mmol), and CPh_2H_2 (37.9 mg 0.225 mmol) were added to a 5.0 mL volumetric flask and diluted with d_8-toluene. 1 ml of this solution was placed in an NMR tube with a septum. The monomer solution was placed in the spectrometer and equilibrated to 25°C by a VT controller. An initial concentration of monomer was taken. The catalyst solution was drawn out of the vial into the syringe and then added to the activator/monomer solution by piercing the NMR tube's septum while the syringe remained in the N_2 bag. The reaction mixture was shaken for ca. 30 s and returned to the spectrometer. Spectra were acquired at predetermined time intervals until completion. Each sample was prepared for GPC analysis by evaporation of solvent under low heat, dissolution in hexanes, and then filtration through an alumina plug to remove dead catalyst. After evaporation of hexanes, polymer was placed

under reduced pressure overnight to yield clear, colorless poly(1-hexene). ^{1}H spectrum was collected on an INOVA 600 MHz spectrometer and analyzed using MestReNova.

Batch Polymerization of 1-Hexene. The procedure for manual quench was conducted similarly to the array experiments. After an initial point measurement, catalyst was injected and the reaction was shaken for ca. 30 s. The reaction proceeded to a predetermined time before being quenched with d_4-methanol. The quenched reaction was analyzed by ^{1}H NMR to verify monomer conversion. The same work up analysis was used to yield clear, colorless poly(1-hexene). For vinyl end group analysis, the resulting polymer was dissolved in $CDCl_3$ and analyzed by ^{1}H NMR using CPh_2H_2 as an internal standard by method of standard additions. For ^{2}H analysis of active sites, the polymer was dissolved in CH_2Cl_2 and analyzed by ^{2}H NMR. D_6-benzene was used as an internal standard, and the method of standard additions was used in quantification of active sites by ^{2}H NMR. Both vinyl and active sites were measured using a Bruker DRX500 spectrometer at 25 °C.

Gel Permeation Chromatography (GPC) Analysis. Poly(1-hexene) was dissolved in THF to concentrations between 5 and 10 mg mL^{-1} for 4 hours. The samples were filtered and injected at 35 °C into a Viscotek TDAmax GPC equipped with refractive index, viscosity, and two light scattering detectors (7° and 90°). Calibration was performed using a known narrow polystyrene standard. The data analysis was performed on the proprietary OmniSEC software with triple detection methodology.

3.3 Results

The strategy we used to produce a kinetics-based model to describe the polymerization data was as follows:

1. Choose the simplest mechanism (i.e. least number that will account for the types of chemical species observed. For example, if vinylidene groups are observed through the appropriate NMR measurements then a reaction must exist in the model that accounts for their creation.
2. For the given reactions, attempts to fit the data to the model by varying the values of the rate constants or other model parameters.
3. If the given model cannot be made to fit the data for any set of model parameters, modify the model by adding a minimal amount of new reactions to account for the discrepancies between the model and data, then repeat step 2 until the model is satisfactory.

As an example, we present here the method used to develop the model for catalyst **1a**, that is, the catalyst with a titanium metal center and a tetrahydrofuran-based pendant ligand. In addition to the molecular weight distributions, ^{1}H NMR signals were collected and interpreted to represent the monomer concentration, vinylidene and vinylene end group concentration, and both primary and secondary carbon bonded to titanium. The reaction steps modeled are shown in Scheme 3.7.

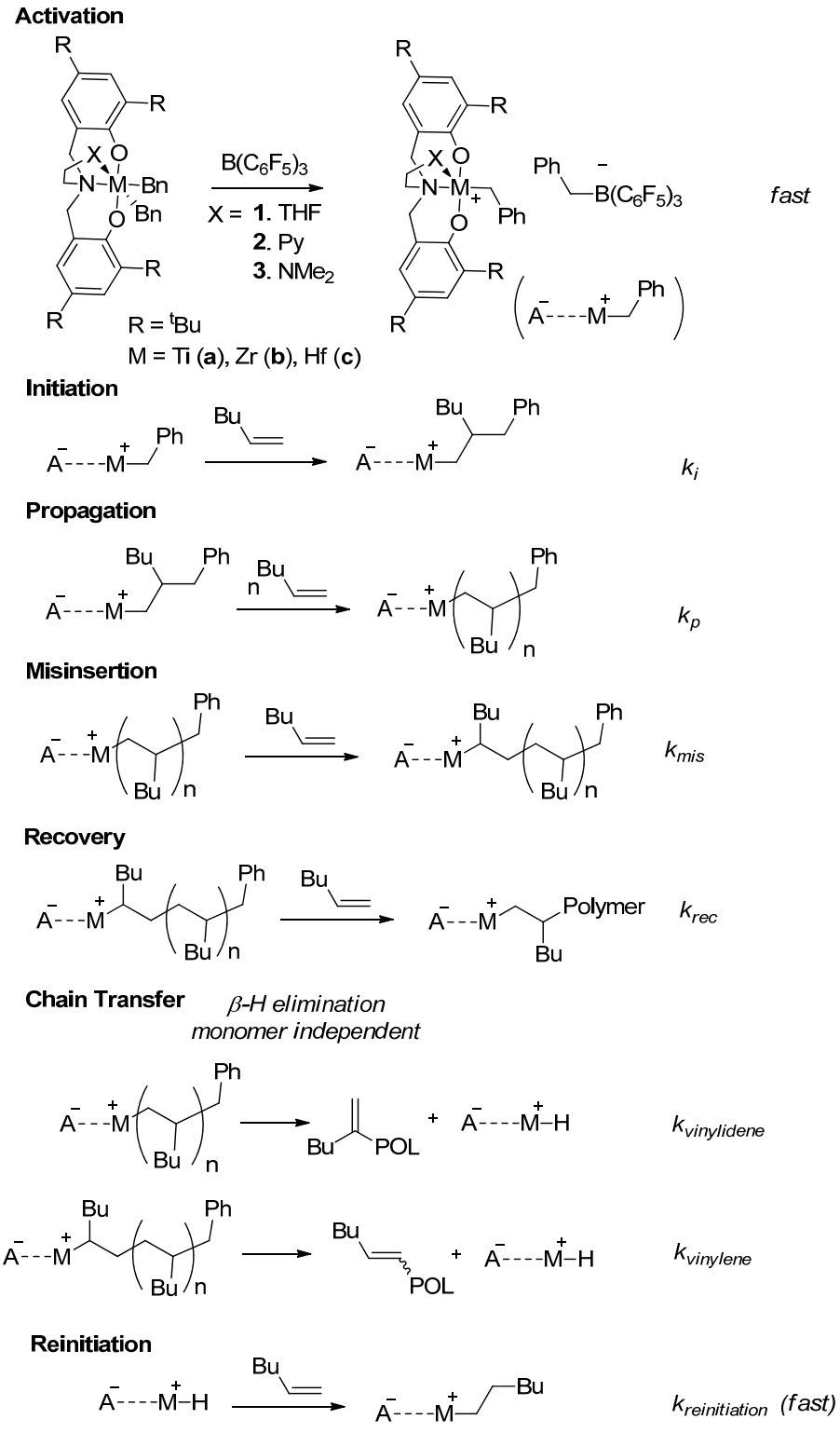

Scheme 3.7 Elementary reaction rate constants used in the modeling of **1a**-**3a**

3.3.1 Detailed Kinetic Modeling

3.3.1.1 Kinetic Modeling of Ti[^{t}Bu-ON^{THF}O]Bn$_2$ Catalyst System (**1a**)

Model A: Base Model

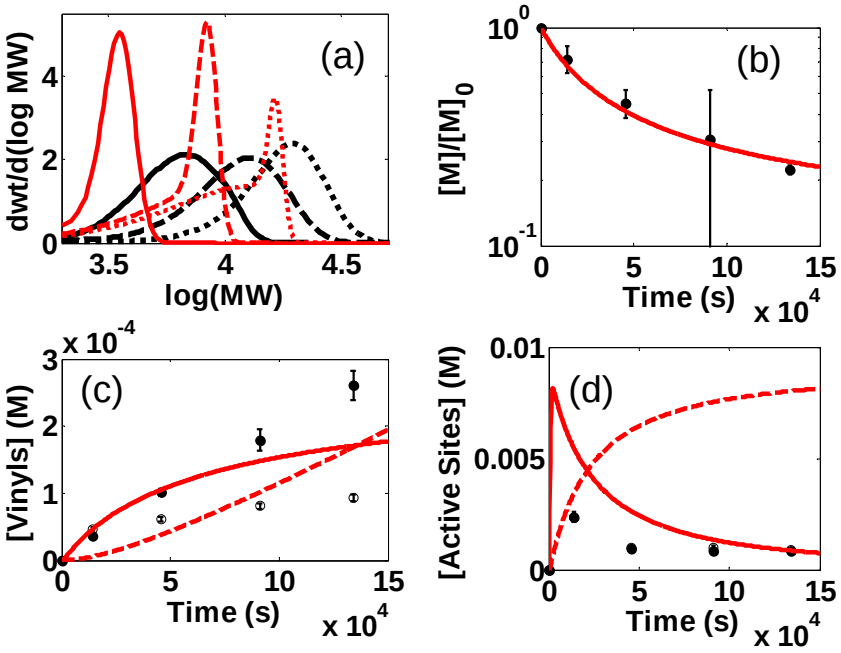

Figure 3.2. Polymerization data (black) and kinetic fits (red) for **1a**/B(C_6F_5)$_3$/1-hexene at 25°C. Reaction conditions: [**1a**] = 9.0 mM, [B(C_6F_5)$_3$] = 9.9 mM, [1-hexene] = 900 mM. (a) MWDs at 14150 s (solid), 45630 s (dashed), 134040 s (dotted). (b) Monomer concentration, (c) vinyl concentration (filled points and solid line represent vinylidene, open points and dashed line represent vinylene), and (d) active site concentration (filled points and solid line represent primary carbon–metal active sites resulting from 1,2-insertion, open points and dashed line represent secondary carbon–metal active sites resulting from 2,1-insertion/misinsertion). The model used is Model A described in the supplementary information.

Based solely on the presence of the aforementioned species, the simplest mechanism that describes the presence of these chemical groups includes the following reactions:

1. Chain growth by propagation (k_p)
2. 2,1-misinsertion of monomer (k_{mis})
3. Chain transfer of catalyst site to form vinylidene ($k_{vinylidene}$)
4. Chain transfer of misinserted site to form vinylene ($k_{vinylene}$)

This model would also assume that the rate constants for the initiation process (insertion of the first monomer following activation) and the re-initiation process (insertion of the first monomer following chain transfer) are equal to the propagation rate constant. It also assumes that activation is rapid and complete. With these four rate constants as parameters certain features of the data can be fit (Figure 3.3); however, the complete set of data cannot be fit simultaneously. The main features that the model fails to fit are (i) the broadness and peak positions in the molecular weight distributions, (ii) the curvature in the vinyl concentration (both for vinylidene and vinylene), and (iii) the drop in secondary active sites. Since none of the reactions in the current model can be removed, we conclude that at least one additional reaction pathway must be added to model the experimental data.

Model B: Model A + Recovery of Misinserted Site

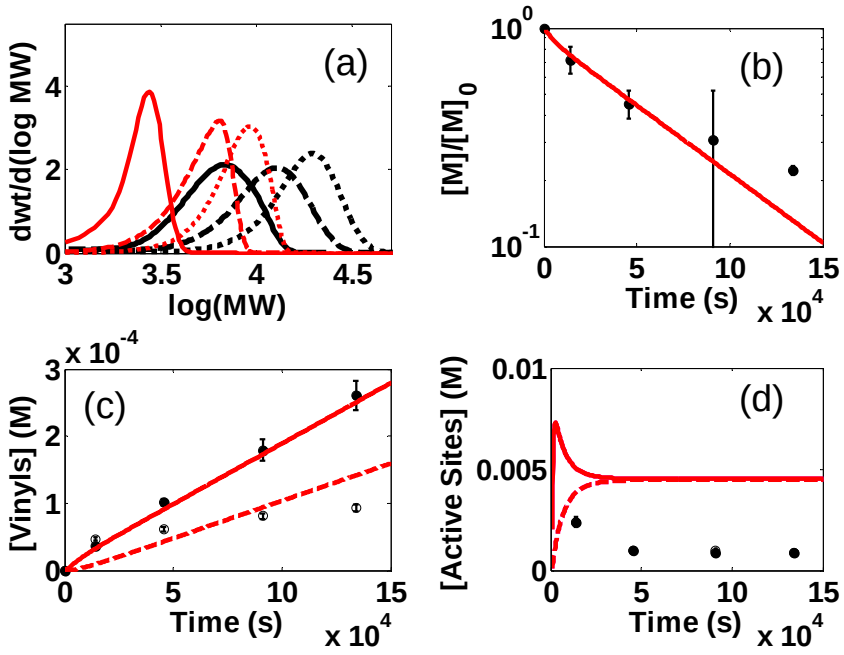

Figure 3.3. Polymerization data (black) and kinetic fits (red) for **1a**/B(C_6F_5)$_3$/1-hexene at 25°C. Description of figures is the same as in Figure S1. The model used is Model B described in the supplementary information.

One of the key deficiencies of Model A was the continuous accumulation of secondary active sites, while the data show that secondary sites follow closely with primary active sites and decrease after an initial maximum. Model A does allow for consumption of secondary sites through vinylene formation, but the low measured value of vinylene concentration limits the rate at which these groups can be consumed. Therefore, we add the following reaction:

5. 1,2-insertion of monomer following 2,1-misinsertion (k_{rec})

This additional reaction converts secondary sites to primary sites, which allows the two sites to interconvert without creating additional vinyls. Allowing the rate constants to adjust to produce the best possible fit (Figure 3.4), we see that there are still deficiencies in this model, including (i) the molecular weight distributions are still too narrow, (ii) the rate of monomer consumption does not decrease late in the reaction, and (iii) active site concentrations are over-predicted.

Model C: Model B + Slow Initiation

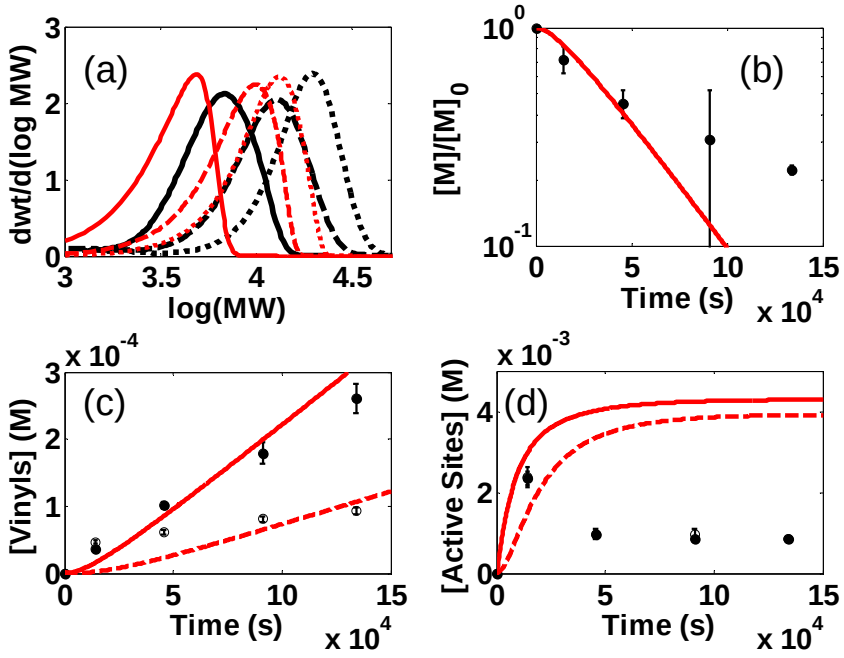

Figure 3.4. Polymerization data (black) and kinetic fits (red) for **1a**/B(C_6F_5)$_3$/1-hexene at 25°C. Description of figures is the same as in Figure S1. The model used is Model C described in the supplementary information.

We observe that the molecular weight distributions in Models A and B are too narrow and have too low of a molecular weight. One reaction pathway known to create this effect is a slow chain initiation reaction:

6. Chain initiation (k_i)

In the earlier models this reaction was implicitly included; however the rate constant was assumed to be equal to the propagation rate constant. The difference here is that initiation is allowed to be much slower than propagation. The initiation reaction involves the very first insertion of a monomer into an activated catalyst site. Chemically, initiation involves

inserting a monomer into a metal–benzyl bond rather than into an already growing polymer chain, and a different reaction rate constant may be expected.

The best model fit of the experimental data based on the six reactions of Model C is shown in Figure S3. The broad molecular weight distribution can now be modeled; however the peak positions are still found to be too low. One way to allow the model to produce higher molecular weight distributions is to increase the ratio of the propagation rate constant to the chain transfer rate constants. From Figure 3.5, we see that we can neither increase k_p nor decrease $k_{vinylene}$ or $k_{vinylene}$ without drastically reducing the quality of the monomer consumption fit or the vinyl fit. Another fault of the model is its inability to match the slowdown in the monomer consumption rate late in the reaction.

Model D: Model C + Catalyst Deactivation

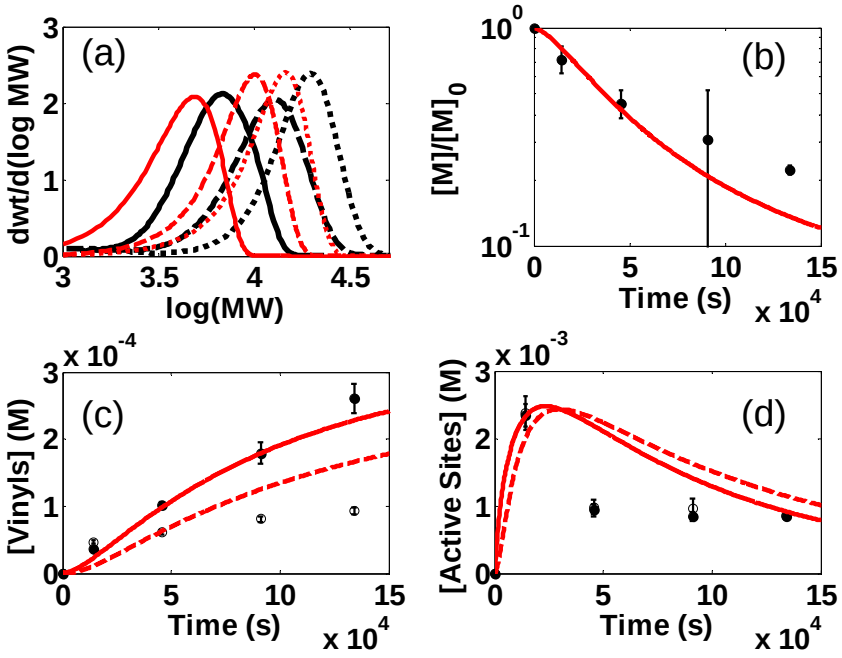

Figure 3.5. Polymerization data (black) and kinetic fits (red) for **1a**/B(C_6F_5)$_3$/1-hexene at 25°C. Description of figures is the same as in Figure 3.2. The model used is Model D described in the supplementary information.

Both the monomer consumption data and the active site concentration data can be interpreted as describing a system where the total concentration of active catalyst decreases over time. Based on this interpretation, the following reaction is included:

7. Catalyst deactivation (k_d)

The reaction is assumed to be independent of monomer concentration. Chemically, the reaction may be interpreted as the reaction of the catalyst with oxygen or some other agent that irreversibly deactivates the site from further polymer growth. No vinyl group is formed in this reaction. Because the polymerization is so slow, it is not unusual to assume that there is a slow rate of deactivation that becomes apparent at long reaction times.

The improvement of Model D over the previous models can be seen in Figure S4, specifically with the monomer consumption and the active site concentration predictions, which now have the same qualitative features as the data. However, the molecular weight distribution predictions are still low while the active site concentrations are mostly too high. As with Model C, increasing the ratio of the propagation rate constant to the chain transfer rate constants will not improve the overall fit.

Model E: Model D + Partial Active Sites

So far, the models used have assumed that the initial concentration of catalyst is fixed at the experimentally measured value. However, many single-site olefin catalysts are known to not fully participate in polymerization. It remains unclear whether this is due to incomplete activation, catalyst poisoning, or some other route. In any case, the following parameter is added to the mechanism:

8. Active catalyst fraction (X_{active})

In terms of modeling, this parameter serves as a multiplication factor for the initial catalyst concentration. The inclusion of this parameter allows for the following adjustments to the model fit: As X_{active} is decreased from 1, the primary and secondary active site concentrations will drop. This means that for a fixed k_p the slope of the monomer consumption curve will decrease toward zero. To compensate, the model value of k_p is typically increased along with the decrease in X_{active} in order to maintain a monomer consumption fit. However, this change to k_p will increase the ratio of propagation to chain transfer, which increases the peak position of the model molecular weight distributions.

In the case of catalyst **1a** this model addition exactly accounts for the deficiencies found in Model D. The model fit is shown in Figure 3.6. This fit corrects the offset in the molecular

weight distributions while maintaining the monomer consumption and vinyl concentration fits. It also improves over the Model D fit by providing a closer fit to the active site concentrations.

This procedure was also followed for catalyst systems **2a** and **3a**. The same chemical mechanism was found to fit the data, where the rate constants and active catalyst fraction parameter had unique values for each system.

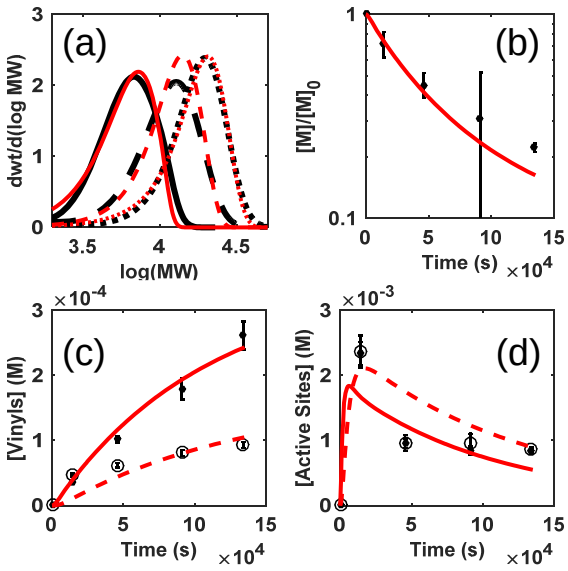

Figure 3.6**.** Data (black) and fits (red) for **1a**/$B(C_6F_5)_3$/1-hexene at 25 °C. Conditions: [**1a**] = 9.0 mM, [$B(C_6F_5)_3$] = 9.9 mM, [1-hexene] = 900 mM. (a) MWDs at 14150 s (solid), 45630 s (dashed), 134040 s (dotted). (b) Monomer concentration, (c) Vinyl concentration (filled points and solid line represent [vinylidene], open points and dashed line represent [vinylene]), and (d) active site concentration (filled points and solid line represent primary active sites resulting from 1,2-insertion, open points and dashed line represent secondary active sites resulting from 2,1-insertion/misinsertion).

3.3.1.2 Kinetic Modeling of Ti[^{t}Bu-ON^{Py}O]Bn$_2$ Catalyst System (**2a**)

Model Predictions for **2a.** The model fit for catalyst system **1a** appears in Figure 3.6. The model fit for catalyst system **2a** appears in Figure 3.7. The rate constants associated with these fits are in the main text Table 3.1.

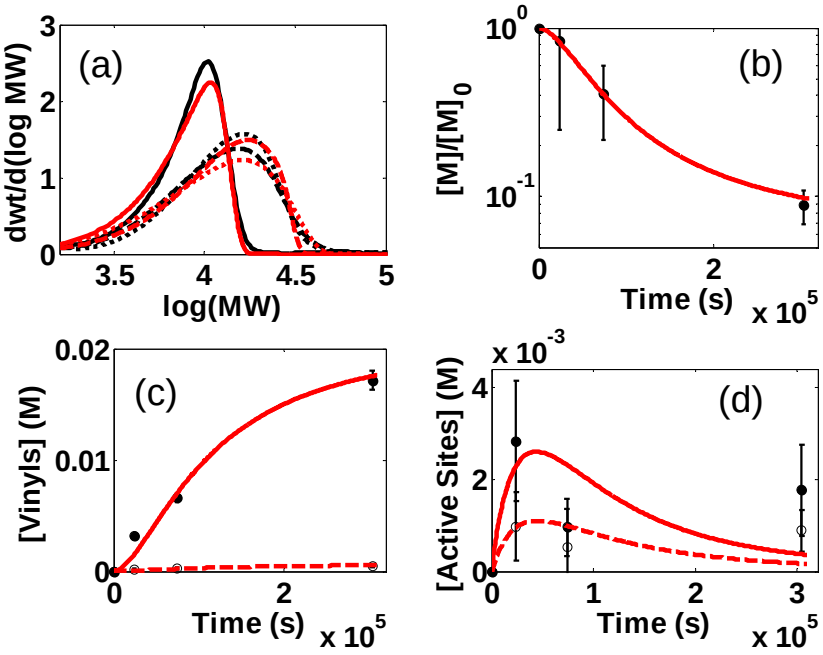

Figure 3.7. Polymerization data (black) and kinetic fits (red) for **2a**/B(C_6F_5)$_3$/1-hexene at 25°C. Reaction conditions: [**2a**] = 9.0 mM, [B(C_6F_5)$_3$] = 9.9 mM, [1-hexene] = 1800 mM. (a) MWDs at 24000 s (solid), 74240 s (dashed), 304282 s (dotted). (b) Monomer concentration, (c) vinyl concentration (filled points and solid line represent vinylidene, open points and dashed line represent vinylene), and (d) active site concentration (filled points and solid line represent primary carbon–metal active sites resulting from 1,2-insertion, open points and dashed line represent secondary carbon–metal active sites resulting from 2,1-insertion/misinsertion). The rate constants from the kinetic fitting appear in Table 3.1.

3.3.1.3 Kinetic Modeling of Ti[^{t}Bu-ON^{NMe2}O]Bn$_2$ Catalyst System (**3a**)

Model Predictions for **3a**. The model fit for catalyst **3a** appears in Figure 3.8. The rate constants associated with these fits are in the main text Table 3.1.

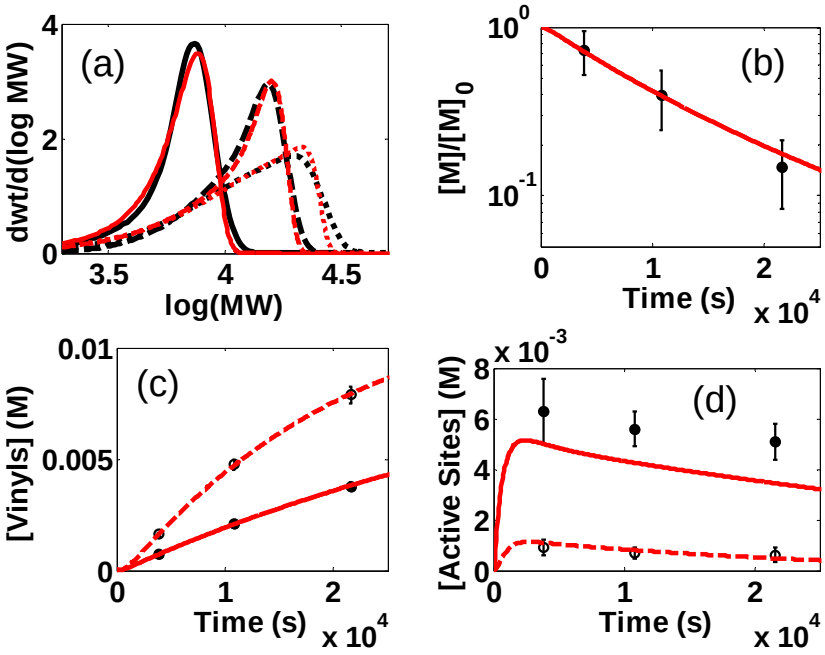

Figure 3.8. Polymerization data (black) and kinetic fits (red) for **3a**/B(C_6F_5)$_3$/1-hexene at 25°C. Reaction conditions: [**3a**] = 9.0 mM, [B(C_6F_5)$_3$] = 9.9 mM, [1-hexene] = 1800 mM. (a) MWDs at 3870 s (solid), 10800 s (dashed), 21600 s (dotted). (b) Monomer concentration, (c) vinyl concentration (filled points and solid line represent vinylidene, open points and dashed line represent vinylene), and (d) active site concentration (filled points and solid line represent primary carbon–metal active sites resulting from 1,2-insertion, open points and dashed line represent secondary carbon–metal active sites resulting from 2,1-insertion/misinsertion). The rate constants from the kinetic fitting appear in Table 3.1.

3.4 Discussion

Herein, we present the experimental data and a quantitative kinetic analysis for 1-hexene polymerization by Ti catalysts **1a**–**3a**. The procedure used to eliminate inadequate mechanisms and to arrive at the final polymerization mechanism for **1a**–**3a** is provided in Chapter 3.3. Each system was studied independently and no a priori assumptions were made with respect to elementary steps. The principle of parsimony (Occam's razor) was applied, where the mechanism with the least number of reactions that can satisfy the kinetic data was adopted. From this independent analysis of the Ti catalysts, **1a**–**3a**, the kinetic mechanism was found to be similar to that observed for the Zr and Hf analogues.

The mechanism includes activation, initiation, propagation via 1,2-insertion, 2,1-misinsertion, recovery from misinsertion, and monomer-independent chain transfer reactions that give vinylidene and vinylene end groups. The elementary kinetic steps are shown in Scheme 1. For each system, we followed a previously developed kinetic modeling method analyzing (1) monomer consumption, (2) MWD, (3) active site concentration, and (4) vinyl end group concentration over the course of the reaction. Active sites were determined by quenching the reaction with d_4-methanol and using ^{2}H NMR spectra in quantifying polymer–deuterium tags. Active sites that underwent 1,2-insertion of 1-hexene are defined as primary sites and those that underwent 2,1-insertion as secondary sites. Both are distinguishable and quantified by the ^{2}H NMR analysis. The complete kinetic analysis for the Zr (**1b**–**3b**) and Hf (**1c**–**3c**) based systems has been reported previously.[9a–9c]

Examination of the rate constants in Table 3.1 shows the rate of initiation for the Ti-based catalysts is slower than that for propagation for all three catalysts. For **1a** and **3a** initiation is 20–40 times slower than propagation; for **2a** initiation is approximately 300

times slower than propagation. The rates of misinsertion for the three catalysts are between 15–50 times slower than for propagation, while the rates of misinsertion and recovery are always the same order of magnitude within each system. Vinyl formation (both vinylidene and vinylene) is monomer independent. For **1a** and **2a** vinylidene formation is much faster than vinylene formation, but for **3a** vinylene formation dominates.

Table 3.1. Rate constants for 1-hexene polymerization with the Ti/Zr/Hf[tBu-ON^{X}O]Bn$_2$/B(C$_6$F$_5$)$_3$ catalysts **1a-3c**.[a]

M	Ti			Zr			Hf		
[ON^{x}O]	THF	Py	NMe$_2$	THF	Py	NMe$_2$	THF	Py	NMe$_2$
M—X[b]/ Å	2.26	2.43	2.55	2.37	2.51	2.59	2.33	2.47	2.56
k_i(10^4)/ M^{-1} s^{-1}	2.97 (+/-.48)	.172 (+/-.047)	7.5 (+/-.5)	800 (+200/-100)	170 (+/-200)	1,600 (+400/-200)	400 (+200/-100)	17 (+2/-1)	400 (+100/-0)
k_p(10^4)/ M^{-1} s^{-1}	121 (+12/-14)	48 (+5/-6)	179 (+/-23)	80,000 (+8,000/-2,000)	13,500 (+2,000/-1,000)	110,000 (+/-10,000)	5,300 (+/-600)	2,000 (+0/-200)	9,500 (+700/-900)
k_{mis}(10^4)/ M^{-1} s^{-1}	3.11 (+/-.29	3.3 (+/-.7)	3.6 (+.9/-.5)	540 (+260/-30)	77 (+5/-4)	550 (+70/-40)	81 (+2/-10)	2.8 (+.2/-0)	12 (+3/-0)
k_{rec}(10^4)/ M^{-1} s^{-1}	2.37 (+/-.2)	7.9 (+/-1.1)	13.2 (+3.4/-2.4)	470 (+210/-20)	52 (+12/-9)	400 (+300/-200)	600 (+40/-50)	2 (+0/-2)	0[c]
$k_{vinylidene}$(10^4)/ s^{-1}	.0172 (+/-.001)	.436 (+/-.024)	.423 (+.038/-.043)	1.40 (.14+/-.2)	13.4 (+0/-.1)	122 (+8/-6)	8.4 (+.2/-.4)	38 (+3/-2)	55 (+/-2)
$k_{vinylene}$(10^4)/s^{-1}	.00541 (+.00025/-.00028)	.031 (+/-.0027)	4.72 (+/-.18)	.51 (+.02/-.03)	4.41 (+/-.03)	87.2 (+.7/-.4)	2.7 (+.7/-.6)	2nd Order[d]	Fast[e]

[a]In toluene at 25 ^{0}C. See Figure 1 for pre-catalyst structures. Error bars have been omitted for clarity; a full table with error bars is included in Section 2 of the SI. Error values were typically (± 10%) of the respective rate constant except in the cases of k_{mis} for **2a**/**3a**/**2b**/**3b** (± 20%), and k_{rec} for **3a**/**2b** (± 25%) and **3b** (± 66%). [b]These crystal structure values were obtained from either literature or in the case of **1b** reported herein. [c]A value of zero means that the model did not require the inclusion of this reaction step. [d]The vinylene rate constant is fast and is monomer-dependent. [e]The model requires a vinylene chain transfer to immediately occur after a misinsertion.

The complete set of rate constants for the Ti catalysts from this study allows direct comparisons to the rate constants for the Zr and Hf analogues. All rate constants for the Ti catalysts **1a–3a** are roughly two orders of magnitude slower than those of the Zr catalysts and an order of magnitude slower than for the Hf catalysts. Focusing on the propagation rate constant, Zr (8.0 M^{-1} s^{-1}) is the largest, then Hf (0.53 M^{-1} s^{-1}), and finally Ti (0.0121 M^{-1} s^{-1}) for ligand (**1**). While differences in propagation between Zr/Hf catalysts are possibly due to electronic differences in the metal, as indicated by the larger Hf–carbon bond enthalpy,[27] steric crowding may contribute to the reduced activity of the Ti catalysts for 1-hexene polymerization. The metal-ligand bond distances as detailed in Figure 3.9 were determined from the precatalyst crystal structures and are given in Table 3.2. The metal–ligand bond lengths for Ti catalysts **1a**–**3a** are significantly shorter, i.e. ~0.8 angstroms, than the Zr analogues **1b**–**3b**. Contractions of these key bond lengths result in a smaller active site that partially blocks the interactions between catalyst and monomer.

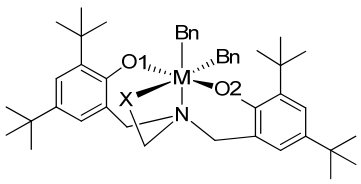

Figure 3.9 Molecular representation of **1a-3b** with key bond distances in Table 3.2

Table 3.2. Key bond lengths for **1a-3b** for Figure 3.9[9,24-26]

Pendant		THF	Py	NMe_2
Metal		Ti/Zr/Hf	Ti/Zr/Hf	Ti/Zr/Hf
Bond Length (Å)	X-M	2.26/2.37/2.33	2.43/2.51/2.47	2.55/2.59/2.56
	N-M	2.36/2.44/2.42	2.35/2.46/2.43	2.38/2.45/2.42
	O1-M	1.88/2.00/1.98	1.86/2.00/1.98	1.85/2.00/1.98
	O2-M	1.87/1.99/1.99	1.90/2.00/1.99	1.87/1.99/1.98

A focus on single active species containing different metal centers reveals that the k_{mis} and k_{rec} rate constants show a unique trend across the ligand family. These rate constants for Ti catalysts increase as the M–X bond distance increases, suggesting a steric influence on 2,1-insertion and recovery. This is in contrast to the changes in k_{mis} and k_{rec} for Zr and k_{mis} for Hf, where the rate constants do not correlate with the pendant bond length. Interestingly, Hf catalysts exhibit a reverse trend from that for Ti with regard to k_{rec}, i.e. Hf catalysts exhibited a decrease in the recovery rate constant as the pendant bond length increased. Combined with fact that Hf-Py and Hf-NMe_2 display rapid chain transfer of secondary inserted sites, Hf catalysts **2c** and **3c** exhibited less dormancy when compared to **1c**, Ti catalysts **1a**–**3a**, and Zr catalysts **1b**–**3b**. This suggests that the changes in metal center and ligand design can have a significant effect on monomer misinsertions, the percent of regioerrors in a polymer chain, and the polymer length via chain transfer following 2,1-insertions.

Calculating the percent of misinserted monomers into a primary polymer site can be done by comparing the rate of the misinsertion reaction rate to the sum of the rates of all monomer insertion reactions for a primary active site; specifically,

$$\%\ \text{Misinsertions} \approx \frac{\text{2,1}-\text{Ins.}}{\text{All Ins.}} \approx \frac{[\text{C}^*][\text{M}]k_{mis}}{[\text{C}^*][\text{M}](k_p+k_{mis})} = \frac{k_{mis}}{k_p+k_{mis}} \qquad \text{Equation 3.1}$$

where [M] = [1-Hexene] and [C*] = concentration of primary active catalyst. The results of these calculations for each metal catalyst are shown in Table 3.3.

Table 3.3 Calculations and values used to calculate the number of regioerrors in each polymer

	Ti-THF	Ti-Py	Ti-NMe_2	Zr-THF	Zr-Py	Zr-NMe_2	Hf-THF	Hf-Py	Hf-NMe_2
$[Catalyst]_0$	0.009	0.009	0.009	0.003	0.003	0.005	0.003	0.003	0.003
$[Monomer]_0$	0.9	1.8	1.8	0.6	0.6	0.5	0.6	0.6	0.6
Time (sec)	134000	304000	21600	331	3200	158	3915	10960	3000
Remaining [Monomer]	1.47E-01	1.77E-01	3.20E-01	1.28E-02	3.31E-04	5.99E-02	2.23E-03	8.28E-02	1.90E-03
[1,2-insertion] + [Recovered]	7.34E-01	1.53E+00	1.45E+00	5.83E-01	5.97E-01	4.38E-01	5.90E-01	5.20E-01	6.03E-01
[Misinsertions]	1.83E-02	9.53E-02	2.81E-02	3.88E-03	3.29E-03	2.14E-03	8.58E-03	6.38E-04	6.98E-04
% Misinserted monomers	2.43%	5.87%	1.90%	0.66%	0.55%	0.49%	1.43%	0.12%	0.12%
Ave. % Misinsertions by Metal	3.40%			0.56%				0.12%	
kmis/kp	2.58%	6.86%	2.01%	0.68%	0.57%	0.50%	1.53%	0.14%	0.13%
[Secondary Sites]	9.00E-04	1.68E-04	4.79E-04	1.51E-03	5.83E-04	6.13E-04	2.05E-04	1.67E-04	0.00
[Vinylene]	1.05E-04	5.45E-04	8.01E-03	2.19E-05	1.41E-03	8.32E-04	3.21E-04	4.16E-04	6.98E-04
% Misinsertions followed by CT	0.603%	0.573%	29.003%	0.924%	51.895%	54.632%	3.837%	88.423%	100%
% Recovered Misinsertions	99.397%	99.427%	70.997%	99.076%	48.105%	45.368%	96.163%	11.577%	0.000%
% Regioerrors in the polymer	2.4%	5.8%	1.3%	0.65%	0.26%	0.22%	1.4%	0.014%	0.000%
Ave. % Regioerrors per Metal	3.2%			0.38%			0.007%		

Going from Ti to Zr to Hf, the number of 2,1-insertions decreases, which is similar to the results seen by Busico and coworkers.[22] On average, the Ti catalysts exhibited ~3.4% 2,1-insertions as compared to Zr and Hf catalysts that exhibit ~0.56% and ~0.12% 2,1-insertions, respectively. The Hf catalyst **1c** stands as an outlier to this trend, as it had an increased amount of 2,1-insertion, 1.43%. Figure 3.10 shows the effect on metal center on Equation 3.1 using data for catalysts **1a-3c** from Table 3.1.

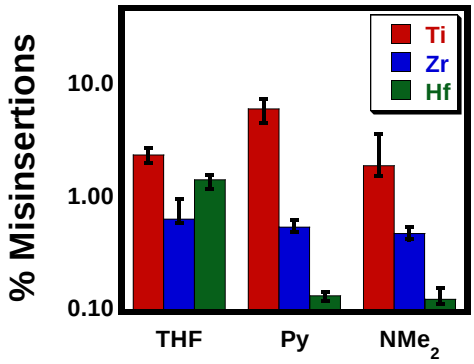

Figure 3.10 % Misinsertions reactions using Equation 3.1 and Table 3.1 for **1a-3c**

The percentage of 2,1-insertion has direct implications on the polymer MWD and the number of regioerrors within the polymer chain. As shown in Scheme 3.7, a catalyst species containing a misinserted monomer can either recover to the active polymerization species by a 1,2-insertion, forming a regioerror polymer defect, or perform a β-hydride elimination to form a metal hydride and a vinylene chain terminated polymer. Using the rate constants from Table 3.1, the number of 1-hexene misinsertions was compared to the concentration of vinylene terminated groups and secondary active sites; thus the percent of

polymer regioerrors, Figure 3.11A, and the percent of vinylene terminated polymers following 2,1-misinsertion were determined. Literature experimental values for regioerrors in poly(1-hexene) by Kol and coworkers[24c] using a Ti amine bis-phenolate catalyst featuring a methoxy pendant and regioerrors in polypropylene by Busico and coworkers[22] using Zr/Hf Salan catalysts are also shown in Figure 3.11A for comparison (catalyst structures shown in Figure 3.11B).

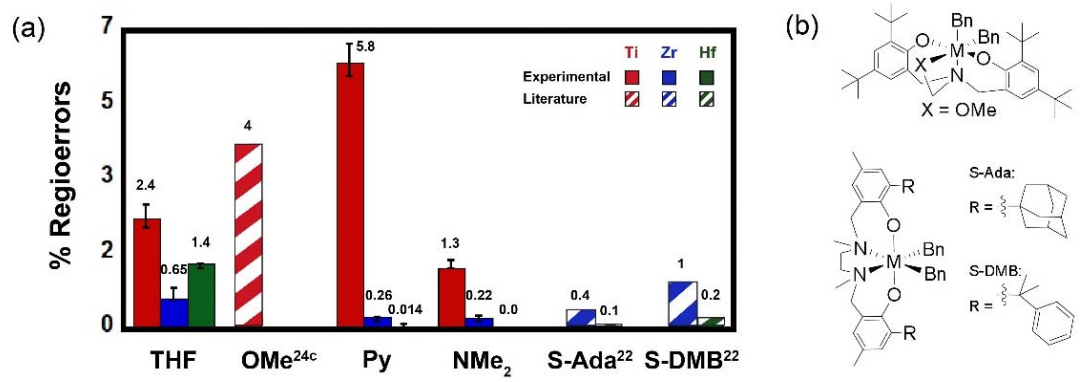

Figure 3.11 (A) % Regioerrors calculate for catalysts **1a-3c** and (B) other catalysts

Comparing values of Equation 3.1 with Figure 3.11, one finds that Ti catalysts **1a**–**3a** exhibited very little chain transfer after a 2,1-insertion but instead produced longer polymers containing an average of ~3.2% regioerrors, compared to 3.4% misinsertions. This is consistent with the regioerrors reported by Kol and coworkers for poly(1-hexene) polymer produced by the Ti[^{t}Bu-ON^{OMe}O]Bn$_2$catalyst, ~4% regioerrors.[24c] However, they reported < 1% regioerrors in poly(1-hexene) produced by catalyst **1c** while the kinetic model using rate constants given in Table 1 predicts a slightly larger 1.3% regioerrors for

the same catalyst.[24c] Zr catalysts **2b**/**3b** consistently exhibit rapid chain transfer after a 2,1-insertion, producing shorter, vinylene-terminated polymer chains and ultimately retained < 0.3% regioerrors in the resulting polymer, compared to the ~0.5% misinsertions calculated from Equation 3.1. The regioerrors incorporated by Hf catalysts **2c**/**3c** into polymer chains were even lower, 0.0014% and 0.0% respectively, because these catalysts preferred rapid chain transfer to produce a vinylene end group over recovery. These results are consistent with Busico and coworkers'[22] findings, Figure 3.11A, where Zr catalysts showed increased amounts of regioerrors when compared to analogous Hf catalysts. However, Zr–THF and Hf–THF catalysts produced more polymer regioerrors, i.e. 0.65% and 1.4%, respectively. The deviation for these catalysts may be due to the increased steric interference caused by the shorter M–X distance. While we do not fully understand the nature of this interaction, we note that Coates *et al.* also reported increased 2,1-insertions as they increased steric bulk in their Ti phenoxyimine catalysts.[16]

In summary, the percentages of regioerrors associated with Ti and Zr catalysts were fairly consistent across the different ligands and monomers, with the Ti catalysts exhibiting the most regioerrors. The regioerrors for the Hf catalysts were typically lower than for the Ti and Zr catalysts but can be influenced by changes with the ligand system.

These observations on the metal's influence on misinsertion and termination rate constants are important for future catalyst design. A higher selectivity toward vinylidene-terminated products may be possible by choosing Hf over Ti/Zr metal centers. Reducing regioerrors within the polymer could also be accomplished by changes in metal center rather than designing bulkier ligand architectures. In fact, Rieger and coworkers have already shown that the reduction in regioerrors by using Hf catalysts produces higher

quality ultrahigh molecular weight polypropylene elastomers when compared to Zr analogues.[28] Furthermore, regioselectivity in the insertion α-olefins into metal–carbon bonds seems to follow the trend hinted at by Oliva, Nozaki, and others; specifically, the number of 2,1-insertion increases as the reaction center becomes electron deficient, and the number of 1,2-insertion increases as the electron density increases. This trend is also seen for 1-hexene insertions as the metal center changes from Ti to Zr to Hf. This observation may be applicable to the design of other nonpolymerization catalyst systems that involve the insertion of α-olefins, such as hydroformylation or for cross-coupling Heck reactions.

The number of 1,2-insertions a polymer undergoes at a single primary active site before chain termination is given by the ratio of the propagation rate and the termination rate. Ignoring all other reactions except 1,2-insertion and vinylidene reaction rates, we can estimate the propensity of a catalyst to produce longer or shorter chains; specifically,

$$\text{Prop. vs. Term.} \quad \frac{\text{Rate 1,2}-\text{ins.}}{\text{Rate 1,2}-\text{term.}} \approx \frac{k_p[C^*][M]}{k_{vinyldene}[C^*]} = \frac{k_p[M]}{k_{vinyldene}} \qquad \text{Equation 3.2}$$

where [M] = [1-Hexene], [C*] = concentration of the primary active catalyst. For a constant [M], the average length of polymers from different catalyst systems can be ordered along the trend found by computing $k_p/k_{vinylidene}$. At 25°C the Zr catalysts **1b**–**3b** should produce longer polymer chains than the Ti (**1a**–**3a)** and Hf (**1c**–**3c**) based on the rate constants from Table 3.1 and Equation 3.2, shown in Figure 3.12.

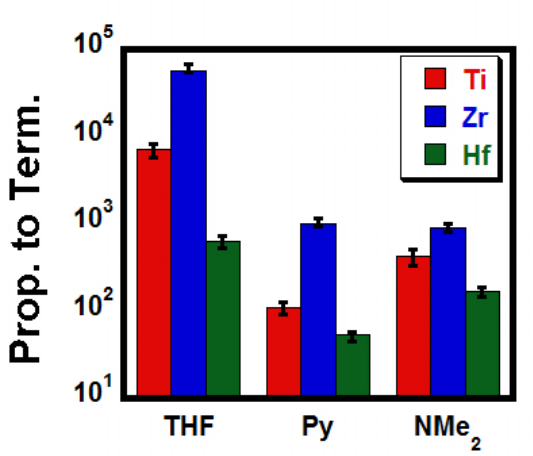

Figure 3.12 Ratio of propagation to termination for **1a-3c** using Table 3.1/Equation 3.2

However, this result is not consistent with previous literature that suggests that Ti catalysts produce the highest M_W.[24-26] To determine if the other reactions had an effect on the polymer length, calculations using the rate constants from Table 3.1 for batch polymerization were performed with the initial conditions of $[1\text{-Hexene}]_0$ = 600 mM and $[\text{Catalyst}]_0$ = 3.0 mM for each of the nine catalysts. To control for incomplete catalyst participation and catalyst deactivation reactions, the catalyst participation was fixed at 100% and modeled without a catalyst deactivation step. The results of these computer simulations conducted to 95% monomer consumption are shown in Figure 3.13. When identical initial monomer concentration and catalyst participation were enforced, the resulting M_n with respect to the metal center are ordered as Zr > Ti > Hf. However, the trend for M_n as reported in the literature is Ti > Zr > Hf, as the Ti catalysts were reported as essentially living poly(1-hexene) catalysts.[24-26]

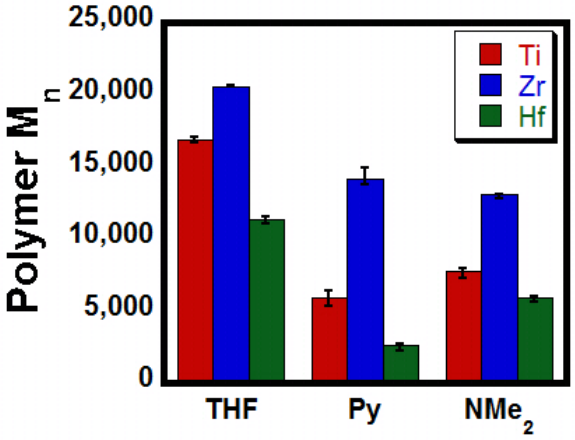

Figure 3.13 Polymer M_n calculated using *k*'s from Table 3.1 with identical initial conditions and complete catalyst participation

The apparent discrepancy can be resolved by understanding the conditions in which the reported activity experiments in the literature were conducted. Zr/Hf catalysts, when tested for reactivity in neat solutions of 1-hexene, were active enough to raise the reaction media temperature to a boil from the exothermic ΔH_{rxn} to produce polymers with shorter M_n, commiserate to reactions held at higher temperatures.[25] Kol and coworkers then "tamed" the reactivity by diluting the reaction media with an inert, nonpolar solvent that gave both a lower catalytic activity and longer polymer chains, indicative of a lower reaction temperature.[25] In both of these experiments, the reaction temperature was neither controlled nor monitored. The effect of temperature on the catalytic mechanism has tremendous effect on the polymer M_n, influencing both the values of k_p and $k_{vinylidene}$ in Equation 3.2, for each of these active catalysts. In contrast, the 1-hexene activities for the amine bis(phenolate) Ti catalysts were reported from experiments in neat 1-hexene; the TOFs for these systems were low enough that the experiments did not bring the reaction

media to a boil despite the higher concentration of 1-hexene.[24] Therefore, the polymer M_n of the Ti catalysts are influenced by the effect of the monomer concentration, a larger [M] in Equation 3.2 produces an inflated polymer M_n value compared to experiments run at lower monomer concentrations, while the M_n of the Zr/Hf catalysts is affected strongly by the reaction temperature, changing k_p and $k_{vinylidene}$ in Equation 3.2. Combined with the fact that activity experiments do not account for the percent of active catalysts participating in the catalytic cycle, another key factor affecting polymer M_n, activity measurements and end point MWD analysis should be used with caution when comparing catalysts when potential reaction temperature changes, inequivalent monomer loading, catalyst participation, or even catalyst deactivation can distort actual chemical trends.

The implications of this more detailed knowledge in terms of polymer engineering should not be ignored. Consider a process to produce long chains of poly(1-hexene). This could be accomplished by using a high monomer batch process with a Ti amine bis-phenolate catalyst. Alternatively, a semibatch process featuring a Zr metal centered catalyst could be utilized, where cooled 1-hexene is continually fed into a thermally-regulated reactor to maintain a constant temperature. Between the two processes, the Zr system could potentially produce longer polymers with fewer regioerrors, use less catalyst material, and be faster than the alternative Ti batch system. The design of this polymerization reactor system comes directly from knowing the polymer mechanism and associated rate constants in Table 3.1.

With regard to the polymer termination process, it has been previously shown that the chain transfer rate constant ($k_{vinylidene}$) for **1b**–**3b**/**1c**–**3c** catalysts correlates to the metal–pendant (M–X) bond lengths.[9c] A plot of the logarithm of $k_{vinylidene}$ for catalysts **1a**–**3a**

versus the M–X bond length in the precatalyst structures forms a linear relationship as shown in Figure 3.14. Surprisingly, the Ti catalysts have a slope comparable to that for the Hf catalysts. At this time, we do not have a clear understanding of the features of the molecular structure that govern the β-hydride agostic interactions necessary for chain transfer other than that the size of a catalyst's active site (M-X bond distance) can be directly correlated to the monomer-independent vinylidene chain transfer rate constant. The pendant sterics could directly influence the polymer chain transfer or some other factor could influence both the M–pendant bond length and the β-hydride elimination reaction. Regardless, this key bond length is a chemical descriptor that can be used in designing processes that are targeted either to reduce the vinylidene termination rate, producing long polymers, or increase the vinylidene termination rate, thus producing oligomers.

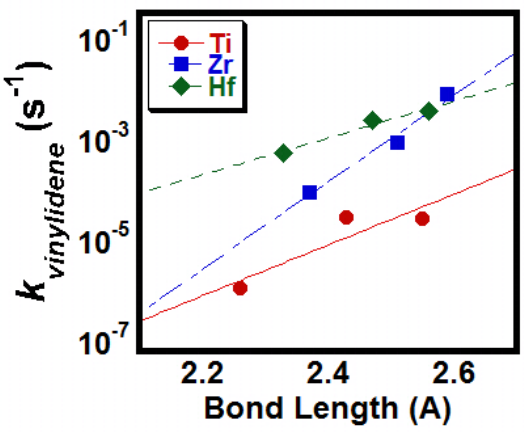

Figure 3.14 Log $k_{vinylidene}$ vs **1a-3c** M-X bond lengths

3.5 Conclusions

A comprehensive kinetic study of three catalytic systems based on hafnium amine bis-phenolate complexes has been completed, and the relevant rate constants and elementary reaction steps were robustly determined for each system. The mechanism includes initiation, normal propagation, misinsertion, recovery, and chain transfer. In conjunction with the previous study of zirconium analogs, this report allows for the first quantitative comparison between similarly ligated hafnium and zirconium based olefin polymerization catalysts. The most important findings are: the one order of magnitude decrease in k_p for the hafnium catalysts; an overall decrease in all monomer dependent reaction steps; and the correlation between the logarithm of monomer independent chain transfer and the hafnium pendant ligand (Hf-X) bond distance. The last observation is similar to the one previously reported for zirconium systems, but in case of the hafnium catalysts the dependence is 2.7 times weaker. However, it is also interesting that there does not appear to be such a correlation that can be drawn for the propagation rate constant. Subsquent studies are ongoing to ascertain the dependence of k_p on the steric and electronic nature of the pendant. Furthermore, this work has been submitted to ACS Catalysis.[29]

3.6 References

(1) (a) Chen, E. Y-X.; Marks, T. J. *Chem. Rev.* **2000**, *100*, 1391-1434. (b) Li, H.; Marks, T. J. *Proc. Natl. Sci. U.S.A.* **2006**, *103*, 15295-15302. (c) Delferro, M.; Marks, T. J. *Chem. Rev.* **2011**, *111*, 2450-2485.

(2) (a) Krauledat, H.; Brintzinger, H.H. *Angew. Chem., Int. Ed.* **1990**, *29*, 1412-1413. (b) Piers, W. E.; Bercaw, J. E. *J. Am. Chem. Soc.* **1990**, *112*, 9406-9707. (c) Coates, G. W.; Waymouth, R. M. *J. Am. Chem. Soc.* **1991**, *113*, 6270-6271. (d) Coates, G. W.; Waymouth, R. M. *Science* **1995**, *267*, 217-218.

(3) Manz, T.A.; Phomphrai, K.; Medvedev, G. A.; Krishnamurthy, B. B.; Sharma, S.; Haq, J.; Novstrup, K. A.; Thomson, K. T.; Delgass, W. N.; Caruthers, J. M.; Abu-Omar, M. M. *J. Am. Chem. Soc.* **2007**, *129*, 3776-3777.

(4) Britovsek, G. J. P.; Gibson, V. C.; Wass, D. F. *Angew. Chem., Int. Ed.* **1999**, *38*, 428-447.

(5) Markets and Markets, Inc. Polyolefins Market By Types (Low, Linear & High Density Polyethylene, Polypropylene And Ethylene Vinyl Acetate),

(6) Huang, J.; Rempel, G. L. *Prog. Polym. Sci.*, **1995**, 20, 459-526.

(7) (a) Möhring, P. C.; Coville, N. J. *Coord. Chem. Rev.* **2006**, *250*, 18-35. (b) Möhring, P. C.; Coville, N. J. *J. Organometallic Chem.* **1994**, *479*, 1-29.

(8) (a) Moscato, B. M.; Zhu, B.; Landis, C. R. *Organometallics* **2012**, *31*, 2097-2107. (b) Liu, Z.; Somsook, E.; Landis, C. R. *J. Am. Chem. Soc.* **2001**, *123*, 2915-2916. (c) Liu, Z.; Somsook, E.; White, C. B.; Rosaaen, K. A.; Landis, C. R. *J. Am. Chem. Soc.* **2001**, *123*, 11193-11207. (d) Novstrup, K. A.; Travia, N. E.; Medvedev, G. A.; Stanciu, C; Switzer, J. M.; Thomson, K. T.; Delgass, W. N.; Abu-Omar, M. M.; Caruthers, J. M. *J. Am. Chem. Soc.* **2010**, *132*, 558-566.

(9) (a) Switzer, J. M.; Travia, N. E.; Steelman, K. D.; Medvedev, G. A.; Thomson, K. T.; Delgass, W. N.; Abu-Omar, M. M.; Caruthers, J. M. *Macromolecules* **2012**, *45*, 4978-4988. (b) Steelman, D. K.; Xiong, S.; Pletcher, P. D.; Smith, E.; Switzer, J. M.; Medvedev, G. A.; Delgass, W. N.; Caruthers, J. M.; Abu-Omar M. M. *J. Am. Chem. Soc.* **2013**, *135*, 6280-6288. (c) Steelman, D. K.; Pletcher, P. D.; Switzer, J. M.; Xiong, S.; Medvedev, G. A.; Delgass, W. N.; Caruthers, J. M.; Abu-Omar M. M. *Organometallics* **2013**, *32*, 4862-4867. (d) Steelman, D. K.; Xiong, S.; Medvedev, G. A.; Delgass, W. N.; Caruthers, J. M.; Abu-Omar M. M. *ACS Catal.* **2014**, *4*, 2186-2190. (e) Xiong, S.; Steelman, D. K.; Medvedev, G. A.; Delgass, W. N.; Abu-Omar M. M.; Caruthers, J. M. *ACS Catal.* **2014**, *4*, 1162-1170.

(10) (a) Alt, H. G.; Köppl, A. *Chem. Rev.* **2000**, *100*, 1205-1221. (b) Kaminsky, W.; Schlobohm, M. *Makromol. Chem., Macromol. Symp.* **1986**, *4*, 103-118. (c) D'Agnillo, L.; Soares, J. B. P.; Penlidis, A. *Macromol. Chem. Phys.* **1998**, *199*, 955-962. (d) Silveira, F.; Simplício, L. M. T.; Rocha, Z. N.; dos Santos, J. H. Z. *Appl. Catal. A.* **2008**, *344*, 98–106. (e) Quijada, R.; Dupont, J.; Silveira, D. C.; Miranda, M. S. L.; Scipioni, R. B.; *Macromol. Rapid Commun.* **1995**, *16*, 357-362. (f) Soga, K.; Kim, H. J.; Shiono, T.; *Makromol. Chem., Rapid Commun.* **1993**, *14*, 765-770. (g) Martinho Simões, J. A.; Beauchamp, J. L. *Chem. Rev.* **1990**, *90*, 629-688. (h) Ihm, S. I.; Chu, K. J.; Yin, J. H.; Soga,K. Studies in Surface Science and Catalysis Advisory, Proceedings of the International Symposium on Catalyst Design for Tailor-Made Polyolefins, Terano, M. Kanazawa, Japan, (1994), pp. 299–306.

(11) (a) Xie, Z. *Coord. Chem. Rev.* **2006**, *250*, 3850-3855. (b) Zi, G.; Li, H.-W.; Xie, Z. *Organometallics* **2002**, *21*, 3850-3855. (c) Britovsek, G. J.; Gibson, V. C.; Wass, D. F. *Angew. Chem. Int. Ed.* **1999**, *38*, 428-447 (d) Gibson, V. C.; Spitzmesser, S. K. *Chem. Rev.* **2003**, *103*, 283-315. (e) Makio, H.; Kashiwa, N.; Fujita, T. *Adv. Synth. Catal.* **2002**, *344*, 477-493 (f) Makio, H.; Terao, H.; Iwashita, A.; Fujita, T. *Chem. Rev.* **2011**, *111*, 2363-2449.

(12) Margl, P.; Deng, L.; Ziegler, T. *J. Am. Chem. Soc.* **1998**, *120*, 5517-5525.

(13) (a) Nakata, N.; Toda, T.; Ishii, A. *Polym. Chem.* **2011**, *2*, 1597-1610. (b) Cohen, A.; Kopilov, J.; Lamberti, M.; Vednitto, V.; Kol, M. *Macromolecules* **2010**, *43*, 1689-1691.

(14) (a) Roll, W.; Britzinger, H-H.; Rieger, B.; Zolk, R. *Angew. Chem., Int. Ed.* **1990**, *29*, 279-280. (b) Chadwick, J. C.; van der Burgt, F. P. T.; Rastogi, S. *Macromolecules* **2004**, *37*, 9722-9727. (c) Klingelhofer, S.; Schellengerg, C.; Pommerehne, J.; Bassler, H.; Greiner, A.; Heitz, W. *Macro. Chem. Phys.* **1997**, *198*, 1511-1530. (d) Busico, V.; Cipullo, R.; Ronca, S. *Macromolecules* **2002**, *35*, 1537-1542.

(15) (a)Esteb, J. J. Stereoselective Polymerization with Single-Site Catalysis. In *Substituted Indenyl and Cyclopentadienyl Catalysts for Stereoselective Propylene Polymerization*; Baugh, L. S.; Canich, J. A. M., Ed.; Taylor & Francis Group; CRC: Boca Raton, FL, 2008; pp 37-82. (b) Ma, H.; Huang, J. Stereoselective Polymerization with Single-Site Catalysis. In *Tactic Polystyrene and Styrene Copolymers*; Baugh, L. S.; Canich, J. A. M., Ed.; Taylor & Francis Group; CRC: Boca Raton, FL, 2008; pp 37-82.

(16) Hustad, P. D.; Tian, J.; Coates, G. W. *J. Am. Chem. Soc.* **2002**, *124*, 3614-3621.

(17) Guo, N.; Li, L.; Marks, T. J. *J. Am. Chem. Soc.* **2004**, *126*, 6542-6543.

(18) (a) von Schneck, H.; Strömberg, S.; Zetterberg, K.; Ludwig, M.; Akermark, B.; Svensson, M. *Organometallics* **2001**, *20*, 2813-2819. (b) Deubel, D.; Ziegler, T. *Organometallics* **2002**, *21*, 4432-4441.

(19) Nakamura, A.; Ito, S.; Nozaki, K. *Chem. Rev.* **2009**, *109*, 5215-5244.

(20) (a) Theaker, G. W.; Morton, C.; Scott, P. *Dalton Trans.* **2008**, 6883-6885. (b) Chirik, P. J.; Bercaw, J. E. *Organometallics* **2005**, *24*, 5407-5423.

(21) Galdi, N.; Izzo, L.; Oliva, L. *Organometallics* **2010**, *29*, 4434-4439.

(22) Cipullo, R; Busico, V.; Fraldi, N.; Pellecchia, R.; Talarico, G. *Macromolecules* **2009**, *42*, 3869-3872.

(23) Margl, P.; Deng, L.; Ziegler, T. *J. Am. Chem. Soc.***1999**, *121*, 154-162.

(24) (a) Groysman, S.; Goldberg, I.; Kol, M.; Genizi, E.; Goldschmidt, Z. *Inorganica Chimica Acta.* **2003**, *345*, 137-144. (b) Tshuva, E. Y.; Goldberg, I.; Kol, M.; Goldschmidt, Z. *Inorganic Chem. Comm.* **2000**, *3*, 611-614. (c) Groysman, S.; Tshuva, E. Y.; Goldberg, I.; Kol, M.; Goldschmidt, Z.; Shuster, M. *Organometallics*, **2004**, *23*, 5291-5299.

(25) (a) Tshuva, E. Y.; Goldberg, I.; Kol, M.; Weitman, H.; Goldschmidt, Z. *Chem. Comm.* **2000**, 379-380. (b) Tshuva, E. Y.; Goldberg, I.; Kol, M. *Organometallics* **2001**, *20*, 3017-3028.

(26) Tshuva, E. Y.; Groysman, S.; Goldberg, I.; Kol, M. *Organometallics* **2002**, *21*, 662-670.

(27) Kissounko, D. A.; Zhang, Y.; Harney, M. B.; Sita, L. R. *Adv. Synth. Catal.* **2005**, *347*, 426−432.

(28) Rieger, B.; Carten, T.; Preuschen, J. *Macromolecules* **2002**, *35*, 5742-5743.

(29) Pletcher, P. D.; Switzer, J. M.; Steelman, D. K.; Medvedev, G. A.; Delgass, W. N.; Caruthers, J. M.; Abu-Omar M. M. *ACS Cat.* Submitted.

CHAPTER 4. KINETIC MODELING FOR THE DETERMINATION OF THERMODYNAMIC ACTIVATION PARAMETERS OF SELECT ZIRCONIUM AMINE BIS-PHENOLATE CATALYSTS FOR 1-HEXENE POLYMERIZATION

4.1 Introduction

The effect of reaction temperature on the polymerization of α-olefins by single-site catalysts has been rigorously studied by a number of research teams. These studies show that catalyst activity increases,[1] polymer chain length decreases[1d-f,2] and stereoregularity decreases[1b,c,e,2-3] with increasing reaction temperature. The clear kinetic reasoning for these effects is that the competing reactions of chain transfer, epimerization, and regioerrors increase more quickly than the increases in the propagation rate constant. Though initial reports by Andresen et al. in the 1970s on ethylene polymerization by alkylaluminum-activated titanium metallocenes exist in the literature,[1a] it has only been very recent that more precise studies have begun to probe activation parameters in single-site polymerization.

The results and discussions sections were contributed by Dr. Jeffery Switzer of Purdue Chemical Engineering.

One of the most difficult problems obtaining reliable activation parameters is the challenge in obtaining robust kinetic rate constants at a series of reaction temperatures. As such, less precise parameters, such as activity, are often measured. Polymerization activity, here described as the growth rate constant for a particular catalyst with the units of polymer mass per catalyst site per unit time, provides a simple measurement on the number of catalytic turnovers for a catalyst, and is both academically and industrially important. Alt and Köppl presented a comprehensive review in 2000 on the activity of ethylene polymerization by Group IV metallocenes in the attempt to correlate catalyst structure to literature reported activity measurements.[4] While they ultimately identified that the amount of steric crowding near the active site influenced polymerization activity, they were unable to find a quantitative relationship based on reported catalyst activity measurements.

The cause for the lack of quantitative correlations between activity and catalyst structure is due to a host of different causes. One of the most commonly accepted reasons is that catalyst dormancy or deactivation can reduce catalytic turnover as the reaction precedes in time. Furthermore, polymerization activity is not equivalent to a catalyst's propagation rate constant as measured in batch reactions; activity decreases over time as less monomer is present while a rate constant is independent on the changing monomer concentration. It is clear that obtaining quantitative rate constants of elementary reactions within the polymerization mechanism is the only reliable method to determine stucture activity relationships and reliable activation parameters

In an attempt to obtain rate constants, Rytter and coworkers analyzed ethylene and propylene polymerization reactions utilizing zirconium dichloride catalysts with methylaluminoxane (MAO) activators.[5] Measuring catalytic activity over a 100 °C

temperature range, they looked at catalytic activity over time. While their models included initiation by first insertion of olefin into the catalysts, propagation, dormant site formation, chain termination, and catalyst deactivation. Modeling the data gave rise to propagation rate constants that would differ over an order of magnitude to the traditionally reported activity measurements and allowed for activation parameters to be calculated. Using these values, they were able to have predict catalytic activity at temperatures not directly studied.

Following Rytter and coworker's success, a series of studies were reported where the propagation,[6] initiation,[6a-c,7] chain transfer,[6a-d,8] and deactivation[9] rate constants were successfully measured. However, the activation parameters for these rate constants were only determined in a few select cases.[6c-g,9] Liu and coworkers published a complete kinetic analysis of the *rac*-(C_2H_4(1-indenyl)$_2$)$ZrMe_2$/$B(C_6F_5)_3$ catalyst system in the polymerization of 1-hexene.[6c] Collecting data over a 60°C temperature range, they calculated activation parameters for the initiation, propagation, and chain transfer reaction rate constants. Interestingly, they chose to analyze the data response of each rate constant separately at different temperature, instead of calculating the rate constants for the entire mechanism at each temperature as a whole, and would apply this methodology to the formation of polypropylene.[6d] These studies have led to a multitude of activation parameter studies for several MAO activated catalysts systems. [6e,f,10] In light of these reports, groups have hypothesized that catalysts having relatively large, more negative entropy's of activation (<–30 cal mol^{-1} K^{-1}) with small enthalpy's of activation (~5-10 kcal mol^{-1}) exhibited slower propagation rate constants when compared to more active, industrially-used catalysts.[10a]

While these insights have provided tremendous new understanding on the nature of catalyst activity, it is important to ensure that the kinetic methods used to study these catalysts are able to produce the most accurate rate constants. In a study by Novstrup et al.,[11] a simultaneous fitting of all kinetic data was applied to the previously mentioned study by Liu and coworkers for 1-hexene polymerization. By also utilizing the precise shape of the molecular weight distribution (MWD) over time, a correction factor was needed for the propagation rate constant at 0°C to correctly fit the data. This suggests that the piecemeal approach to kinetic modeling may not provide the required accuracy for analysis of activation parameters over a large temperature range.

In this chapter, we examine 1-hexene polymerization kinetics and mechanism for three zirconium amine bis-phenolate catalysts, Figure 4.1, over a 40°C temperature range, including the kinetic data at 25 °C that has been discussed in previous work.[12] Models including rate constants for initiation, propagation via 1,2-insertion, misinsertion via 2,1-insertion, recovery, chain transfer, and reinitiation, Scheme 4.1, have been analyzed and different temperatures to examine the thermodynamic activation parameters.

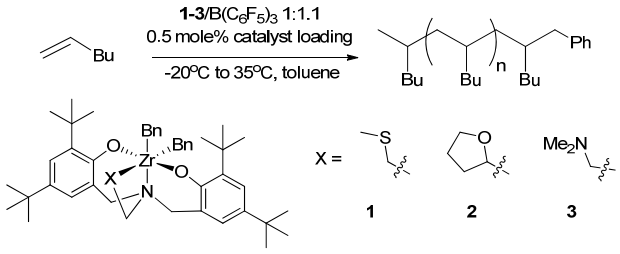

Figure 4.1 Zr amine bis-phenolate catalysts studied in a wide temperature range **1-3**

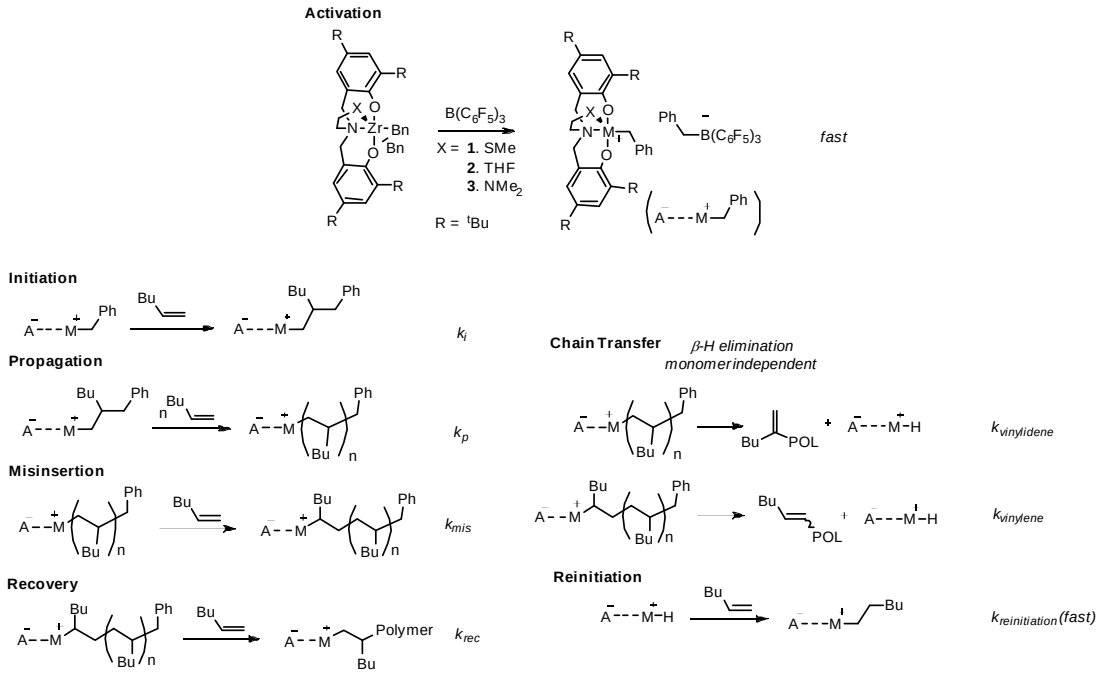

Scheme 4.1 Mechanism and elementary rate constants used for modeling catalysts **1-3**

4.2 Experimental Procedure

General Procedure: All manipulations were performed under dry inert atmosphere in a glove box or in a vacuum manifold using air sensitive techniques under N_2 or Ar atmosphere. Solvents were distilled over activated alumina and a copper catalyst using a solvent purification system (PPT- Pure Process Technology) and degassed before being stored over activated molecular sieves. Tetrabenzylzirconium was purchased from STREM and used as received. The monomer 1-hexene was purchased from Aldrich and purified by distillation over a small amount of dimethyl bis(cyclopentadienyl)zirconium and stored over activated molecular sieves. Tris(pentafluorophenyl)boron was purchased from STREM and purified by sublimation. Diphenylmethane was purchased from Aldrich, degassed, and stored over molecular sieves. CD_3OD was purchased from Cambridge

Isotopes and used as received. D_8-toluene was degassed and stored over molecular sieves. ^1H and ^2H NMR experiments were performed on a Varian INOVA600 MHz or Bruker DRX500 MHz spectrometer. The ligands and precatalysts were prepared following literature procedures.[12]

NMR scale quenched polymerization of 1-hexene with Zr[tBuON^{X}O]Bn$_2$ (X = SMe, THF, NMe$_2$): The time dependent concentrations of different species were monitored by quenching the samples using d_4-methanol at times representing 30%/60%/90% conversion of initial 1-hexene amount. The procedure for NMR scale polymerization is based on literature.[12a,b] As an example of a typical polymerization, Zr[tBuON^{SMe}O]Bn$_2$ (21.0 mg, 0.02625 mmol) was dissolved into 3.5 ml toluene using a stir bar. Three 1 mL aliquots of the precatalyst solution were then separated into vials containing pierceable screw-top caps. A 3 ml syringe, needle, and a vial containing the precatalyst solution were placed into a N_2 bag. The vial in the bag was submerged into a constant temperature bath at the requisite temperature At 35 °C an oil bath was used, at 0 °C an ice bath was used, at –17 °C a dichlorobenzene/dry ice bath was used, and at –20 °C an acetone/dry ice bath was used. Meanwhile, tris(pentafluorophenyl)boron (14.1 mg, 0.0275 mmol), 1-hexene (0.4208 grams, 5 mmol), and diphenylmethane (8.4 mg, 8.33 mmol) were added to a 5 mL volumetric flask and diluted to the mark using d_8-toluene. A 1.5 mL aliquot of this stock solution was added into each of three NMR tubes containing a pierceable septum. These monomer/activator solutions were then placed into a spectrometer and allowed to equilibrate to room temperature, and the initial monomer concentration was taken relative to the diphenylmethane standard. The sample was taken to the respective temperature bath and allowed to equilibrate to temperature. The catalyst solution was then added to the

monomer/activator solution by piercing the cap while the syringe remained in the N_2 bag. The reaction mixture was then shaken for 30 seconds outside of the bath before being returned. The reactions were quenched at different times. Each sample was dried, dissolved in hexane, filtered through alumina to remove dead catalyst, dried again, and placed under vacuum for 12 hours to get a total polymer weight.

The material was analyzed by ^{1}H NMR to verify the conversion of monomer in accordance with literature procedure.[12a,b] For vinyl analysis, 1.2 mL of $CDCl_3$ was added to the dried polymer to completely dissolve the polymer. A 1 mL aliquot was removed and placed into an NMR tube. Diphenylmethane (70.0 mg, 0.42 mmol) dissolved in $CDCl_3$ in a 5 mL volumetric flask was used as an internal standard using the method of standard additions, where 10 microliter aliquots were added to the sample to quantify the amount of end groups through ^{1}H NMR. The sample was then dried and reweighed to compare what percentage of polymer was quantified to determine total concentration of vinyl groups. The two polymer samples were recombined and dried.

For ^{2}H analysis, a similar procedure to vinyl analysis was followed. Following quenching, 1.2 mL of dichloromethane was added to the dried polymer sample, and the polymer was dissolved. A 1 mL aliquot was removed and placed into a NMR tube. As a standard, d_6-benzene (80.0 mg, 0.95 mmol) was dissolved in dichloromethane in a 5 mL volumetric flask. The sample was then analyzed utilizing the method of standard additions. The sample was then dried and weighed to determine the percentage of polymer analyzed and total amount of active sites from deuterium labeling. The procedure listed above was used for all catalyst systems, with the measured amounts adjusted to provide the desired experimental concentrations.

Gel permeation chromatography (GPC) analysis: The procedure used to analyze polymer samples using GPC methods was taken from Novstrup et al.,[11] and it is summarized below. Poly(1-hexene) samples were added to THF at room temperature and allowed to dissolve for 4 h. Solutions were then passed through a 0.2 μm filter to remove any particulate matter. The GPC analysis was performed on a Viscotek TDAmax. Samples were injected through a 200 μL injection loop and passed through three Viscotek T6000M 10 μm General Mixed Org columns in series in a 35 °C oven at a flow rate of 1.0 mL min^{-1}. The analysis made use of the differential RI detector, a viscometer, and two light scattering detectors angled at 90° and 7°. Molecular weights were assigned by way of the triple detection calibration method. System parameters were calibrated with a 99,000 g mol^{-1} polystyrene standard. The calibration was verified through the analysis of a broad standard, SRM 706a, provided by the National Institute of Standards and Technology.

Kinetic modeling analysis: In order to determine the kinetic models for each data set, the methods described in our previous work have been employed.[12a] Such methodology was found sufficient to produce good fits in almost all cases, with poor fits being ascribed to experimental problems. Errors in the rate constants were assigned by using the standard errors as calculated through the weighted least squares optimization routine, also described in our previous work.[12a]

Catalyst synthesis: Catalysts synthesized here are included in Chapter 2.

4.3 Results

Three catalyst systems were studied to gauge the effects of temperature changes on 1-hexene polymerization. The precatalysts were: Zr-tBu$_4$[ON^{X}O]Bn$_2$ [X = SMe (**1**), THF (**2**), NMe$_2$ (**3**)]. In all cases, B(C$_6$F$_5$)$_3$ was used to activate the precatalyst. All experiments were carried out in toluene. Each catalyst system was studied at three temperatures: **1** was studied at –17 °C, 22 °C, and 35 °C; and **2** and **3** were studied at –20 °C, 0 °C, and 25 °C. The mechanisms and rates for **1** at 22 °C and **2**–**3** at 25 °C have been previously published.[12]

Kinetic modeling methods discussed in previous work have been used to obtain kinetic mechanisms and rate constants that provide good fits of the data sets collected. In all cases, the data sets consisted of the following: monomer concentration, vinylidene and vinylene concentration, primary and secondary deuterium incorporation following catalyst quenching, and molecular weight distribution of the polymer product, all as a function of reaction time. The mechanisms were not assumed *a priori* to follow the same mechanism, but many similarities were seen.

In the following figures, the model fits are color-coded by the corresponding catalyst as follows: SMe pendant (**1**): Green; THF pendant (**2**): Red; NMe$_2$ pendant (**3**): Blue. Black will represent experimental data, regardless of the catalyst that was used.

The data and model fits for **1**–**3** that have not been previously published are shown in Figure 4.2. The following comments can be made regarding the data:

(i) In all cases, both primary and secondary deuterium labels were discovered. The labels, which originate on the quenching agent, CD$_3$OD, are assumed to affix to the growing end of the polymer, and their concentrations therefore represent the active

site concentration before quenching. The presence of both primary and secondary sites is evidence that monomer misinsertion (that is, 2,1-insertion) occurs at some rate in all cases.

(ii) In all cases, both vinylidene and vinylene groups were discovered. Vinylidene groups are assumed to originate from a chain transfer pathway (either monomer dependent or independent) where the reactant is a primary active site (a primary carbon is bonded to the metal), whereas vinylene groups originate from secondary active sites (a secondary carbon is bonded to the metal).

(iii) Assuming that active site concentrations are constant (which they all roughly are, as seen in Figure 4.2d), vinyl groups will either form linearly with time (independent of monomer concentration) or will have a decreasing growth rate (dependent on monomer concentration). As seen in Figure 4.2, the vinyl formation rate always decreases late in the reaction at these temperatures. The vinyl formation pathways are therefore monomer dependent. This typically occurs through a β-H transfer to monomer pathway.

(iv) All experiments shown were carried out with a 200:1 ratio for 1-hexene:precatalyst. If polymerization were "living," one would expect a maximum chain length of approximately 16,800 g mol^{-1} (about 4.2 on the log scale). However, despite chain transfer reactions decreasing the chain length, in each case the maximum polymer molecular weight exceeds this value. The mechanism must account for this in some manner. Three possible mechanistic features that will achieve higher-than-living molecular weight are: (i) initiation is slow compared to propagation, (ii) the secondary sites are slow to insert additional monomers, and (iii) not all of the

precatalyst activates or otherwise participates in polymerization. In each of these three cases, the amount of working catalyst is reduced, effectively increasing the 1-hexene:catalyst ratio. Each method has a different effect on the other data features and can therefore be distinguished from the rest. It can be seen from the rate constants, shown in Tables 4.1, 4.2 and 4.3, that all three of these features exist for all catalysts to some degree.

These clues were used to assist in model selection and optimization. The chemical mechanisms include the following reactions: (i) propagation, (ii) initiation (which is sometimes slow compared to propagation), (iii) misinsertion and recovery, (iv) monomer dependent vinylidene and vinylene formation, and in some cases (v) monomer independent catalyst deactivation. Catalyst participation was also less than 100% in all cases. The similarity of all these models allows us to compare rate constants and activation parameters among all reaction temperatures and catalysts. The rate constants corresponding to the models (including previously published rates for comparison) are shown in Tables 4.1, 4.2 and 4.3.

Ultimately, good fits were produced for the majority of the data. The most striking exception is the molecular weight distribution fit for **2** at 0 °C. The early experimental distribution (shown in black in Figure 4.2) is predicted to have a shape quite similar to the later distributions, but shifted to a lower molecular weight. However, the model prediction shows a distribution with a much steeper high molecular weight tail. It is possible to select an alternative model that fits the early distribution well, but all such models heretofore discovered fit the later distributions and the vinyl and active site data poorly.

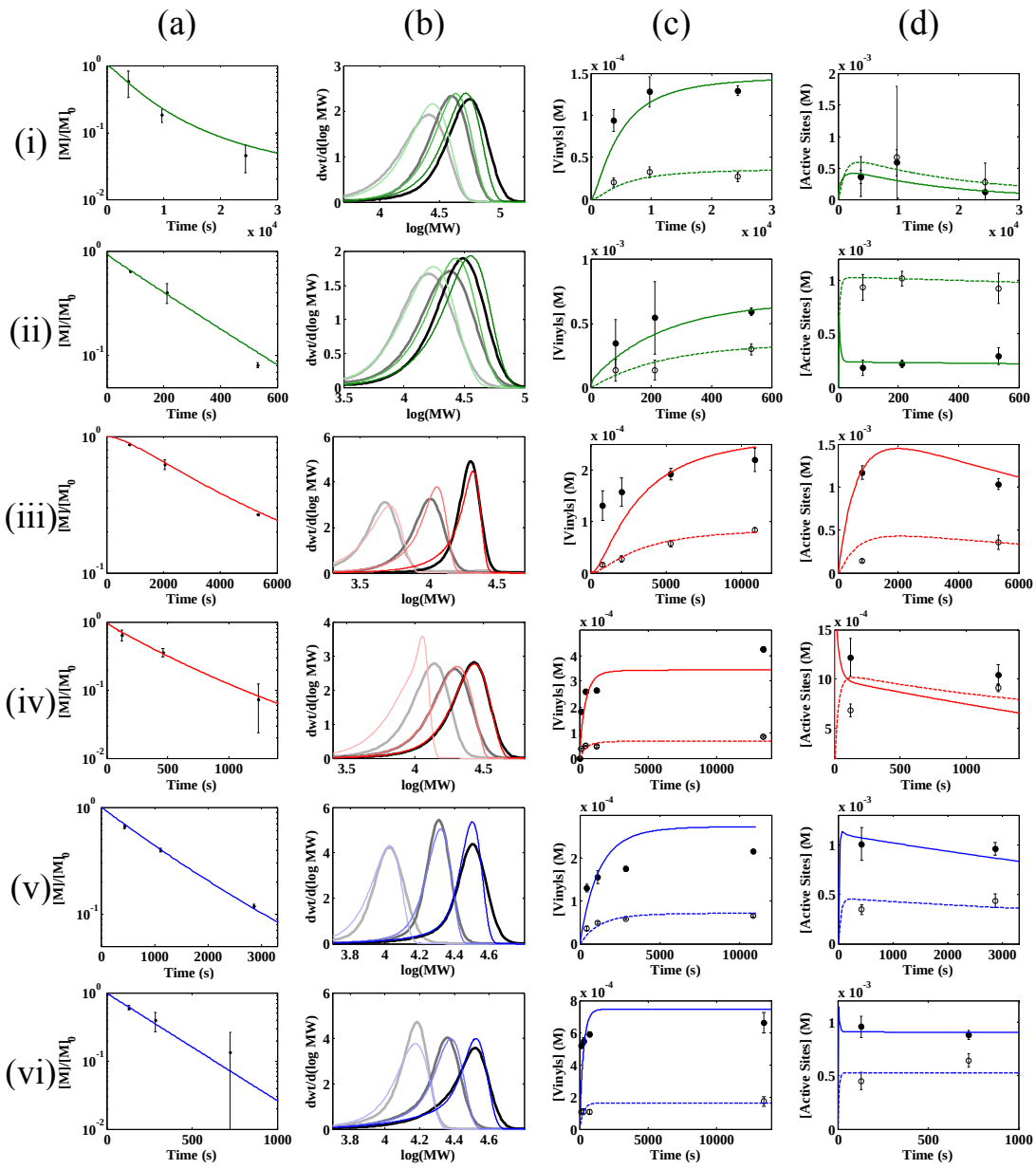

Figure 4.2 Data and model fits for 1-hexene polymerization by **1**–**3**/$B(C_6F_5)_3$ in toluene. $[\mathbf{1}–\mathbf{3}]_0$ = 3 mM; $[B(C_6F_5)_3]_0$ = 3.3 mM; $[1\text{-hexene}]_0$ = 600 mM. Black: data; color: model fits. The rate constants for the models are in Tables 4.1, 4.2, and 4.3. Row (i): **1** at –17 °C; Row (ii): **1** at 35 °C; Row (iii): **2** at –20 °C; Row (iv): **2** at 0 °C; Row (v): **3** at –20 °C; Row (iv): **3** at 0 °C. Column (a): monomer consumption; Column (b): molecular weight distributions at times corresponding to data in column 1; Column (c): vinylidene (solid) and vinylene (open) concentrations; Column (d): primary (solid) and secondary (open) active site concentrations.

Table 4.1. Rate constants for **1** at different temperatures

	−17 °C	22 °C	35 °C
k_p M^{-1} s^{-1}	0.411 ± 0.017	12.3 ± 4.1	16.91 ± 0.27
k_{mis} M^{-1} s^{-1}	0.0051 ± 0.0007	0.20 ± 0.07	0.315 ± 0.014
k_{rec} M^{-1} s^{-1}	0.00348 ± 0.00046	0.0359 ± 0.0009	0.0696 ± 0.0029
$k_{vinylidene}$ (10^{-3}) M^{-1} s^{-1}	0.1054 ± 0.0048	2.2 ± 0.5	19.80 ± .35
$k_{vinylene}$ (10^{-3}) M^{-1} s^{-1}	0.0184 ± 0.0009	0.949 ± 0.028	2.56 ± 0.06
k_i M^{-1} s^{-1}	0.00146 ± 0.00028	0.0172 ± 0.0013	$0.17 < k_i \leq k_p$
k_d (10^{-3}) s^{-1}	0.127 ± 0.013	7.9 ± 1.2	0
Catalyst participation	0.475 ± 0.028	1 ± 0	0.4171 ± 0.0021

Table 4.2. Rate constants for **2** at different temperatures

	–20 °C	0 °C	25 °C
k_p M^{-1} s^{-1}	0.1720 ± 0.0022	1.751 ± 0.016	8.0 ± 0.5
k_{mis} M^{-1} s^{-1}	0.0081 ± 0.0015	0.0173 ± 0.0015	0.054 ± 0.015
k_{rec} M^{-1} s^{-1}	0.0272 ± 0.0049	0.0365 ± 0.0026	0.047 ± 0.012
$k_{vinylidene}$ (10^{-3}) M^{-1} s^{-1}	0.087 ± 0.007	0.381 ± 0.042	1st order
$k_{vinylene}$ (10^{-3}) M^{-1} s^{-1}	0.0949 ± 0.0043	0.46 ± 0.06	1st order
k_i M^{-1} s^{-1}	0.00252 ± 0.00019	0.046	± 0.006 0.015
k_d (10^{-3}) s^{-1}	0.107 ± 0.010	0	0
Catalyst participation	0.815 ± 0.031	0.652 ± 0.009	varies

Table 4.3. Rate constants for **3** for different temperatures

	–20 °C	0 °C	25 °C
k_p M^{-1} s^{-1}	0.723 ± 0.010	3.86 ± 0.10	11.9 ± 1.2
k_{mis} M^{-1} s^{-1}	0.0152 ± 0.0014	0.106 ± 0.009	0.082 ± 0.009
k_{rec} M^{-1} s^{-1}	0.0367 ± 0.0027	0.174 ± 0.012	0.116 ± 0.028
$k_{vinylidene}$ (10^{-3}) M^{-1} s^{-1}	0.406 ± 0.040	5.13 ± 0.16	1st order
$k_{vinylene}$ (10^{-3}) M^{-1} s^{-1}	0.224 ± 0.007	1.90 ± 0.09	1st order
k_i M^{-1} s^{-1}	0.087 ± 0.035	$0.2 < k_i \leq k_p$	0.11
k_d (10^{-3}) s^{-1}	0	0	
Catalyst participation	0.4960 ± 0.0036	0.4787 ± 0.0042	varies

The rate constants in Tables 4.1, 4.2, and 4.3 are shown graphically in Figure 4.3. They are displayed in an Arrhenius plot to identify linearity. Figure 4.3a shows that k_p obeys typical Arrhenius behavior for all catalyst over the temperature range studied. Figure 4.3 also shows that other than k_i, the remaining rate constants (k_{mis}, k_{rec}, $k_{vinylidene}$, and $k_{vinylene}$) for **1** obey Arrhenius behavior as well. For **2** and **3**, k_i, k_{mis}, and k_{rec} have some deviation from Arrhenius behavior. The most striking feature of Figure 4.3 is that in several cases the temperature independent rate constant at 0 °C is about the same or is faster than the value at 25 °C.

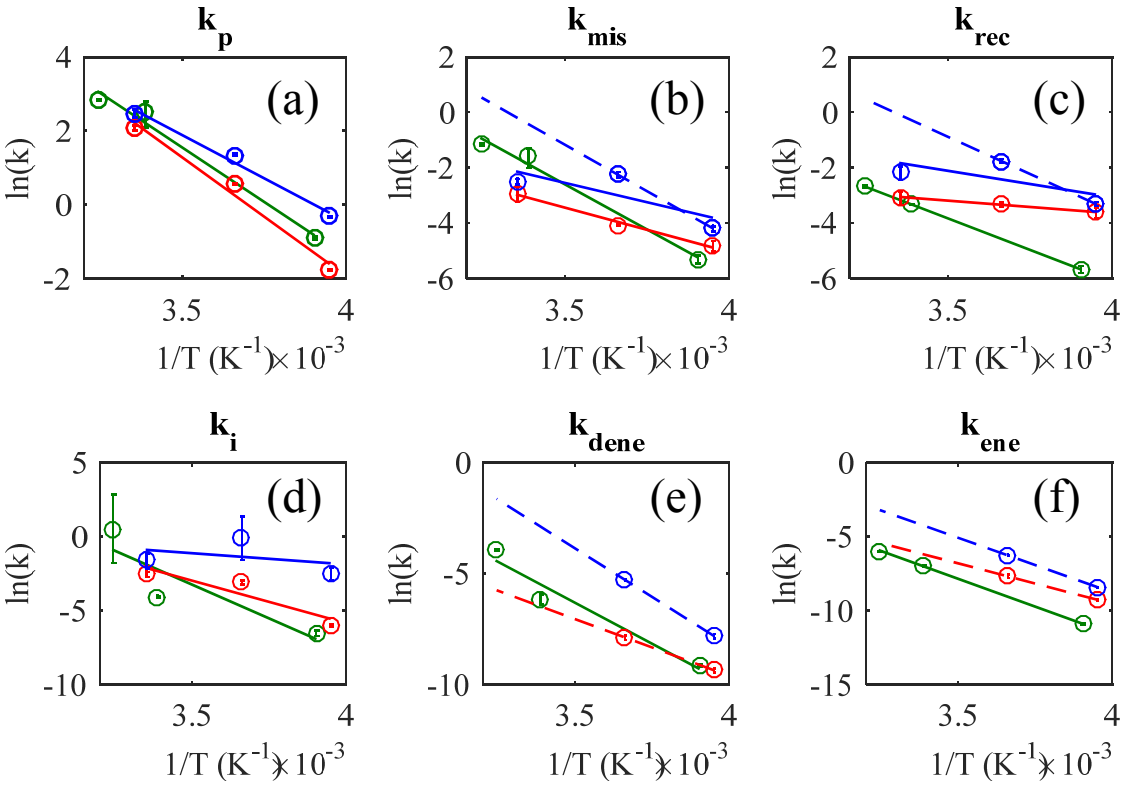

Figure 4.3 Arrhenius plots for kinetic rate constants describing the kinetic behavior of catalysts **1-3**; Green: **1**, Red: **2**, Blue: **3**

With regard to chain transfer, while the mechanism for **1** is the same at all temperatures, there appears to be a change in the chain transfer mechanism for **2** and **3** when the temperature changes. As previously noted, at the lower temperatures (–20 and 0 °C) vinyl groups form more slowly as monomer is consumed. Our published results show that at the higher temperature (25 °C) vinyl groups form at a constant rate regardless of the monomer concentration. Thus the low temperature chain transfer rate constants for **2** and **3** cannot be compared to the high temperature rate constants. We may still extract activation parameters for monomer dependent chain transfer from the two available data points. Figure 4.3e and Figure 4.3f show the line between the two low temperature data points to provide a rough comparison with the results from **1**.

4.4 Discussion

The thermodynamic activation parameters for catalysts **1-3** are given in Table 4.3. These values were calculated under the assumption that the rate constants, shown in Figure 4.2, follow Arrhenius behavior, outlined by the Equation 4.1:

$$k = Ae^{-\frac{E_a}{RT}} \qquad \text{Equation 4.1}$$

Where k is the rate constant, R is the ideal gas constant, and T is the reaction temperature. E_a and A are the model parameters derived from the linear fit of the data in Figure 4.3 and are known as the activation energy and the preexponential factor, respectively. Their connection to the activation parameters comes from applying the Eyring equation of transition state theory, Equation 4.2:

$$k = \kappa \frac{k_B T}{h} e^{\frac{\Delta S^{\ddagger}}{R}} e^{\frac{-\Delta H^{\ddagger}}{RT}} \qquad \text{Equation 4.2}$$

Where k_B is Boltzmann's constant, h is Planck's constant, and $\Delta S^{\ddagger}$ and $\Delta H^{\ddagger}$ are the entropy and enthalpy of activation, respectively. The parameter κ is the transmission coefficient. The connection between these two equations can be readily seen. When the natural logarithm of k is plotted against 1/T, the slope becomes $-\Delta H^{\ddagger}/R$ with the intercept of $\Delta S^{\ddagger}/R + \ln(\kappa \frac{k_B T}{h})$ (Since T varies, an average reaction temperature is used). These values are shown in Table 4.4 below.

Table 4.4. Activation parameters for relevant rate constants of **1-3**

		$\Delta H^{\ddagger}$ kcal mol^{-1}	$\Delta S^{\ddagger}$ cal mol^{-1} K^{-1}
k_i	SMe	18 ± 10	–1 ± 33
	THF	11.5 ± 4.7	–24 ± 17
	NMe_2	3 ± 7	–50 ± 26
k_p	SMe	11.7 ± 1.5	–14.4 ± 5.4
	THF	12.8 ± 1.8	–11 ± 6
	NMe_2	9.3 ± 1.2	–22.1 ± 4.4
k_{mis}	SMe	12.9 ± 1.4	–18 ± 5
	THF	6.4 ± 0.6	–43.0 ± 2.2
	NMe_2	13[a]	–14[a]
k_{rec}	SMe	9.030 ± 0.041	–34.53 ± 0.14
	THF	1.82 ± 0.11	–58.39 ± 0.40
	NMe_2	11[a]	–23[a]
$k_{vinylidene}$	SMe	14.7 ± 3.4	–19 ± 12
	THF	10[a]	–37[a]
	NMe_2	17[a]	–5.0[a]
$k_{vinylene}$	SMe	14.99 ± 0.25	–21.7 ± 0.9
	THF	11[a]	–34[a]
	NMe_2	15[a]	–17[a]

[a.] These values were computed using a linear fit of the experimental data from the two lower temperature experiments only; thus, there is no error value.

In Figure 4.3, only **1** shows Arrhenius behavior for all of its rate constants, excluding k_i. Figure 4.3a reveals that k_p follows Arrhenius behavior for all **1**–**3**. The activation parameters are very similar across all catalysts, with **1** and **2** essentially identical within experimental error. The fact that k_p is the same for all three of these catalysts indicates that the propagation process is relatively unchanged by the identity of the pendant group. This result is somewhat intuitive using the following logic.

The propagation step typically involves two steps: docking of the monomer to the active site and monomer insertion following bond breaking and formation (electron rearrangement). The docking step is monomer dependent while the insertion step is monomer independent. Because monomer consumption is always linear on the semi-log plot of concentration vs. time (Figure 4.2), we conclude that the docking step is rate limiting for olefin propagation.

Monomer docking is governed by two parameters: (a) the energy required for the monomer to displace the anionic counterion at the active site, and (b) the size of the opening for the monomer to approach the active site. The change in pendant will produce a slight change in the charge density of the metal; however, during propagation the counterion is potentially displaced by the growing polymer chain such that the changes in charge density are not important to the ion separation energy. Additionally, the pendants—THF, NMe_2, and SMe—all roughly equal in size. Since neither displacement of the counterion or size of the active site is significantly changed, the activation parameters for the propagation rate constants are **1-3** are nearly consistent.

While k_p is approximately equal among these catalysts, our previous work showed that at 25°C there is a large difference in $k_{vinylidene}$ and $k_{vinylene}$. This temperature study has

uncovered some peculiarity regarding the chain transfer reactions. For **2**, chain transfer is monomer dependent (both vinylidene and vinylene formation) at –20 and 0°C, but appears to become monomer independent at 25°C. The 25°C result comes with the caveat that at this temperature there are very few vinyls formed, and because the concentrations are so low and the error relatively large, the actual mechanisms for chain transfer could in fact be interpreted to be monomer dependent. Yet if these rate constants were assumed to be monomer dependent at 25°C, it would be seen that they are approximately equal to—or lower than—the rates at 0°C, not what would be expected of rate constants following Arrhenius behavior. Furthermore, for **3** vinyl formation is unambiguously monomer independent at 25°C. At this time the reason for the change in mechanism is not understood. It is generally accepted that chain transfer in single-site catalysis preferentially follows a monomer dependent pathway unless monomer concentration is low or the monomer complexation pathway is disfavored,[13] although it is unclear why monomer complexation for chain transfer would be disfavored only at a higher temperature and only for catalyst **3**. Examining polymerization behavior at intermediate temperatures may provide more information, as would experiments at additional initial monomer concentrations, which would provide more discrimination of the reaction order for chain transfer.

Despite the change in mechanism, Figure 4.3 and Table 4.4 can provide some insight regarding monomer dependent chain transfer. The activation enthalpy for both vinylidene and vinylene chain transfer by the monomer dependent pathway are higher for **3** than for **2**, and the activation entropy for both reactions is lower in magnitude (less negative) for **3** than for **2**. The corresponding values for **1** are roughly intermediate to those for **2** and **3**.

The activation entropy for vinylidene formation by **3** is quite low (–5.0 cal mol^{-1} K^{-1}). The reaction involves the docking of a monomer followed by an insertion process (similar to propagation), but the product involves the release of the polymer chain. The overall process should be approximately entropy neutral, with the first step decreasing entropy (two species react to form one) and the second step increasing it (one species reacts to form two). Thus if the activation entropy for the total reaction is low, it may be inferred that the second step is likely to be the rate determining step. Conversely, the activation entropy for vinylene formation is much larger (–17 cal mol^{-1} K^{-1}). In this case, it may be the docking process that is rate limiting. This makes some intuitive sense since the catalyst reactant for vinylene formation, which is a secondary site, is more sterically crowded than the primary site in vinylidene formation, and the entropy loss associated with this reaction will be more substantial (loss of the degrees of freedom of a free monomer). The activation entropy for vinylidene and vinylene formation are approximately equal for both **1** and **2**. In these cases the rate determining step may be the same, and since the values are larger (approx. –20 cal mol^{-1} K^{-1} for **1** and approx. –35 cal mol^{-1} K^{-1} for **2**) the docking step is rate limiting for chain transfer from both a primary and secondary site, perhaps due to the nature of the pendant (SMe and NMe_2 pendants crowd the chain transfer site, while THF does not).

The rate constants for misinsertion and recovery for catalyst **3** do not follow Arrhenius behavior, nor does k_{mis} for **2**. The rate constants at 0°C are equal to or greater than they are at 25°C. If we assume that the data should follow Arrhenius behavior, it is possible that either (i) the calculated rate constants at 25°C are too low, or (ii) those at 0°C are too high (or both). Because the 25°C experiments were done in a different, more easily

contaminated experimental setup (Schlenk flask at high temperature versus sealed NMR tube at low temperature), we will assume that the 0°C data is more reliable than the 25°C data. Figure 4.3 shows Arrhenius fits for these cases using just the two low temperature rate constants using dashed lines. Under these assumptions, we can compare the activation parameters for these rate constants.

When comparing the activation parameters for k_{mis} and k_{rec} for **1–3**, we see for all cases that the activation enthalpy is lower for k_{rec} than for k_{mis}, and the activation entropy is higher (more negative) for k_{rec} than for k_{mis}. This may indicate that a different rate limiting step controls each of these two reactions. As with propagation, misinsertion and recovery require a docking step and an insertion step. Docking will be more difficult when the active site is more crowded, while insertion will be more difficult when the carbon at the active site (that which is closest to the metal) is less highly substituted because there are fewer carbon atoms available to distribute the temporary decrease in charge at the transition state. For the misinsertion reaction, the reacting catalyst has a less crowded, less substituted primary site, indicating that insertion is more likely to be the rate limiting step. Conversely, for the recovery step the reacting catalyst is a more crowded, more substituted secondary site, indicating that docking is more likely to be the rate limiting step. Also, the docking step involves the loss of a free monomer in solution, which will have a large entropy loss and likely a large activation entropy barrier compared with insertion. This agrees with recovery having docking as the rate limiting step.

If monomer insertion is the rate limiting step for the misinsertion reaction, the implication is that the reaction is zero order in monomer and first order overall. However, the kinetic modeling procedure shows that second order misinsertion rate constants provide

a good fit. The reason is that misinsertion is a relatively uncommon event, occurring once for every 50–100 propagation insertions. The reaction order therefore has little influence on the rate of monomer consumption. Another implication is that misinsertion will become more frequent relative to propagation (which is monomer dependent) late in the reaction when monomer concentration is low. However, a decrease in monomer concentration may cause the reaction order of misinsertion to shift to second order due to the decrease in the rate of monomer docking. Ultimately, the data available are not robust enough to distinguish both the docking and insertion rate constants for misinsertion, and so only one rate constant has been reported for the reaction.

For the initiation rate constants, we cannot discuss the activation parameters with much certainty. Table 4.4 lists the errors in these parameters as quite large. The reason for the substantial uncertainty is the large deviation from Arrhenius behavior for all catalysts. Part of this deviation comes from the difficulty of assigning this rate constant from the available data. Much lower monomer conversion or initial monomer concentration data would be needed to assign these rate constants with better accuracy.

We would like to know how the activation parameters for the catalysts studied here compare with those for other catalysts. However, activation parameters are not commonly reported. Rate constants are not often measured for single-site polymerization catalysts; instead, parameters such as activity, which have less kinetic precision, are usually reported. We remarked earlier that the publication by Ciancaleoni, et al., summarizes activation parameters from available data,[10a] and the authors note that the slow propagation rate constants are due to the large (more negative) entropy of activation (–30 cal mol^{-1} K^{-1} or more) along with a relatively moderate enthalpy of activation (5–10 kcal mol^{-1}). Compared

with these values, the results in Table 4.4 show that the activation parameters for propagation for **1**–**3** are of generally the typical magnitude for single-site catalysts.

Landis, et al., did measure actual rate constants and report activation parameters for 1-hexene polymerization by *rac*-(C_2H_4(1-indenyl)$_2$)$ZrMe_2$/$B(C_6F_5)_3$.[6c] The results are summarized in Table. 4.5. For k_p, they report $\Delta H^{\ddagger}$ = 11.2 ± 1.5 kcal mol^{-1} and $\Delta S^{\ddagger}$ = –33 ± 5 cal mol^{-1} K^{-1}. However, further analysis of this system identified that k_p at 0°C was incorrect due to incomplete participation by the precatalyst in the polymerization reaction.[11] This oversight is also present at other reaction temperatures, but the correction needed has not yet been determined. It is difficult to say exactly how much difference there is in the activation parameters without the additional analysis at other reaction temperatures, but preliminary results find that the true activation parameters for k_p are closer to $\Delta H^{\ddagger}$ = 9.4 kcal mol^{-1} and $\Delta S^{\ddagger}$ = –21.4 cal mol^{-1} K^{-1}. These parameters are nearly equal to those for **3** despite the large difference in catalyst structure.

Table 4.5 Select activation parameters for *rac*-(C_2H_4(1-indenyl)$_2$)$ZrMe_2$/$B(C_6F_5)_3$[6c]

	$\Delta H^{\ddagger}$ kcal mol^{-1}	$\Delta S^{\ddagger}$ cal mol^{-1} K^{-1}
k_p	6.4 ± 1.5	–33 ± 5
k_i	11.2 ± 1.5	–24 ± 5
"k_{mis}"[a]	9.7 ± 1.2	–35 ± 4
$k_{vinylidene}$ (1st order)	16.2 ± 3	–12 ± 6

[a] In the publication, vinylene formation is recognized to follow immediately from 2,1 insertion, or misinsertion, which is the rate limiting step.

While noting the modeling error, we may still compare the remaining rate constants. Even though we have not determined k_i very well, we see that for k_{mis} the reported enthalpy for the indenyl catalyst is somewhat lower and the reported entropy is somewhat higher than for the amine bis-phenolate catalysts, the same trend that was seen for k_p; however, nothing more can be said without a corrected kinetic model.

The vinylidene chain transfer reaction is first order with the indenyl catalyst, whereas the activation parameters in Table 4.4 represent a second order process. These processes are quite different, and we cannot reasonably compare the rate constant $k_{vinylidene}$ between these different catalyst systems. We do note, however, the relatively small (less negative) value of the activation entropy (–12 cal mol^{-1} K^{-1}), which we have associated with the reactions where we hypothesize that insertion (rather than docking) is the rate limiting step. In first order chain transfer, there is only an electron rearrangement step (similar to insertion), so a low value for activation entropy is not surprising.

4.5 Conclusions

Polymerization data at multiple temperatures have been collected for a series of three zirconium amine bis-phenolate catalysts, with each catalyst varying only in its pendant group. The data were used to extract chemical mechanisms and rate constants, and the rate constants were used to determine activation enthalpy and entropy for each reaction. The parameters were compared among the three catalysts. The following conclusions come from the analysis. The propagation rate constant is mostly unaffected by changes to the pendant as there are only small changes to both activation enthalpy and entropy for this reaction. For catalyst **3**—and perhaps **2** as well—the mechanism for chain transfer changes from monomer dependent at lower temperature to monomer independent at higher temperature. The reason is unclear, as this effect is not seen with **1**. For all catalysts, misinsertion and vinylidene formation reactions (which both have the same reactants—a primary active site and a monomer) have a higher activation enthalpy and a lower (less negative) activation entropy than recovery and vinylene formation reactions (which also share reactants—a secondary active site and a monomer). We postulate that these two groups of catalysts have different rate limiting steps—monomer docking for recovery and vinylene formation, and insertion for misinsertion and vinylidene formation. When insertion is rate limiting, the overall reaction may appear to be zeroth order in monomer, at least early in the reaction when monomer concentration is high. Exceptions to this rule may arise when the catalyst pendant provides additional crowding, specifically in regards to chain transfer, which is highly pendant dependent.[12b]

While there are no completely reliable systems to compare these results to, the calculated activation parameters are fairly similar to what is seen for other catalysts.

Ultimately, understanding the temperature dependent nature of these catalysts will help future scientists to select the best reaction conditions to produce a desired polymer product. For instance, when the activation enthalpy is greater for k_{mis} than for k_p (as it is for **1** and **3**), a lower reaction temperature would increase the k_p:k_{mis} ratio, resulting in a smaller percentage of misinsertions, although at the cost of a slower reaction. Yet to have a good understanding of the temperature behavior of single-site catalysts a complete and reproducible data set is required. The data reported herein provide accurate results for many parameters, but they are lacking in some places, such as early monomer conversion data to compute k_i. Additional discriminating experiments would help to provide more reliable parameters where they are currently missing and allow for better predictive ability of coordination insertion polymerization catalysis.

4.6 References

(1) (a) Andresen, A.; Cordes, H. G.; Herwig, J.; Kaminsky, W.; Merck, A.; Mottweiler, R.; Pein, J.; Sinn, H.; Vollmer, H. J. *Angewandte Chemie-International Edition in English* **1976**, *15*, 630; (b) Chien, J. C. W.; Sugimoto, R. *J. Polym. Sci. Pol. Chem.* **1991**, *29*, 459; (c) Ewen, J. A.; Elder, M. J.; Jones, R. L.; Haspeslagh, L.; Atwood, J. L.; Bott, S. G.; Robinson, K. *Makromolekulare Chemie-Macromolecular Symposia* **1991**, *48-9*, 253; (d) Razavi, A.; Ferrara, J. *Journal of Organometallic Chemistry* **1992**, *435*, 299; (e) Rieger, B.; Jany, G.; Fawzi, R.; Steimann, M. *Organometallics* **1994**, *13*, 647; (f) Miyake, S.; Okumura, Y.; Inazawa, S. *Macromolecules* **1995**, *28*, 3074.

(2) Busico, V.; Cipullo, R.; Chadwick, J. C.; Modder, J. F.; Sudmeijer, O. *Macromolecules* **1994**, *27*, 7538.

(3) (a) Erker, G.; Fritze, C. *Angewandte Chemie-International Edition in English* **1992**, *31*, 199; (b) Busico, V.; Cipullo, R.; Cutillo, F.; Vacatello, M.; Castelli, V. V. *Macromolecules* **2003**, *36*, 4258.

(4) Alt, H. G.; Koppl, A. *Chemical Reviews* **2000**, *100*, 1205.

(5) (a) Thorshaug, K.; Stovneng, J. A.; Rytter, E.; Ystenes, M. *Macromolecules* **1998**, *31*, 7149; (b) Wester, T. S.; Johnsen, H.; Kittilsen, P.; Rytter, E. *Macromolecular Chemistry and Physics* **1998**, *199*, 1989.

(6) (a) Song, F.; Cannon, R. D.; Bochmann, M. *J Am Chem Soc* **2003**, *125*, 7641; (b) Song, F. Q.; Hannant, M. D.; Cannon, R. D.; Bochmann, M. *Macromolecular Symposia* **2004**, *213*, 173; (c) Liu, Z. X.; Somsook, E.; White, C. B.; Rosaaen, K. A.; Landis, C. R. *Journal of the American Chemical Society* **2001**, *123*, 11193; (d) Sillars, D. R.; Landis, C. R. *J Am Chem Soc* **2003**, *125*, 9894; (e) Busico, V.; Cipullo, R.; Esposito, V. *Macromol. Rapid Commun.* **1999**, *20*, 116; (f) Mehrkhodavandi, P.; Schrock, R. R.; Pryor, L. L. *Organometallics* **2003**, *22*, 4569; (g) Chen, M. C.; Roberts, J. A.; Marks, T. J. *J Am Chem Soc* **2004**, *126*, 4605l; (h) Keaton, R. J.; Jayaratne, K. C.; Henningsen, D. A.; Koterwas, L. A.; Sita, L. R. *J Am Chem Soc* **2001**, *123*, 6197; (i) Manz, T. A.; Phomphrai, K.; Medvedev, G.; Krishnamurthy, B. B.; Sharma, S.; Haq, J.; Novstrup, K. A.; Thomson, K. T.; Delgass, W. N.; Caruthers, J. M.; Abu-Omar, M. M. *J Am Chem Soc* **2007**, *129*, 3776; (j) Bochmann, M.; Cannon, R. D.; Song, F. *Kinet. Catal.* **2006**, *47*, 160.

(7) Liu, Z. X.; Somsook, E.; Landis, C. R. *Journal of the American Chemical Society* **2001**, *123*, 2915.

(8) Naga, N.; Mizunuma, K. *Polymer* **1998**, *39*, 5059.

(9) Dornik, H. P.; Luft, G.; Rau, A.; Wieczorek, T. *Macromol. Mater. Eng.* **2004**, *289*, 475.

(10) (a) Ciancaleoni, G.; Fraldi, N.; Budzelaar, P. H.; Busico, V.; Cipullo, R.; Macchioni, A. *J Am Chem Soc* **2010**, *132*, 13651; (b) Goodman, J. T.; Schrock, R. R. *Organometallics* **2001**, *20*, 5205.

(11) Novstrup, K. A.; Travia, N. E.; Medvedev, G. A.; Stanciu, C.; Switzer, J. M.; Thomson, K. T.; Delgass, W. N.; Abu-Omar, M. M.; Caruthers, J. M. *J Am Chem Soc* **2010**, *132*, 558.

(12) (a) Switzer, J. M.; Travia, N. E.; Steelman, D. K.; Medvedev, G. A.; Thomson, K. T.; Delgass, W. N.; Abu-Omar, M. M.; Caruthers, J. M. *Macromolecules* **2012**, *45*, 4978; (b) Steelman, D. K.; Xiong, S.; Pletcher, P. D.; Smith, E.; Switzer, J. M.; Medvedev, G. A.; Delgass, W. N.; Caruthers, J. M.; Abu-Omar, M. M. *J Am Chem Soc* **2013**, *135*, 6280; (c) Steelman, D. K.; Pletcher, P. D.; Switzer, J. M.; Xiong, S. L.; Medvedev, G. A.; Delgass, W. N.; Caruthers, J. M.; Abu-Omar, M. M. *Organometallics* **2013**, *32*, 4862.

(13) Margl, P.; Deng, L. Q.; Ziegler, T. *Journal of the American Chemical Society* **1999**, *121*, 154.

CHAPTER 5. EFFECTS OF ACTIVATOR AND LEWIS BASES ON THE OLIGOMERIZATION AND POLYMERIZATION OF 1-HEXENE CATALYZED BY A 5-COORDINATE, SINGLE-SITE ZIRCONIUM AMINE BIS-PHENOLATE COMPLEX

5.1 Introduction

The ability to polymerize or oligomerize olefins has been an area of intense research for the past few decades.[1] In that time, there have been significant advances in understanding both the fundamental chemical reaction pathways and overall catalyst design.[1] Understanding both the fundamental controls that affect both activity and the length of polymer product distribution has been the important challenge in designing catalyst systems. Even beyond controlling the product's molecular weight, changing the catalyst design to transform the different kinds of vinyl chain termination products allows for a new class of oligomer feedstock materials. However, once the catalyst has been synthesized, there is only a limited number of controls that can be used to change catalytic activity.

One key factor used to bias the size of the polymer chain has been to increase or decrease the polymerization reaction temperature.[2] Decreasing the reaction temperature has been a useful tool in suppressing chain transfer to create "living" polymerization systems.[2] While increasing the reaction temperature does increase rate of propagation, chain transfer rate constants are more sensitive to changes in temperature and will reduce the size of the polymer chains to produce oligomeric products.[2] It is clear that controlling the reaction temperature is a useful tool to either help produce oligomers or "living" polymeric materials.

Another method used to control polymerization has been to use a substoichiometric ratio of activator to catalyst.[3] Electropositive Group IV polymerization catalysts are electron deficient species that have been known to dimerize through a process known as degenerative chain transfer. A pre-catalyst with two alkyl groups can form a dimer with an activated catalyst by displacing the coordinating anion and forming an alkyl bridge between the two metals. Literature reports on this style of catalytic control has been shown to influence copolymerization,[3a] affect chain length size or polydispersity index in batch reactions by allowing all active sites to enter the catalytic cycle,[3b] or even produce polymer chains that contain blocks of isotactic α-olefins.[3c] Unfortunately, we are unaware of any literature reports of this technique used with oligomerization catalysts.

In recent publications,[4,5] it was shown that a 5-coordinate, N-heterocyclic carbene (NHC) Zr catalysts could be used to control the type of 1-hexene oligomer products based on a coordinating Lewis base to the active zirconium metal center. In fact, it was shown that the identity of the Lewis base would modulate the catalyst to produce polymers with a variety of lengths based upon the sterics of the coordinating trialkyl phosphine.[4] These

reports show the potential for modular catalysis, the ability to tune product characteristics using a single, well-defined catalyst without requiring further synthesis. At this time, we are not aware of a single catalyst system that has been studied on the effects of temperature, degenerative transfer, and Lewis base additive within a single system.

In this chapter, we report the oligomerization of α-olefins using a 5-coordinate amine bis-phenolate Zr catalyst featuring a propyl pendent,[6] labeled Zr[Pr], in conjunction with a trityl tetrakis(pentafluoroaryl) borate (Trityl) activator, overall reaction shown in Figure 5.1. By analyzing the consumption of α-olefin and the production of different vinyl groups, we are able to show the propagation of α-olefin through 1,2-insertion, 2,1-misinsertion, chain transfer to either vinylidene or vinylene chains, reinitiation by 1,2-insertion of α-olefin, and chain walking via insertion of a vinylidene into a metal hydride before subsequent β-hydrogen chain transfer to form a tri-substituted vinyl end group. Test reactions were also run using tris(pentafluoroaryl) borane (FAB) and N,N-dimethyl anilinium tetrakis(pentafluoroaryl) borate (Anilinium) activators. Additionally, further control over the chain terminated products was studied by increasing the reaction temperature or through degenerate group transfer. These effects were shown to also reduce the molecular weight (M_w) of products. Particularly the effect on the degree of polymerization (DP), the average number of monomer subunits in an oligomer or polymer, is noted. Furthermore, reactions were studied with the addition of a Lewis base after activation with the goal of producing polymeric products.

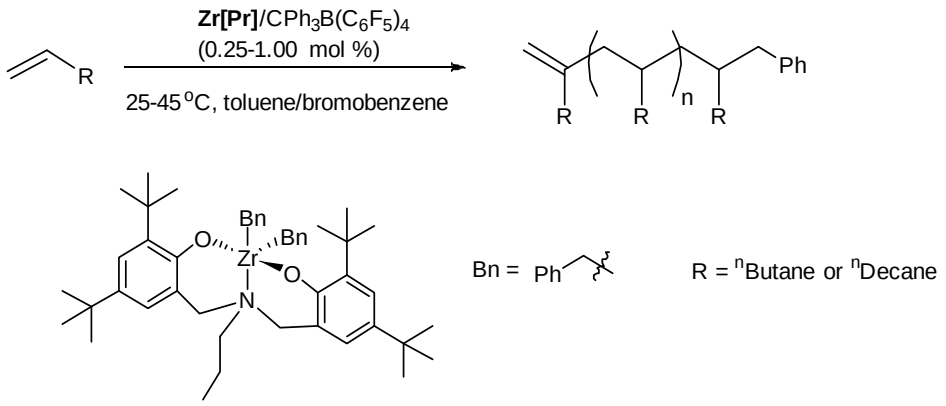

Figure 5.1. Oligomerization catalyst system Zr[Pr] for α-olefins

5.2 Experimental Procedure

General Procedure. All manipulations were performed under dry inert atmosphere in a glove box or at a vacuum manifold using air sensitive techniques under N_2 or Ar atmosphere. Pentane, toluene, bromobenzene, and acetonitrile (MeCN) were dried and degassed through a Solvent Drying System (Pure Process Technologies, LLC.) Trimethylamine (NEt_3) and pyridine (Py) were dried over CaH_2, degassed, and stored over sieves before use. 2,4-di-tBu phenol, 37% formaldehyde solution, propyl amine, triphenyphospine (PPh_3), trityl tetrakis(pentafluoroaryl) borate, anilinium tetrakis(pentafluoroaryl) borate, tris(pentafluoroaryl) borane, and 1 M trimethylphospine (PMe_3) in toluene solution were purchased from Sigma. Tetrabenzyl zirconium was purchased and used as received from Strem. Synthesis of the ^{t}Bu-ON^{Propyl}O ligand and Zr[Pr] catalyst was done following literature procedures.[6] Methodology for kinetic experiments followed previously described methods. Kinetic modeling was done by fitting

the concentration data collected by NMR or GPC to chemical mechanisms unique to the catalyst. ^{1}H NMR experiments were performed on a Varian INOVA600 MHz.

The Pr ligand was prepared following modified literature procedures.[6]

Synthesis of 6,6'-((propylazanediyl)bis(methylene))bis(2,4-di-tert-butylphenol), tBu-ON^{Pr}O ligand. The synthesis procedure is based on literature,[6] Scheme 5.1. In a typical synthesis, a 100 mL reaction vessel was charged with 2,4-di-tert-butylphenol (15. g, 72.8 mmol), propyl amine (2.15 g, 36.4 mmol) and 37% histological grade formaldehyde (5.43 mL, 72.8 mmol), and distilled water, and a stir bar while to a volume of 40 mL. The biphasic reaction mixture was refluxed for 48 hrs. The reaction was cooled to room temperature initially and cooled further to 0 °C in an ice bath. The aqueous layer was decanted, and a minimal amount of cold, dry methanol was added to the organic phase. This mixture was sonicated for 30 min, and the resulting solid isolated by vacuum filtration. The crude ligand product was purified by crystallization from ethanol (82% yield). ^{1}H NMR ($CDCl_3$): δ 7.23 (s, 2H), 6.92 (s, 2H), 3.68 (s, 4H), 2.51 (m, 2H), 1.40 (s, 18H), 1.28 (s, 18H), 0.88 (t, 3H). ^{13}C NMR ($CDCl_3$): δ 152.4, 141.5, 136.0, 125.0, 123.4, 121.7, 57.2, 55.5, 34.8, 34.2, 31.6, 29.7, 19.4, 11.7.

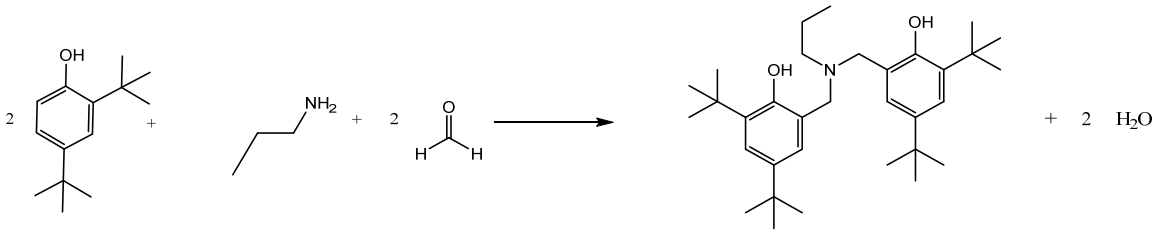

Scheme 5.1. Synthesis of the ^{t}Bu-ON^{Pr}O ligand

Synthesis of Zr[Pr]Bn$_2$. The synthesis procedure is based on literature,[6] Scheme 5.2. In a typical synthesis, a 100 mL flask was charged with tetrabenzylzirconium (0.5 g, 0.11 mmol), 20 mL toluene, and a stir bar and fitted with a rubber septum. A second 100 mL flask was charged with the tBu-ON^{Pr}O ligand (0.545 g, 0.11 mmol) and 20 mL of toluene. The two flasks were placed under an inert atmosphere, and the ligand solution was added to the tetrabenzylzirconium solution via a cannula. The reaction was stirred for 2 hours resulting in a clear solution. The solution was evaporated to dryness and washed with cold pentane. The resulting solid (91 % yield) was recrystallized in pentane to afford an analytically pure complex. ^{1}H NMR (C_6D_6): δ 7.76 (d, 2H), 7.57 (d, 2H), 7.28 (t, 2H), 7.12 (t, 1H), 6.94 (d, 2H), 6.92 (d, 2H), 6.74 (t, 2H), 6.62 (t, 1H), 3.30 (d, 2H), 2.99 (s, 2H), 2.98 (d, 2H), 2.03 (m, 2H),1.95 (s, 2H), 1.79 (s, 18H), 1.35 (s, 18H), 1.05 (m, 2H), -0.03 (t, 3H). ^{13}C NMR (C_6D_6): δ 158.3, 148.3, 142.1, 137.4, 136.8, 131.4,129.5, 125.8, 125.4, 125.2, 125.1, 122.7, 60.9, 58.9, 45.5, 36.1, 35.0, 32.6, 31.3, 14.0, 11.2.

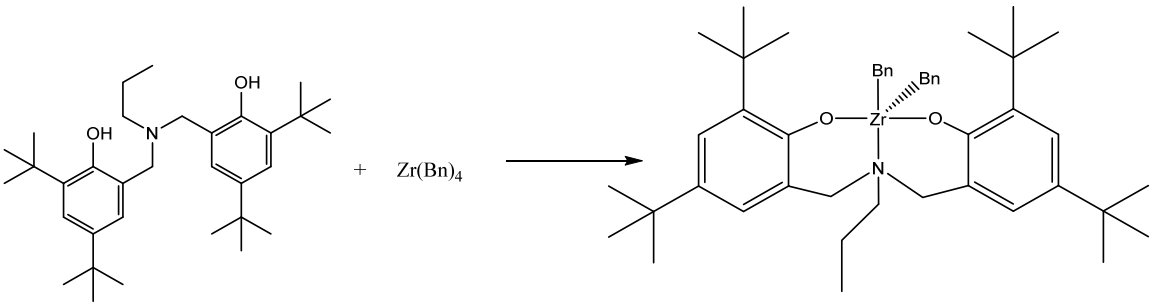

Scheme 5.2. Synthesis of the Zr[Pr]Bn$_2$ catalyst

NMR scale oligomerization of 1-hexene (or 1-dodecene) with Zr[Pr]Bn_2 at 25 ºC. The procedure for NMR scale polymerization is based on literature.[7] For a typical polymerization, Zr[Pr]Bn_2 (6.1 mg, 0.0075 mmol) was dissolved in a 0.5 mL mixture of d_8-toluene/bromobenzene 50/50 v/v in a small vial and sealed with a screw-cap septum. The vial containing the precatalyst solution was pierced with a 1 mL syringe. The vial and syringe were placed in an N_2 bag and allowed to equilibrate to 25 ºC. Tris(pentafluorophenyl)boron (4.2 mg, 0.0083 mmol), 1-hexene (0.126 grams, 1.50 mmol), and diphenylmethane (9.7 mg 0.058 mmol) were added to a 2 mL volumetric flask and diluted to the mark with d_8-toluene/bromobenzene 50/50 v/v. This solution was placed in an NMR tube and sealed with a septum. The monomer/activator solution was placed in the spectrometer and allowed to equilibrate to 25 ºC using a VT controller. A measurement was taken to determine the initial concentration of monomer relative to the internal standard. The NMR tube was removed from the spectrometer, and the catalyst precursor solution was added to the activator/monomer solution by piercing the septum while the syringe remained in the N_2 bag. The reaction mixture was shaken for 30 seconds and injected back into the spectrometer. Measurements were taken at predetermined time intervals until the reaction reached completion. Each sample was prepared for GPC analysis by filtration through an alumina plug to remove the quenched catalyst. Evaporation of solvent yielded clear, colorless oligomers of 1-hexene. The array of spectra was collected on an INOVA 600 MHz spectrometer and analyzed using MestReNova.

Polymerization and oligomerization of 1-hexene with Zr[Pr]Bn_2 in the presence of Lewis Base. For a typical polymerization experiment, Zr[Pr]Bn_2 (6.1 mg, 0.0075 mmol) was dissolved in a 0.5 mL mixture of d_8-toluene/bromobenzene 50/50 v/v

in a small vial and mixed with 0.5 ml of trityl tetrakis(pentafluorophenyl)borate (4.2 mg, 0.0083 mmol). A solution of 1-hexene (0.126 grams, 1.50 mmol), .0083 ml of a Lewis base, and diphenylmethane (9.7 mg 0.058 mmol) were added to a 2 mL volumetric flask and diluted to the mark with d_8-toluene/bromobenzene 50/50 v/v. This solution was added to the activated catalyst solution and measurements were taken at predetermined time intervals until the reaction reached completion. Each sample was prepared for GPC analysis by filtration through an alumina plug to remove the quenched catalyst. Evaporation of solvent yielded clear, colorless oligomers or polymers of 1-hexene. The array of spectra was collected on an INOVA 600 MHz spectrometer and analyzed using MestReNova.

5.3 Results and Discussion

A series of test reactions were conducted using different activators. Using FAB, Trityl borate, and Anilinium borate, a series of test reactions were run with 200 equivalents of 1-hexene and analyzed after 48 hr reaction time. FAB and Anilinium activators with the Zr[Pr] catalyst exhibited incomplete reactivity exhibiting < 12% conversion to produce oligomer products while the Trityl borate showed > 99% conversion of 1-hexene to produced oligomers containing three different chain ends – vinylidene, vinylene, and a tri-substituted chain end, with signals in the ^{1}H NMR at δ 4.9, 5.3, and 5.6, respectively.[4,8] The formation of the different terminated vinyl groups is shown in Scheme 5.3.

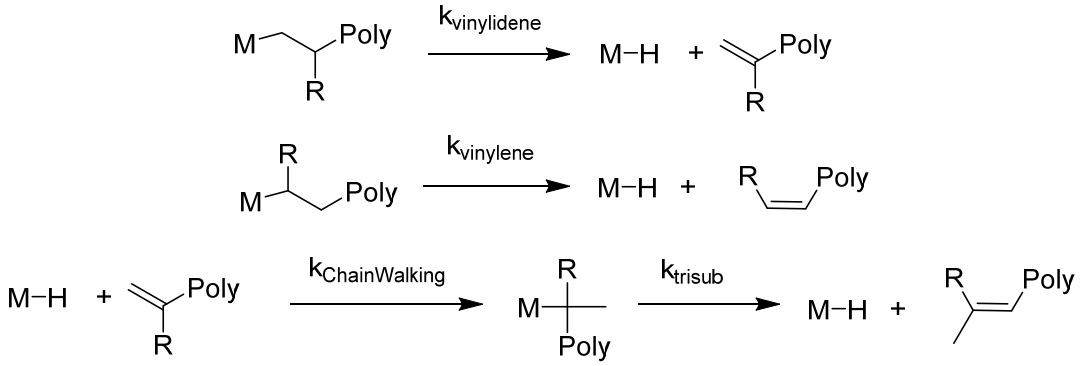

Scheme 5.3. Elementary reactions for the formation of vinyl terminated groups

As illustrated in Scheme 5.3, the formation of vinylidene and vinylene occur through the β-hydrogen elimination reactions between a Zr-primary carbon and Zr-secondary carbon, respectively. The formation of the tri-substituted species is believed to be formed through a chain walking mechanism: a vinylidene terminated group inserts into a metal-hydride before subsequent β-hydrogen elimination reaction to form a stable tri-substituted vinyl group. The monomer conversion, % vinyl groups, and the degree of polymerization, average number of monomers within each polymer or oligomer, are presented in Table 5.1.

Table 5.1. Results from initial activity study of Zr[Pr]/activator at 30 °C

Run #	Activator	T °C	% Conv.	%Vinylidene	%Tri-substituted	%Vinylene	DP[a]
1	FAB	30	11	80	0	20	-[b]
2	Anilinium	30	12%	60	0	40	-[b]
3	Trityl	30	99	13	35	52	11

Reaction were peformed at 30 °C quenched with methanol after 48 hours. [a]The degree of polymerization was determined by dividing the change from the initial 1-hexene vinyl signals to the sum of the vinyl signals of the oligomeric products. [b]The average length could not be determined since the vinyl signals overlapped each other.

These results are in an agreement with the literature. The initial report by Moshe Kol showed a rapidly deactivating, oligomerization catalyst system when paired with the FAB co-catalyst.[6] However, contrary reports in the patent literature revealed that the Zr[Pr] catalyst could be stabilized by using methyl aluminoxane (MAO) as an activator.[9] Furthermore, in other reports, some 5-coordinate Group IV catalysts paired with the FAB co-catalysts showed no reactivity but exhibited reactivity when paired with Trityl or MAO activators.[4,5] The lack of reactivity between these catalysts, when paired with FAB co-catalysts, has been traditionally explained by the formation of a stable inner-coordination zwitterion pair, as shown in Scheme 5.4, while the use of Trityl co-catalysts produced outer-sphere zwitterion pair that is reactive towards olefin insertion.[4,5]

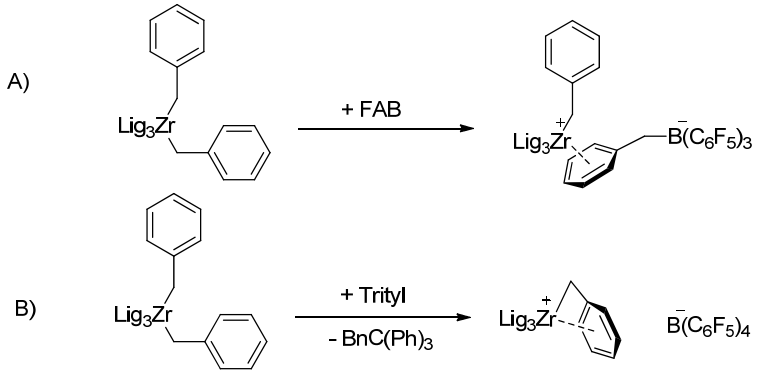

Scheme 5.4. A) Inner-sphere zwitterion pair with FAB while B) shows the outer-sphere zwitterion pair formed with a Trityl with a 5 coordinate Zr catalyst featuring Bn groups

^{19}F experiments were taken of the Zr[Pr]/FAB to understand the nature of the zwitterionic coordination environment and is shown in Figure 5.2. Catalyst and activator

were added together at -40 °C and allowed to warm in the NMR to the -25 °C and 25 °C before spectrum was collected.

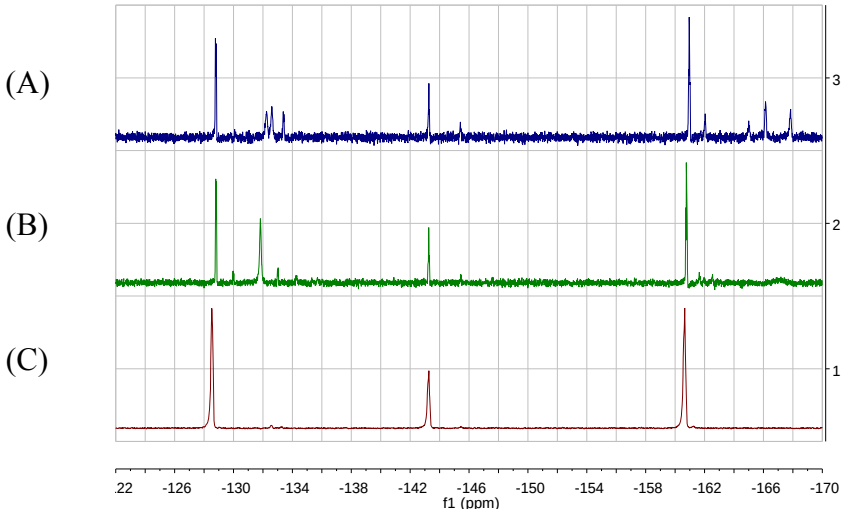

Figure 5.2. ^{19}F NMR of (A) Zr[Pr]/FAB at -25 ºC, (B) Zr[Pr]/FAB at 25 ºC, and (C) FAB at 25 ºC

Looking at Figure 5.2A, we see that Zr[Pr]/FAB shows a series of different peaks at -25 °C. The peaks in the region of -162 ppm to -168 ppm correspond to both inner-sphere and outer-sphere complexes, -165 to -168 ppm for inner-sphere and -162 to -166 ppm for outer-sphere.[10] This suggests that the catalyst activation process at low temperature may follow the same process observed for group IV systems by Bochmann and coworkers, shown in Scheme 5.5.[11] The activation process for metallocene compounds have been shown to form binuclear complexes bridged by an alkyl groups in a reaction between two catalyst complexes with a Lewis acid activator. The formation of the binuclear complex pushes the anionic borate to the outer-coordination sphere. This species will further react

with another equivalent of activator to form a mono-catalyst-activator zwitterion pair. Similar to other Zr complexes with open coordination sites that interact with Lewis bases, that structure may exhibit an inner-sphere coordination sphere and may explain the signals in the ^{19}F NMR.

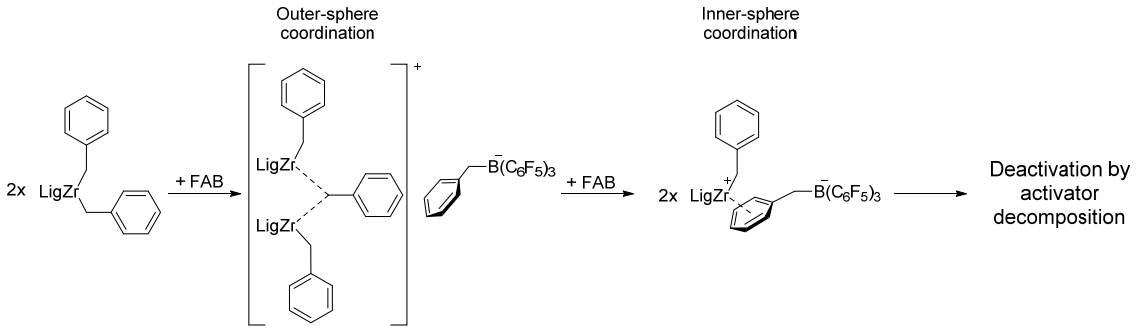

Scheme 5.5. Proposed activation pathway of Zr[Pr]/FAB

Allowing the reaction to warm to room temperature, the spectrum changes dramatically. In Figure 5.2B at 25 °C, the inner- and outer-sphere activator signals have diminished and only a series of deactivated products are -132 ppm. The disappearance of other ^{19}F signals may have occurred through precipitation of the deactivated products. This may explain how the Zr/FAB catalyst pair only exhibits limited 1-hexene oligomerization – the unstable anion, or potentially the binuclear complex, is able to turnover a few times before decomposition with the inner-sphere benzyl borate occurs. This reasoning can help explain the reports of the Zr[Pr]/MAO[9] and Zr[Pr]/Trityl oligomerization reactivity; the outer-sphere nature of these catalyst/activator ion pairs may overcome the decomposition pathway and allow for nearly complete α-olefin conversion.

Interestingly, the reactivity of the Zr[Pr]/Anilinium system also exhibited incomplete 1-hexene conversion. This stands in contrast to both the work by Bercaw et al. with a 5-coordinate Zr NHC catalyst that exhibited no catalytic activity and the Romain et al. Zr NHC catalyst system which completely converted 1-hexene into oligomers when using the Anilinium co-catalyst.[4,5] The coordination of the N,N-dimethyl aniline to the different catalyst centers was reported to both cause the lack of reactivity in the Bercaw system[4] and the selective production of 2,1-insertion products by the Romain catalyst systems.[5] It seems likely that the coordination of the free N,N-dimethyl aniline may reduce 1-hexene conversion as well as increased vinylene chain termination groups from 2,1-insertion when used with the Zr[Pr] catalyst, as seen in Table 5.1.

Kinetic studies were undertaken to measure the conversion of α-olefins and identity of the oligomer vinyl populations for the Zr[Pr]/Trityl reaction pair. The effect of temperature and the ratio of catalyst to activator for 1-hexene and 1-dodecene consumption were probed. The appearance and changes to the three other vinyl peaks over time were also noted – an increase then a decrease of vinylidene terminated groups, growth of vinylene terminated groups, and the growth of internal, tri-substituted vinyl groups.

To establish a base line reactivity, 1-hexene and 1-dodecene were studied with the Zr[Pr]/Trityl catalyst system at 25 °C; kinetic profiles are shown in Figures 5.3A and B, respectively.

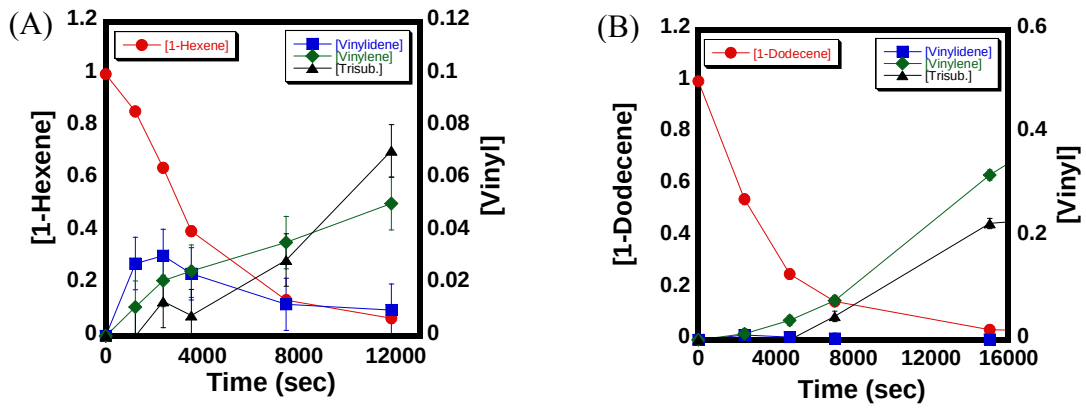

Figure 5.3. Zr[Pr]/Trityl at 1:1 ratio with (A) 200 equivalents of 1-Hexene at 25 °C and (B) 100 equivalents of 1-dodecene at 25 °C. Monomer concentrations are on the left y-axis while the vinyl product concentration values are shown on the right y-axis. Error bars of ±.02 M are included.

Due to the difference in chain length, it has been reported in other systems that the propagation rate drops as the monomer size increases from 1-hexene to 1-dodecene.[12] This is indeed the case with the Zr[Pr]/Trityl system; the propagation rate of 1-hexene is roughly three times faster than 1-dodecene. Furthermore, looking at the DP for this system for both monomers, we see that the 1-dodecene oligomers are roughly 70% the length compared to the oligomers made from 1-hexene. This suggests that the chain termination reactions for the different monomers are not the same. If the termination reactions were exactly the same, the ratio of the DP_{hex}/DP_{dec} would be closer to the $k_{p,hex}/k_{p,dec}$.

Table 5.2. Zr[Pr]/Trityl reactivity towards 1-hexene (Run 4) and 1-dodecene (Run 5) at 25 °C

Run #	% Conv.	Mono	T °C	k_p (s^{-1})	% -dene	%Tri-	% -lene	DP
4	93	Hex	25	1.63e-4	1.0	26.2	72.8	11.3
5	98	Dec	25	5.03e-5	7.8	3.3	88.9	8.1

Another interesting fact is the percentage of vinylene chain ends near the end of the reaction. The formation of vinylene terminated products are the result of 2,1-insertions of α-olefin into a metal-polymeric bond and subsequent chain transfer of that species. Comparing the 1-hexene and 1-dodecene chain ends, it follows that the oligomerization of 1-dodecene has a higher percentage of vinylene, 88.9%, when compared to the oligomerization of 1-hexene, 72.8%. This suggests that 2,1-insertion may be dependent on the size of the last inserted monomer. Shown in Scheme 5.6, it may be possible that the monomer inserts in either a frontside approach that brings the monomer close to the growing oligomeric chain, or the monomer inserts by a backside approach that interacts with the propyl chain attached to the amine group. The steric bulk from 1-dodecene oligomers attached to the Zr center may increase the number of backside approaches for 1-dodecene exhibit a larger percentage of 2,1-insertions/vinylene terminated products. Redesign of the catalyst structure by converting the propyl- group to a bulkier substituent or to a pendant that binds weakly to the Zr center may reduce the number of 2,1-insertions and increase the percentage of vinylidene terminated oligomers.

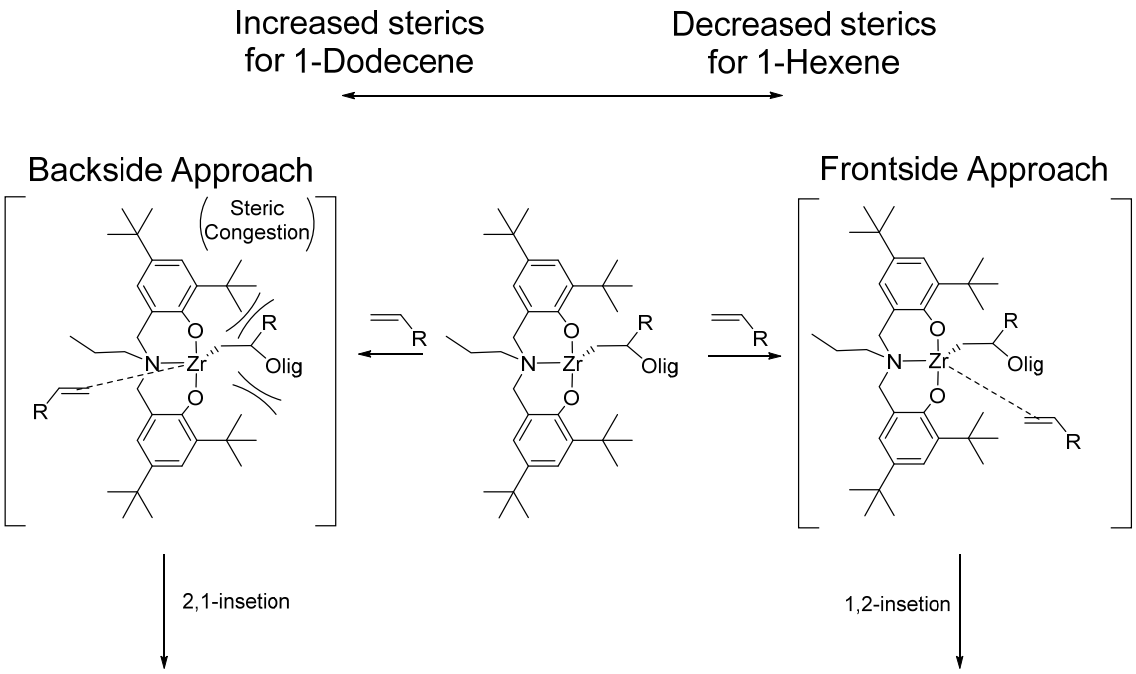

Scheme 5.6. Possible backside or frontside approaches of α-olefin for monomer insertion

Another interesting fact to note about the vinyl groups for the oligomer chain ends is the distinctive difference between the number of tri-substituted chain ends. Examining Figure 5.4A, the oligomerization of 1-hexene shows an increase and then decrease of vinylidene chain ends in solution that corresponds with the appearance and growth of tri-substituted chain ends. In Figure 5.4B for 1-dodecene, there is virtually no vinylidene terminated groups in solution. In contrast, tri-substituted chain ends do appear in solution. This suggests that the dissociation of the 1-dodecene oligomer from the Zr catalyst is slow compared to the chainwalking reaction that converts vinylidene chain ends to tri-substituted chain ends at this temperature.

One of the traditional methods used to reduce the M_w oligomer distributions has been to increase the reaction temperature. Shown in Figure 5.5, the kinetic plots for the

consumption of 1-hexene and changes in vinyl groups are plotted vs time at 25 °C and 45 °C.

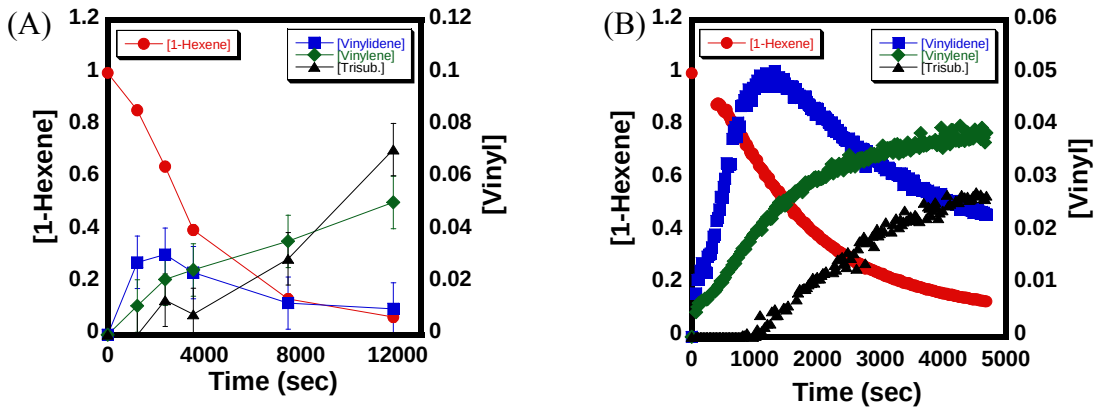

Figure 5.4. Zr[Pr]/Trityl at 1:1 ratio with 200 equivalents of 1-Hexene at (A) 25 °C and (B) 45 °C Monomer concentrations are on the left y-axis while the vinyl product concentration values are shown on the right y-axis. Error bars of ±.02 M are included in plot (A) and are omitted from plot (B) for clarity.

Comparing Figure 5.4A and Figure 5.4B, increasing the temperature by 20 °C has a tremendous effect on increasing catalyst reactivity, reducing the oligomer PD, and influencing the percentage of vinyl groups, shown below in Table 5.3.

Table 5.3. Zr[Pr]/Trityl reactivity towards 1-hexene at 25 °C (Run 4) and at 45 °C (Run 6)

Run #	% Conv.	Mono	T °C	k_p (s^{-1})	% -dene	%Tri-	% -lene	DP
4	93	Hex	25	1.63e-4	1.0	26.2	72.8	11.3
6	86	Hex	45	1.99e-4	26.2	30.2	43.6	5.7

The effect of increasing temperature on olefin conversion and reducing product Mw has been well established in the literature.[2] For the Zr[Pr]/Trityl system, there was only a slight increase in k_p increasing the temperature to 45 °C for the conversion of 1-hexene. However, the DP of the oligomers was effectively cut in half and produced much shorter oligomers. However, the changes to the percentage of different vinyl groups is different to the established literature on olefin polymerization. The percentage of vinylene groups decreased as the temperature increases from 72.8% to 43.6%, which runs opposite to the trends seen for increasing numbers of regioerrors in polymers as the temperature rises. At this point in time, it is not exactly clear why this occurs. However, this suggests that increasing the temperature can both reduce the Mw of the oligomer products and increase the vinyl chain ends selectively to vinylidene terminated groups.

The effect of temperature on 1-dodecene oligomerization exhibited the same trend as that for 1-hexene. The kinetics are shown in Figure 5.5 and the percentage of vinyl chain ends and DP shown in Table 5.4.

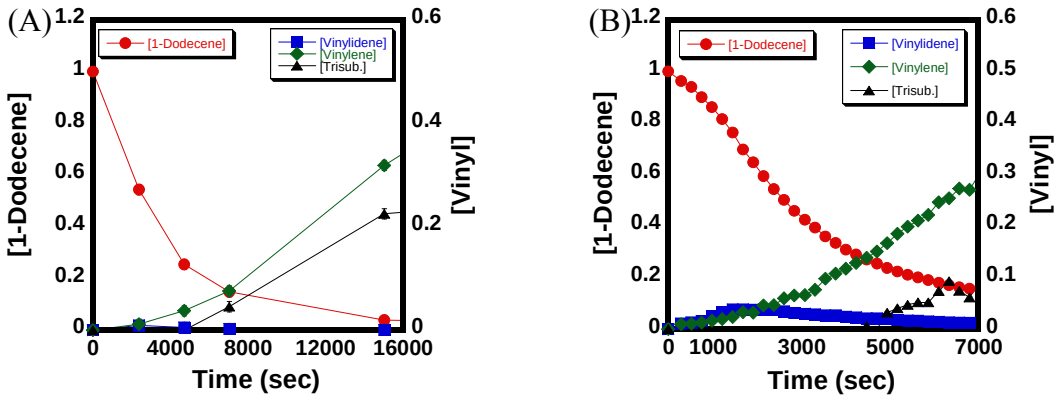

Figure 5.5. Zr[Pr]/Trityl at 1:1 ratio with 100 equivalents of 1-dodecene at (A) 25 °C and (B) 45 °C. Monomer concentrations are on the left y-axis while the vinyl product concentration values are shown on the right y-axis. Error bars of ±.02 M are included.

Table 5.4. Zr[Pr]/Trityl reactivity towards 1-dodecene at 25 °C (Run 5) and at 45 °C (Run 7)

Run #	% Conv.	Mono	T °C	k_p (s^{-1})	% -dene	%Tri-	% -lene	DP
5	98	Dec	25	5.03e-5	7.8	3.3	88.9	8.1
7	97.8	Dec	45	1.54e-4	<.1	32.8	67.2	3.6

Again the propagation rate constant increased, the DP decreased roughly by a half, and the percentage of vinylene terminated groups decreased from 88.9% to 67.2%. Interestingly, vinylidene chain ends were observed at 45 °C but were eventually converted to tri-substituted chain ends by the end of reaction. This shows that temperature offers a unique control on both the oligomer MW and identity of chain ends.

One of the most interesting features of Group IV catalysts is their ability to dimerize into binuclear complexes (BNC) through a degenerative group transfer. By using a substoichiometric amount of activator, an activated catalyst species can react with a bis-alkyl precatalyst species. The subsequent transfer of this alkyl group from one catalyst site to the other catalyst site allows one catalyst site to be active for a certain period before the BNC is reformed. Depending on the temperature, activator, and catalyst, the system may exhibit a rapid equilibrium between the BNC to free active catalyst and precatalyst.[3b] This mechanism, as well as the initial activation steps, is shown in Scheme 5.7.

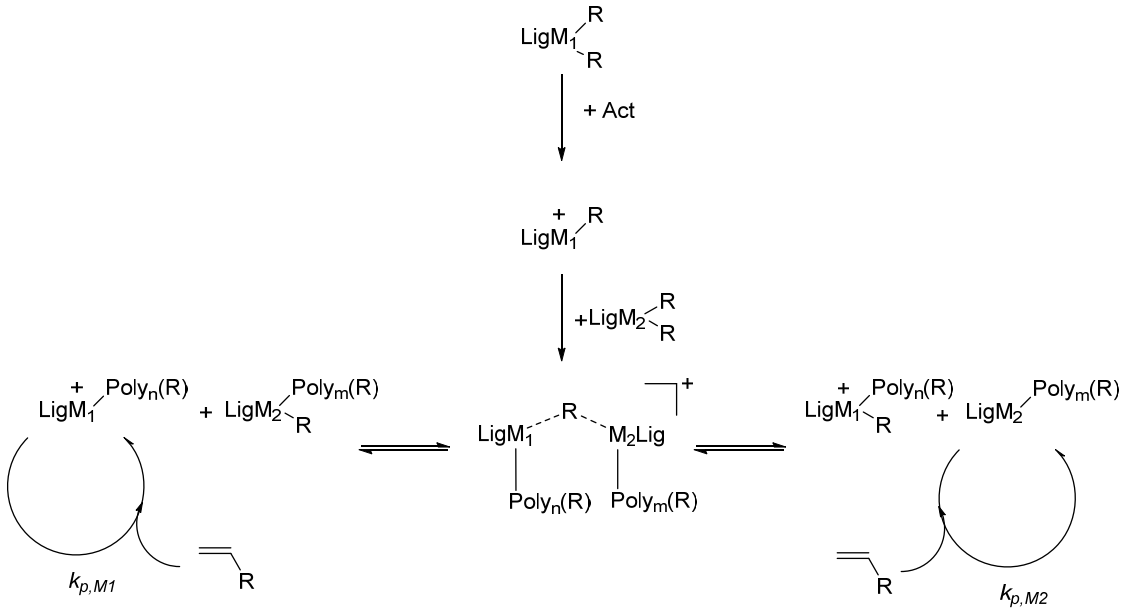

Scheme 5.7. BNC formation/catalysis with Group IV catalysts induced by substiochiometric activator

The oligomerization of 1-hexene was repeated with substoichiometric amounts of trityl activator, in a 2:1 ratio of precatalyst to activator. Kinetic experiments were conducted at 25 ^{o}C for 1-hexene. These are shown in Figure 5.6 and the monomer conversion, percent vinyl groups, and DP are reported in Table 5.5.

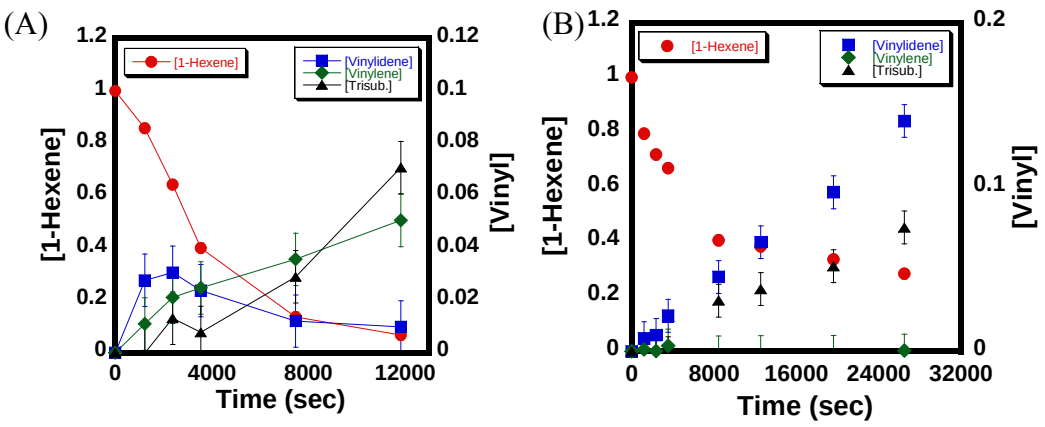

Figure 5.6 Zr[Pr]/Trityl at with 200 equivalents of 1-Hexene at 25 ºC with (A) Cat:Act ratio of 1:1 ratio and (B) a Cat:Act ratio of 2:1 ratio with. Monomer concentrations are on the left y-axis while the vinyl product concentration values are shown on the right y-axis.

Table 5.5. Zr[Pr]/Trityl reactivity towards 1-hexene at 25 °C with 1:1 (Run 4) and 2:1 (Run 8) ratios of catalyst to activator

Run #	% Conv.	Mono	T °C	k_p (s^{-1})	% -dene	%Tri-	% -lene	DP
4	93	Hex	25	1.63e-4	1.0	26.2	72.8	11.3
8	73	Hex	25	3.15e-5	61.7	36.1	1.4	4.7

The effect of substoichiometric activator produces interesting results. The propagation rate constant decreases and monomer conversion plateaus around 70% monomer conversion. While it makes intuitive sense that the reaction slows down as there are potentially less active sites available to react with 1-hexene, it is surprising to see incomplete monomer conversion since this stable catalyst/activator pair shows nearly complete monomer conversion given enough time. However, the most interesting effects occur with the DP and identity of vinyl groups at the end of reaction. The use of

substoichiometric activator drastically reduced the number of vinylene chain ends from 72.8% to 1.4% and reduced the DP of the oligomer faction from 11.3 to 4.7 units long. Furthermore, the conversion of vinylidene to tri-substituted remained the same while the percentage of vinylidene terminated groups grew from 1% to over 60%. These findings suggest that the formation of a BNC has a tremendous effect on both the selectivity of monomer insertion and chain termination. These results suggest that the BNC disfavors 2,1-insertion of 1-hexene and raises the region-selectivity towards 1,2-insertion.

This reaction was also subjected to a reaction temperature of 45 °C. The kinetics are shown in Figure 5.7 with the vinyl group identity and DP tabulated in Table 5.6.

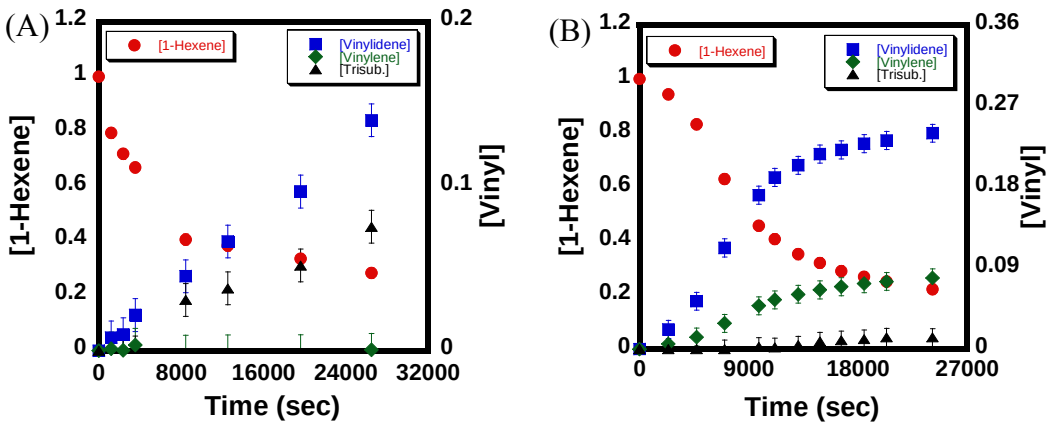

Figure 5.7 Zr[Pr]/Trityl at 2:1 ratio with 200 equivalents of 1-Hexene at (a) 25 °C and (b) 45 °C. Monomer concentrations are on the left y-axis while the vinyl product concentration values are shown on the right y-axis.

Table 5.6. Zr[Pr]/Trityl at a 2:1 catalyst to activator ratio reactivity towards 1-hexene at 25 °C (Run 8) and 45 °C (Run 9)

Run #	% Conv.	Mono	T °C	Cat:Act	k_p (s^{-1})	% -dene	%Tri-	% -lene	DP
8	73	Hex	25	2:1	3.15e-5	61.7	36.1	1.4	4.7
9	77	Hex	45	2:1	3.34e-6	72.3	3.9	23.8	2.5

The combined effect of temperature and substoichiometric activator have an additive effect on the both 1-hexene oligomer DP and chain ends identity. The average chain lengths decrease again to form shorter chains and the % vinylidene chain ends increases from 61.7% to 72.3%. Interestingly, the percentage of vinylene groups increases from 1.4% to 23.8%, in contrast to the temperature effect of the 1:1 ratio of catalyst to activator that decreased the number of vinylene groups. This suggests that the BNC dissociates more at this temperature and allows for the free activated catalyst to insert 1-hexene in a 2,1- fashion, bringing the % vinylene closer to that seen in reaction 6 in Table 5.3, % vinylene = 43.6.

Strangely, the propagation rate constant drops by an order of magnitude as the temperature increases. While at this time we do not have a clear understanding as to why the reactivity of the system decreases, the reappearance of vinylene terminated groups may indicate 2,1-insertions are again occurring and the existence of the BNC with these secondary inserted carbons may have a detrimental effect on the overall catalytic reactivity. Furthermore, this system slows down and eventually reaches a plateau of 1-hexene

conversion around 80%. It appears that the catalyst deactivation or dormancy that occurs at 25 °C still exists at 45 °C.

Another method of studying the effect of substoichiometric activator is to compare the endpoint molecular weight distributions of 1:1 catalyst to activator at 25 °C and 45 °C and 2:1 catalyst to activator at 25 °C and 45 °C. These distributions are shown in Figure 5.8 below.

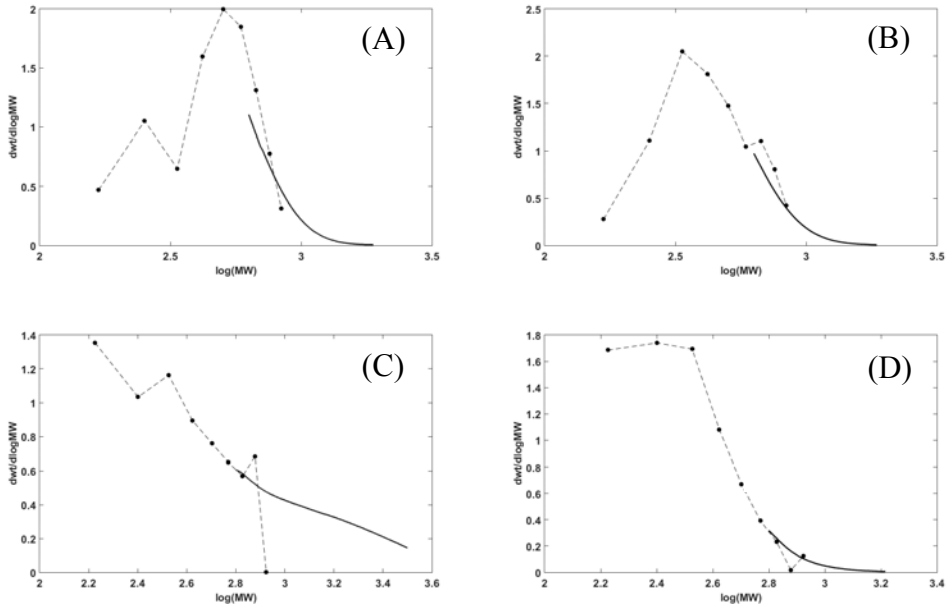

Figure 5.8 GPC traces of 1-hexene oligomerization with (A) 1:1/Cat:Act at 25 °C, (B) 1:1/Cat:Act at 45 °C, (C) 2:1/Cat:Act at 25 °C, and (D) 2:1/Cat:Act at 45 °C

The GPCs under these conditions are informative in terms of the effect of the BNC at different temperatures. Comparing the 1:1 (Figure 5.8A) and 2:1 (Figure 5.8C) ratios of catalyst to activator at 25 °C, the distributions look fundamentally different. The substoichiometric system shows a very broad distribution while the stoichiometric

activator conditions shows a Schultz-Flory distribution centered around hexamers. This may indicate that there is a slow interconversion between the BNC and cationic free activated catalyst and precatalyst. A fast equilibrium between the different species should produce a tight distribution instead of a broader one containing longer MW oligomers. Furthermore, an equilibrium that favors the formation of BNC would help explain the decrease in monomer conversion as there would be less active sites in solution available to convert α-olefins into oligomers.

By increasing the temperature, the MWD shifts downwards for both the substoichiometric and stoichiometric systems. The experiments 1:1 (Figure 5.8B) ratio of catalyst to activator at 45 °C have now shifted from a distribution centered around hexamers to a distribution centered around tetramers. However, the 2:1 ratio of catalyst to activator (Figure 5.8D) at 45 °C now shows a narrower distribution of products when compared to the 2:1 (Figure 5.8C) ratio of catalyst to activator at 25 °C. Furthermore, the green curve shows a distribution centered around dimers and trimers. Looking at Scheme 5.8, it is possible that the BNC of Zr[Pr]/Trityl again exhibits equilibrium rate constants, K_{eq1} and K_{eq2}, that favor of the formation of the BNC. This would explain the decreased monomer consumption rate by 3x compared to the kinetics of run 4 from Table 5.2. However, by increasing the reaction temperature to 45 °C, the rate of exchange between the cationic catalyst and BNC, K_{eq1} and K_{eq2}, must increase since the MWD in the GPC shows a much narrower oligomer product distribution. Furthermore, the changes to the % vinylene chain ends suggests that the equilibrium in Scheme 5.8 has shifted towards free activated catalyst and pre-catalyst. However, this runs contrary to the kinetic data from Table 5.6. The kinetic data shows that the consumption of 1-hexene is slower at higher

temperature. It is possible that the BNC formation at higher temperature may contain metal-hydrides instead of metal-oligomeric groups. Such a species may shift the equilibrium to form a dormant BNC and could explain why there is incomplete conversion of 1-hexene when using substoichiometric amounts of activator for oligomerization of α-olefins. Regardless, the use of substoichiometric amounts of activator at different reaction temperatures has been shown to be a viable method to reduce the M_w and control the vinyl chain ends in oligomerization reactions.

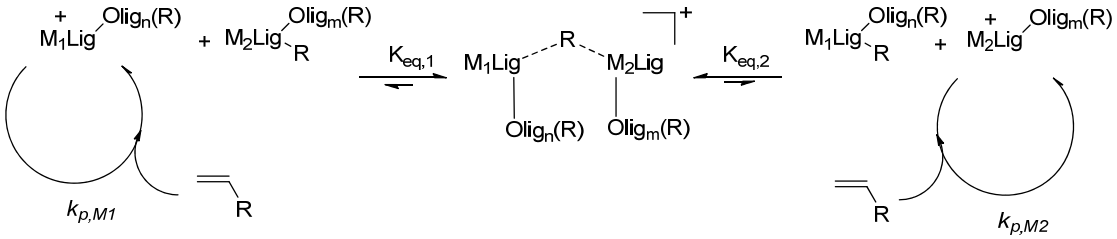

Scheme 5.8. BNC of Group IV catalysts induced by substiochiometric activator

Recently, it was reported that a 5-coordinate Zr NHC catalyst system could be switched from an oligomerization system into a polymerization system by coordination of Lewis base to the activated zwitterion pair.[4] Reactions with substoichiometric amounts of PMe_3, PPh_3, NEt_3, Py, and MeCN with the Zr[Pr]/Trityl catalyst system were conducted to test if a switch existed with this catalyst system. When these systems were conducted with Zr[Pr]/Trityl in the presence of a 4:1 ratio of catalyst to additive, oligomer products were seen with PMe_3, PPh_3, and MeCN systems after 72 hours of reaction. Unexpectedly, the reaction with PMe_3 and MeCN additive produced polymer fractions in addition to

oligomers with very similar PDs. The results of these tests are summarized below in Table 5.7.

Table 5.7 Results of Zr[Pr]/Trityl/LB reactivity studies

Run #	Lewis Base	% Conv.	Mono	T °C	Cat:Act:LB	k_p,obs s^{-1}	% -dene	% -lene	%Tri-	PD
10[a]	PMe_3	>99	Hex	30	4:4:1	-	-	-	-	74.8
11	PPh_3	96	Hex	30	4:4:1	-	59.3	33.1	7.6	3.9
12[b]	NEt3	<3	Hex	30	4:4:1	-	-	-	-	-
13[b]	Py	<3	Hex	30	4:4:1	-	-	-	-	-
14[a]	MeCN	>99	Hex	30	4:4:1	-	-	-	-	79.8

[a]An oligomer peak and a polymer peak were observed and the PD for the polymer distribution is reported; [b]Low conversion prevented complete analysis of products and end groups.

To probe the effect of Lewis base on the Zr[Pr]/Trityl catalyst system, NMR spectroscopic studies were undertaken. ^{31}P NMR spectra were collected with solutions of PMe_3 and PPh_3 in the presence and absence of the activated catalyst system. Shown in Figures 5.9 and 5.10, it is unclear if there is any coordination between the cationic metal center and the Lewis base, contrary to the results seen by the Bercaw lab with their 5-coordinate NHC Zr system in the presence of different alkyl phosphine bases.[4] The peaks seen around 24 ppm and 37 ppm are the known coupling products of phosphine and Trityl activator.[13] Interestingly, the peaks for the Zr[Pr]/Trityl/Phosphine systems in Figures 5.9 and 5.10 are much broader than the free phosphine.

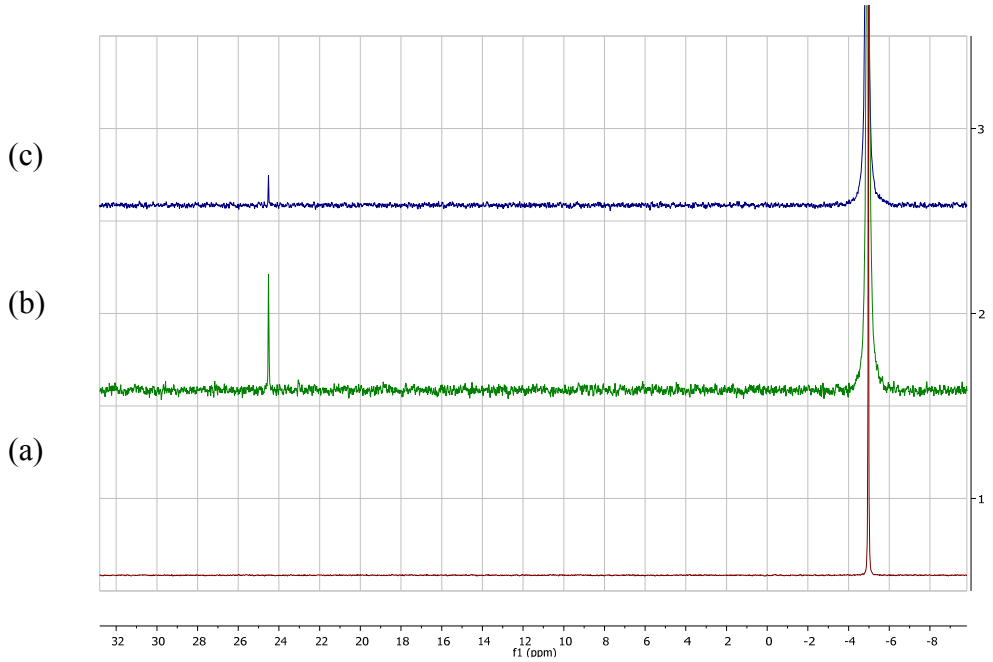

Figure 5.9 ^{31}P NMR of Zr[Pr]/Trityl/PPh_3 (a) is only PPh_3 (b) 1:1:1 Zr[Pr]/Trityl/PPh_3, and (c) 1:1:2.5 Zr[Pr]/Trityl/PPh_3

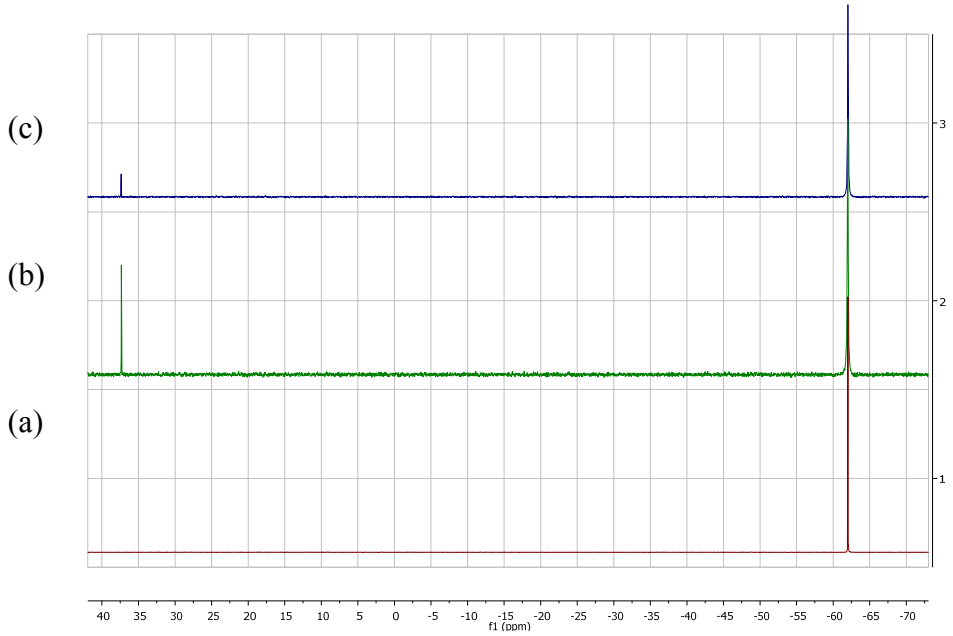

Figure 5.10 ^{31}P NMR of Zr[Pr]/Trityl/PMe_3 (a) is only PMe_3 (b) 1:1:1 Zr[Pr]/Trityl/PMe_3, and (c) 1:1:2.5 Zr[Pr]/Trityl/PMe_3

The effect of Lewis base also has affect on the distribution of different sized products for both oligomers or the formation of oligomers and polymers. The results of the Zr/Trityl/PPh_3 system suggest that the catalyst system produces lower molecular weight products (PD of 3.9) with higher percentage of vinylidene products (59.3%) when compared to the Zr[Pr]/Trityl system at identical conditions, run 3 in Table 5.1. This may have been caused by coordination of the phosphine to the activated Zr center. Additionaly, coordination complexes between Zr[Pr]/Trityl with MeCN and PMe_3 may generate a polymerization system similar to that seen by Bercaw et al.[4], Scheme 5.9, that affords linear 1-hexene polymers. However, this stands in contrast to the ^{31}P NMR experiments that do not show coordination of the PPh_3 or PMe_3 to the activated Zr[Pr]/Trityl system.

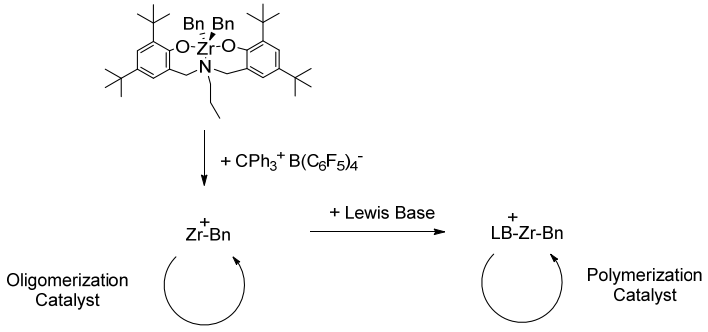

Scheme 5.9. Suggested oligomerization and polymerization mechanisms for Zr[Pr]/Trityl and Zr[Pr]/Trityl/Lewis base systems based off of Bercaw's catalyst/Trityl/Lewis base system

Control reactions were conducted to test the reactivity between the Tirtyl activator, Lewis base, 1-hexene, and 1-hexene oligomers. After 72 hours, there was no reaction between Trityl/Lewis base/1-hexene. The reaction between Trityl activator and oligomers, however, instantly converted the 1-hexene oligomers to polymers, concievably through a

carbocationic mechanism. It is known that Trityl borate salts can be used as cationic intiators for isobutylene, through a mechanism shown below in Scheme 5.10.[13]

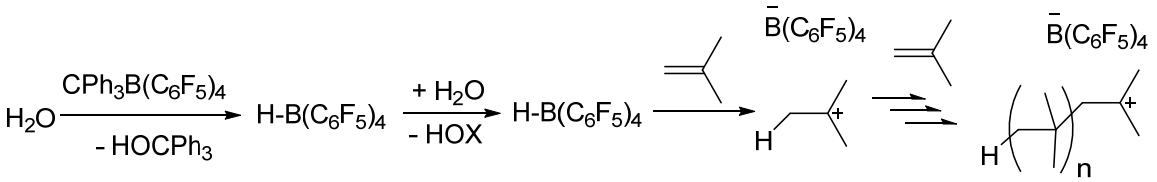

Scheme 5.10. Carbocationic initiation using Trityl borate salts with trace amount of water

Based off this information, it is possible that the polymerization system between Zr[Pr]/Trityl/MeCN and Zr[Pr]/Trityl/PMe_3 are instead due to a tandem catalysis system between the Zr[Pr]/Trityl oligomerization system and unreacted Trityl borate with MeCN/PMe_3 and vinylidene oligomers to form a carbocationic polymerization center, Scheme 5.11.

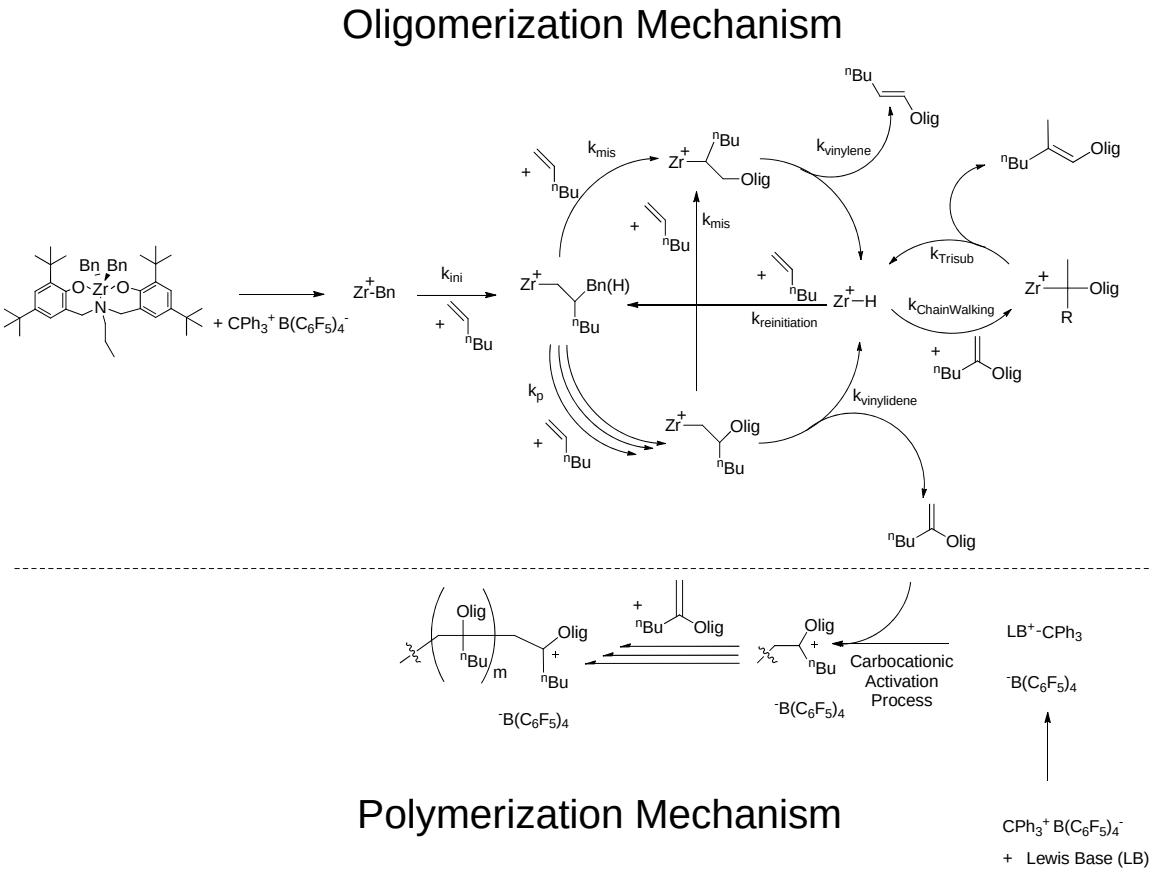

Scheme 5.11. Possible tandem catalysis system with a Zr/Trityl oligomerization system and a carbocationic polymerization system

If the system does produce polymers by this tandem catalysis method involving carbocationic polymerization of vinylidene oligomers, then the polymers produced should have different properties from linear poly(1-hexene), such as a different dN/dC. Isolation and testing of these polymers from the oligomers would allow one of these mechanisms to be disproven and offer new insights to this polymer producing system.

5.4 Conclusions

A comprehensive α-olefin insertion reactivity study on a 5-coordinate Zr amine bis-phenolate complex has been completed. Fundamental oligomerization reactivity of 1-hexene was changed by the identity of the co-catalyst activator. Studies with 1-hexene and 1-dodecene with Zr[Pr]/Trityl system were undertaken at different temperatures and ratios of catalyst to Trityl co-catalyst, with substoichiometric amounts of activator produced binuclear complexes (BNCs). Increasing the temperature increased catalyst activity, reduced the DP, and reduced the percent of vinylene chain ends for the different oligomers. Using substoichiometric activator reduced the propagation rate, reduced the DP, and vastly reduced the percent of vinylene chain ends. By increasing the temperature and using BNCs, the distribution was drastically reduced to form a distribution of trimers with 1-hexene monomer. The addition of different Lewis bases produced polymers with PMe_3 and MeCN while PPh_3 lowered the DP of 1-hexene oligomers. This stands in contrast to ^{31}P NMR experiments that did not show coordination of the trialkyl phosphines to the Zr[Pr]/Trityl system. Two possible polymerization mechanisms were discussed to explain the new reactivity. One mechanism requires coordination of the Lewis base to the catalyst center to form a new polymerization catalyst that produces linear poly(1-hexene) through a coordination insertion mechanism while the other mechanism requires an oligomerization site using the Zr[Pr]/Trityl system and a carbocationic polymerization site that converts vinylidene oligomers to nonlinear brush polymers from 1-hexene oligomers. Further characterization of the resulting polymers should delineate and clarify which of the two mechanisms is operabale.

5.5 References

(1) (a) Alt, H. G.; Koppl, A. *Chem. Rev.* **2000**, *100* (4), 1205-1222. (b) Britovsek, G. J. P.; Gibson, V. C.; Wass, D. F. *Angew. Chem. Int. Ed.* **1999**, *38*, 428-447.

(2) (a) Andresen, A.; Cordes, H. G.; Herwig, J.; Kaminsky, W.; Merck, A.; Mottweiler, R.; Pein, J.; Sinn, H.; Vollmer, H. J. *Ange. Chemie Int. Ed.* **1976**, *15*, 630.; (b) Chien, J. C. W.; Sugimoto, R. *J. Polym. Sci. Pol. Chem.* **1991**, *29*, 459.; (c) Ewen, J. A.; Elder, M. J.; Jones, R. L.; Haspeslagh, L.; Atwood, J. L.; Bott, S. G.; Robinson, K. *Makromol. Chem. Macromol. Symposia* **1991**, *48-9*, 253.; (d) Razavi, A.; Ferrara, J. *J. Organometallic Chem.* **1992**, *435*, 299.; (e) Rieger, B.; Jany, G.; Fawzi, R.; Steimann, M. *Organometallics* **1994**, *13*, 647.; (f) Miyake, S.; Okumura, Y.; Inazawa, S. *Macromolecules* **1995**, *28*, 3074.

(3) (a) Chen, Y. X.; Metz, M. V.; Li, L.; Stern, C. L.; Marks, T. J. *J. Am. Chem. Soc.* **1998**, *120* (25), 6287-6305. (b) Xiong, S.; Steelman, D. K.; Medvedev, G. A.; Delgass, W. N.; Abu-Omar, M. M.; Caruthers, J. M. *ACS Cat.* **2014**, *4* (4), 1162-1170. (c) Zhang, Y.; Keaton, R. J.; Sita, L. R. *J. Am. Chem. Soc.* **2003**, *125*, 9062–9069. (d) Bochmann, M.; Lancaster, S. J. *Angew. Chem., Int. Ed. Engl*. **1994**, *33*, 1634–1637.

(4) Despagnet-Ayoub, E.; Takase, M. K.; Henling, L. M.; Labinger, J. A.; Bercaw, J. E. *Organometallics* **2015**, *34*, 4707-4716.

(5) Dagprme. S.; Bellemin-Laponnaz, S.; Romain, C. *Organometallics* **2013**, *23*, 2736-2743.

(6) Tshuva, E. Y.; Goldberg, I.; Kol, M.; Goldschmidt, Z. *Organometallics* **2001**, *20* (14), 3017-3028.

(7) Steelman, D. K.; Xiong, S.; Pletcher, P. D.; Smith, E.; Switzer, J. M.; Medvedev, G. A.; Delgass, W. N.; Caruthers, J. M.; Abu-Omar, M. M. *J. Am. Chem. Soc.* **2013**, *135* (16), 6280-6288.

(8) Grumel, V.; Brull, R.; Pasch, H.; Raubenheimer, H. G.; Sanderson, R.; Wahner, U. M. *Macromol. Mater. Eng.* **2001**, *286* (8), 480-487.

(9) Hlavinka, M. L; Yang, Q.; Small, B. L.; Yu, Y. Catalyst systems for production of alpha olefin oligomers and polymers. US 20130172498[a]1, July 4, 2013.

(10) Horton, A. D.; de With, J. *Organometallics* **1997**, *16*, 5424-5436.

(11) Bochmann, M. *Organometallics* **2010**, *29*, 4711-4740.

(12) Cai, Z.; Ohmagari, M.; Nakayama, Y.; Shiono, T. *Macromol. Rapid Commun.* **2009**, *30*, 1812.

(13) Cabrera, L.; Welch, G. C.; Masuda, J. D.; Wei, P.; Stephan, D. W. *Inorganica Chemica Acta* **2006**, *359*, 3066-3071.

VITA

VITA

Born at Andrew's Airforce Base outside of Belleville, IL on March 24th 1988, Paul Daniel Pletcher joined his family of two older sisters (Jennifer and Diane), older brother (Christopher), and parents (Sunae and David Pletcher). After moving several places, he and his family eventually settled down in 1998 in Farmville, VA. At the high school level, Paul focused his varsity soccer, became a key member on the academic bowl team, graduated Valedictorian before moving onward to the University of Virginia's School of Engineering and Applied Science in the fall of 2006. Initially majoring solely in Chemical Engineering, Paul would eventually expand to a second major of Chemistry and began conducting analytical research under the tutelage of Professor James Demas on measuring the physical properties of ionic liquids. After graduating in 2010 with B.S. Chemical Engineering and B.S. Chemistry, Paul took some time before entering Chemistry Graduate Department at Purdue University in West Lafayette, IN to work in the laboratory of Professor Mahdi Abu-Omar. In his personal life, Paul met the love of his life in graduate school, Chelsey Del Grosso, and has built a happy life with their two yorkies, Bella and Teddy.

PUBLICATIONS

JACS
JOURNAL OF THE AMERICAN CHEMICAL SOCIETY

Article

pubs.acs.org/JACS

Effects of Pendant Ligand Binding Affinity on Chain Transfer for 1-Hexene Polymerization Catalyzed by Single-Site Zirconium Amine Bis-Phenolate Complexes

D. Keith Steelman,[†] Silei Xiong,[‡] Paul D. Pletcher,[†] Erin Smith,[†] Jeffrey M. Switzer,[‡] Grigori A. Medvedev,[‡] W. Nicholas Delgass,[‡] James M. Caruthers,*[,‡] and Mahdi M. Abu-Omar*[,†,‡]

[†]Brown Laboratory, Department of Chemistry, Purdue University, 560 Oval Drive, West Lafayette, Indiana 47907, United States

[‡]School of Chemical Engineering, Purdue University, Forney Hall of Chemical Engineering, 480 Stadium Mall Drive, West Lafayette, Indiana 47907, United States

Supporting Information

ABSTRACT: The kinetics of 1-hexene polymerization using a family of five zirconium amine bis-phenolate catalysts, Zr[tBu-ON^{X}O]Bn$_2$ (where X = THF (**1**), pyridine (**2**), NMe$_2$ (**3**), furan (**4**), and SMe (**5**)), has been investigated to uncover the mechanistic effect of varying the pendant ligand X. A model-based approach using a diverse set of data including monomer consumption, evolution of molecular weight, and end-group analysis was employed to determine each of the reaction specific rate constants involved in a given polymerization process. The mechanism of polymerization for **1**−**5** was similar and the necessary elementary reaction steps included initiation, normal propagation, misinsertion, recovery from misinsertion, and chain transfer. The latter reaction, chain transfer, featured monomer independent β-H elimination in **1**−**3** and monomer dependent β-H transfer in **4** and **5**. Of all the rate constants, those for chain transfer showed the most variation, spanning 2 orders of magnitude (ca. (0.1−10) × 10^{-3} s^{-1} for vinylidene and (0.5−87) × 10^{-4} s^{-1} for vinylene). A quantitative structure−activity relationship was uncovered between the logarithm of the chain transfer rate constants and the Zr−X bond distance for catalysts **1**−**3**. However, this trend is broken once the Zr−X bond distance elongates further, as is the case for catalysts **4** and **5**, which operate primarily through a different mechanistic pathway. These findings underscore the importance of comprehensive kinetic modeling using a diverse set of multiresponse data, enabling the determination of robust kinetic constants and reaction mechanisms of catalytic olefin polymerization as part of the development of structure−activity relationships.

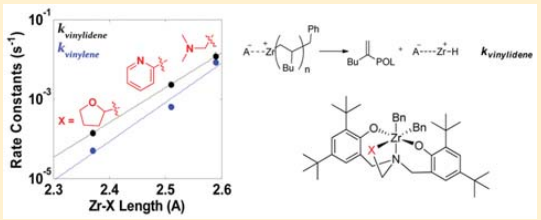

INTRODUCTION

Production of polyolefins is a major industrial process with a current capacity of ca. 110 billion kg per year globally.[1] While polyolefins are primarily produced using heterogeneous Ziegler catalysts, homogeneous single-site catalysts, the so-called metallocenes, have attracted attention because they offer potential control of the various kinetic steps, which in turn can be manipulated by "catalyst design".[2−4] One of the drawbacks of metallocenes, beside sensitivity to polar functional groups, is their thermal sensitivity. Beyond metallocenes, the next generation of thermally stable catalysts includes group 4 coordination complexes featuring phenolate amine ligands.[5] While high-throughput screening has accelerated the discovery process with group 4 coordination complexes leading to Dow's catalysts for olefin block copolymer synthesis,[6] the promise of directly correlating kinetic constants to descriptors of the catalyst has not yet been realized. A major obstacle in the way of rational catalyst design is the lack of proper quantitative kinetic analysis of all the relevant processes (i.e., kinetic steps) that are involved in catalytic olefin polymerization.[7,8] Nevertheless, the study of single-site catalysts for olefin polymerization is particularly attractive because of the potential of correlating directly the physical properties of the resulting polymer to structural features of the catalyst based on first principles.[9] This correlation allows one to draw conclusions on how a catalyst structure may be manipulated to yield specific polymeric architectures.

One specific family of nonmetallocene catalysts, first pioneered by Kol and co-workers, that has sparked interest utilizes an amine bis-phenolate (Salan) ligand system (see Figure 1).[10,11] The reason for choosing this particular family of ligands as part of our detailed kinetic studies is the relative ease of synthesis and the ability to tune the catalyst's coordination environment.[12] Furthermore, these catalysts exhibit high activity, comparable to metallocene catalysts, with 1-hexene in conventional organic solvents such as toluene. This feature enables the collection of kinetic data in the condensed phase and eliminates mass transfer limitations that are inherent with gaseous substrates. Following up on Kol's earlier qualitative

Received: February 8, 2013
Published: March 22, 2013

   dx.doi.org/10.1021/ja401474v | J. Am. Chem. Soc. 2013, 135, 6280−6288

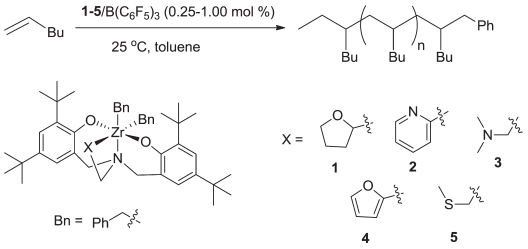

Figure 1. 1-Hexene polymerization catalyzed by zirconium salan-type catalysts **1**–**5** when combined with the activator $B(C_6F_5)_3$.

observations that the nature of the pendant ligand (X) and its distance from the metal center (Zr–X) influence chain transfer,[13] we have undertaken a comprehensive kinetic study of the five catalysts shown in Figure 1. We will show in the following sections the minimally required set of rate constants needed to describe completely the rich data set for each catalyst including the molecular weight evolution. The rate constant affected the most by changing the pendant ligand (X) is that for chain transfer that results in vinyl terminated polymer.

Four chemical mechanisms have been noted for chain transfer in single-site homogeneous olefin polymerization catalysts. Normally chain transfer occurs via β-H elimination to give vinylidene terminated polymer chains. This process is independent of monomer concentration and the resulting metal hydride undergoes reinitiation. If the catalyst is susceptible to 2,1-misinsertion (which results in regio-errors), the resulting polymeryl chain can undergo unimolecular β-H elimination to give vinylene terminated polymer chains.[14] In some cases for propylene, a second mechanism has been recognized in which β-methyl instead of β-H elimination occurs to give M-CH_3, which can reinitiate by inserting a monomer.[15] It should be noted that ethyl or higher alkane elimination has not been observed. A third mechanism is second-order chain transfer in which vinylidene and vinylene end groups result from H-transfer to a monomer.[7,8] In this mechanism the chain transfer rate constant is second-order and the rate is dependent on the monomer concentration. The last recognized chemical mechanism for chain transfer is that to the activator. This is usually a minor pathway observed with aluminum alkyl activators, although exceptions where it is dominant have been noted in the literature.[16]

Suppression of chain transfer while maintaining a high propagation rate can provide easy access to new block copolymers via controlled sequential addition of monomer.[17] Therefore, quantitative understanding of factors that control the rate of chain transfer exclusively is valuable from a fundamental standpoint as well as for practical applications. In semiquantitative studies, two parameters, catalyst activity (TOF or g polymer mol^{-1} catalyst h^{-1}) that is taken as indicative of the propagation rate constant and the molecular weight average of the resulting polymer (M_w), have been used to infer how catalyst structure influences the chain transfer rate. The consensus from these studies pointed to steric bulk as the major contributor to retardation of chain transfer as long as there is a weakly coordinating ligand or an available coordination site for monomer docking.[18] Bercaw and co-workers observed that the use of a more open metal center leads to faster propagation by allowing more space for a more facile monomer insertion and an increase in the propensity for β-H elimination due to more available space to accommodate the β-H agostic bonding interactions necessary for β-H elimination.[19] This empirical insight has been responsible for the development of late transition metal catalysts based on Fe, Co, and Ni that can effect ethylene polymerization rather than producing oligomers.[18]

Ziegler and co-workers performed a detailed computational study of ethylene polymerization using a wide range of d^0 metal catalysts,[20] finding that the energy barrier for chain transfer is strongly influenced by sterically bulky ligands and, to some degree, the identity of the metal. They also observed that, for the systems studied, β-H transfer to monomer, a second-order chain transfer process, is preferred over β-H elimination, except when monomer concentration is small or when monomer coordination to the metal is severely hindered. This observation was used successfully by Busico and co-workers to design catalysts that were shown experimentally to have hindered chain transfer reactions.[21] In addition, Camacho and Guan have attributed the steric blocks present in their cyclophane-based nickel catalyst to its ability to polymerize olefins even at high temperatures where chain transfer typically dominates,[22] and Rieger and co-workers have used sterically hindered nickel and palladium catalysts to produce high molecular weight polyethylene rather than α-olefin oligomers.[23]

Earlier work by Doi and co-workers showed that for $V(acac)_3$–$Al(C_2H_5)_2Cl$ the identity of the alkylaluminum cocatalyst influences the amount of chain transfer.[24] Later work by Naga and Mizunuma showed similar activator effects on the amount of chain transfer using zirconium metallocenes, with an additional observation that the β-H chain transfer pathway was preferred with one alkylaluminum activator while chain transfer to activator was dominant with another.[25] More

Table 1. Rate Constants for 1-Hexene Polymerization with the $Zr[tBu\text{-}ON^XO]Bn_2/B(C_6F_5)_3$ Catalysts 1–5[a]

X	THF (1)	Pyridine (2)	NMe2 (3)	Furan (4)	SMe[b] (5)
Zr–X/ Å	2.37	2.51	2.59	2.69	2.89
k_i/ M^{-1} s^{-1}	0.08 (+0.02/ −0.01)	>0.05	0.16 (+0.04/-0.02)	0.0031 (+0.0003/-0.0004)	0.017 (+0.002/-0.001)
k_p/ M^{-1} s^{-1}	8.0 (+0.8/ −0.2)	1.8 (+0.2/-0.1)	11 (+1/-1)	3.52 (+0.03/-0.04)	12 (+5/-4)
k_{mis}/ M^{-1} s^{-1}	0.054 (+0.026/-0.003)	0.031 (+0.004/-0.005)	0.055 (+0.007/-0.004)	0.0064 (+0.0002/-0.0004)	0.20 (+0.08/-0.06)
k_{rec}/ M^{-1} s^{-1}	0.047 (+0.021/-0.002)	0.028 (+0.004/-0.005)	0.04 (+0.03/-0.02)	0[c]	0.036 (+0.001/-0.001)
$k_{vinylidene}$ (10^{-3})/ s^{-1}	0.14 (+0.014/ −0.02)	2.4 (+0.1/-0.1)	12.2 (+0.8/-0.6)	1.00 (+0.07/-0.08)	0
$k_{vinylene}$ (10^{-3})/ s^{-1}	0.051 (+0.002/ −0.003)	0.65 (+0.06/ −0.05)	8.72 (+0.07/ −0.04)	0	0
$k_{vinylidene}$ (10^{-3})/ M^{-1} s^{-1}	0	0	0	12.1 (+0.7/-0.6)	2.2 (+0.6/-0.4)
$k_{vinylene}$ (10^{-3})/ M^{-1} s^{-1}	0	0	0	6.9 (+0.07/-0.06)	0.95 (+0.06/-0.04)

[a]In toluene at 25 °C. See Figure 1 for precatalyst structures and Scheme 1 for reactions steps. Errors are in parentheses. [b]In toluene at 22 °C. [c]A value of zero means the fit did not require the inclusion of this reaction step.

dx.doi.org/10.1021/ja401474v | J. Am. Chem. Soc. 2013, 135, 6280–6288

recently, Marks and co-workers have studied the effects of ion pair structure and dynamics on polymerization activity, stereoselectivity, and chain transfer in C_s-symmetric zirconium metallocene precatalysts using various fluorinated aryl borane and aluminum activators.[26] They found that ion pairing dictates the relative rate of termination to propagation as well as the preferred termination pathway.

In this study, we describe a detailed kinetic analysis for catalysts **1**−**5**, culminating in Table 1, which contains all of the rate constants for each system. The following sections will discuss observations and trends that only become apparent through the generation and examination of the full kinetic constants presented in Table 1. These kinetic constants represent the minimal number of necessary reaction steps needed to describe the entire data set for each of the catalysts, which includes monomer consumption kinetics, molecular weight evolution as determined by GPC (gel permeation chromatography), active-site count, and analysis of terminated end groups in the resulting polymer. The mechanism of chain transfer and its corresponding rate constants as the pendant ligand (X) changes have been pinpointed. A linear quantitative structure−activity relationship (QSAR) between the logarithm of the chain transfer rate constant and the Zr−X bond length will be shown and discussed.

EXPERIMENTAL PROCEDURES

General Procedure. All manipulations were performed under dry inert atmosphere in a glovebox or at a vacuum manifold using air sensitive techniques under N_2 or Ar atmosphere. Toluene and pentane were distilled over activated alumina and a copper catalyst using a solvent purification system (Anhydrous Technologies) and degassed through freeze−pump−thaw cycles. Both solvents were stored over activated molecular sieves. Tetrabenzylzirconium was purchased from STREM and used as received. The monomer 1-hexene was purchased from Aldrich and purified by distillation over a small amount of dimethyl bis(cyclopentadienyl)zirconium and stored over molecular sieves. Tris(pentafluorophenyl)boron was purchased from STREM and purified by sublimation. Diphenylmethane was purchased from Aldrich and stored over molecular sieves. CH_3OD was purchased from Cambridge Isotopes and used as received. d_8-Toluene was used as received and stored over molecular sieves. ^1H and ^2H NMR experiments were performed on a Varian INOVA600 MHz or Bruker DRX500 MHz spectrometer.

The ligands and precatalysts (**1**−**5**) were prepared following modified literature procedures.[12,27,28] We describe herein the details for one representative procedure and provide the others in the Supporting Information.

Synthesis of 6,6′-((((Tetrahydrofuran-2-yl)methyl)-azanediyl)bis(methylene))bis(2,4-di-*tert*-butylphenol), tBu-ON^{THF}O ligand. In a typical synthesis, an 80 mL reaction vessel was charged with 2,4-di-*tert*-butylphenol (6.19 g, 30.0 mmol), 2-(aminomethyl)tetrahydrofuran (1.55 mL, 15 mmol), and 37% histological grade formaldehyde (6.00 mL, 80 mmol), distilled water, and a stir bar while maintaining a maximum volume of 80 mL. The biphasic reaction mixture was placed in a CEM microwave reactor and allowed to warm to 100 °C over 5 min while stirring. The reaction was allowed to stand at 100 °C for 30 min, and then cooled to room temperature. The aqueous layer was removed, and cold, dry methanol was added to the organic phase. This mixture was shaken for 30 min, and the resulting solid isolated by vacuum filtration. The crude ligand product was purified by crystallization from ethanol (28% yield).

Synthesis of Zr[tBu-ON^{THF}O]Bn$_2$ (1). In a typical synthesis, a 100 mL flask was charged with tetrabenzylzirconium (0.557 g, 1.22 mmol), 20 mL toluene, and a stir bar and fitted with a rubber septum. A second 100 mL flask was charged with the ^{t}Bu-ON^{THF}O ligand (0.609 g, 1.13 mmol) and 20 mL of toluene. The two flasks were placed under an inert atmosphere, and the ligand solution was added to the tetrabenzylzirconium solution via a cannula. The reaction was allowed to warm to 60 °C and stir for 2 h resulting in a bright yellow solution. The solution was concentrated to about 10 mL and placed into a −10 °C freezer. Yellow crystals formed within 2 days and the mother liquor was removed via a cannula. The crystals were dried under vacuum (84% yield). The precatalyst was recrystallized by vapor diffusion of pentane into a precatalyst/toluene solution to afford an analytically pure complex.

NMR Scale Polymerization of 1-Hexene. The procedure for NMR scale polymerization is based on the literature.[29] For a typical polymerization, Zr[tBu-ON^{THF}O]Bn$_2$ (**1**) (6.1 mg, 0.0075 mmol) was dissolved in 0.5 mL toluene in a small vial and sealed with a screw-cap septum. The vial containing the precatalyst solution was pierced with a 1 mL syringe. The vial and syringe were placed in an N_2 bag and allowed to equilibrate to 25 °C. Tris(pentafluorophenyl)boron (4.3 mg, 0.0084 mmol), 1-hexene (0.1265 g, 1.50 mmol), and diphenylmethane (9.5 mg 0.056 mmol) were added to a 2 mL volumetric flask and diluted to the mark with d_8-toluene. This solution was placed in an NMR tube and sealed with a septum. The monomer/activator solution was placed in the spectrometer and allowed to equilibrate to 25 °C using a VT controller. A measurement was taken to determine the initial concentration of monomer relative to the internal standard. The NMR tube was removed from the spectrometer, and the catalyst precursor solution was added to the activator/monomer solution by piercing the septum while the syringe remained in the N_2 bag. The reaction mixture was shaken for ca. 30 s and placed back into the spectrometer. Spectra were acquired at predetermined time intervals until the reaction reached completion. Each sample was prepared for GPC analysis by evaporation over mild heat before dissolution in hexanes and filtration through an alumina plug to remove the quenched catalyst. Evaporation of solvent yielded clear, colorless poly(1-hexene). The array of ^1H spectra was collected on an INOVA 600 MHz spectrometer and analyzed using MestReNova.

Batch Polymerization of 1-Hexene. The procedure for Manual Quench is based on literature.[30] For a typical polymerization, Zr[tBu-ON^{THF}O]Bn$_2$ (0.073 g, 0.090 mmol) was dissolved in 5.0 mL toluene in a small vial that was sealed with a screw-cap septum. The vial containing the precatalyst solution was pierced with a 10 mL syringe. The vial and syringe were placed in an N_2 bag and allowed to equilibrate to 25 °C. Tris(pentafluorophenyl)boron (0.053 g, 0.099 mmol), and 1-hexene (1.575 g, 18.71 mmol) were added to a 25 mL flask and diluted to the mark with toluene. This solution was diluted to 26 mL with 1 mL of toluene, and 1 mL of the resulting solution was removed for quantification of the initial monomer concentration through NMR analysis. The flask was sealed with a septum and moved from an N_2 filled glovebox to a vacuum manifold and placed under argon. The monomer/activator solution was allowed to equilibrate to 25 °C using a temperature-controlled silicone oil bath. The catalyst precursor solution was added to the activator/monomer solution by piercing the septum while the syringe remained in the N_2 bag. The resulting yellow solution was allowed to stir while aliquots were removed at selected times and each was injected into a 10 mL volumetric flask containing 1 mL of deutero-methanol. A 1 mL aliquot from the quenched solutions was removed and a 0.5 mL solution of *d*-toluene spiked with diphenylmethane as an internal standard for quantification of 1-hexene consumption (via ^1H NMR on Varian Inova 600). Each sample was prepared for GPC analysis by evaporation over mild heat before dissolution in hexanes and filtration through an alumina plug to remove the quenched catalyst. Evaporation of solvent yielded clear, colorless poly(1-hexene).

In the case of vinyl end group analysis, a 1 mL aliquot was worked up as described above. The resulting polymer was dissolved in $CDCl_3$, and diluted to the mark in a 2 mL volumetric flask. Diphenylmethane was used as an internal standard and the method of standard additions was used in quantification of the end groups by ^1H NMR. All end-group analysis measurements were taken on a Bruker DRX500 spectrometer at 25 °C.

In the case of ^2H analysis for active-site counting, the remaining quenched reaction solution (8 mL) was worked up as described above. The resulting polymer was dissolved in CH_2Cl_2, and diluted to the

dx.doi.org/10.1021/ja401474v | J. Am. Chem. Soc. 2013, 135, 6280−6288

mark in a 2 mL volumetric flask. d_6-Benzene was used as an internal standard and the method of standard additions was used in quantification of active sites by ^{2}H NMR. All active site measurements were taken on a Bruker DRX500 spectrometer at 25 °C.

Gel Permeation Chromatography (GPC) Analysis. The procedure used to analyze polymer samples using GPC methods was taken from Novstrup et al.,[7] and it is summarized below. Poly(1-hexene) samples were added to THF at room temperature and allowed to dissolve for 4 h. Solutions were then passed through a 0.2 μm filter to remove any particulate matter. The GPC analysis was performed on a Waters GPCV 2000 for system **1** and **3**, and on a Viscotek GPCmax VE 2001 for system **2**, **4**, and **5**. On the Waters GPCV 2000, samples were injected through a 101.3 μL injection loop and passed through two Polymer Laboratories PLGel 5 μm Mixed-C columns in series in a 45 °C oven at a flow rate of 1.0 mL min^{-1}. On Viscotek GPCmax VE 2001, samples were injected through a 200 μL injection loop and passed through three Viscotek T6000 M 10 μm General Mixed Org columns in series in a 35 °C oven at a flow rate of 1.0 mL min^{-1}. The analysis made use of the differential RI detector and a capillary viscometer. Molecular weights were assigned by way of a universal calibration curve created with polystyrene standards ranging from 580 g mol^{-1} to 3 114 000 g mol^{-1}. The calibration was verified through the analysis of a broad standard, SRM 706a, provided by the National Institute of Standards and Technology.

RESULTS

Here we present a complete kinetic analysis for 1-hexene polymerization by catalysts **1**−**5**. In approaching each system, we followed our previously developed kinetic modeling method[7,29] based on the analysis of multiresponse data that includes GPC traces where we did not make any a priori assumptions about the elementary reaction steps taking place. However, when this independent analysis was completed for each catalyst system, it emerged that all five systems described herein follow a similar kinetic mechanism including initiation, propagation via normal insertion, 2,1-misinsertion, recovery from misinsertion, and two types of chain transfer resulting in the formation of vinylidene and vinylene species. The kinetic steps are illustrated in Scheme 1. The activation step is fast on the time scale of polymerization and as a result was not used in the kinetic modeling. Chain transfer resulting in vinylidene and vinylene follows either unimolecular (monomer independent) β-H elimination or bimolecular β-H transfer to monomer.

Examining the available data, the reasons for the mechanism above (Scheme 1) are as follows:

I. Misinsertion (k_{mis}) and recovery (k_{rec}) are necessary because of the following:

1. We observe two types of chains attached to the active sites (primary and secondary) in active-site counting experiments with MeOD quenches (^{2}H NMR of isolated polymer gives δ 0.83 (DH_2C−Polymer) and 1.22 (DH(Bu)C−Polymer).
2. When analyzing the produced polymer, there are two types of vinyl end groups observed: one with a terminal double bond at the end of the chain (vinylidene), and another with an internal double bond inside the chain (vinylene). We believe, in agreement with the literature,[30] that the latter arises from chain transfer of misinserted chains.
3. The secondary sites (Zr-CH(Bu)−Polymer) do not accumulate over time. We assume this is the case because they are able to recover via normal 1-hexene insertion.
4. Although there is an alternative explanation for points 1 through 3, namely, that there are two different sites growing separately, it is expected that such a mechanism would at least under some experimental conditions produce bimodal MWD. The fact that none of the five systems exhibit a bimodal MWD and all yield narrow PDI values strongly suggest that these systems are single-site catalysts.

Scheme 1. Elementary Kinetic Steps Used in Fitting the Data for Catalysts 1−5[a]

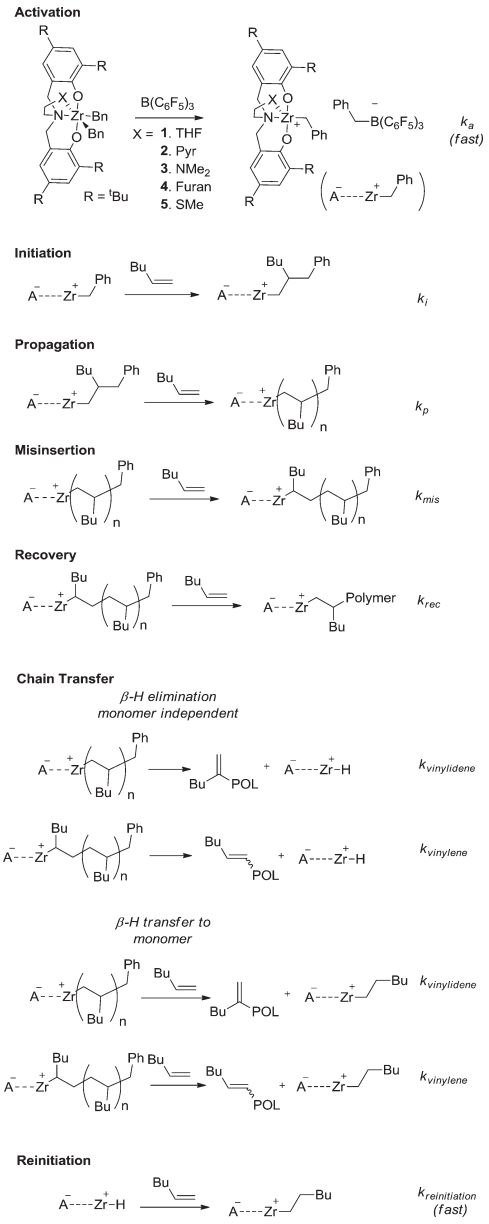

[a]The ordinary differential equations (ODEs) that describe the mass-action kinetics associated with this mechanism are provided in the Supporting Information.

dx.doi.org/10.1021/ja401474v | J. Am. Chem. Soc. 2013, 135, 6280−6288

II. Chain transfer reactions are necessary because we observe polymer chains with vinyl end groups. It should be noted that there are two possible mechanisms through monomer dependent and monomer independent pathways. The monomer dependent pathway (β-H transfer to monomer) results in an active site with one repeat unit, while the monomer independent pathway (β-H elimination) results in the formation of a zirconium hydride. There is an ongoing discussion in the literature whether the insertion of a monomer in the zirconium hydride, i.e., reinitiation ($k_{reinitiation}$) is facile or hindered as compared to the normal initiation (k_i) for a given catalyst system.[31] If the rate constant of reinitiation ($k_{reinitiation}$) of the zirconium hydride is slow, it effectively renders affected catalyst sites inactive, which in turn has an effect on the monomer consumption curve, active sites count, and the MWDs. As a result the value of the reinitiation rate constant ($k_{reinitiation}$) can be determined. On the other hand, when the rate constant of the reinitiation of zirconium hydride is fast, the data are usually not sensitive enough to determine its value precisely, similarly to how the data are not sensitive enough to determine the normal initiation rate when it is not significantly slower than the propagation rate. In practice we have set the reinitiation rate to be equal to the propagation rate in cases when the reinitiation rate is determined to be fast.

An important caveat is that the catalyst participation for each system may vary and not be 100%. The catalyst participation can be estimated from the active site counting experiments (quench with MeOD followed by ^{2}H NMR analysis of polymer chains). Also, for the systems where the chain transfer is low (catalysts **1** and **5**) the catalyst participation is readily estimated from the slope of M_w vs conversion plot, which is linear in these cases. When applicable, these two methods give consistent results. The catalyst participation information for **1**−**5** is provided in the Supporting Information.

For each system we simultaneously fit the following: (1) monomer consumption, (2) MWD, (3) active site counts, and (4) end group counts. The data set usually includes several initial conditions of different $[C]_0$ (C = precatalyst/$B(C_6F_5)_3$) and $[M]_0$ (M = 1-hexene). For some conditions, multiple repeats were carried out, and the results were consistent when small variation in active-site catalyst participation was accounted for; however, only one repeat is shown in the figures below.

In determining error margins of the estimates for the six rate constants for each catalyst system (see Scheme 1), the following considerations apply: (1) the experimental data has an inherent error resulting from the measurement procedure. Specifically, the NMR spectrum is characterized by the uncertainty of roughly 5% for the peak integration; the GPC trace is characterized by the uncertainty of the weight average, M_w, of approximately 3%, where the uncertainty in the shape of the distribution is more difficult to ascertain (see discussion in reference 29). However, these estimates are based on the best experimental conditions, such sufficient concentration of the species of interest in the case of NMR, which holds for the monomer concentration. (2) In the case of the active sites and vinyl end group analyses, the concentrations are relatively low, causing the uncertainty to increase. Three separate measurements were performed for each sample, where the concentration varied slightly from measurement to measurement. The standard deviation calculated on the basis of these three measurements is compared to the inherent NMR integration error, and the larger error is chosen. (3) In the case of the GPC measurements, repeat runs result in minimal scatter such that the GPC curves appear overlapping. This, however, should not be taken as an actual estimate of the experimental error, since the error in the GPC measurements may be systematic rather than random due to various reasons described in the literature.[29] Instead, we assumed that the potential error in the GPC outputs caused by the uncertainty in the dn/dc values, interdetector time, and so forth, amounts to at most a 10% up or down shift of each slice molecular weight and hence the shift of the entire MWD. (This actually translates in the −0.05/+0.04 shifts on log scale).[7] For most of the studied systems, error from the GPC measurements were determined to cause the largest uncertainty in the rate constants, and therefore this method was used to generate the uncertainty reported in this paper.

In the rest of this section we provide first the detailed analysis including fits to the data for each catalyst system, and then a summary of all the rate constants in Table 1.

Zr-THF Catalyst 1. The experimental data along with the kinetic modeling fits are presented in Figure 2.

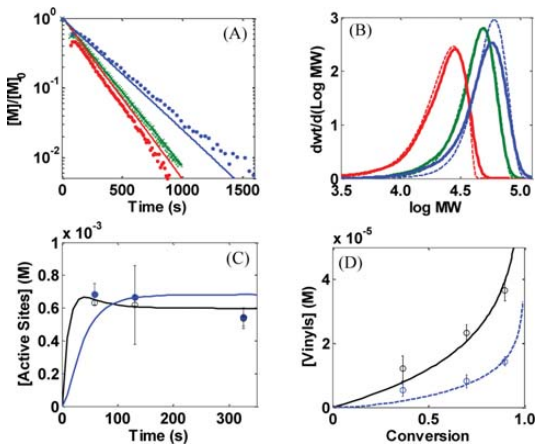

Figure 2. Multiresponse data set with fits for Zr[^{t}Bu-ON^{THF}O]Bn_2/$B(C_6F_5)_3$ catalyst **1**. (A) Monomer consumption of selected NMR scale reactions having catalyst to monomer ratios of 1:100 (red, $[C]_0$ = 3.0 mM, $[M]_0$ = 0.30 M), 1:200 (green, $[C]_0$ = 3.0 mM, $[M]_0$ = 0.60 M), and 1:400 (blue, $[C]_0$ = 1.5 mM, $[M]_0$ = 0.60 M). Symbols are data; solid lines are modeling fits. (B) MWDs of the polymer resulting from the reactions shown in (A). Solid curves are data, dashed curves are fits. (C) Active site counts of selected batch scale reaction with three quenches using MeOD at different reaction times. $[C]_0$ = 3.0 mM, $[M]_0$ = 0.60 M. Black symbols: primary active-site count; blue symbols: secondary active-site count. Solid curves are modeling fits. (D) Vinyl analyses of selected batch scale reaction with three quenches at different reaction time. $[C]_0$ = 3.0 mM, $[M]_0$ = 0.60 M. Black symbols: vinylidene count; blue symbols: vinylene count. Lines represent kinetic modeling fits.

The specific features of this system are (1) very few chain transfer events and (2) catalyst participation is around 50%.

Zr-Pyridine Catalyst 2. The experimental data along with the kinetic modeling fits are presented in Figure 3.

The specific features of this system are (1) catalyst participation around 50%, (2) initiation is fast, i.e., no more than 40 times slower than propagation, and (3) the monomer consumption, i.e., the logarithm of the normalized monomer

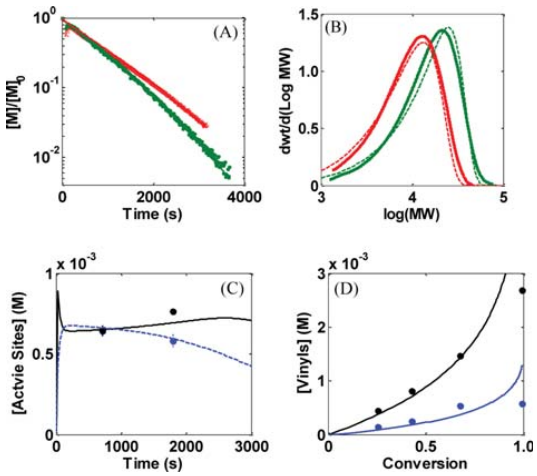

Figure 3. Multiresponse data set with fits for Zr[^{t}Bu-ON^{Py}O]Bn_2/$B(C_6F_5)_3$ catalyst **2**. (A) Monomer consumption of selected NMR scale reactions having catalyst to monomer ratios of 1:100 (red, $[C]_0$ = 3.0 mM, $[M]_0$ = 0.30 M), and 1:200 (green, $[C]_0$ = 3.0 mM, $[M]_0$ = 0.60 M). Symbols are data; solid lines are modeling fits. (B) MWDs of the polymer resulting from the reactions shown in (A). Solid curves are data; dashed curves are fits. (C) Active site counts from three selected NMR scale reactions. Each reaction is quenched using MeOD at different reaction time. $[C]_0$ = 3.0 mM; $[M]_0$ = 0.60 M. Black symbols: primary active-site count; blue symbols: secondary active-site count. Solid curves are modeling fits. (D) Vinyl analyses of three selected NMR scale reactions quenched at different reaction time. $[C]_0$ = 3.0 mM; $[M]_0$ = 0.60 M. Black symbols: vinylidene count; blue symbols: vinylene count. Lines represent kinetic modeling fits.

concentration vs time (Figure 3a), appears bent downward. The explanation for this effect is that the overall rate of consumption is controlled by the primary sites, while the secondary sites are dormant. The exit from the secondary sites can happen via two pathways: (1) recovery by normal monomer insertion and (2) monomer independent chain transfer resulting in an activated catalyst ready to initiate a new chain and start consuming monomers. Toward the end of the reaction, when the monomer concentration becomes low, the rate of misinsertion slows down but the second recovery pathway (chain transfer) does not (since it is independent of monomer). As a result, the number of primary sites increases and the number of secondary sites decreases (Figure 3c), producing the apparent acceleration of monomer consumption.

Zr-NMe$_2$ Catalyst 3. The data and model fits for this catalyst have been published in a previous article.[29] The specific features of this system are as follows: (1) Catalyst participation is generally around 45%, although the exact value varied from 20% to 60% depending on the experiment. (2) Initiation is roughly 70 times slower than propagation. (3) Chain transfer occurred moderately frequently, with both vinylidene and vinylene end groups detected. The data suggest that monomer independent pathways, β-H elimination, lead to both types of observed vinyl end groups. (4) The error estimation in the referenced work[29] was calculated via a different method than the one used here. For consistency, the current method has been applied to the data to produce error estimates for the rate constants shown in Table 1. The error estimation is based on the error from the GPC measurement.

Zr-Furan Catalyst 4. The experimental data along with the kinetic modeling fits are presented in Figure 4.

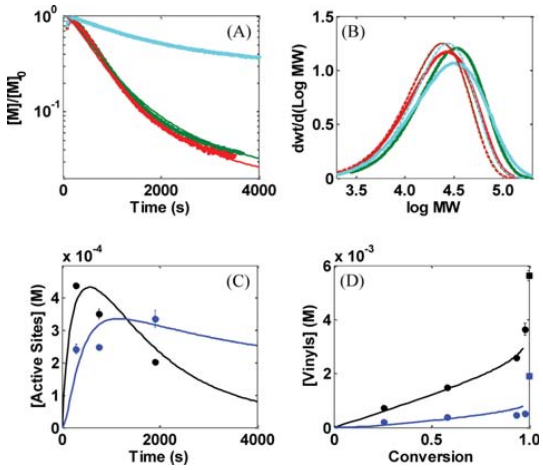

Figure 4. Multiresponse data set with fits for Zr[^{t}Bu-ON^{furan}O]Bn_2/$B(C_6F_5)_3$ catalyst **4**. (A) Monomer consumption of selected NMR scale reactions having catalyst to monomer ratios of 1:100 (red, $[C]_0$ = 3.0 mM, $[M]_0$ = 0.30 M), 1:200 (green, $[C]_0$ = 3.0 mM, $[M]_0$ = 0.60 M), and 1:400 (cyan, $[C]_0$ = 1.5 mM, $[M]_0$ = 0.60 M). Symbols are data; solid lines are modeling fits. (B) MWDs of the polymer resulting from the reactions shown in (A). Solid curves are data; dashed curves are fits. (C) Active site counts of selected batch scale reaction with three quenches using MeOD at different reaction time. $[C]_0$ = 3.0 mM; $[M]_0$ = 0.60 M. Black symbols: primary active-site count; blue symbols: secondary active-site count. Solid curves are modeling fits. (D) Vinyl analyses of selected batch scale reaction with three quenches at different reaction time. $[C]_0$ = 3.0 mM; $[M]_0$ = 0.60 M. Black symbols: vinylidene count; blue symbols: vinylene count. Squares are vinyls counts taken after 12 h. Lines represent kinetic modeling fits.

The specific features of this system are as follows: (1) Catalyst participation is around 50%. (2) Initiation is slow, evidenced by the apparent induction period on the monomer consumption curve (Figure 4a). (3) Chain transfer reactions are monomer dependent, β-H transfer to monomer, supported by the following arguments: (a) under different initial catalyst and monomer concentrations, the MWD does not change significantly (Figure 4b); and (b) the relationship between the end group concentrations and monomer conversion during most of the reaction is linear. These two features indicate that the ratio of the chain transfer rate to the propagation rate is a constant independent of the initial concentrations, and that monomer dependent chain transfer reactions control the MW in this system. (4) There is a continuous increase in the end group counts when the batch system is allowed to run overnight after the monomer has already been fully consumed (Figure 4d). It is, hence, concluded that monomer independent chain transfer reaction must take place when there is no monomer, and this chain transfer reaction most likely arises from normal insertion. As mentioned before, this type of chain transfer results in formation of zirconium hydride. However, in order to model the monomer consumption data for this catalyst system, it is necessary for the reinitiation rate constant to be zero, which effectively creates a deactivation pathway that is responsible for the bending observed in the monomer

dx.doi.org/10.1021/ja401474v | J. Am. Chem. Soc. 2013, 135, 6280−6288

consumption curve (Figure 4a) and the drop in primary site count (Figure 4c). It is known that, for some systems, the reinitiation rate is slow for metal hydride.[31] (5) Given that the primary active site count drops and the secondary active sites accumulate, we believe there is no recovery from misinsertion in this system ($k_{reinitiation} \sim 0$).

Zr-SMe Catalyst 5. The experimental data along with the kinetic modeling fits are presented in Figure 5.

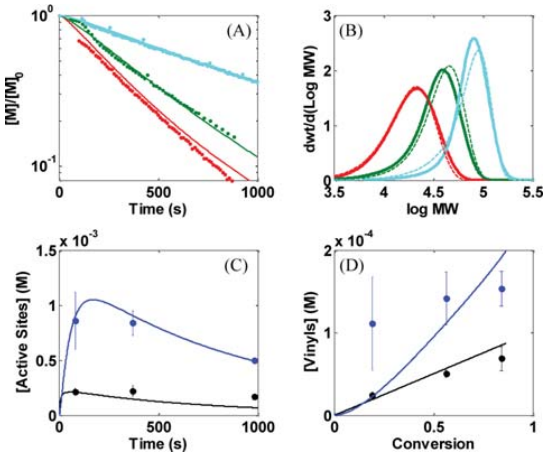

Figure 5. Multiresponse data set with fits for Zr[^{t}Bu-ON^{SMe}O]Bn_2/$B(C_6F_5)_3$ catalyst **5**. (A) Monomer consumption of selected NMR scale reactions having catalyst to monomer ratios of 1:100 (red, $[C]_0$ = 3.0 mM, $[M]_0$ = 0.30 M), 1:200 (green, $[C]_0$ = 3.0 mM, $[M]_0$ = 0.60 M), and 1:400 (cyan, $[C]_0$ = 1.5 mM, $[M]_0$ = 0.60 M). Symbols are data; solid lines are modeling fits. (B) MWDs of the polymer resulting from the reactions shown in (A). Solid curves are data, dashed curves are fits. (C) Active site counts of selected batch scale reaction with three quenches using MeOD at different reaction time. $[C]_0$ = 3.0 mM; $[M]_0$ = 0.60 M. Black symbols: primary active site count; blue symbols: secondary active site count. Solid curves are modeling fits. (D) Vinyl analyses of selected batch scale reaction with three quenches at different reaction time. $[C]_0$ = 3.0 mM; $[M]_0$ = 0.60 M. Black symbols: vinylidene count; blue symbols: vinylene count. Squares are vinyls counts taken after 12 h. Lines represent kinetic modeling fits.

The specific features of this system are as follows: (1) Secondary Zr-polymer sites (Zr-CH(Bu)-Polymer) resulting from misinsertion dominate over primary active-sites (Zr-CH_2-Polymer). The model-based explanation is that the k_{mis}/k_p ratio is high while k_{rec}/k_p is low. The values for this catalyst are similar to those for catalyst **1**, where secondary sites are roughly equal to primary sites. (2) Vinylene end groups, which are formed from chain transfer of secondary sites, are more abundant than vinylidene end groups. This is because of the higher concentration of secondary sites rather than a larger $k_{vinylene}$ rate constant. (3) Vinyl groups form via chain transfer to monomer, affording second-order rate constants. The data, however, is not definitive, and a first-order reaction (β-H elimination) cannot be definitively ruled out. In either case, the vinyl concentrations are relatively small, and the effect of the chain transfer rate constants on the responses other than the vinyl end group analysis data (e.g., the MWDs) is small. (4) The total active site concentration (primary plus secondary) decreases over the course of the reaction. In addition, the monomer consumption slows late in the reaction. These behaviors imply a first-order (in catalyst) deactivation reaction. The deactivation rate constant is approximately half of the initiation rate constant, with the result that the total active site concentration remains low throughout the reaction. (5) While 100% of the catalyst is available to initiate (in contrast to the other systems where only a fraction participates), no more than about one-third (ca. 33%) of the zirconium active sites contain a growing polymer chain at any given time.

DISCUSSION

In this study, the complete set of kinetic rate constants for five zirconium amine bis-phenolate catalyst systems have been presented. For each system, a rich data set including MWD has been collected and successfully fitted by comprehensive kinetic modeling. The mechanism of 1-hexene polymerization for these catalysts (**1**−**5**) consists of the following elementary reaction steps: initiation, normal propagation, misinsertion, recovery, and chain transfer. The values of the rate constants are shown in Table 1.

In the first row in Table 1, the Zr−X bond distance as determined by single crystal X-ray crystallography is shown for each catalyst precursor.[10,11,13] Catalysts **1**−**5** are characterized by a progressively longer Zr−X bond distance. From examination of the data given in Table 1, the chain transfer reaction rates (chain transfer following normal insertion, $k_{vinylidene}$, and chain transfer following misinsertion, $k_{vinylene}$) for systems **1**, **2**, and **3** are monomer independent, whereas, for systems **4** and **5**, the predominant chain transfer reactions are monomer dependent. We speculate that once a certain Zr−X bond distance has been reached, there is enough steric freedom to accommodate monomer dependent chain transfer processes as is the case for systems **4** and **5**. As shown in Figure 4d (see caption), when left overnight, system **4** shows an increase in chain transfer products even after all available monomer has been consumed within 1 h suggesting that there is some amount of monomer independent chain transfer (β-H elimination) events taking place. It follows that although monomer dependent chain transfer is the preferred pathway for systems containing a longer Zr-X bond distance, the possibility of monomer independent chain transfer events remains.

While the literature has ample support from empirical observations and semiquantitative measurements that steric constraints of the ligand contribute significantly to chain transfer rates and the mechanism by which chain transfer occurs, i.e., unimolecular β-H elimination versus transfer to monomer,[18] we present a quantitative measure of the rate constants and illustrate at what point a crossover in the chain transfer mechanism occurs. An important point that should not be passed over lightly is that in the analysis of systems **1**−**5** the chain transfer rate constants presented in this work are not obtained just by analysis of vinyl end groups in isolation from all the other rate constants that are pertinent to the catalytic cycle, but rather the full suite of rate constants describing the entire data set for each of the catalyst systems. It is only when this level of quantitative analysis has been employed that one can make definitive QSAR describing how catalyst structure affects properties of the resulting polymer. For example, often in the literature observation of changes in M_w is taken as a direct measure of chain transfer rates as long as activity (TOF) of the catalysts under study remained comparable.[5,18] The assumption in such comparisons is that TOF is a direct measure of k_p and that all other constants did not change. By applying our quantitative analysis methods such assumptions

and pitfalls that arise from comparing activities rather than rate constants can be eliminated.

A close examination of the unimolecular (β-H elimination) chain transfer rate constants $k_{vinylidene}$ and $k_{vinylene}$ for systems **1**, **2**, and **3** revealed a very intriguing trend. There appears to be a direct correlation between the length of the Zr-X bond distance and $k_{vinylidene}$ and $k_{vinylene}$ (Figure 6). Remarkably, the logarithms

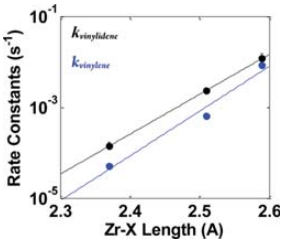

Figure 6. Plot of monomer independent chain transfer rate constants ($k_{vinylidene}$ and $k_{vinylene}$) versus Zr-X bond length for catalysts **1**, **2**, and **3**. Black symbols: chain transfer rate constants from primary sites ($k_{vinylidene}$); blue symbols: chain transfer rate constants from secondary sites ($k_{vinylene}$).

of both chain transfer rate constants appear to depend linearly on the aforementioned bond length. It can be speculated that this increase in bond distance allows for more steric freedom to accommodate the β-hydride agostic interaction necessary for chain transfer to occur, causing an increase in $k_{vinylidene}$ and $k_{vinylene}$ for catalysts **1**, **2**, and **3**. This observation implies that the activation energy, which is proportional to the logarithms of the rate constants at constant temperature, is linearly related to the Zr−X bond length at least for the three systems investigated. Although $k_{vinylidene}$ is always larger than $k_{vinylene}$, as seen in Figure 6, both rate constants are affected in a similar way by the increase of the Zr−X bond length as evidenced by their similar slopes.

Marks and co-workers have probed the effects of using different activators in Zr-based metallocene systems and showed that ion pairing does modulate chain transfer among other rates of polymerization and stereodefects.[26] The work presented in this study has been able to elucidate the role variations have on the rates of chain transfer in a way that can be quantified in terms of the simple Zr−X bond distance. The QSAR presented in Figure 6 is useful because it establishes a relationship for this catalyst family that is based on robust rate constants rather than a relative trend or estimated ordering of rates that represents a composite of elementary reaction steps. Of course, robustly establishing a QSAR model will require the analysis of more systems than just the five reported in this paper; however, these results are the start toward developing a fundamental understanding of the relationship between chemical structure and catalytic activity.

However, in systems **4** and **5** the further increase in the Zr−X bond length does not result in the expected increase in vinyl terminated chains, breaking the aforementioned trend and, moreover, leads to a different chain transfer mechanism: a monomer dependent β-H transfer. To illustrate that this change in the trend is quite significant, we show in Figure 7 the predicted vinyl concentrations for system **4** when it is assumed that the trend would continue. Specifically, the hypothetical values $k_{vinylidene}$ = 0.093 s^{-1} and $k_{vinylene}$ = 0.063 s^{-1} are obtained by extrapolating linearly to the Zr−X bond length for system **4**,

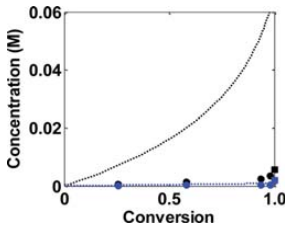

Figure 7. Predicted vinyl formation (dashed curves) using rate constants: k_i = 0.08 M^{-1} s^{-1}, k_p = 8 M^{-1} s^{-1}, $k_{misinsertion}$ = 0.054 M^{-1} s^{-1}, k_{rec} = 0.047 M^{-1} s^{-1}, $k_{vinylidene}$ = 0.093 s^{-1}, and $k_{vinylene}$ = 0.063 s^{-1} for catalyst **4**. Black symbols: measured vinylidene counts; blue symbols: measured vinylene counts. $[C]_0$ = 3.0 mM; $[M]_0$ = 0.60 M.

which is 2.69 Å. The predicted vinylidene concentration is more than 1 order of magnitude higher than the measured experimental value at the end of the reaction. It should be noted that the monomer independent chain transfer is not eliminated completely. As mentioned above, when system **4** was allowed to run for 12 h after the monomer had been consumed an increase in vinyl concentrations was detected.

In the above, we attributed the emergence of the monomer dependent chain transfer mechanism in systems **4** and **5** to increased steric freedom availed by greater Zr−X bond distance. While this may explain the greater ease with which monomer can coordinate to effect chain transfer, it by itself does not explain why the monomer independent reaction should become hindered. We speculate that once the Zr−X distance is large enough (or alternatively the pendent zirconium interaction is weak enough), some other agent, most likely the counterion, may occupy the spot thereby precluding the β-H agostic bond from forming.[26]

Catalyst **5** also exhibits monomer dependent chain transfer with fairly low rate constants. This result is less surprising than that of system **4** as the sulfur atom of the pendant group in **5** is significantly different than the second row pendant ligand atoms (N or O) in **1**−**4** according to HSAB theory. It is speculated that this effect accounts for the mechanistic change observed in system **5**.

The rest of the rate constants shown in Table 1 do not seem to exhibit clear trends with respect to Zr−X bond length. Specifically, k_p is large for systems **1**, **3**, and **5**, and several times lower for catalysts **2** and **4**. This effect alludes to the fact that other catalyst descriptors, i.e., electronic effects, derived from the sp^2 nature of the donor, are perhaps responsible.[10]

Rate constants for misinsertion (k_{mis}) are similar for systems **1**, **2**, and **3**, whereas in the case of **4**, k_{mis} is an order of magnitude slower. For system **5**, k_{mis} is an order of magnitude faster. It stands to reason that the longer Zr−X bond distance would allow for more steric freedom for the misinsertion of monomer resulting in an increased misinsertion rate. However, this line of logic fails to describe catalyst **4**, which appears, yet again, to be an outlier.

Rate of recovery from misinsertion (k_{rec}) is similar for systems **1**, **2**, **3**, and **5**. For system **4**, k_{rec} is zero within the uncertainty of the kinetic analysis. This suggests that the recovery rate for these systems is not governed by sterics.

As discussed in the literature,[10,11] these catalysts produce atactic poly(1-hexene); so, it is not clear if the change in the nature of the pendant effects the degree of tacticity in the resulting polymer product in a way that is easily defined.

dx.doi.org/10.1021/ja401474v | J. Am. Chem. Soc. 2013, 135, 6280−6288

CONCLUSIONS

A comprehensive kinetic study of five catalytic systems based on Zr amine bis-phenolate complexes has been completed, and the relevant rate constants and elementary reaction steps were robustly determined for each system. The mechanism includes initiation, normal propagation, misinsertion, recovery, and chain transfer. The most significant finding was an apparent correlation between the zirconium pendant ligand (Zr−X) bond distance and the rate constants of chain transfer. Specifically, for catalysts **1**−**3**, the logarithm of the chain transfer rate constants ($k_{vinylidene}$ and $k_{vinylene}$) increase linearly with the Zr−X bond distance. Once a certain Zr−X bond distance is reached, the chain transfer mechanism changes from monomer independent β-H elimination to monomer dependent β-H transfer (to monomer), as observed for systems **4** and **5**. This study has also shown that, with the exception of **4**, the rate of misinsertion (k_{mis}) increases for a longer Zr−X bond distance, which is most likely due to an increase in the steric freedom allowing for an increase in misinsertion events, regio errors.

ASSOCIATED CONTENT

Supporting Information

Synthesis of all ligands and precatalysts, as well as a complete set of experimental procedures for each system and kinetic modeling. This material is available free of charge via the Internet at http://pubs.acs.org.

AUTHOR INFORMATION

Corresponding Author

*E-mail: caruther@purdue.edu (J.M.C.); mabuomar@purdue.edu (M.M.A.-O.).

Author Contributions

All authors have given approval to the final version of the manuscript.

Notes

The authors declare no competing financial interest.

ACKNOWLEDGMENTS

Financial support was provided by the U.S. Department of Energy by Grant No. DE-FG02-03ER15466. This research was supported in part by the National Science Foundation through TeraGrid resources provided by Purdue University under grant number TG-CTS070034N. Computing resources were also provided by Information Technology at Purdue.

REFERENCES

(1) Chemical Market Associates, Inc. (CMAI), 2005 *World Polyolefins Analysis*, www.cmaiglobal.com.

(2) (a) Chen, E. Y-X.; Marks, T. J. *Chem. Rev.* **2000**, *100*, 1391−1434. (b) Li, H.; Marks, T. J. *Proc. Natl. Acad. Sci. U.S.A.* **2006**, *103*, 15295−15302.

(3) Manz, T. A.; Phomphrai, K.; Medvedev, G. A.; Krishnamurthy, B. B.; Sharma, S.; Haq, J.; Novstrup, K. A.; Thomson, K. T.; Delgass, W. N.; Caruthers, J. M.; Abu-Omar, M. M. *J. Am. Chem. Soc.* **2007**, *129*, 3776−3777.

(4) (a) Krauledat, H.; Brintzinger, H. H. *Angew. Chem., Int. Ed.* **1990**, *29*, 1412−1413. (b) Piers, W. E.; Bercaw, J. E. *J. Am. Chem. Soc.* **1990**, *112*, 9406−9707. (c) Coates, G. W.; Waymouth, R. M. *J. Am. Chem. Soc.* **1991**, *113*, 6270−6271.

(5) Britovsek, G. J. P.; Gibson, V. C.; Wass, D. F. *Angew. Chem., Int. Ed.* **1999**, *38*, 428−447.

(6) Arriola, D. J.; Carnahan, E. M.; Hustad, P. D.; Kuhlman, R. L.; Wenzel, T. T. *Science* **2006**, *312*, 714−719.

(7) Novstrup, K. A.; Travia, N. E.; Medvedev, G. A.; Stanciu, C.; Switzer, J. M.; Thomson, K. T.; Delgass, W. N.; Abu-Omar, M. M.; Caruthers, J. M. *J. Am. Chem. Soc.* **2010**, *132*, 558−566.

(8) Liu, Z. X.; Somsook, E.; White, C. B.; Rosaaen, K. A.; Landis, C. R. *J. Am. Chem. Soc.* **2001**, *123*, 11193−11207.

(9) (a) Angermund, K.; Fink, G.; Jensen, V. R.; Kleinschmidt, R. *Chem. Rev.* **2000**, *100*, 1457−1470. (b) Bochmann, M. *J. Organomet. Chem.* **2004**, *689*, 3982−3998. (c) Mohring, P. C.; Coville, N. J. *Coord. Chem. Rev.* **2006**, *250*, 18−35. (d) Wang, B. *Coord. Chem. Rev.* **2006**, *250*, 242−258.

(10) Tshuva, E. Y.; Goldberg, I.; Kol, M.; Goldschmidt, Z. *Organometallics* **2001**, *20*, 3017−3028.

(11) Tshuva, E. Y.; Groysman, S.; Goldberg, I.; Kol, M.; Goldschmidt, Z. *Organometallics* **2002**, *21*, 662−670.

(12) Kerton, F. M.; Holloway, S.; Power, A.; Soper, R. G.; Sheridan, K.; Lynam, J. M.; Whitwood, A. C.; Willans, C. E. *Can. J. Chem.* **2008**, *86*, 435−443.

(13) Groysman, S.; Goldberg, I.; Kol, M.; Genizi, E.; Goldschmidt, Z. *Organometallics* **2003**, *22*, 3013−3015.

(14) (a) Gahleitner, M.; Severn, J. R. *Designing Polymer Properties*. In *Tailor-Made Polymers*; Wiley-VCH Verlag GmbH & Co., 2008. (b) Resconi, L.; Cavallo, L.; Fait, A.; Piemontesi, F. *Chem. Rev.* **2000**, *100*, 1253−1346.

(15) Resconi, L.; Piemontesi, F.; Franciscono, G.; Abis, L.; Fiorani, T. *J. Am. Chem. Soc.* **1992**, *114*, 1025−1032.

(16) Mogstad, A.-L.; Waymouth, R. M. *Macromolecules* **1992**, *25*, 2282−2284.

(17) Coates, G. W.; Hustad, P. D.; Reinartz, S. *Angew. Chem., Int. Ed.* **2002**, *41*, 2236−2257.

(18) Mecking, S. *Angew. Chem., Int. Ed.* **2001**, *40*, 534−540 and references therein.

(19) Agapie, T.; Henling, L. M.; DiPasquale, A. G.; Rheingold, A. L.; Bercaw, J. E. *Organometallics* **2008**, *27*, 6245−6256.

(20) Margl, P.; Deng, L. Q.; Ziegler, T. *J. Am. Chem. Soc.* **1999**, *121*, 154−162.

(21) Busico, V.; Cipullo, R.; Friederichs, N.; Ronca, S.; Talarico, G.; Togrou, M.; Wang, B. *Macromolecules* **2004**, *37*, 8201−8203.

(22) Camacho, D. H.; Guan, Z. B. *Macromolecules* **2005**, *38*, 2544−2546.

(23) (a) Meinhard, D.; Wegner, M.; Kipiani, G.; Hearley, A.; Reuter, P.; Fischer, S.; Marti, O.; Rieger, B. *J. Am. Chem. Soc.* **2007**, *129*, 9182−9191. (b) Anselment, T. M. J.; Wichmann, C.; Anderson, C. E.; Herdtweck, E.; Rieger, B. *Organometallics* **2011**, *30*, 6602−6611.

(24) Doi, Y.; Ueki, S.; Keii, T. *Macromolecules* **1979**, *12*, 814−819.

(25) Naga, N.; Mizunuma, K. *Polymer* **1998**, *39*, 5059−5067.

(26) Chen, M.-C.; Roberts, J. A. S.; Marks, T. J. *J. Am. Chem. Soc.* **2004**, *126*, 4605−4625.

(27) Groysman, S.; Goldberg, I.; Kol, M.; Genizi, E.; Goldschmidt, Z. *Inorg. Chim. Acta* **2003**, *345*, 137−144.

(28) Tshuva, E. Y.; Gendeziuk, N.; Kol, M. *Tetrahedron Lett.* **2001**, *42*, 6405−6407.

(29) Switzer, J. M.; Travia, N. E.; Steelman, D. K.; Medvedev, G. A.; Thomson, K. T.; Delgass, W. N.; Abu-Omar, M. M.; Caruthers, J. M. *Macromolecules* **2012**, *45*, 4978−4988.

(30) Liu, Z.; Somsook, E.; Landis, C. R. *J. Am. Chem. Soc.* **2001**, *123*, 2915−2916.

(31) Christianson, M. D.; Tan, E. H. P.; Landis, C. R. *J. Am. Chem. Soc.* **2010**, *132*, 11461−11463.

ORGANOMETALLICS

Article

pubs.acs.org/Organometallics

Comparison of Selected Zirconium and Hafnium Amine Bis(phenolate) Catalysts for 1-Hexene Polymerization

D. Keith Steelman,[†] Paul D. Pletcher,[†] Jeffrey M. Switzer,[‡] Silei Xiong,[‡] Grigori A. Medvedev,[‡] W. Nicholas Delgass,[‡] James M. Caruthers,*[,‡] and Mahdi M. Abu-Omar*[,†,‡]

[†]Brown Laboratory, Department of Chemistry, Purdue University, 560 Oval Drive, West Lafayette, Indiana 47907, United States

[‡]School of Chemical Engineering, Purdue University, Forney Hall of Chemical Engineering, 480 Stadium Mall Drive, West Lafayette, Indiana 47907, United States

Supporting Information

ABSTRACT: The kinetics of 1-hexene polymerization using a family of three zirconium and hafnium amine bis-phenolate catalysts, M[*t*-Bu-ON^{X}O]Bn$_2$ (where M = Zr (**a**) or Hf (**b**), and X = THF (**1**), pyridine (**2**), or NMe$_2$ (**3**)), have been investigated to uncover the mechanistic effect of varying the metal center M. A model-based approach using a diverse set of data including monomer consumption, evolution of molecular weight, and end-group analysis was employed to determine each of the reaction-specific rate constants involved in a given polymerization process. This study builds upon the mechanism of polymerization for **1a**−**3a**, which has been previously reported by applying the same methodology to the hafnium containing analogues, **1b**−**3b**. It has been observed that each elementary step-specific rate constant that involves the insertion of a monomer is reduced by an order of magnitude. As previously reported for catalysts **1a**−**3a**, a quantitative structure−activity relationship was uncovered between the logarithm of the monomer-independent chain transfer rate constants and the Hf−X bond distance for catalysts **1b**−**3b**. However, this dependence on the pendant ligand is 2.7 times weaker for the Hf-containing analogues versus those containing Zr. These findings underscore the importance of comprehensive kinetic modeling using a diverse set of multiresponse data, enabling the determination of robust kinetic constants and reaction mechanisms of catalytic olefin polymerization as part of the development of structure−activity relationships.

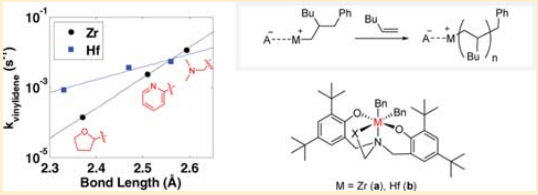

INTRODUCTION

Production of polyolefins is a major industrial process with a current capacity of ca. 110 billion kg per year globally.[1] Today polyolefins are produced primarily using heterogeneous Ziegler-Natta catalysts; however, in recent years, homogeneous single-site catalysts, specifically metallocene-type catalysts, have attracted attention because they offer potential control of the various kinetic steps, which in turn can be manipulated by "catalyst design".[2−4] While high-throughput screening has accelerated the discovery process with group 4 coordination complexes leading to Dow's catalysts for olefin block copolymer synthesis,[5] the promise of directly correlating kinetic constants to descriptors of the catalyst has not yet been realized. A major obstacle in the way of rational catalyst design is the lack of proper quantitative kinetic analysis of all the relevant processes (i.e., kinetic steps) that are involved in catalytic olefin polymerization.[6,7] Nevertheless, the study of single-site catalysts for olefin polymerization is particularly attractive because of the potential to directly correlate the physical properties of the resulting polymer to structural features of the catalyst based on first principles.[8] These types of correlations enable one to draw conclusions on how a catalyst structure may be manipulated to yield specific polymeric architectures. One particular avenue of interest is to investigate the effect that changing the metal center will have on the polymerization process.

Of the group IV elements, the metal that has received the most attention as a homogeneous polymerization catalyst is zirconium. Hafnium is another group IV element that is known to act as a homogeneous polymerization catalyst. Zirconium and hafnium in the +4 oxidation state are remarkably similar, having the same number of outer shell d-electrons and the same ionic radii due to the lanthanide contraction. Many of the analogous zirconium and hafnium complexes reported in the literature have virtually identical crystal structures.[9−11] Despite their similarities, these two metals behave drastically differently as polymerization catalysts. When studying β-Me elimination chain transfer pathways in propylene oligomers, Fiorani et al. observed that as a general rule zirconocene type catalysts have increased activity over their hafnocene type catalysts; however, for bis(Cp*)-metallocenes, hafnium has a significantly larger activity than its zirconium analogue, making it one of the few examples where the general rule is broken.[10] Further studies by Collins and Ferrara showed the same phenomenon with an

Received: June 22, 2013
Published: August 26, 2013

   dx.doi.org/10.1021/om4006005 | *Organometallics* 2013, 32, 4862−4867

additional note that the hafnium analogues produce polymers with a significantly larger molecular weight, M_w.[11]

One specific family of nonmetallocene catalysts, first pioneered by Kol and co-workers, that has sparked interest utilizes an amine bis-phenolate (salan) ligand system (see Figure 1).[12,13] The reason for choosing this particular family of

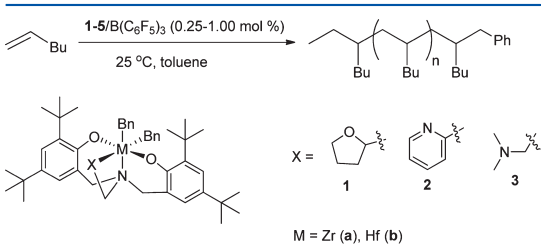

Figure 1. 1-Hexene polymerization catalyzed by zirconium/hafnium salan-type catalysts **1a**–**3b** when combined with the activator $B(C_6F_5)_3$.

ligands as part of our detailed kinetic studies is the relative ease of synthesis and the ability to tune the catalysts' coordination environment.[14] Furthermore, these catalysts exhibit high activity, comparable to metallocene catalysts, with 1-hexene in conventional organic solvents such as toluene. This feature enables the investigation of kinetic data in the condensed phase thereby eliminating mass transfer limitations that are inherent in gas phase polymerization reactions. Following up on Kol's earlier qualitative observations that the nature of the pendant ligand (X) and its distance from the metal center (Zr–X) influence chain transfer,[15] we have shown a linear correlation between the logarithm of the chain transfer rate constants, $k_{vinylidene}$ and $k_{vinylene}$, and the Zr–X bond distance, which was probed by quantitative kinetic modeling of a diverse set of multiresponse data.[16,17] In this study, we continre the use of quantitative kinetic modeling of multiresponse data for the salan-type catalysts to elucidate the effect of changing the metal center from Zr to Hf on the rate constants that comprise the olefin polymerization mechanism.

EXPERIMENTAL PROCEDURE

General Procedure. All manipulations were performed under dry inert atmosphere in a glovebox or at a vacuum manifold using air-sensitive techniques under N_2 or Ar atmosphere. Toluene and pentane were distilled over activated alumina and a copper catalyst using a solvent purification system (Anhydrous Technologies) and degassed through freeze–pump–thaw cycles. Both solvents were stored over activated molecular sieves. Tetrabenzylzirconium was purchased from STREM and used as received. The monomer 1-hexene was purchased from Aldrich and purified by distillation over a small amount of dimethyl bis(cyclopentadienyl)zirconium and stored over molecular sieves. Tris(pentafluorophenyl)boron was purchased from STREM and purified by sublimation. Diphenylmethane was purchased from Aldrich and stored over molecular sieves. CH_3OD was purchased from Cambridge Isotopes and used as received. Toluene-d_8 was used as received and stored over molecular sieves. ^1H and ^2H NMR experiments were performed on a Varian INOVA600 MHz or Bruker DRX500 MHz spectrometer.

The ligands and precatalysts (**1a**–**3b**) were prepared following modified literature procedures.[12,13] We describe herein the details for one representative procedure and provide the others in the Supporting Information.

Synthesis of 6,6′-((((Tetrahydrofuran-2-yl)methyl)-azanediyl)bis(methylene))bis(2,4-di-*tert*-butyl-phenol), *t*-Bu-ON^{THF}O Ligand (1). In a typical synthesis, an 80 mL reaction vessel was charged with 2,4-di-*tert*-butylphenol (6.19 g, 30.0 mmol), 2-(aminomethyl) tetrahydrofuran (1.55 mL, 15 mmol) and 37% histological grade formaldehyde (6.00 mL, 80 mmol), distilled water, and a stir bar while a maximum volume of 80 mL was maintained. The biphasic reaction mixture was placed in a CEM microwave reactor and allowed to warm to 100 °C over 5 min while stirring. The reaction was allowed to stand at 100 °C for 30 min and then cooled to room temperature. The aqueous layer was removed, and cold, dry methanol was added to the organic phase. This mixture was shaken for 30 min, and the resulting solid isolated by vacuum filtration. The crude ligand product was purified by crystallization from ethanol (28% yield).

Synthesis of Zr[*t*-Bu-ON^{THF}O]Bn$_2$ (1a). In a typical synthesis, a 100 mL flask was charged with tetrabenzylzirconium (0.557 g, 1.22 mmol), 20 mL of toluene, and a stir bar and fitted with a rubber septum. A second 100 mL flask was charged with the *t*-Bu-ON^{THF}O ligand (0.609 g, 1.13 mmol) and 20 mL of toluene. The two flasks were placed under an inert atmosphere, and the ligand solution was added to the tetrabenzylzirconium solution via a cannula. The reaction was allowed to warm to 60 °C and stir for 2 h resulting in a bright yellow solution. The solution was concentrated to about 10 mL and placed into a −10 °C freezer. Yellow crystals formed within 2 days, and the mother liquor was removed via a cannula. The crystals were dried under vacuum (84% yield). The precatalyst was recrystallized by vapor diffusion of pentane into a precatalyst/toluene solution to afford an analytically pure complex.

NMR Scale Polymerization of 1-Hexene. The procedure for NMR scale polymerization is based on literature.[17] For a typical polymerization, Zr[*t*-Bu-ON^{THF}O]Bn$_2$ (**1**) (6.1 mg, 0.0075 mmol) was dissolved in 0.5 mL of toluene in a small vial and sealed with a screw-cap septum. The vial containing the precatalyst solution was pierced with a 1 mL syringe. The vial and syringe were placed in a N_2 bag and allowed to equilibrate to 25 °C. Tris(pentafluorophenyl)boron (4.3 mg, 0.0084 mmol), 1-hexene (0.1265 g, 1.50 mmol), and diphenylmethane (9.5 mg 0.056 mmol) were added to a 2 mL volumetric flask and diluted to the mark with toluene-d_8. This solution was placed in an NMR tube and sealed with a septum. The monomer/activator solution was placed in the spectrometer and allowed to equilibrate to 25 °C using a VT controller. A measurement was taken to determine the initial concentration of monomer relative to the internal standard. The NMR tube was removed from the spectrometer, and the catalyst precursor solution was added to the activator/monomer solution by piercing the septum while the syringe remained in the N_2 bag. The reaction mixture was shaken for ca. 30 s and placed back into the spectrometer. Spectra were acquired at predetermined time intervals until the reaction reached completion. Each sample was prepared for GPC analysis by evaporation over mild heat before dissolution in hexanes and filtration through an alumina plug to remove the quenched catalyst. Evaporation of solvent yielded clear, colorless poly(1-hexene). The array of ^1H spectra was collected on an INOVA 600 MHz spectrometer and analyzed using MestReNova.

Batch Polymerization of 1-Hexene. The procedure for Manual Quench is based on literature.[18] For a typical polymerization, Zr[*t*-Bu-ON^{THF}O]Bn$_2$ (0.073 g, 0.090 mmol) was dissolved in 5.0 mL of toluene in a small vial that was sealed with a screw-cap septum. The vial containing the precatalyst solution was pierced with a 10 mL syringe. The vial and syringe were placed in a N_2 bag and allowed to equilibrate to 25 °C. Tris(pentafluorophenyl)boron (0.053 g, 0.099 mmol), and 1-hexene (1.575 g, 18.71 mmol) were added to a 25 mL flask and diluted to the mark with toluene. This solution was diluted to 26 mL with 1 mL of toluene, and 1 mL of the resulting solution was removed for quantification of the initial monomer concentration through NMR analysis. The flask was sealed with a septum and moved from a N_2 filled glovebox to a vacuum manifold and placed under argon. The monomer/activator solution was allowed to equilibrate to 25 °C using a temperature-controlled silicone oil bath. The catalyst precursor solution was added to the activator/monomer solution by piercing the septum while the syringe remained in the N_2 bag. The resulting yellow solution was allowed to stir while aliquots were removed at selected times, and each was injected into a 10 mL

dx.doi.org/10.1021/om4006005 | *Organometallics* 2013, 32, 4862–4867

volumetric flask containing 1 mL of deuteromethanol. A 1 mL aliquot from the quenched solutions was removed, and a 0.5 mL solution of toluene-*d* spiked with diphenylmethane as an internal standard for quantification of 1-hexene consumption (via ^{1}H NMR on Varian Inova600). Each sample was prepared for GPC analysis by evaporation over mild heat before dissolution in hexanes and filtration through an alumina plug to remove the quenched catalyst. Evaporation of solvent yielded clear, colorless poly(1-hexene).

In the case of vinyl end group analysis, a 1 mL aliquot was worked up as described above. The resulting polymer was dissolved in $CDCl_3$ and diluted to the mark in a 2 mL volumetric flask. Diphenylmethane was used as an internal standard, and the method of standard additions was used in quantification of the end groups by ^{1}H NMR. All end-group analysis measurements were taken on a Bruker DRX500 spectrometer at 25 °C.

In the case of ^{2}H analysis for active-site counting, the remaining quenched reaction solution (8 mL) was worked up as described above. The resulting polymer was dissolved in CH_2Cl_2, and diluted to the mark in a 2 mL volumetric flask. Benzene-d_6 was used as an internal standard, and the method of standard additions was used in quantification of active sites by ^{2}H NMR. All active site measurements were taken on a Bruker DRX500 spectrometer at 25 °C.

Gel Permeation Chromatography (GPC) Analysis. The procedure used to analyze polymer samples using GPC methods was taken from Novstrup et al.,[6] and it is summarized below. Poly(1-hexene) samples were added to THF at room temperature and allowed to dissolve for 4 h. Solutions were then passed through a 0.2 μm filter to remove any particulate matter. The GPC analysis was performed on a Waters GPCV 2000 for systems **1a** and **3a**, and on a Viscotek TDAmax for systems **1b**, **2a**, **2b**, and **3b**. On the Waters GPCV 2000, samples were injected through a 101.3 μL injection loop and passed through two Polymer Laboratories PLGel 5 μm Mixed-C columns in series in a 45 °C oven at a flow rate of 1.0 mL min^{-1}. On the Viscotek TDAmax, samples were injected through a 200 μL injection loop and passed through three Viscotek T6000M 10 μm General Mixed Org columns in series in a 35 °C oven at a flow rate of 1.0 mL min^{-1}. The analysis made use of the differential RI detector and a viscometer. Molecular weights were assigned by way of a universal calibration curve created with polystyrene standards ranging from 580 g mol^{-1} to 3 114 000 g mol^{-1}. The calibration was verified through the analysis of a broad standard, SRM 706a, provided by the National Institute of Standards and Technology.

RESULTS

The complete kinetic analysis for the zirconium-based systems **1a**, **2a**, and **3a** has been reported in previous publications.[16,17] Here we present the experimental data and a complete kinetic analysis for 1-hexene polymerization by hafnium-based analogues **1b**, **2b**, and **3b**. For each system, we followed our previously developed kinetic modeling method[6,16,17] based on the analysis of multiresponse data that includes (1) monomer consumption, (2) MWD, (3) active site counts, and (4) vinyl end group counts as measured by ^{1}H NMR. We determine the active site count at any point in the course of the reaction as the number measured by quenching with methanol-d_4 and performing ^{2}H NMR measurement of the concentration of chains with deuterated end groups. The sites that have undergone 1,2-insertion are defined as primary sites, and the sites that have undergone 2,1-misinsertion are defined as secondary sites. Within this analysis, each system is studied independently, and no a priori assumptions are made with respect to the elementary steps. As explained in detail in the Supporting Information, the analysis procedure begins with the most basic mechanism, i.e., initiation and propagation, and fitting is attempted to the entire data set; only after a simple mechanism is shown to fail, a new elementary step, e.g., chain transfer, is added, and the fitting is attempted again.

As a result, a minimal set of elementary steps is determined that can fit the multiresponse data. For the zirconium-based systems **1a**, **2a**, and **3a**, such a minimal set turned out to include initiation, propagation via normal insertion, 2,1-misinsertion, recovery from misinsertion, and chain transfer[16] resulting in the formation of vinylidene and vinylene species (see Scheme 1).

Scheme 1. Elementary Kinetic Steps Used in Fitting the Data for Catalysts 1−5[a]

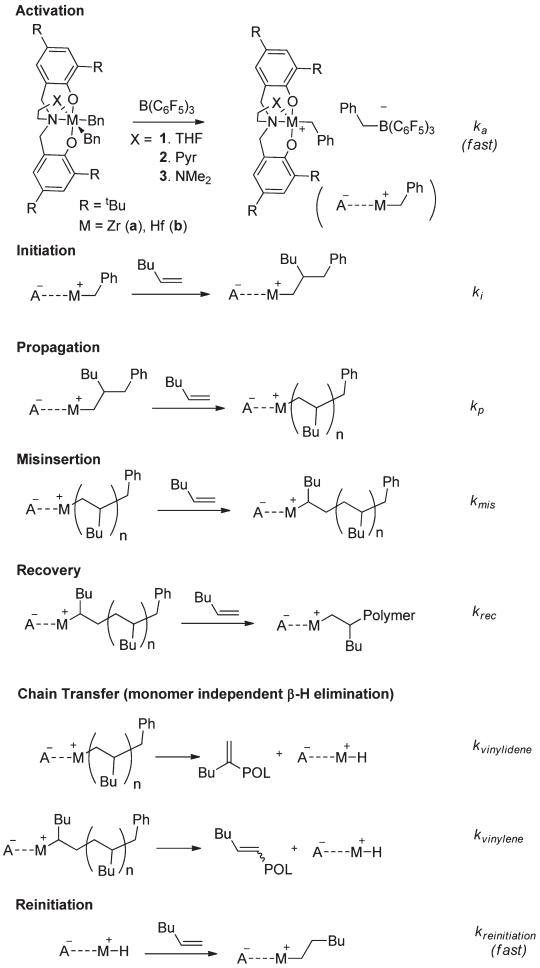

[a]The ordinary differential equations (ODEs) that describe the mass-action kinetics associated with this mechanism are provided in the Supporting Information.

Also it is noted that the catalyst participation may not be 100% of the nominal precatalyst amount, and it may vary from system to system and experiment to experiment. By catalyst participation, here we mean the fraction of precatalyst that can be activated and initiated once the reactant species are combined. This is separate from time-dependent deactivation. For the hafnium-based systems **1b**, **2b**, and **3b**, the results of the kinetic analysis are here presented. We chose the system **2b** to illustrate the quality of kinetic fitting. The similar figures for

dx.doi.org/10.1021/om4006005 | *Organometallics* 2013, 32, 4862−4867

systems **1b** and **3b** are in the Supporting Information. The main conclusion is that the kinetic mechanism for hafnium-based systems is essentially the same as for zirconium analogues.

Hf–Pyridine Catalyst 2b. The experimental data along with the kinetic modeling fits are presented in Figure 2.

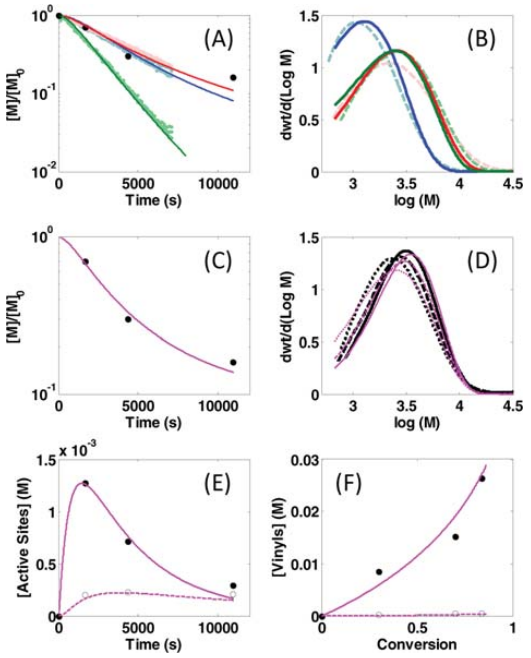

Figure 2. Multiresponse data set with fits for catalyst **2b**. NMR-scale experiments: (A) Monomer consumption. Data, symbols; fits, lines. (B) MWDs at the end. {Blue, Red, Green}, $[C]_0$ = {3.0, 3.0, 6.0} mM and $[M]_0$ = {0.30, 0.60, 0.60} M. Data, solid; fits, dashed. Batch scale experiments ($[C]_0$ = 3.0 mM, $[C]_0$ = 0.60 M): (C–F). (C) Monomer consumption. Data, symbols; fit, line. (D) MWDs at (solid) 1694 s, (dashed) 4352 s, (dotted) 10963 s. Data, black; fits, magenta. (E) Active site counts. Primary, filled circles (data)/solid line (fit); secondary, open circles (data)/dashed line (fit). (F) End group analysis. Filled circles (data)/solid line (fit), vinylidene; open circles (data)/dashed line (fit), vinylene. In (A), black circles same as in (C) for comparison.

The specific features of this system are as follows: (1) Catalyst participation is nearly 100%. (2) In the case of the batch scale experiments, significant catalyst deactivation is observed as evidenced by bending of the monomer consumption curve in Figure 2C and the steep decline in primary active site counts over the course of the reaction in Figure 2E. In the case of the NMR scale experiments, the deactivation either does not occur or is much less significant. For that reason, deactivation is not considered as part of the catalytic reactions. (3) The amount of chain transfer is relatively high as evidenced by the significant vinylidene concentration in Figure 2F and the fact that the MWD does not change much after 30% conversion of the monomer. The vinylidene formation is via a monomer-independent reaction as evidenced by the upward curvature in the vinylidene concentration versus monomer conversion plot (Figure 2F). (4) The vinylene end group concentration is much lower than that of vinylidene (Figure 2F), where the vinylene formation is via monomer-dependent reaction as evidenced by the linear accumulation in Figure 2F.

Hf–THF Catalyst 1b. The experimental data along with the kinetic modeling fits are presented in the Supporting Information. The specific features of this system are as follows: (1) Catalyst participation is approximately 50%. (2) Faster chain transfer rate and slower propagation rate compared to its zirconium analogue result in a much higher chain transfer frequency (i.e., the measured vinyl terminated groups are 100 times higher at the end of the reaction). However, the chain transfer rate of this catalyst remains the lowest compared to catalyst **2b** and **3b**. (3) Fewer secondary sites are formed, meaning there is less dormancy as compared to the zirconium analogue. The vinylene count is quite small, indicating that the actual chain transfer rate from secondary sites is negligible.

Hf–NMe_2 Catalyst 3b. The experimental data along with the kinetic modeling fits are presented in the Supporting Information. The specific features of this system are as follows: (1) Catalyst participation is approximately 40%. (2) There is a decline in active catalyst sites over the course of the reaction, although it is not as steep as in systems **1b** and **2b**. (3) No secondary catalyst sites were measured, although a small amount of vinylene end groups was detected. This peculiar behavior was also observed for the $EBIZrMe_2/B(C_6F_5)_3$ catalyst.[6,7] Vinylene is typically expected to form following chain transfer of secondary sites. It is likely in this system that secondary sites do form, but they rapidly undergo either chain transfer or monomer-dependent recovery. Since no secondary

Table 1. Rate Constants for 1-Hexene Polymerization with the $M[t\text{-Bu-ON}^XO]Bn_2/B(C_6F_5)_3$ Catalysts 1a–3b[a]

X	Zr-THF (**1a**)	Hf-THF (**1b**)	Zr-Pyr (**2a**)	Hf-Pyr (**2b**)	Zr-NMe_2 (**3a**)	Hf-NMe_2 (**3b**)
M–X/Å	2.37	2.33	2.51	2.47	2.59	2.56
$k_i/M^{-1}\ s^{-1}$	0.08 (+0.02/−0.01)	0.04 (+0.02/−0.01)	>0.05	0.0017 (+0.0002/−0.0001)	0.16 (+0.04/−0.02)	0.04 (+0.01/−0)
$k_p/M^{-1}\ s^{-1}$	8.0 (+0.8/−0.2)	0.53 (+0.06/−0.06)	1.8 (+0.2/−0.1)	0.20 (+0/−0.02)	11 (+1/−1)	0.95 (+0.07/−0.09)
$k_{mis}/M^{-1}\ s^{-1}$	0.054 (+0.026/−0.003)	0.0081 (+0.0002/−0.001)	0.031 (+0.004/−0.005)	0.00028 (+0.00002/−0)	0.055 (+0.007/−0.004)	0.0012[b] (+0.0003/−0)
$k_{rec}/M^{-1}\ s^{-1}$	0.047 (+0.021/−0.002)	0.06 (+0.004/−0.005)	0.028 (+0.004/−0.005)	0.0002 (+0/−0.0002)	0.04 (+0.03/−0.02)	N/A
$k_{vinylidene}$ $(10^{-3})/s^{-1}$	0.14 (+0.014/−0.02)	0.84 (+0.02/−0.04)	2.4 (+0.1/−0.1)	3.8 (+0.3/−0.2)	12.2 (+0.8/−0.6)	5.5 (+0.2/−0.2)
$k_{vinylene}$ $(10^{-3})/s^{-1}$	0.051 (+0.002/−0.003)	0.27 (+0.07/−0.06)	0.65 (+0.06/−0.05)	2nd order	8.72 (+0.07/−0.04)	[b]

[a]In toluene at 25 °C. See Figure 1 for precatalyst structures and Scheme 1 for reactions steps. Errors are in parentheses. [b]The misinsertion reaction in the system **3b** mechanism is followed immediately by monomer-independent β-H elimination to form vinylene.

dx.doi.org/10.1021/om4006005 | *Organometallics* 2013, 32, 4862–4867

sites are observed even late in the reaction when monomer concentration is low, a fast monomer-independent chain transfer event is more probable.

DISCUSSION

In this study, the complete set of kinetic rate constants for three zirconium amine bis-phenolate catalyst systems and three hafnium analogues have been presented. For each system, a rich data set including MWD has been collected and successfully fitted by comprehensive kinetic modeling. With one possible exception, the mechanism of 1-hexene polymerization for these catalysts (**1a**−**3b**) consists of the following elementary reaction steps: initiation, normal propagation, misinsertion, recovery, and chain transfer. For system **3b**, there is not enough information to include or exclude a recovery reaction.

The values of the rate constants are shown in Table 1 including error bounds, which were determined using the methodology for determining error bounds discussed in the previous paper.[16] Examining the summarized kinetic data in Table 1, the following conclusions emerge: (1) The monomer-dependent rate constants k_i, k_p, k_{mis}, and k_{rec} are slower for the Hf systems than for the Zr systems. In particular, the propagation rate is 1 order of magnitude slower in all the hafnium-based systems. (2) $k_{vinylidene}$, which is monomer-independent chain transfer, is not uniformly slower for Hf versus Zr. It depends on the pendant of the ligand. For example, for the THF pendant (**1a** and **b**), $k_{vinylidene}$ for Hf is larger than that for Zr, and the rate constants are comparable for both metals in the case of the pyr pendant (**2a** and **b**). (3) Vinylene formation does not behave consistently across all pendants with Hf as it does for Zr. For Hf−Pyr it appears second order; for Hf−NMe_2 it is apparently fast (consistent with fast $k_{vinylidene}$). We do not currently have an explanation for this behavior. (4) Each hafnium complex exhibits less secondary site formation than its zirconium analogue.

A possible reason for the reduction in the rate of all elementary steps that require the insertion of a monomer is due to the larger metal−carbon bond enthalpy of the hafnium systems as compared with the analogous zirconium systems.[19] In our previous paper we pointed out a linear correlation between the logarithm of the rate of monomer-independent chain transfer and the bond distance between the zirconium and the pendant group observed in the precatalyst.[16] A similar linear relationship appears to be holding for the monomer-independent chain transfer rate for the hafnium-based systems as shown in Figure 3. However, the hafnium-based system exhibits a much weaker dependence on the bond length, as the slope of this correlation is 2.7 times smaller. In our previous study,[16] we speculated that this increase in bond distance allows for more steric freedom to accommodate the β-hydride agostic interaction necessary for chain transfer to occur. Since the effective size of the hafnium metal center is generally believed to be similar to that of zirconium, it is unclear why this correlation is weaker in hafnium-based systems. However, it is likely that the exact reason lies with the intrinsic properties of the metal center and how these properties control the β-hydrogen transfer reactions.

CONCLUSIONS

A comprehensive kinetic study of three catalytic systems based on hafnium amine bis-phenolate complexes has been completed, and the relevant rate constants and elementary reaction steps were determined for each system. The mechanism includes initiation, normal propagation, misinsertion, recovery, and chain transfer. In conjunction with the previous study of zirconium analogues, this report allows for the first quantitative comparison between similarly ligated hafnium and zirconium-based olefin polymerization catalysts. The most important findings are as follows: the 1 order of magnitude decrease in k_p for the hafnium catalysts; an overall decrease in all monomer-dependent reaction steps; and the correlation between the logarithm of monomer-independent chain transfer and the hafnium pendant ligand (Hf−X) bond distance. The last observation is similar to the one previously reported for zirconium systems, but in case of the hafnium catalysts the dependence is 2.7 times weaker. However, it is also interesting that there does not appear to be such a correlation that can be drawn for the propagation rate constant. Subsequent studies are ongoing to ascertain the dependence of k_p on the steric and electronic nature of the pendant.

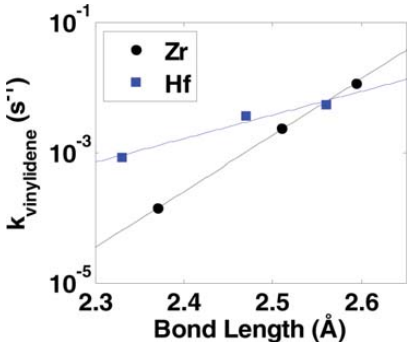

Figure 3. Log($k_{vinylidene}$) vs M−X bond length.

ASSOCIATED CONTENT

Supporting Information

The synthesis of all ligands and precatalysts, as well as a complete set of experimental procedures for each system and kinetic modeling material, and crystal data (CIF). These materials are available free of charge via the Internet at http://pubs.acs.org.

AUTHOR INFORMATION

Corresponding Author

*E-mail: mabuomar@purdue.edu; caruther@purdue.edu.

Notes

The authors declare no competing financial interest.

ACKNOWLEDGMENTS

Financial support was provided by the U.S. Department of Energy by Grant No. DE-FG02-03ER15466. This research was supported in part by the National Science Foundation through TeraGrid resources provided by Purdue University under Grant No. TG-CTS070034N. Computing resources were also provided by Information Technology at Purdue.

REFERENCES

(1) *World Polyolefins Analysis*, Chemical Market Associates, Inc. (CMAI), 2005; www.cmaiglobal.com.

(2) (a) Chen, E. Y-X.; Marks, T. *J. Chem. Rev.* **2000**, *100*, 1391−1434. (b) Li, H.; Marks, T. J. *Proc. Natl. Acad. Sci. U. S. A.* **2006**, *103*, 15295−15302.
(3) Manz, T. A.; Phomphrai, K.; Medvedev, G. A.; Krishnamurthy, B. B.; Sharma, S.; Haq, J.; Novstrup, K. A.; Thomson, K. T.; Delgass, W. N.; Caruthers, J. M.; Abu-Omar, M. M. *J. Am. Chem. Soc.* **2007**, *129*, 3776−3777.
(4) (a) Krauledat, H.; Brintzinger, H. H. *Angew. Chem., Int. Ed.* **1990**, *29*, 1412−1413. (b) Piers, W. E.; Bercaw, J. E. *J. Am. Chem. Soc.* **1990**, *112*, 9406−9707. (c) Coates, G. W.; Waymouth, R. M. *J. Am. Chem. Soc.* **1991**, *113*, 6270−6271.
(5) Arriola, D. J.; Carnahan, E. M.; Hustad, P. D.; Kuhlman, R. L.; Wenzel, T. T. *Science* **2006**, *312*, 714−719.
(6) Novstrup, K. A.; Travia, N. E.; Medvedev, G. A.; Stanciu, C.; Switzer, J. M.; Thomson, K. T.; Delgass, W. N.; Abu-Omar, M. M.; Caruthers, J. M. *J. Am. Chem. Soc.* **2010**, *132*, 558−566. Caruthers, J. M.; Abu-Omar, M. M. *J. Am. Chem. Soc.* **2007**, *129*, 3776−3777.
(7) Landis, C. R.; Rosaaen, K. A.; Sillars, D. R. *J. Am. Chem. Soc.* **2003**, *125*, 1710−1711.
(8) (a) Angermund, K.; Fink, G.; Jensen, V. R.; Kleinschmidt, R. *Chem. Rev.* **2000**, *100*, 1457−1470. (b) Bochmann, M. *J. Organomet. Chem.* **2004**, *689*, 3982−3998. (c) Mohring, P. C.; Coville, N. J. *Coord. Chem. Rev.* **2006**, *250*, 18−35. (d) Wang, B. *Coord. Chem. Rev.* **2006**, *250*, 242−258.
(9) (a) Gauthier, W. J.; Corrigan, J. F.; Taylor, N. J.; Collins, S. *Macromolecules* **1995**, *28*, 3771−3778. (b) Razavi, A.; Ferrara, J. *J. Organomet. Chem.* **1992**, *435*, 299−310.
(10) Resconi, L.; Piemontesi, F.; Franciscono, G.; Abist, L.; Fioranit, T. *J. Am. Chem. Soc.* **1992**, *114*, 1025−1032.
(11) Abbas, R.; Ferrara, J. *J. Organomet. Chem.* **1992**, *435*, 299−310.
(12) Tshuva, E. Y.; Goldberg, I.; Kol, M.; Goldschmidt, Z. *Organometallics* **2001**, *20*, 3017−3028.
(13) Tshuva, E. Y.; Groysman, S.; Goldberg, I.; Kol, M.; Goldschmidt, Z. *Organometallics* **2002**, *21*, 662−670.
(14) Kerton, F. M.; Holloway, S.; Power, A.; Soper, R. G.; Sheridan, K.; Lynam, J. M.; Whitwood, A. C.; Willans, C. E. *Can. J. Chem.* **2008**, *86*, 435−443.
(15) Groysman, S.; Goldberg, I.; Kol, M.; Genizi, E.; Goldschmidt, Z. *Organometallics* **2003**, *22*, 3013−3015.
(16) Steelman, D. K.; Xiong, S.; Pletcher, P. D.; Smith, E.; Switzer, J. M.; Medvedev, G. A.; Delgass, W. N.; Caruthers, J. M.; Abu-Omar, M. M. *J. Am. Chem. Soc.* **2013**, *135*, 6280−6288.
(17) Switzer, J. M.; Travia, N. E.; Steelman, D. K.; Medvedev, G. A.; Thomson, K. T.; Delgass, W. N.; Abu-Omar, M. M.; Caruthers, J. M. *Macromolecules* **2012**, *45*, 4978−4988.
(18) Liu, Z.; Somsook, E.; Landis, C. R. *J. Am. Chem. Soc.* **2001**, *123*, 2915−2916.
(19) Kissounko, D. A.; Zhang, Y.; Harney, M. B.; Sita, L. R. *Adv. Synth. Catal.* **2005**, *347*, 426−432.